Technische Universität München
TUM School of Natural Sciences

Expanding the Biomedical Application Scope: Tailoring of Poly(vinyl phosphonates) via Side- and End-Group Functionalization

Kerstin Petra Halama

Vollständiger Abdruck der von der TUM School of Natural Sciences der Technischen Universität München zur Erlangung einer

Doktorin der Naturwissenschaften (Dr. rer. nat.)

genehmigten Dissertation.

Vorsitz: Priv.-Doz. Dr. Alexander Pöthig

Prüfende der Dissertation:

1. Prof. Dr. Dr. h.c. Bernhard Rieger
2. Prof. Dr. Thomas Brück

Die Dissertation wurde am 18.03.2024 bei der Technischen Universität München eingereicht und durch die TUM School of Natural Sciences am 13.05.2024 angenommen.

"What doesn't kill you makes you stronger"

- Kelly Clarkson

Für meine Eltern

Acknowledgments

Zuerst möchte ich Prof. Dr. Dr. h.c. Bernhard Rieger meinen aufrichtigen Dank für seine Unterstützung und für die Freiheiten eigene Ideen zu verfolgen, aussprechen. Ich konnte in meiner Zeit am WACKER-Lehrstuhl für Makromolekulare Chemie sehr viel lernen und habe sie sehr genossen.

Ein großes Dankeschön geht an die guten Seelen des WACKER-Lehrstuhls, ohne welche Vieles nicht so problemlos laufen würde. Besonderer Dank gilt Dr. Carsten Troll, der für jede technische Problemstellung eine Lösung findet und die Organisation des Lehrstuhls fest im Griff hat. Ebenso möchte ich Dr. Sergei Vagin danken, der für jede chemische Herausforderung eine weiterhelfende Idee oder Erklärung parat hat und Frau Bauer, die den Bürokratie-Dschungel für uns erheblich entschärft hat.

Des Weiteren möchte ich meinen ehemaligen und aktuellen Lehrstuhlkollegen aus der Makro danken, für die Unterstützung und schöne Zeit in und außerhalb des Labors. Danke für die (Aperol) Abende und gemeinsamen Erlebnisse, sowie die vielen Dinge, die ich von euch lernen durfte. Ein besonderes Dankeschön geht hierbei an meinen Benchpartner Anton Maier und meinen Masterarbeitsbetreuer Andreas Schaffer, sowie an Moritz Kränzlein und Philipp Weingarten für die gute Zusammenarbeit bezüglich unserer Polymere, aber auch bei der Bändigung der (MALS-) GPC.

Marina Wittig und Brigita Bratić verdienen besondere Erwähnung, nicht nur als hervorragende Kolleginnen, sondern auch als wunderbare Freundinnen. Die gemeinsamen Wochenendtrips bleiben für mich unvergessliche Erinnerungen, und ich hoffe, dass noch viele folgen werden.

Ein ausdrücklicher Dank geht an meine Auszubildenden Jakob, Chantal, Marie und Marius, sowie meine Studenten Lena, Johannes, Fabio, Leo, Marc, Markus, Maxi, Sebi, Ines und Hannah. Ohne eure Unterstützung wäre diese Arbeit nicht möglich gewesen. Ein besonderer Dank gilt meinem Masteranden Marvin Foith – es war mir eine Ehre, mit dir zusammenzuarbeiten.

Ebenso möchte ich mich bei unterschiedlichen Mitgliedern der Arbeitskreise Fischer, Inoue, Boekhoven und Bach bedanken, die stets bereit waren, bei kurzfristig fehlenden Chemikalien, Geräten und Messungen auszuhelfen.

Ein weiterer Dank geht an meine Schwimm-Gruppe, mit der ich über die Jahre hinweg schöne Abende am See oder im Hallenbad nach der Uni erleben durfte.

Fabian Späth, Karina Hemmer, Katrin Kollmannsberger und Lilla Koser – euch gebührt ein außerordentliches Dankeschön. Ohne euch wäre nicht nur meine Promotion, sondern auch

mein ganzes Studium nicht so unterhaltsam, lustig und schön gewesen. Danke, dass ihr immer für mich da seid.

Andreas Saurwein, dir möchte ich für deine jahrelangen Freundschaft danken, sowie für die schönen Momente und deine Unterstützung besonders in letzter Zeit.

Zum Schluss möchte ich von ganzem Herzen bei meiner Familie bedanken. Danke Matthias, dass du ein so wichtiger Teil in meinem Leben bist. Die durch dich geprüfte Durchsetzungsfähigkeit, konnte ich während meines Studiums gut gebrauchen. Und danke an Anna, die Teil unserer Familie geworden ist und die Einzige die Zuhause versteht was ich von der Chemie erzähle. Mama und Papa, ohne euch wäre ich nicht da, wo ich heute bin. Danke, dass ihr immer hinter mir steht und an mich glaubt. Danke, dass ihr mich unterstützt und für mich da seid. Danke, dass ihr mir so viele Dinge beigebracht habt, die (zum Glück) gar nichts mit Chemie zu tun haben.

Table of Contents

List of abbreviation

2VP	2-vinyl pyridine
AAC	azide-alkyne cycloaddition
AFM	atomic force microscopy
AIBN	azobis(isobutyronitrile)
Ar	aryl
ATRP	atom transfer radical polymerization
CHEMS	3*β*-Hydroxy-5-cholesten-3-hemisuccinate
Chol	cholesterol
CMC	critical micelle concentration
CNT	carbon nanotube
Cp	cyclopentadienyl ligand
Cp*	1,2,3,4,5-pentamethyl cyclopentadienyl ligand
CuAAC	Cu(I)-catalyzed azide-alkyne cycloadditions
CuAACP	copper(I)-catalyzed azide-alkyne click polymerization
Đ	polydispersity index [-]
DAlVP	diallyl vinyl phosphonate
DAVP	dialkyl vinylphosphonates
DCM	dichlormethane
DEEP	diethylethyl phosphonate
DEVP	diethyl vinyl phosphonate
DIVP	diisopropyl vinyl phosphonate
DLS	dynamic light scattering
DMVP	dimethylvinyl phosphonate
dn/dc	refractive index increment [mL/g]
DNA	desoxyribonucleic acid

DOX	doxorubicin
DPrTMSVP	dipropargyl vinyl phosphonate
DPVP	di-*n*-propyl vinyl phosphonate
DWCNT	double-walled carbon nanotube
EA	elementar analysis
EPR	enhanced permeability and retention
ESI-MS	electrospray ionization mass spectrometry
Et	ethyl
EWG	electron withdrawing group
FA	folate
FR	folate receptor
I.E.	initiation efficiency [%]
IPOx	2-*iso*-propenyl-2-oxazoline
LCST	lower critical solution temperature
Me	methyl
MeCN	acetonitrile
MMA	methyl methacrylate
M_n	number average molecular weight [kg/mol]
MW	weight average molecular weight [kg/mol]
MWCNT	multi-walled carbon nanotube
N-(2-HPMA))	N-(2-Hydroxypropyl)methacrylamide
NMP	nitroxide-mediated radical polymerization
NMR	nuclear magnetic resonance spectroscopy
NR	nile red
Nu	nucleophil
PAMAM	poly(amidoamine)

PANI	poly(aniline)
PCL	poly(caprolactone)
PDEVP	poly(diethyl vinyl phosphonate)
PDI	polydispersity index
PEG	poly(ethylene glycol)
PGMA	poly(glycidylmethacrylate)
PLA	poly(lactic acid)
PLGA	poly(lactic-co-glycolic acid)
PMMA	poly(methylmethacrylate)
Pol	polymer
PPEs	poly(phosphoester)s
PPO	poly(propylene oxide)
PS	polystyrene
PVA	poly(vinyl alcohol)
PVPA	poly(vinyl phosphonic acid)
R	rest
RAFT	reversible addition-fragmentation chain transfer
REM-GTP	rare earth metal-mediated group transfer polymerization
RES	reticuloendothelial system
R_f	retention factor
RNA	ribonucleic acid
ROP	ring-opening polymerization
RuAAC	ruthenium-catalyzed azide-alkyne click conditions
SKA	silyl ketene acetals
SKA-GTP	silyl ketene acetal-initiated group transfer polymerization
SWCNT	single-walled carbon nanotube

sym-Col	1,3,5-trimethylpyridine
T	temperature
^{t}Bu	*tert*-butyl-
TCPS	tissue culture polystyrene
TEM	transmission electron microscopy
TGA	thermal gravimetric analysis
THF	tetrahydrofuran
TLC	thin layer chromatography
TMPy	tetramethylpyrazine
TMS	trimethylsilyl
TOC	abstract graphic

List of Publication

- M. Kränzlein*, T.M. Pehl*, K. Halama*, P.F. Großmann, T. Kratky, A. Mühlbach and B. Rieger, *Macromol. Mater. Eng.* **2022**, *308*, 2200635 “Azide-Modified Poly(diethyl vinylphosphonates) for Straightford Graft-To Carbon Nanotube Functionalization”.

- K. Halama*, A. Schaffer* and B. Rieger, *RSC Adv.* **2021**, *11*, 38555-38564 “Allyl Group-Containing Polyvinylphosphonates as a Flexible Platform for the Selective Introduction of Functional Groups via Polymer-Analogous Transformations”.

- K. Halama, M. T. Lin, A. Schaffer, M. Foith, F. Adams and B. Rieger, *Macromolecules*, **2024**, *57*,1438-1447 “Cytocompatible Triblock Copolymers with Controlled Microstructure enabling Orthogonally Functionalized Bio-Polymer-Conjugates”

Publication beyond the scope of this Thesis:

- F. Späth, A.S. Maier, M. Stasi, A.M. Bergmann, K. Halama, M. Wenisch, B. Rieger and J. Boekhoven, *Angew. Chem. Int. Ed.* **2023**, *62*, e202309318 “The Role of Chemically Innocent Polyanions in Active, Chemically Fueled Complex Coacervate Droplets”

Abstract

Due to their outstanding properties, such as thermoresponsive behavior and high biocompatibility, poly(vinyl phosphonates) present a promising foundation for various applications, particularly in the biomedical field. The precise designability of these polymers through rare earth metal-mediated group transfer polymerization (REM-GTP) allows for targeted variation and customization to meet specific requirements for subsequent applications. In the context of this thesis, different approaches to the modification of poly(vinyl phosphonates) are explored, with a particular focus on the introduction of alkynes and azides, which serve as the starting points for the frequently utilized azide-alkyne cycloaddition (AAC) in a biological context. Initially, the targeted introduction of functional end groups on α-methylpyridines, which act as initiators coordinating with Yttrium/Lutetium catalysts through C–H bond activation and subsequently covalently binding to the polymer chain, is investigated. To expand the repertoire of functional initiator motifs, silyl-protected alkynes, and unprotected azides are synthesized, and poly(diethyl vinyl phosphonate) (PDEVP) is then functionalized with these end groups. In the domain of side-chain modifications, allyl bonds in the static poly(vinyl phosphonate), based on diethyl vinyl phosphonate (DEVP) and diallyl vinyl phosphonate (DAlVP), are initially transformed through polymer-analogous reactions. This involves bromination, epoxidation, and thiol-ene click reactions of the integrated allyl bonds, as well as subsequent nucleophilic substitution, nucleophilic ring opening, and hydrazone formation to integrate azides and other functional groups. These serve as anchor points for attaching various substrates via AAC and allow for additional multiple functionalizations through further thiol-ene click reactions of the previously unreacted double bonds. For a more precise introduction of functional groups, dipropargyl vinyl phosphonate (DPrTMSVP), a vinyl phosphonate with protected propargyl groups, is generated, enabling the controlled adjustment of the architecture of poly(vinyl phosphonates) through controlled monomer addition. The resulting terpolymer P(DAlVP-DEVP-DPrTMSVP) forms the basis for orthogonal functionalization through thiol-ene click reactions and AAC, thereby facilitating the development of specifically multiply modifiable polymer chains. Particularly noteworthy is the attachment of biologically active substrates such as folic acid and cholesterol, along with the excellent biocompatibility of the resulting polymer, highlighting the diverse possibilities of targeted modification of these polymers.

Zusammenfassung

Aufgrund ihrer herausragenden Eigenschaften, wie ihr thermoresponsives Verhalten und ihre hohe Biokompatibilität, stellen Poly(vinyl phosphonate) eine vielversprechende Grundlage für diverse Anwendungen vor allem im biomedizinischen Bereich dar. Die präzise Designbarkeit dieser Polymere durch REM-GTP ermöglicht eine gezielte Variation und Anpassung der Poly(vinyl phosphonate) für zukunftsorientierte Anwendungen. Im Rahmen dieser Arbeit werden verschiedene Ansätze zu Modifizierung von Poly(vinyl phosphonaten) getestet, wobei der Fokus insbesondere auf die Integration von Alkinen und Aziden gelegt wird, da diese als Ausgangsgruppen für die häufig im biologischen Kontext genutzten Azid-Alkin Cycloaddition (AAC) fungieren. Zum einen wird die gezielte Einführung funktionaler Endgruppen an α-Methylpyridinen untersucht. Diese koordinieren über C–H Bindungsaktivierung an Yttrium/Lutetium -Katalysatoren und werden anschließend kovalent an die Polymerkette gebunden. Zur Erweiterung des Spektrums funktionaler Initiator Motive werden silyl-geschützte Alkine und ungeschützte Azide synthetisiert, um anschließend über Endgruppenfunktionalisierung an Poly(diethylvinyl phosphonate) (PDEVP) angebracht zu werden. Zum anderen werden im Bereich der Seitenkettenmodifikationen Allylbindungen im statischen Poly(vinyl phosphonaten), basierend auf Diethylvinyl phosphonat (DEVP) und Diallylvinyl phosphonat (DAlVP), durch Polymer-analoge Reaktionen umgesetzt. Dies erfolgt mittels Bromierung, Epoxidierung und Thiol-En Klick-Reaktionen, sowie durch nachfolgende nukleophile Substitution und Ringöffnung, sowie Hydrazonbildung, um Azide und andere funktionelle Gruppen einzufügen. Diese Funktionalitäten dienen als Ankerpunkte zur Anbindung unterschiedlicher Substrate über AAC sowie zur mehrfachen Funktionalisierung mittels zusätzlicher Thiol-En Klick-Reaktionen der bis dahin unreagierten Doppelbindungen. Um eine präzisere Einführung von funktionellen Gruppen zu gewährleisten, wird Dipropargylvinyl phosphonat (DPrTMSVP), ein Vinylphosphonat mit geschützten Propargylseitenketten, entwickelt. Dadurch kann anhand von kontrollierte Monomer Zugabe, die Architektur der Poly(vinyl phosphonate) präzise eingestellt werden. Das daraus resultierende Terpolymer P(DAlVP-DEVP-DPrTMSVP) bildet die Grundlage für eine orthogonale Funktionalisierung mittels Thiol-En Klick-Reaktionen und AAC, was wiederum die Entwicklung von gezielt und mehrfach modifizierbarer Polymerketten ermöglicht. Insbesondere die Anbindung biologisch aktiver Substrate wie Folsäure und Cholesterol, sowie die gute Biokompatibilität des resultierenden Polymers unterstreichen die vielfältigen Möglichkeiten der zielgerichteten Modifikation dieser Polymere.

1. Introduction – Polymers in Biomedical Application

Macromolecular materials gain significance for medical purposes. Polymers play a crucial role in diverse biomedical fields, including tissue engineering, the implantation of medical devices and artificial organs, as well as applications in prosthetics, ophthalmology, dentistry, bone repair, and many more (Figure 1.1). Additionally, delivery platforms based on polymers enable the controlled, slow release of drugs into the body, as well as the targeted administration of drugs to inflammation sites or tumors.[1, 2]

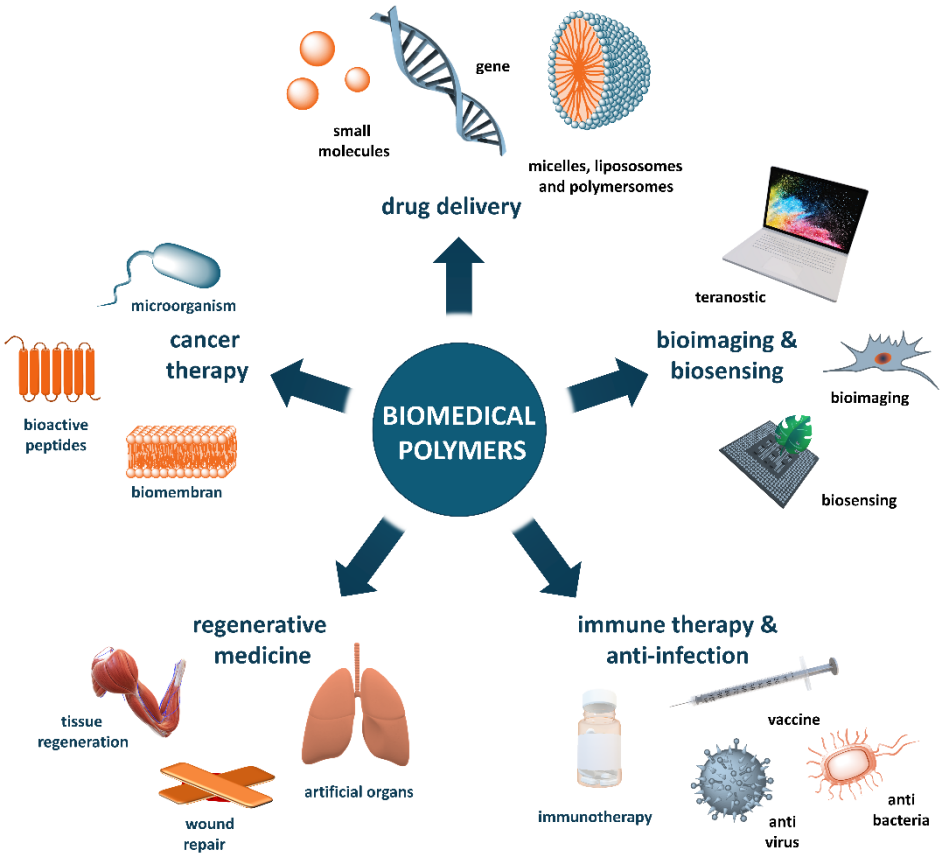

Figure 1.1: Schematical illustration of polymers in biomedical applications.[2]

For selecting materials for these applications, it is essential to consider different criteria, such as biocompatibility, wettability, and biological degradability. The wide range of chemical and functional properties exhibited by polymers makes it possible to design specific structures tailored for biomedical applications.[3-5] Among the polymers used, two categories can be distinguished: natural and synthetic polymers. Natural polymers have long been used to produce biomaterials due to their biocompatibility and low immunogenic properties. Collagen, a natural protein found in the skin and other connective tissues, is often used to manufacture implants for tissue cultivation and regeneration. In addition to collagen, other natural polymers such as fibrin and keratin, as well as various polysaccharides, are being investigated or already

used for their suitability.[6, 7] However, natural polymers, characterized by rapid degradability, low mechanical properties, and a high risk of contamination with microbial immunogens, are not conducive to causing chronic immunological inflammations. In contrast, synthetic polymers exhibit significantly superior properties compared to their natural counterparts.[8] The first synthetic polymer reported for medical purposes is poly(methylmethacrylate) (PMMA).[9] Ongoing research focuses on other synthetic polymers, such as poly(ethylene glycol) (PEG), poly(lactic acid) (PLA), poly(vinyl alcohol) (PVA), poly(caprolactone) (PCL), and poly(lactic-co-glycolic acid) (PLGA), due to their effectiveness in biomedical applications.[3, 10] Special interest is given to the development of "smart polymers," which are materials where one or more properties can be changed by external stimuli. This allows the creation of tunable and personalized macromolecules that can overcome the many limitations in the heterogeneous environment of the human body.[11] Various external stimuli, including temperature, redox reactions, pH changes, and light intensity, serve as triggers for intelligent materials.[12-15] The adaptable properties and environmental responsiveness of intelligent polymeric materials offer the prospect of developing personalized biomedical products.[13] Given the diverse applications of polymeric biomaterials, there is no singular ideal polymer or polymer family. Instead, researchers need to access a library of materials that can be synthesized and manipulated to meet specific requirements for a specific biomedical function. This thesis proposes the inclusion of poly(vinyl phosphonate)s into this material family.

2. Theoretical Background

2.1 Poly(vinyl phosphonate)s

Desoxyribonucleic acid (DNA) and ribonucleic acid (RNA) are two of the most renowned naturally occurring phosphorus-containing polymers. These macromolecules feature nucleosides connected to the phosphate backbone, enabling the storage of genetic information vital for the growth, evolution, operation, and reproduction of all living organisms.[16, 17] The synthetic production of these polymers is complex due to the inherent sensitivity of the polymers, notably their susceptibility to hydrolysis. Therefore, a careful distinction is required between the phosphorus-containing functional groups and those designated for polymerization when using the employed monomers. Cyclic monomers are subjected to ring-opening polymerization (ROP), whereas olefinic monomers are utilized in chain growth polymerization processes (Scheme 2.1).[18]

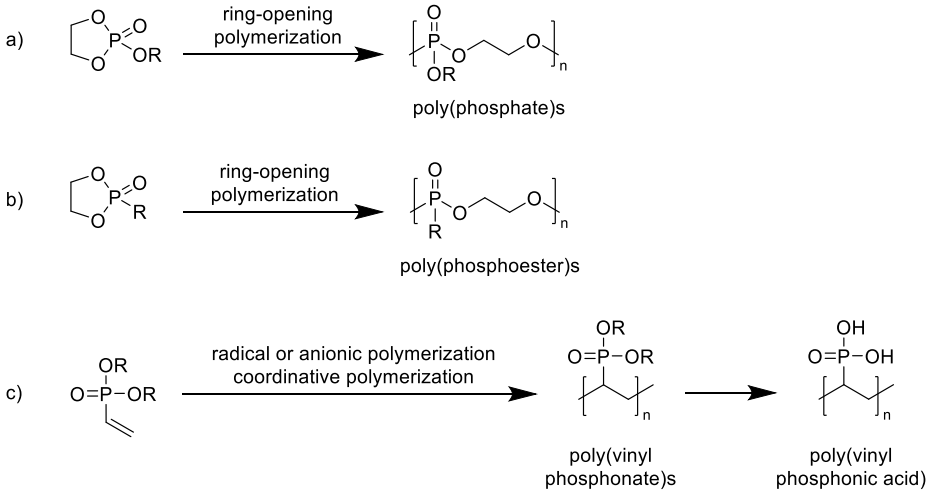

Scheme 2.1: Phosphorus-containing monomers and their corresponding polymers: a) poly(phosphate)s, b) poly(phosphoester)s, and c) poly(vinyl phosphonate)s and poly(vinyl phosphonic acid).[18]

A noteworthy and well-explored class of synthetically manufactured phosphorus-containing polymers is exemplified by poly(phosphoester)s (PPEs). These macromolecules, characterized by their repetitive phosphor ester units, exhibit similarities to naturally occurring structures. Additionally, they demonstrate remarkable biocompatibility and biodegradability, owing to their susceptibility to hydrolysis and enzymatic cleavage. Through the adjusting incorporation of tailored side chain modifications, PPEs exhibit considerable structural diversity, making them a promising platform for various biomedical applications.[19-21] Another exciting group of phosphorus-containing polymers is represented by poly(vinyl phosphonate)s, which exhibit good biocompatibility and water solubility. Remarkably, substantial coverage of the dialkyl vinylphosphonates (DAVP) class, including the monomer and the corresponding

polymer with the nearest phosphorus distance to the C-C backbone of the polymer, did even occur in only a few reports until 2010. [22, 23]

2.1.1 Vinyl phosphonates

Various synthesis pathways are available for vinyl phosphonates, one of the simplest and longest-known phosphorus-containing monomers, yielding high yields and starting from common feedstock materials. The most widely recognized method involves a *Michaelis-Arbusov* rearrangement created from trialkyl phosphite, followed by *E1cb* elimination to form the final dialkylvinyl phosphonate (Scheme 2.2, a). [24-26] An alternative synthesis route can be utilized for more complex syntheses and sterically demanding vinyl phosphonates. This pathway initiates with a *Kabachnik* rearrangement starting from commercially available tris(2-chloroethyl)phosphite to yield (2-chloroethyl)phosphonic dichloride. Subsequently, chlorination with thionyl chloride is carried out to obtain (2-chloroethyl)phosphonic dichloride, which can then be esterified with various alcohols. The corresponding DAVP compound is obtained through a subsequent base-induced elimination step (Scheme 2.2, b). The group of *Rieger et al*. further simplified this process into a two-stage synthesis route, wherein vinyl phosphonic acid, also commercially available, is first transformed into the chloride with oxalyl chloride, followed by esterification as the final step (Scheme 2.2, c).[27]

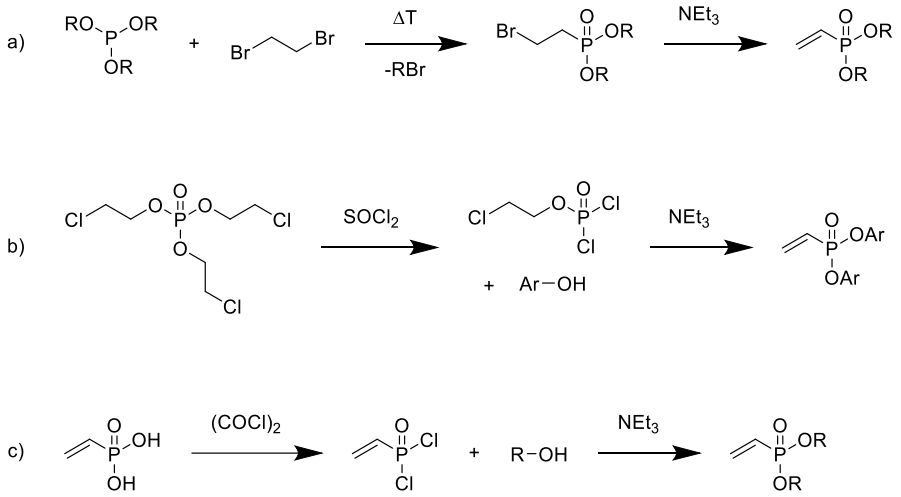

Scheme 2.2: Monomer synthesis of vinyl phosphonates a) via *Michaelis-Arbusov* reaction, b) via *Kabachinik* rearrangement and c) as a two-stage synthesis route.In addition to their role in polymerization, DAVPs are employed to incorporate phosphorus functionalities into macromolecules through various chemical processes, including *Diels-Alder* cyclization, thiol-ene click reactions, 1,4-*Michael*-addition, and cross-coupling reactions.[28-32]

2.1.2 Polymerization of Poly(vinyl phosphonate)s

While vinyl phosphonates were early and frequently associated with the previously mentioned organic reactions, there was initially minimal research regarding their polymerizability. This can be attributed to the limited performance of these monomers using classic polymerization techniques, thereby constraining the exploration of their material properties and potential applications. The initial efforts to polymerize DEVP and diisopropyl vinyl phosphonate (DIVP) via free radical polymerization yielded only oligomers. This outcome can be attributed to several underlying factors. One reason is the low propagation rate, which is due to the high stability of the formed radical species. Additionally, frequent chain transfer reactions occurred, leading either to monomers or the formed polymers, hindering the production of larger macromolecules. Furthermore, side reactions involving intramolecular hydrogen transfer from the phosphonate ester unit to the primary alkyl radical occurred. The newly formed radical is inserted into another monomer, creating an unstable P-O-C motif in the polymer backbone. This instability, caused by thermal lability, resulted in chain fragmentation (Scheme 2.3).[33 34]

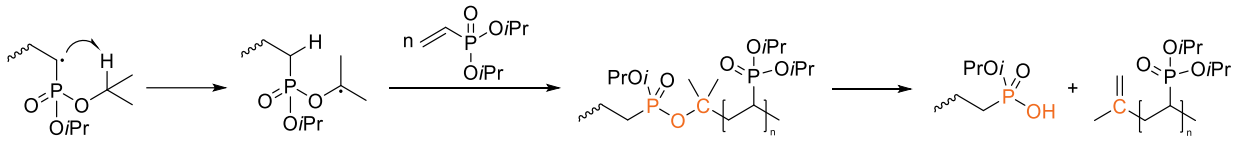

Scheme 2.3: Intramolecular chain scission of oligomeric DIVP during radical polymerization.[34]

To circumvent this problem, subsequent research has focused on non-radical polymerization methods. At first glance, anionic polymerization of vinyl phosphonates holds promise due to its generally increased reactivity, which should yield improved conversion rates and higher molecular weights. However, like radical polymerization, this approach encounters various side reactions that lead to poly(vinyl phosphonate)s exhibiting high polydispersity.[35] A primary contributing factor to this phenomenon is the presence of the α-acidic proton within the vinyl group, which can initiate termination reactions with initiation or propagation species (Scheme 2.4, a).[36] Furthermore, anionic initiators with high nucleophilicity can attack the electrophilic phosphorus atom, subsequently eliminating an alcoholate (Scheme 2.4, b). A third side reaction involves a nucleophilic attack on the vinyl bond (Scheme 2.4, c). Additionally, extended reaction times are requisite for achieving complete monomer conversion, indicative of low polymerization rates. The resonance stabilization of the anionic chain end by the phosphonate unit diminishes its reactivity, and the limited initiator efficiency of the employed metals may be one reason for the observed reduced activity.[18, 36]

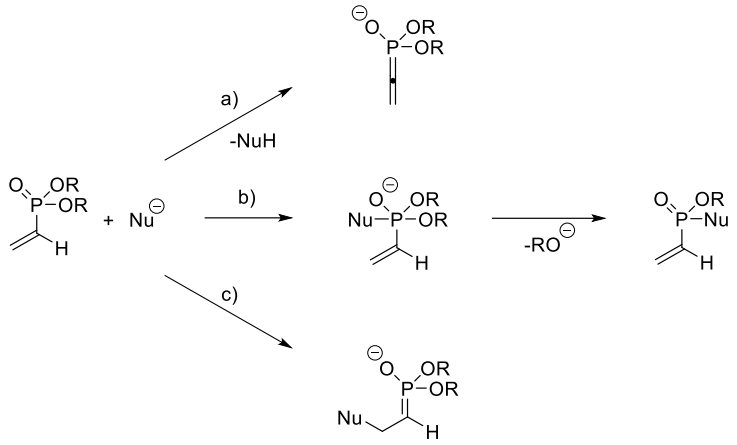

Scheme 2.4: Possible side reactions during anionic polymerization of vinyl phosphonates: a) abstraction of the *α*-acidic proton, b) nucleophilic attack at the electrophilic phosphorus and subsequent elimination of an alcoholate and c) nucleophilic attack at the vinyl moiety.[36]

Rare Earth Metal-mediated Group Transfer Polymerization

Due to the reasons previously outlined, high-molecular-weight poly(vinyl phosphonate)s remained inaccessible for an extended period. Nevertheless, vinyl phosphonates share electronic and structural similarities with other *Michael*-type acceptor monomers, such as methyl methacrylate (MMA), 2-vinyl pyridine (2VP), or 2-*iso*-propenyl-2-oxazoline (IPOx) (Scheme 2.5).[18, 36] Among numerous polymerization techniques, also rare earth metal-mediated group transfer polymerization emerges as a promising method for polymerizing MMA. REM-GTP combines the advantageous characteristics of ionic and coordinative polymerization with its living nature, enabling the synthesis of strictly linear polymers with a remarkably narrow polydispersity index (PDI < 1.1).[37]

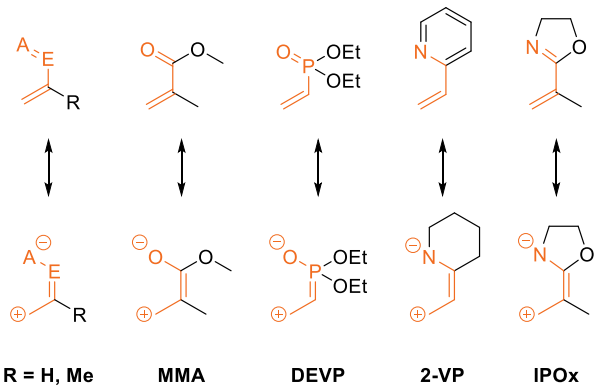

Scheme 2.5: Structural and electronic similarity between different typical *Michael*-type monomers.[36]

This polymerization method can be attributed to the silyl ketene acetal-initiated group transfer polymerization (SKA-GTP) developed by *Webster* and *DuPont*.[38] In this process, silyl ketene acetals (SKA)s are used as initiators, and *Lewis* acids are employed to activate monomers. Repeated conjugate addition reactions transfer the SKA group from the initiator to the monomer. This living polymerization is characterized by a linear increase in molar mass and

high monomer conversion, and facilitates the production of block copolymers through sequential polymerization.[18] Building upon this foundation, *Yasuda*, *Collins*, and *Ward* polymerized MMA using metallocene, laying the foundational principles for REM-GTP.[39, 40] In contrast to *Yasuda et al.* who employed the neutral complex $[(C_5Me_5)_2SmH]_2$ as their catalyst, *Collins* and *Ward* utilized a two-component system comprising Cp_2ZrMe_2 and $[Cp_2ZrMe(THF)][BPh_4]$. This approach facilitates the synthesis of syndiotactic, high-molecular-weight PMMA with a narrow polydispersity index (PDI < 1.05).[40, 41] The process initiates with the activation of the hydrido-bridged dimer through the coordination of a MMA monomer. In this step, the hydride group of the catalyst attacks the vinylic CH_2 group of MMA (Scheme 2.6, a). Subsequently, another molecule of MMA coordinates with the resulting intermediate through an 1,4-addition (*Michael* addition) reaction. This sequence leads to the formation of a monometallic, cyclic, eight-membered transition state, which is confirmed through the isolated crystal structure of the MMA adduct (Scheme 2.6, b). Following this stage, another monomer coordinates to the active species, causing the displacement of the ester group and forming another eight-membered transition state (Scheme 2.6, c). The polymerization using the cationic zirconocene catalyst follows a comparable mechanism. However, it necessitates the presence of co-catalysts that negatively affect both the polymerization activity and stereoselectivity.[18]

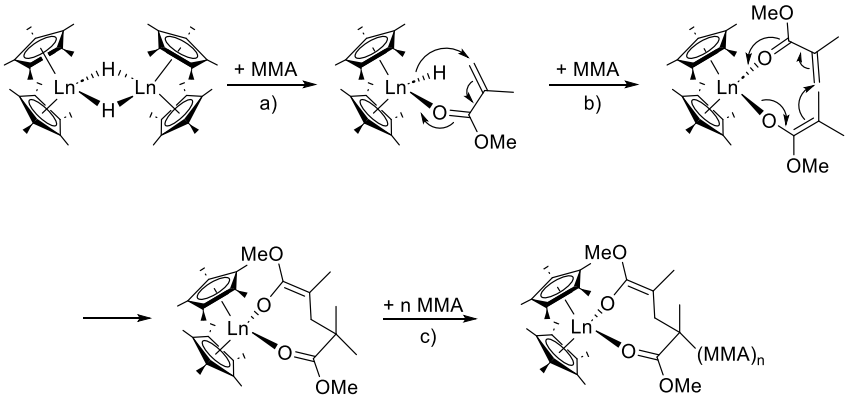

Scheme 2.6: *Yasuda*-type REM-GTP of MMA: a) dissociation and coordination of MMA. b) hydride transfer to MMA and formation of the eight-membered transition state. c) repeated conjugate addition of MMA.[18]

Rieger et al. used the REM-GTP mechanism, predicated on the 1,4 *Michael* addition, to facilitate the polymerization of well-known vinyl phosphonates in these reactions. Initially, using simple rare-metal alkyl precursors lead to the polymerization of dimethyl vinyl phosphonate (DMVP) and DIVP oligomers.[42] However, a significant enhancement in activity and increased yields of polymerization were observed with lanthanide tri(bisdimethylsilylamide) complexes (Ln = La, Nd, Sm, Y) when employing metal centers with a smaller ionic radius (Figure 2.1).[18] NMR studies revealed the coordination of oxygen moiety instead of vinyl group, indicating a group transfer polymerization mechanism. Nevertheless, the consistently broad PDI suggests a non-uniform, slow initiation or possibly initiation involving more than one σ-donor ligand.[42]

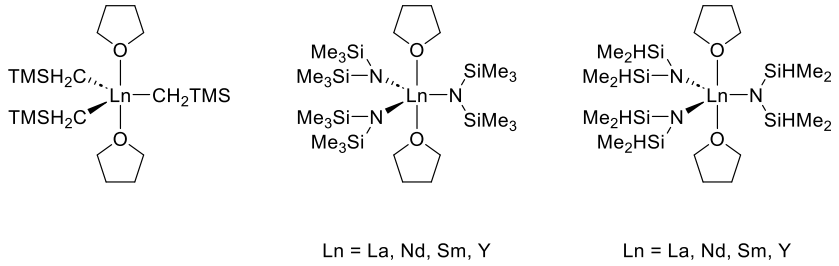

Figure 2.1: Rare earth alkyl complexes for the oligomerization of DMVP and DIVP.

A significant advancement was made by successfully executing the controlled polymerization of high-molecular-weight PDEVP using rare earth metallocenes of the type Cp_2LnX (Ln = Gd-Lu, X = Cp, Me, CH_2TMS, Cl). While cyclopentadiene (Cp) serves as a versatile and strongly coordination ligand, methyl (Me) acts as a strong nucleophile, leading to rapid initiation, whereas chloride (Cl) functions as a comparatively weaker nucleophile, resulting in fewer side reactions.[43] The assumption that the polymerization of DEVP follows a group transfer polymerization mechanism was further supported by the copolymerization of DEVP and MMA. It was postulated that a DEVP unit coordinates to the metal center, inducing a rearrangement of the Cp ligands from η^5- to η^1-coordination. This Cp group then engages in a 1,4-addition reaction with the vinyl group of the monomers, allowing for the coordination of another DEVP molecule to the metal center (Scheme 2.7).[44]

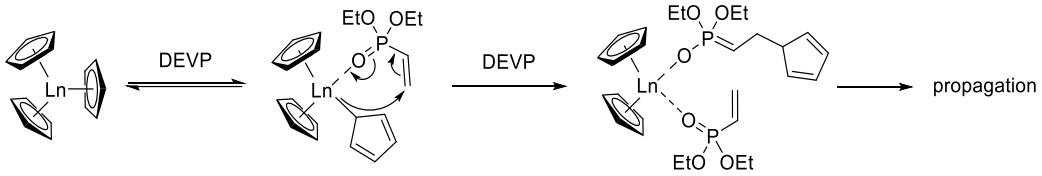

Scheme 2.7: Postulated initiation mechanism for the polymerization of DEVP with Cp_3Ln.[44]

Furthermore, the living character of the REM-GTP of DAVPs was confirmed, leading to higher polymerization degrees and narrower molecular weight distributions. Additionally, the previously hypothesized influence of the ionic radius of the metal center on the polymerization rate, as proposed by *Yasuda*[41], was validated. In the case of metallocene complexes employed for DEVP polymerization, a noticeable enhancement in initiator efficiency was observed as the ionic radius decreased. Moreover, the impact of different ligands on the initiation mechanism of REM-GTP for vinyl phosphonates was demonstrated. Highly nucleophilic ligands like CH_2TMS or Me prefer initiation by abstracting the acidic α-proton of the vinyl unit (Scheme 2.8, a). Ligands with lower nucleophilicity, such as Cl or alkoxides, induce ligand exchange driven by the monomer (Scheme 2.8, b). Exclusive nucleophilic transfer of the ligands and consequent monomer coordination occurred only with ligands like Cp or thiolates (Scheme 2.8, c).[45]

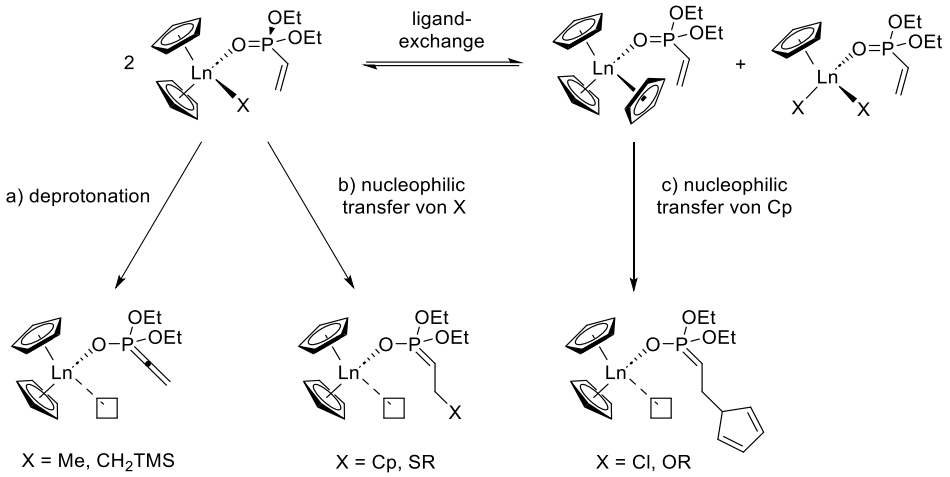

Scheme 2.8: Initiation of vinyl phosphonates using rare earth metallocenes *via:* a) deprotonation of the acidic *α*-CH, b) nucleophilic transfer of X, or c) a monomer-induced ligand-exchange reaction.[45]

The coordination of vinyl phosphonates to the employed complexes was investigated through NMR spectroscopy studies to better understand the initiation mechanism. This investigation used diethylethyl phosphonate (DEEP) due to its analogous structure and comparable steric requirements to DEVP. However, DEEP is not capable of subsequent polymerization. An occurrence of ligand exchange induced by the monomer was noted, wherein the metallocene $Cp_2LnX(DEEP)$ achieved equilibrium with the complexes $Cp_3Ln(DEEP)$ and $CpLnX_2(DEEP)$ (Scheme 2.9).[45]

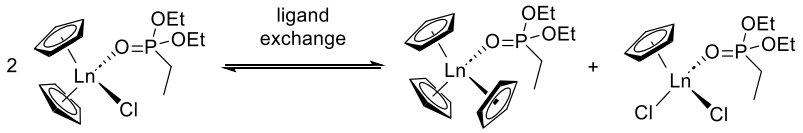

Scheme 2.9: Ligand exchange of Cp_2LnX induced by DEEP.[45]

The crystal structure analysis of the complexes $Cp_3Y(DEEP)$ and Cp_2LnCl (Ln = Ho, Yb) confirmed the thesis that the vinyl phosphonate coordinates *via* the oxygen atom and not *via* the double bond. Furthermore, these investigations have demonstrated that *the Michael*-system of the vinyl phosphonates adopts the necessary conformation for repeated conjugate addition, thus enabling REM-GTP.[43, 45] Based on various experimental studies, the group of *Rieger et al.* proposed a mechanism for the polymerization of DAVP through REM-GTP. In this process, the existing polymer is substituted by a newly introduced monomer through an intermediate pentacyclic stage *via* S_N2-type associative displacement. This first transition state is the rate-determining step of the reaction. Complexes with smaller metal centers have a more considerable steric demand in the eight-membered metal cycle, destabilizing propagation and consequently speeding up the process. Additionally, longer side chains in the polymers result in greater steric hindrance during the formation of the new polymer in the transition state, leading to a higher activation barrier (Scheme 2.10).[18, 45]

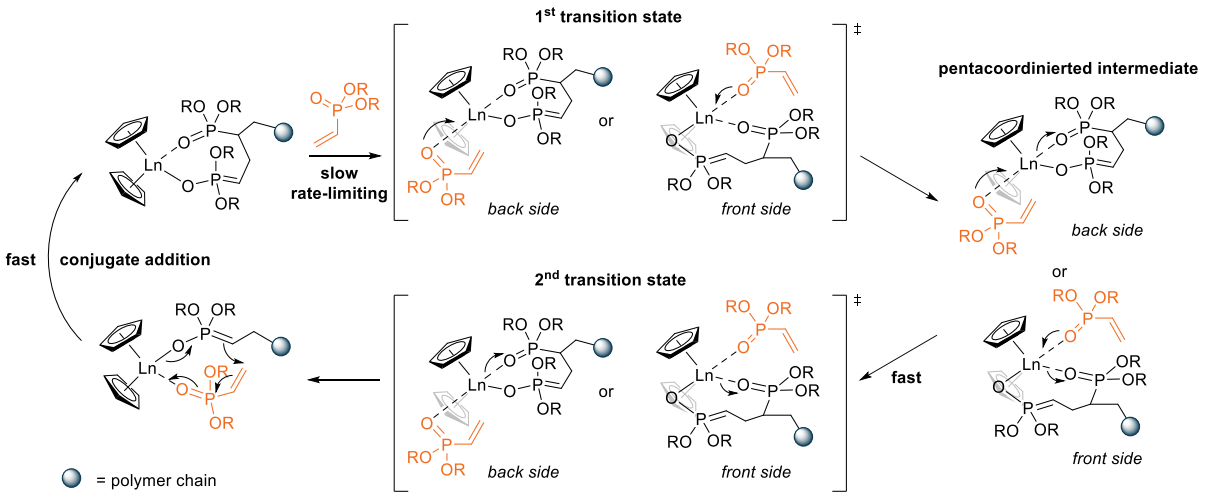

Scheme 2.10: Reaction mechanism of REM-GTP of DAVPs.[45]

Various catalysts with different initiators and metal centers were tested for detailed REM-GTP mechanistic studies of vinyl phosphonate. Notably, DAVP exhibited the highest levels of activity and efficiency in thiolate complexes. Nevertheless, these complexes exhibit certain drawbacks, such as end-group elimination and forming $[Cp_2LnS^tBu]_2$ dimers, which hinder the polymerization of less coordinated monomers. Consequently, the search for highly active and efficient initiators for REM-GTP was pursued.[18]

C–H bond activation through σ-bond metathesis

The typical initiation method for REM-GTP of methacrylate, involving the nucleophilic transfer of strongly basic ligands to a coordinated monomer, has proven ineffective for vinyl phosphonates.[45, 46] These initiators lead to various side reactions, such as the abstraction of the *α*-acidic proton, resulting in reduced initiator efficiency and longer initiation times.[45] Inspired by the enolate initiators employed in zirconium-mediated GTP, which utilize a faster initiation mechanism through an eight-proton process to overcome the limitations of alkyl initiators, *Rieger et al.* focused on the development and investigation of enolate and enamine initiators.[47, 48] These initiators mimic the active propagation species, bypassing the inefficient initiation step of alkyl initiators. However, the formed complexes exhibit long initiation times, which could be attributed to a preference for nucleophilic transfer over deprotonation. Consequently, achieving a successful synthesis without side products was not feasible. Instead, σ-bond metathesis was chosen as a potential method to bypass the initiation limitations. *σ*-bond metathesis enables intramolecular C-H activation in trivalent lanthanides and d^0 transition metals without altering the oxidation state.[49, 50] This allows for hydrogen (H-H) activation through hydrogenolysis or C-H and C-C bonds through alkanolysis. This concerted reaction proceeds through a four-membered transition state in the form of a [2σ+2σ] cycloaddition and can be illustrated as the exchange of the metal-ligand *σ*-bond with a σ-bond of the substrate (Scheme 2.11).[51, 52]

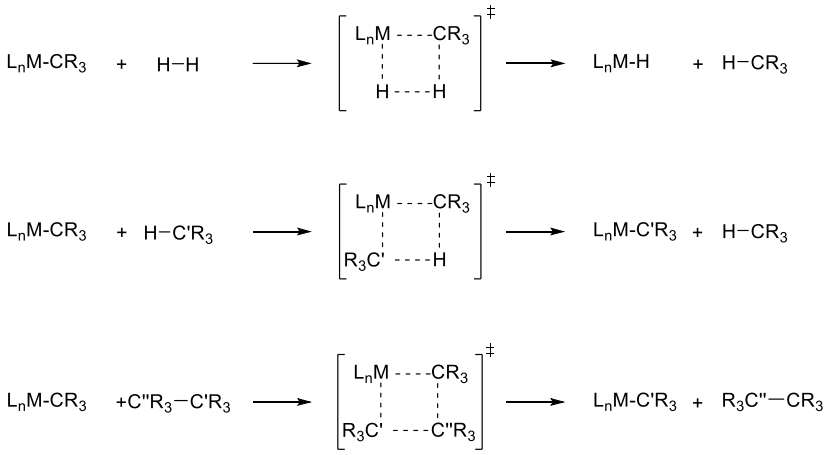

Scheme 2.11: Hydrogenolysis and alkanolysis through σ-bond metathesis.

Teuben et al. systematically explored the activation of C-H bonds activation of various metallocene and non-metallocene compounds with diverse substrates, ranging from ethylene to alkyl-substituted pyridine derivatives.[53] Notably, they identified a highly selective C-H bond activation of the sp^3-alkyl group *via* a η^3-(*C*, *C*, *N*)-*aza*-allylic motif for α-picoline and ethyl-pyridine.[54, 55] The group of *Mashima et al*. applied this approach for the introduction of chain end moieties in the polymerization of 2-vinyl pyridine, a *Michael-type* system. Therefore, various catalysts were generated and tested through in situ σ-bond metathesis of a yttrium complex with different alkynes and α-picolyl initiators, such as phenylpyridine, 1-trimethylsilyl-1-propyne and 2,4,6-trimethylpyridine (*sym*-collidine) (Scheme 2.12).[56]

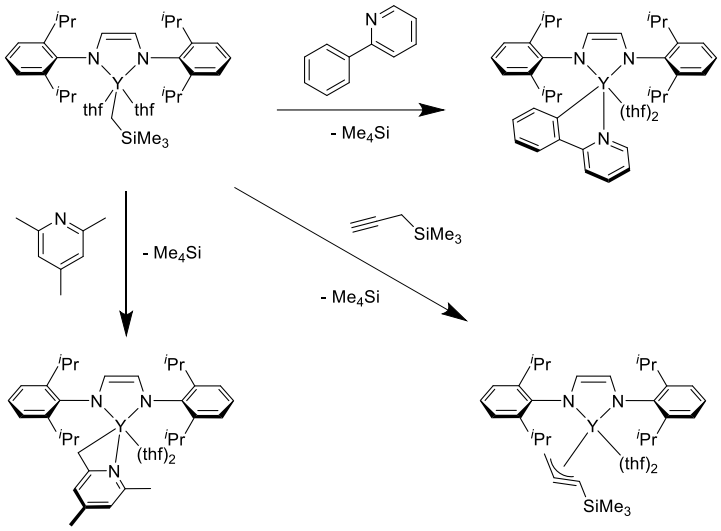

Scheme 2.12: C-H bond activation of various, non-classical CH-acidic compounds.[56]

Rieger et al. applied this technique to introduce pyridine initiators to the REM-GTP of dialkylvinyl phosphonates. In this context, they activated the cyclopentadienyl systems Cp_2LnCH_2TMS (Ln= Y or Lu) using *sym*-collidine. While the Yttrium complexes exhibited complete conversions within a short time at room temperature, the Lutetium catalysts required higher temperatures and longer reaction durations to achieve the same results. Through

crystallographic analysis, it was confirmed that the binding of pyridine occurs through the sp^3-alkyl group *via* a η^3-(*C*, *C*, *N*)-*aza*-allylic motif, which is attributed to the resonance structure of the carbanion or enamine (Scheme 2.13).[18, 48]

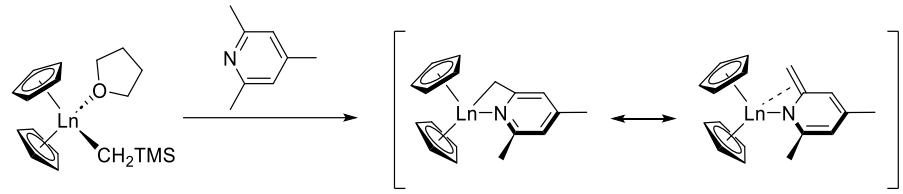

Scheme 2.13: Formation of mesomeric equilibrium of the carbanionic and the enamine form during C-H bond activation of *sym*-collidine.[48]

End group analysis through electrospray ionization mass spectrometry (ESI-MS) measurements of DEVP-oligomers confirmed the functionalization of chain ends with (4,6-dimethylpyridin-2-yl) methyl and indicated a nucleophilic transfer of the *sym*-collidine initiator to the first monomer during the initiation process. It is assumed to be a eight-electron process. Subsequent polymerization studies of Cp_2Ln(*sym*-collidine) (Ln = Y or Lu) with DEVP not only demonstrated the suitability of the system for REM-GTP but also exhibited high activity, high initiator efficiency, narrow molecular weight distribution, and a living polymerization character (Scheme 2.14).[18, 48]

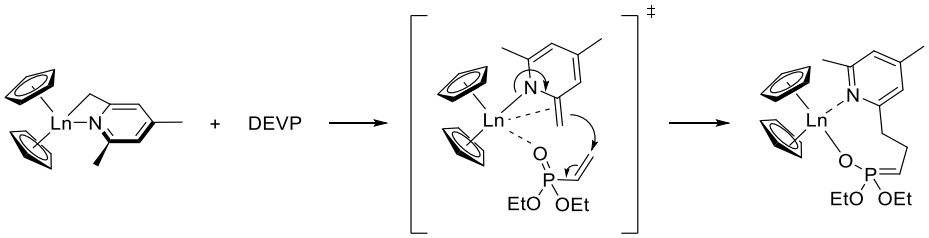

Scheme 2.14: Proposed initiation mechanism for DEVP *via* eight-membered transition state.[48]

Its efficiency and straightforward handling for catalyst functionalization, making it an ideal platform for end-group modifications, characterize the new initiator system. Through σ-bond metathesis, a wide range of pyridine derivatives can be utilized to generate various polymer architectures or introduce different functional end groups through a targeted design approach.[57, 58] For instance, by employing 1,3,5-tris(3,5-dimethyl-4-pyridinyl) benzene, where three pyridine groups are activated for C-H bond activation using Cp_2YCH_2TMS in a one-pot synthesis, star-shaped polymers can be produced.[59] Similarly, the bifunctional 2,3,5,6-tetramethylpyrazine (TMPy) allows for dual activation of the initiator, enabling linear polymerization in two different directions.[60] Another bifunctional pyridine hydroquinone ether offers the additional advantage of introducing a highly fluorescent marker.[61]

Beyond varying polymer architecture, this system also offers the flexibility to incorporate different functional end groups for subsequent post-polymerization functionalization. For example, a vinyl group, which enables following thiol-ene click reactions, can be introduced

through the C-H activation of 2,6-dimethyl-4-(4-vinylphenyl) pyridine with Cp_2YCH_2TMS.[62, 63] When inserting other functionalities, it becomes essential to protect the original functional group to prevent catalyst degradation. Studies involving silyl, pyrrole, and trityl-protected initiators have demonstrated high initiator efficiency and narrow polydispersity indices, even in cases of incomplete C-H activation. After deprotecting the end groups, these initiators can be employed for further polymer modifications (Scheme 2.15).[64]

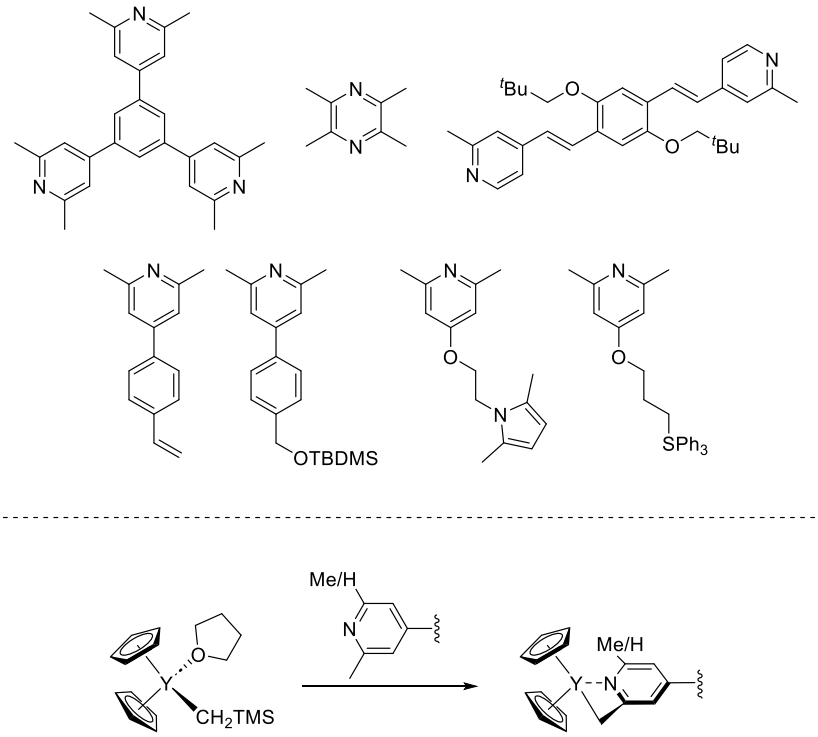

Scheme 2.15: Examples of functional pyridine-based initiators for C-H bond activation of $Cp_2Y(CH_2TMS)(thf)$ and the subsequent vinyl phosphonate polymerization.

2.1.3 Introduction of Functionality to Polymer Chain

Copolymerization of different vinyl phosphonates and other monomers

In addition to end-group modification of polymers, the structure and functionality can be altered by varying the polymer chain. The unique nature of REM-GTP allows for the polymerization of a wide range of *Michael*-type monomers. The living nature of the polymers enables the formation of block copolymers with AB, ABC, or multiblock structures through the sequential addition of monomers. Consequently, producing copolymers using diverse vinyl phosphonates and other Michael monomers, such as 2VP, becomes feasible.[58] This allows the development of amphiphilic polymers consisting of hydrophilic and hydrophobic blocks. When reaching a specific concentration known as the critical micelle concentration (CMC), these polymers exhibit the capability to form micelles (thoroughly discussed in Chapter 2.3.1). *Rieger et al.* polymerized BAB block copolymers using 2VP and DEVP, forming more stable micelles with a lower CMC compared to similar structures (Scheme 2.16). These block copolymers exhibit the narrow polydispersity expected from REM-GTP and pH- and thermoresponsive behavior.[60] Notably, thermoresponsive behavior can be observed in all poly(vinyl phosphonate)s, as elaborated upon in chapter 2.1.4.

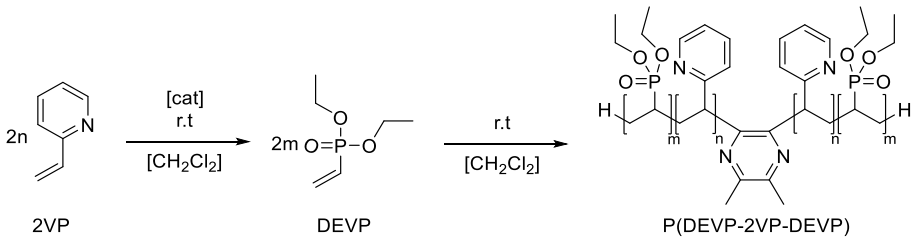

Scheme 2.16: Sequential REM-GTP of 2VP and DEVP with $[(ONOO)^tBuY(thf)]_2$ ((dimethylpyrazine-diyl)dimethyl)) at room temperature.[60]

Due to these promising results, efforts are being directed towards adjusting the temperature-sensitive behavior of the formed micelles. The modification of the lower critical solution temperature (LCST, more precisely explained in chapter 2.1.4) of PDEVP is intended to be achieved by introducing additional vinyl phosphonates. By incorporating hydrophilic or hydrophobic side chains into the monomers, changes in the LCST can be controlled.[65] Consequently, AB and ABB'-type block copolymers comprised of 2VP and DAVP have been synthesized. The BB' block is formed based on the statistical distribution of DEVP with di-*n*-propyl vinyl phosphonate (DPVP) or DMVP (Scheme 2.17). These polymers exhibit excellent initiator efficiency and maintain a narrow molecular weight distribution, making them promising candidates for biomedical applications. This is further reinforced by unimodal copolymers with identical compositions, leading to the formation of similar micelles with a homogeneous size distribution. Furthermore, the targeted manipulation of the LCST can be proven, as it can be

decreased through copolymerization with the hydrophobic DPVP and increased by copolymerization with the hydrophilic DMVP.[66]

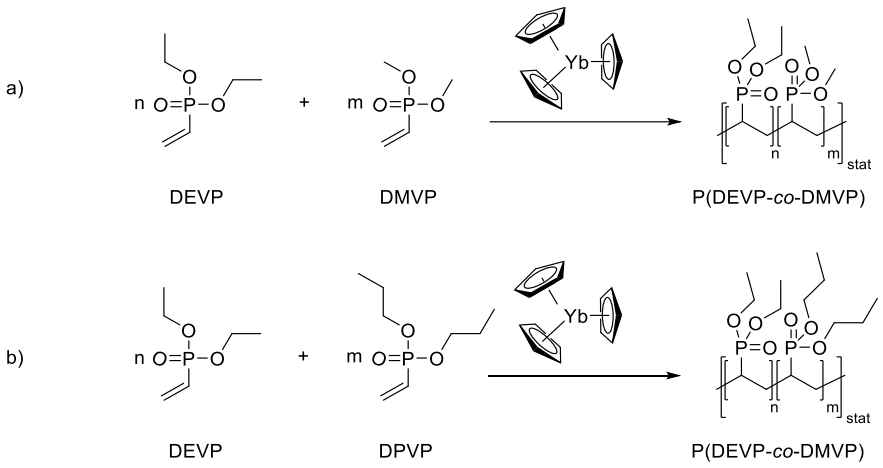

Scheme 2.17: Statistical copolymerization of DEVP with a) DMVP and b) DPVP *via* Cp_3Yb-initiated GTP.[65]

In further studies, poly(vinyl phosphonate)s with a triblock structure ABB' were synthesized. This structure includes 2VP, DEVP, and DAIVP blocks. These precisely defined copolymers exhibit the promising qualities observed in previously developed polymers and offer the potential for post-polymerization functionalization of the allyl side chains of DAIVP through a radical thiol-ene click reaction (Scheme 2.18). In this case, they were used with the crosslinking agent 3,6-dioxa-1,8-octanedithiol to form nanoparticles, bypassing the CMC and creating continuous and stable drug transport carriers.[67]

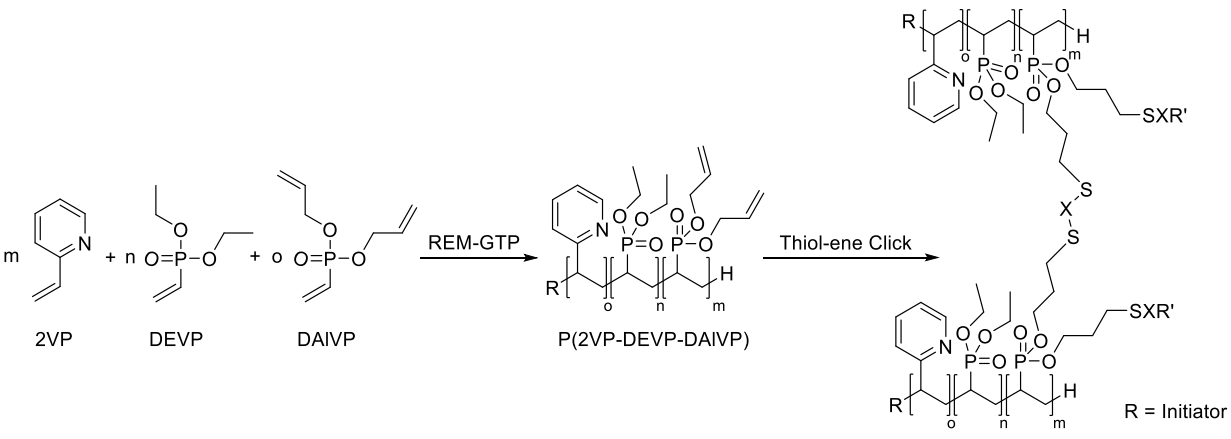

Scheme 2.18: Block copolymerization of 2VP, DEVP, and DAIVP with $Cp_2Y(CH_2(C_5H_2Me_2N))$, followed by thiol-ene click reaction towards cross-linked nanoparticles.[67]

Modification of the ester side groups of Poly(vinyl phosphonate)s

In addition to the insertion of various monomers, it is also possible and sometimes essential to change the properties of poly(vinyl phosphonate)s by transesterification of the ester side groups. The first functionalization of poly(vinyl phosphonate)s involved poly(vinyl phosphonic acid) synthesis. This approach cannot be achieved through REM-GTP or anionic

polymerization due to the degradation of the catalyst during the process. Various reaction conditions can be employed for this modification. Subjecting the polymers to thermal treatment or utilizing strong acids represents harsh conditions that lead to polymer degradation (Scheme 2.19, a-c).[36] *Mayer et al.* introduced a method for transesterification followed by hydrolysis under milder conditions by employing trimethylsilyl bromide (Scheme 2.19, d, f).[35] However, complete conversion was not attained with this method. *Rieger et al.* achieved full conversion, starting from PDEVP and using TMSCl.[44] The ensuing intermediate naturally tends toward hydrolysis, necessitating direct subsequent use for transesterification. This transesterification can be accomplished using TBAF and the corresponding bromide, such as benzyl bromide (Scheme 2.19, e). The ensuing intermediate naturally tends toward hydrolysis, necessitating direct, subsequent use for transesterification.[44] Subsequently, *Rieger et al.* employed transesterification of the side chains to attach pyrene for the fluorescence labeling of polymer-biomolecule conjugates (Scheme 2.19, g).[62]

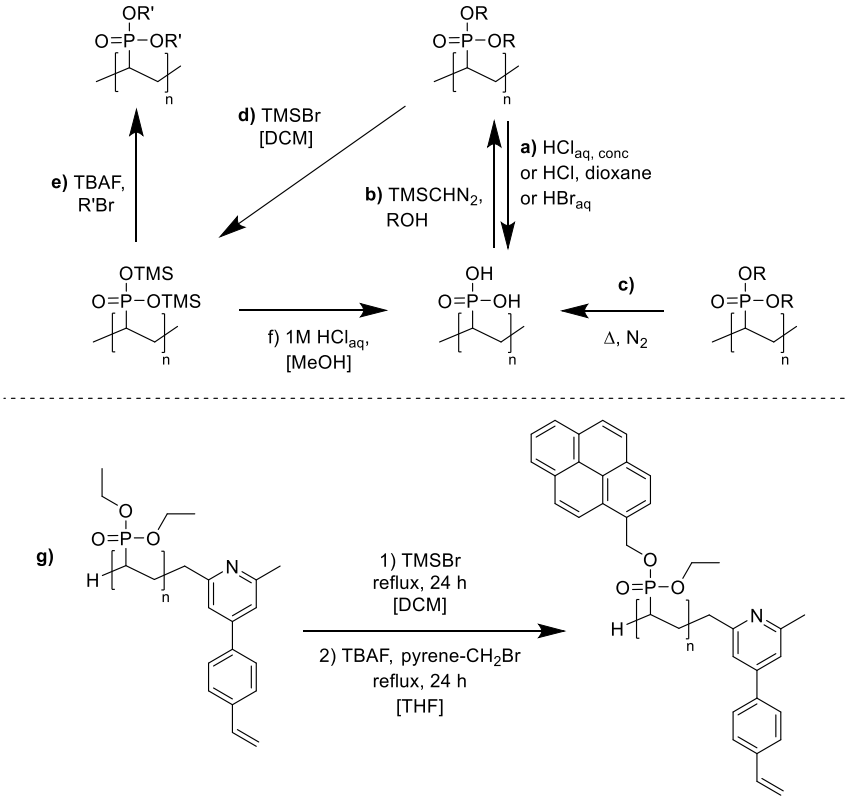

Scheme 2.19: Hydrolysis (a,c,f) and transesterification (b,d,e, and g) of poly(vinyl phosphonate)s.

2.1.4 Outstanding characteristics of Poly(vinyl phosphonate)s

Thermoresponsive behavior of Poly(vinyl phosphonates)

The various methods of modifying poly(vinyl phosphonate)s through end groups and side-chain modifications provide a promising avenue for designing complex materials with tailored material properties. Additionally, these polymers exhibit remarkable solubility characteristics due to their thermoresponsive behavior. In the field of polymer chemistry, where temperature-dependent solubility is a well-studied area, two distinct cases are distinguished: the lower critical solution temperature (LCST) and the upper critical solution temperature (UCST) (Figure 2.2). The LCST represents the temperature below which the aqueous polymer solution appears as a homogeneous phase while a two-phase system forms above it. In the case of UCST, the inverse behavior occurs, with the polymer precipitating when the temperature falls below the specified point.[18, 68, 69] Thermo-responsive polymers undergo a rapid, steep, and reversible phase transition in response to temperature changes, which the entropy change of the polymer chains in the aqueous solution can explain.[68] Due to their LCST behavior, these polymers exhibit hydrophilic behavior at low temperatures and hydrophobic behavior at high temperatures. Below the LCST, the polymer chains can form hydrogen bonds with the surrounding water molecules, leading to hydration. As the temperature increases, these water bonds weaken, causing the polymers to dehydrate and aggregate. This phenomenon is commonly known as the coil-globule transition.[70]

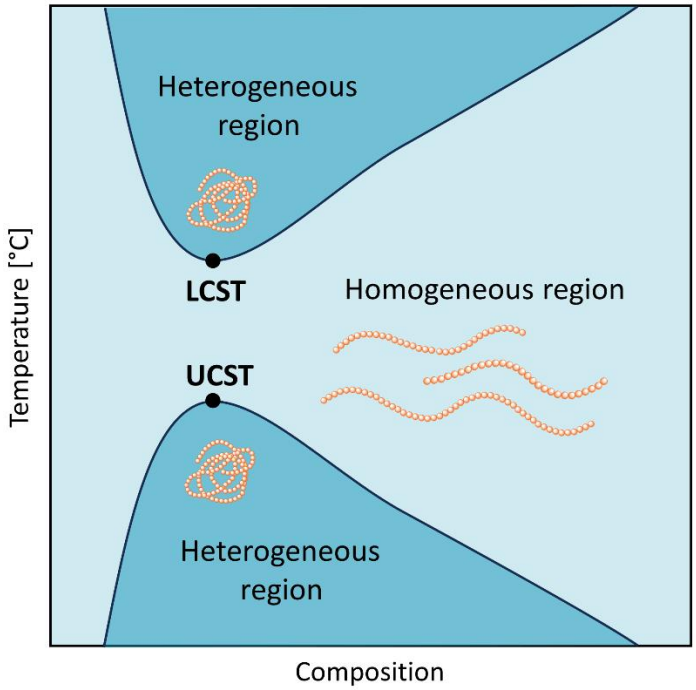

Figure 2.2: Phase diagram of LCST and UCST polymers in aqueous solution.

The solubility properties of poly(vinyl phosphonate)s depend on the specific side chains of the polymers. Hydrophilic PDMVP is soluble in water but poorly soluble in organic solvents, whereas PDIVP exhibits good solubility in organic solvents. PDEVP displays amphiphilic behavior and is soluble in both water and organic solvents.[44] Aqueous solutions of PDEVP have a low LCST close to the physiological range (T_{LCST} = 40 – 46 °C), making it an exciting property for various applications. The cloud point of poly(vinyl phosphonate)s is influenced by multiple conditions, such as the polarity of the solvent or the polymer concentration. The composition and molecular weight of poly(vinyl phosphonate)s also have a significant impact. In the case of PDEVP, the cloud point decreases with increasing molar mass of the polymer. By synthesizing copolymers of DEVP with the hydrophilic DMVP or the hydrophobic DPVP, the LCST of water-soluble polymers can be precisely adjusted within a range from 5 to 95 °C. A linear correlation between the hydrophilic or hydrophobic monomer composition and the LCST of the copolymers can be observed.[18] For biomedical applications, it is essential to consider the influence of salts and other complex media that are present in biological processes on the thermal behavior of these polymers. This is particularly important regarding its good biocompatibility and the resulting potential applications in the biomedical field.[71]

Good Biocompatibility

In addition to their adjustable thermoresponsive properties, the biocompatibility of poly(vinyl phosphonate)s is of significant interest. Mainly, poly(vinyl phosphonic acid) (PVPA) has been widely established. Numerous studies have been published on phosphorus-containing polymers concerning bone tissue and PVPA-coated surfaces for the growth of various cell types.[72-75] However, the interaction with living cells was only later investigated by coating mesenchymal stem cells with PDEVP, making this polymer a suitable material for this cell type compared to the reference material, tissue culture polystyrene (TCPS).[76] A significant advantage of this coating material was its efficient cell adhesion, attributed to low cell-coating interaction and coating cytotoxicity. Due to the covalent binding of water-soluble polymers, the detachment of polymers from the surface was prevented. Another study examined the impact of dissolved PDEVP on living cells, where only minimal cytotoxicity was observed at different molar masses of the polymers.[63] After demonstrating the low cell toxicity of PDEVP, poly(vinyl phosphonate)s with various biological interest applications are investigated. Initially, PDEVP was modified *via* end-group functionalization with cholesterol or folic acid. These polymer conjugates exhibited similar biocompatibility to the non-functionalized polymers (Scheme 2.20).[63]

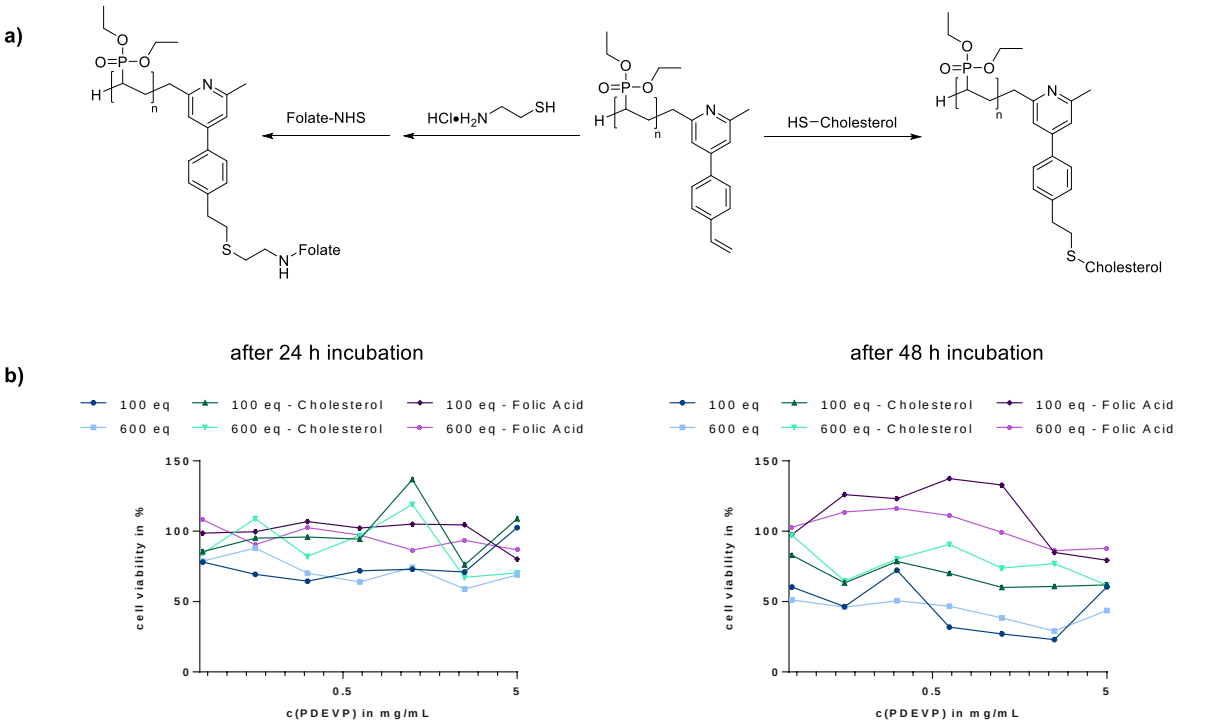

Scheme 2.20: a) Post-polymerization functionalization of PDEVP *via* thiol-ene click chemistry with folate and cholesterol derivates and b) cell viability of HEK-293 cells after 24 h and 48 h with these polymer-conjugates.[63]

Subsequently, these polymers were further modified with pyrene, a photoluminescent marker, *via* esterification (as described above in chapter 2.1.3), and their interaction with HMEC-1 cells was examined through confocal microscopy, confirming that the polymers penetrated the cells. However, the polymers modified with the photoluminescence marker exhibited high cell toxicity. For this reason, the search for an alternative labeling system for further investigations was necessary.[77] To address this, PDEVP was synthesized with a highly fluorescent laser dye as an initiator, which yielded high cell viability values in tests with sensitive endothelial cells.[61] Furthermore, as previously mentioned, block copolymers composed of 2VP, DEVP, and DAIVP were synthesized and interconnected into nanoparticles through a thiol-ene click reaction. These nanoparticles exhibit promising drug loading and release profiles, as well as low cytotoxicity, dependent on the specific monomer composition.[67]

2.2 Post-Polymerization Functionalization

Controlled "living" polymerization methods, such as REM-GTP, enable the precise synthesis of polymers with specific molecular weight, composition and polymer architecture. Among these methods, the direct polymerization of monomers with functional side groups is the most attractive strategy. Traditional living cationic and anionic polymerization techniques have several limitations regarding the range of monomers that can be used. Many side-chain functionalities cannot be incorporated through direct polymerization or can only be introduced with a significant loss of control. While living radical and catalytic polymerization techniques offer better tolerance for functional groups, they also have limitations due to catalyst decomposition and other side reactions. Therefore, post-polymerization functionalization represents an interesting approach for the synthesis of polymers with functional side groups, bypassing the limitations of living polymerization for modified polymers. This principle is based on modifying the functionalities of previously synthesized precursor polymers. Post-polymerization modification offers the advantage of introducing functional groups and altering polymer properties while maintaining the polymerization degree. In addition, a reactive precursor polymer can be synthesized from a single monomer, which can then be modified in various ways using simple synthesis methods. This results in a wide range of chemical structures with great diversity.[78]

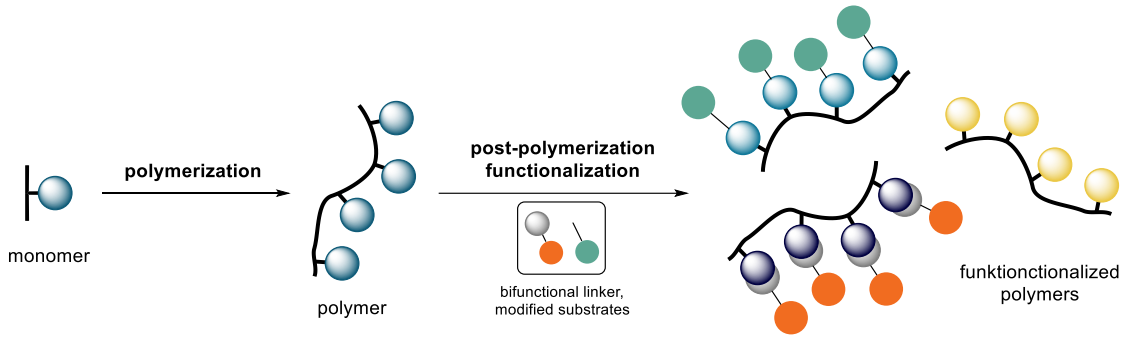

Scheme 2.21: Schematic illustration of post-polymerization-modification.

2.2.1 Click-Reaction

For the post-polymerization functionalization of synthetic polymers, it is necessary to employ processes that facilitate the efficient integration of new functional groups. In 2001, *Sharpless et al.* revolutionized various areas of chemical research by introducing click chemistry.[79] This chemical reaction method is characterized by its exceptional stereo- and regioselectivity, resulting in nearly complete conversions. Furthermore, these types of reactions can be carried out in various solvents and the presence of a wide range of functional groups. For these reasons, the concept of click chemistry has found a broad range of applications in recent years in the synthesis of various polymeric materials.[79-81]

Azide-Alkyne Click Reaction (AAC)

One of the most prominent and commonly observed click reactions is the 1,3-dipolar (3+2) cycloaddition, extensively investigated by *Huisge*n in the 1960s.[82, 83] In this reaction, a five-membered, double-substituted triazole ring is formed when a terminal alkyne reacts with an azide. In the thermally activated *Huisgen* reaction, which does not require catalysts and produces 1,4- and 1,5-triazoles. In contrast, Cu(I)-catalyzed azide-alkyne cycloadditions (CuAAC) exhibit a high degree of regioselectivity, yielding in 1,4-disubstituted 1,2,3-triazoles. This reaction occurs efficiently at room temperature under mild reaction conditions (Scheme 2.22).[84-86]

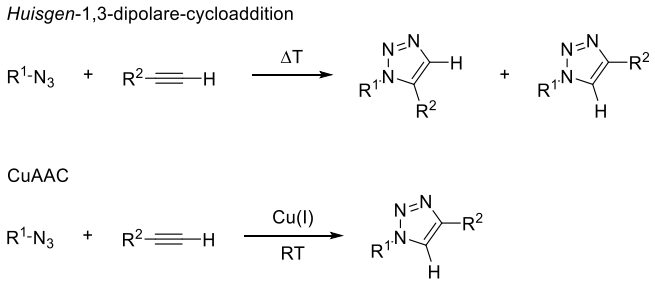

Scheme 2.22: Illustration 1,3-dipolar (3+2) cycloaddition between alkyne and azide.

The thermodynamically controlled CuAAC is characterized by its excellent compatibility with a wide range of functional groups and various solvents, including water. It operates under simple and mild reaction conditions while exhibiting a high tolerance for pH variations. As a result, CuAAC has become a valuable tool for synthesizing and modifying complex organic frameworks and biologically relevant molecules.[87, 88] After extensive investigations into the reaction mechanism of CuAAC, the group of *Fokin et al*. proposed a mechanism in which two copper atoms are involved in each catalytic cycle. The active Cu(I) species can be generated using either Cu(I) salts or Cu(II) salts in combination with sodium ascorbate. In this process, copper coordinates to the acetylene, but this does not expedite the 1,3-dipolar cycloaddition; instead, a *σ*-bonded copper acetylide carrying a *π*-bonded copper coordinates to the azide.

Subsequently, a six-membered copper-metal cycle is formed, with the second copper atom acting as a stabilizing donor ligand. Ring contraction to yield a triazole copper derivative is followed by a protonolysis step, leading to the final triazole product and closing the catalytic cycle (Scheme 2.23).[89, 90]

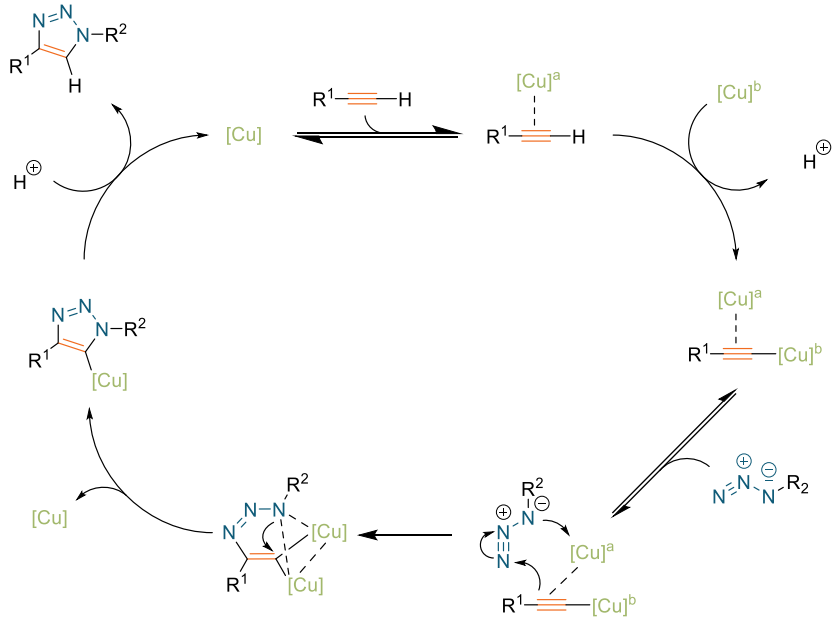

Scheme 2.23: Proposed catalytic mechanism of the CuAAC with two copper atoms.[89]

In addition to CuAAC, the Diels-Alder reaction and other 1,3-dipolar cycloadditions also exist as further click reactions that can be utilized to functionalize polymers and surfaces.

Thiol-ene Click Reaction

Thiol-ene chemistry takes advantage of the positive attributes of click chemistry and demonstrates almost quantitative conversions even under mild conditions after short reaction times. Thiols are of significant interest due to their relatively weak S-H bond, making them suitable for initiation under mild conditions. In thiol-ene click reactions, a distinction is made between the free radical addition of thiols to C-C double bonds and the catalytic *Michael*-addition of thiols to electron-poor olefins (Scheme 2.24).[91]

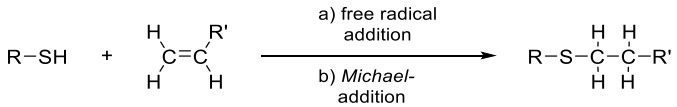

Scheme 2.24: General thiol-ene reactions: a) free radical addition, b) catalyzed *Michael* addition.[91]

The formation of bonds in the free radical thiol-ene reaction proceeds mechanistically through a chain growth process involving initiation, propagation, chain transfer, and termination steps. Radicals can be generated in various ways, but the most used variants are thermal and

photochemical initiation. Radical initiators are classified into two distinct categories: activated through cleavage (Type I) and hydrogen atom abstraction (Type II). Type I initiators include azo compounds such as azobis(isobutyronitrile) (AIBN), peroxides, and photoinitiators like 2,2-Dimethoxy-2-phenylacetophenone. When exposed to high temperatures or UV light, these components decompose into two radical species. Type II initiators, such as benzophenone, are notably less efficient than Type I initiators.[92] The thiol radical formed during initiation is incorporated into the olefin during a propagation step, forming a new carbon-sulfur bond. Subsequently, the radical from the intermediate carbon radical is transferred by the re-abstraction of a hydrogen atom from a thiol group, producing the anti-*Markovnikov* product.[91-93] The alternating two-stage process described can be repeated multiple times before termination occurs through radical-radical recombination. In an ideally progressing thiol-ene reaction, no homopolymerization occurs, which involves the reaction between the carbon radical and additional olefins. Typically, the rate-determining step is the chain transfer, which is highly influenced by the structure of thiol and the solvent used. However, in cases where the reactivity of the olefin is significantly low, the exothermic propagation step progresses slowly, becoming the limiting factor in the reaction (Scheme 2.25).[91]

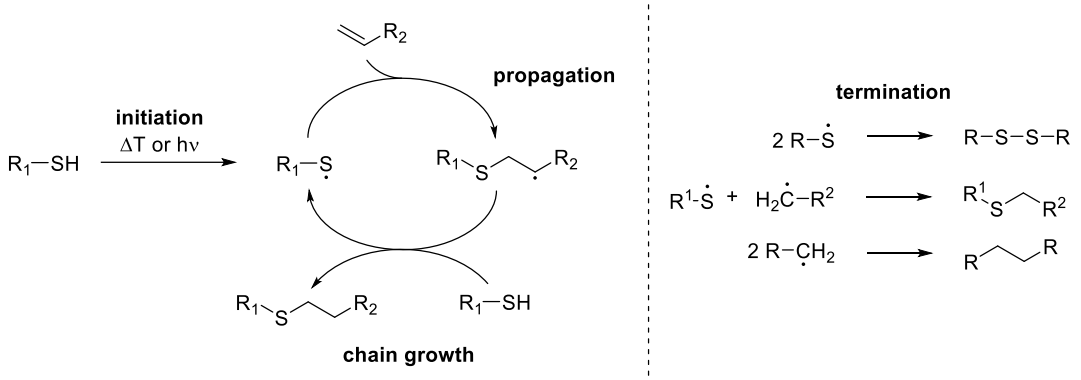

Scheme 2.25: Radical reaction mechanism of the thiol-ene click reaction.[91]

The thiol-ene reaction can also proceed *via* a nucleophilic pathway, where mild bases such as triethylamine or nucleophilic substrates such as phosphines act as catalysts. The thia-*Michael* addition follows a mechanism like the radical variant. In the base-catalyzed method, deprotonation of the thiol is highly efficient under mild conditions due to its high pKa value. In the subsequent crucial step, the resulting thiolate anion adds nucleophilically to the double bond of the substrate at the β-position, forming a highly reactive enolate. This carbanion then abstracts a proton from either the thiol or the triethylammonium cation, ultimately creating the regioselective *anti-Markovnikov* thiol-ene adduct. In the case of the nucleophilic catalytic reaction, the nucleophile directly attacks the activated double bond. The resultant zwitterionic ester enolate species then deprotonates a thiol, yielding the thiolate anion (Scheme 2.26).[91-93]

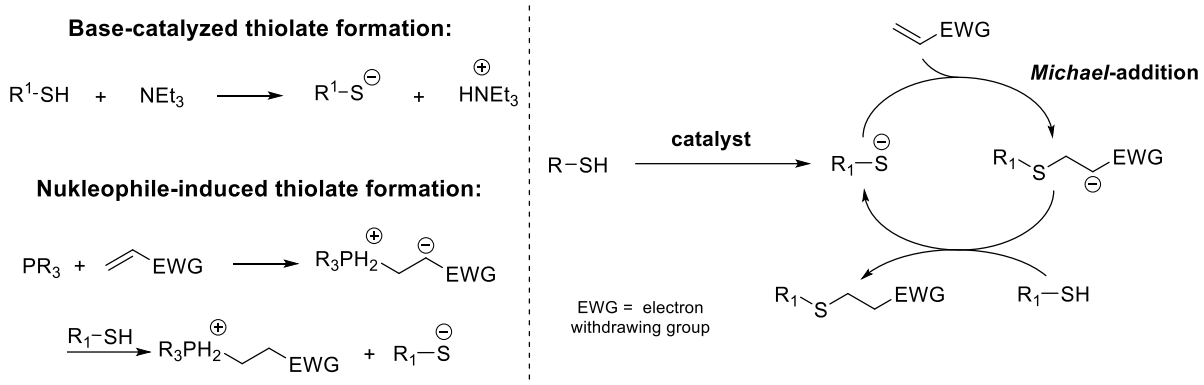

Scheme 2.26: Reaction mechanism of the thia-*Michael* reaction.[91]

2.2.2 Functionalization of Polymers *via* Click-Chemistry

Click reactions are a promising method for polymer modification. They are primarily utilized for functionalizing end groups and side groups. In some cases, direct polymerization can also be achieved through step-growth polymerization, employing A_2 and B_2-type monomers or AB-type monomers.[90]

Azide-Alkyne Click (AAC)

Copper(I)-catalyzed azide-alkyne click polymerization (CuAACP) is one of the most well-known polymerization methods employed to synthesize linear and highly branched polymers.[83, 94] Various catalysts have been developed for this purpose, and they have been utilized in both aqueous and organic solutions, depending on the monomer properties. In many cases, Cu(II) salts are used to generate Cu(I) species in situ through irradiation, ensuring precise control over the timing and spatial aspects of the reaction.[95-97] CuAACP exclusively yields 1,4-triazole linkages, enabling a detailed examination of regioisomers within the polymers, which arise from subtle variations in how two units are connected. For instance, *Tang* conducted experimental and computational investigations on varying substituents at the 1,4-positions of the triazole ring, which had a minor impact on the emission profile of poly(triazole)s. This work laid the foundation for synthetic strategies in developing new luminescent polymers.[98] In addition to 1,4-poly(triazole)s, 1,5-regioregular poly(triazole)s can be produced using Ru(II) catalytic systems. Regioselectivity is determined by the ligands on the ruthenium, with $Cp^*Ru(PPh_3)_2Cl$ favoring 1,5-triazoles, while $RuH_2(CO)(PPh_3)_3$ prefers 1,4-triazoles. Since both 1,4- and 1,5-polytriazoles are easily accessible, the relationship between regioselectivity and thermal stability, refractive index, photophysical properties, and the electrochemical behavior of poly(triazole)s has been examined (Scheme 2.27).[99]

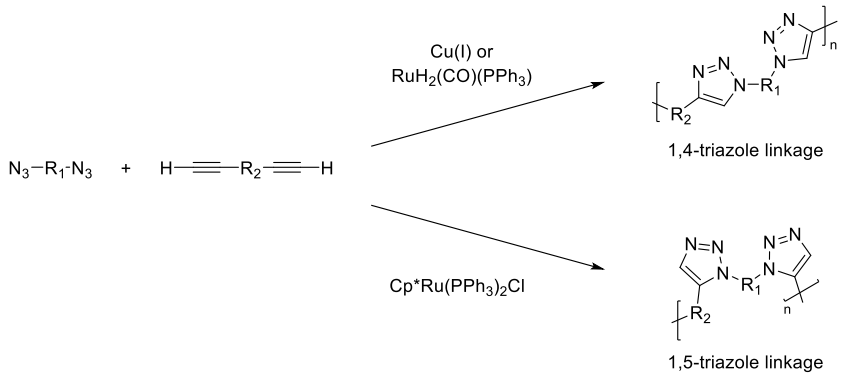

Scheme 2.27: Azide-alkyne click polymerization for preparation of 1,4- and 1,5-regioregular poly(triazole)s.[99]

An alternative approach for efficiently constructing well-defined macromolecular structures involves incorporating clickable functional groups into side chains or end groups. This can be achieved through direct polymerization of clickable monomers using functionalized initiators or through post-polymerization functionalization.[90]

Azide and alkyne groups should be incorporated through post-polymerization modification. This is because alkynes are incompatible with radical polymerization, and azide-functional monomers can participate in cycloaddition reactions with alkene monomers.[100, 101] For instance, *Matyjaszewski* and his group presented a precise atom transfer radical polymerization (ATRP) of 3-azidopropylmethacrylate, carefully controlling reaction conditions to retain the azide functionality (Scheme 2.28, a).[90, 100] Alternatively, direct ROP of cyclic esters containing azide or alkyne moieties has been successfully demonstrated (Scheme 2.28, b+c). An early example involved the utilization of α-propargyl-δ-valerolactone in generating cyclic esters, including alkyne-functionalized lactide and propargyl-3-methylpentenoate oxide. These were subsequently employed in ROP to produce alkyne-functionalized polyesters with low dispersity (PDI<1.3).[90, 102, 103]

The predominant strategy relies on halide substitution for introducing azide groups through post-polymerization modification. A well-studied monomer, 4-vinylbenzyl chloride (or bromide), can be readily polymerized using nitroxide-mediated radical polymerization (NMP) or reversible addition-fragmentation chain transfer (RAFT) methods.[104] Subsequent quantitative substitution of the halides with NaN_3 enables the incorporation of azide as a functional group (Scheme 2.28, d). It is also possible to convert chlorine-substituted poly(lactide) into substituted poly(lactide), either through direct substitution with azide-substituted alkanethiol or through an elimination-addition pathway under mild conditions, without concerns regarding the cleavage of ester groups in the polymer backbone.[105] Furthermore, the nucleophilic ring opening of epoxides in poly(glycidylmethacrylate) (PGMA) with NaN_3 can lead to the formation of azide and secondary hydroxyl groups (Scheme 2.28, e).[106] To create polymers with alkyne functionality through post-polymerization modification, monomers with protected alkynes (Scheme 2.26, f) have been utilized. Trimethylsilyl (TMS) is the most employed protective group, which has been coupled with various styrene, acryl, and acrylamide monomers for ATRP and RAFT polymerization.[90, 107]

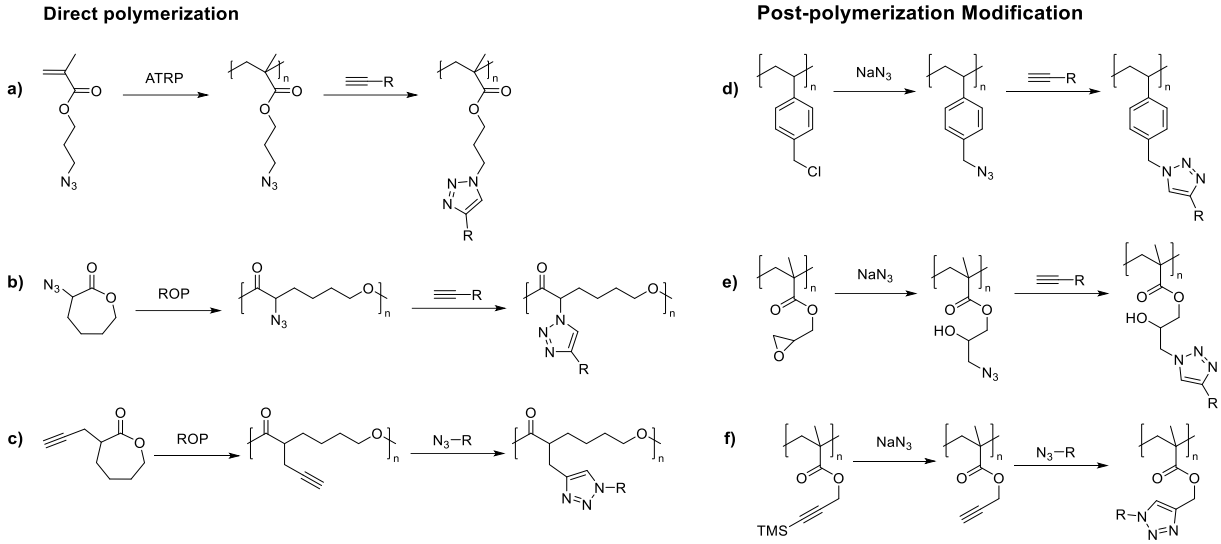

Scheme 2.28: Illustrative examples of direct polymerization (a-c) and post-polymerization functionalization (d-f) approaches for introducing azide or alkyne functionalities onto polymer side chains.[90]

Thiol-ene Click

Thiol-ene click reactions are also a promising method for polymer modification. These reactions primarily involve the functionalization of end groups and side groups. Notable cases include the functionalization of dendrimers and biomacromolecules. The polymer-analogous reaction *via* thiol-ene click chemistry can be achieved in two ways: either the polymer possesses thiol end groups that react with olefins or, conversely, allyl groups that react with thiols (Scheme 2.29).[92]

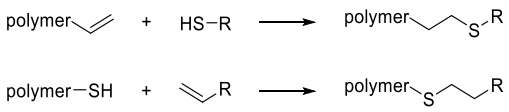

Scheme 2.29: Strategies of post-polymerization functionalization *via* thiol-ene click reaction.[92]

Polymer-analogous reactions are primarily carried out using radical thiol-ene chemistry and less frequently *via thia-Michael* addition. Typically, the double bonds of allylic polymer side chains are modified with thiols through thermal or photochemical radical reactions.[91, 93] Poly(thiol)s are seldom employed due to the potential for oxidation and intra-/intermolecular cross-linking. Radical thiol addition is often applied in the modification of rubber, poly(butadiene), poly(siloxane)s, and poly(urethane)s. Many well-defined homo- and block copolymers have been studied through the functionalization of 1,2-poly(butadiene) with various thiols. This reaction allows for exploring the conditions and specificities relevant to a click reaction across a diverse and comprehensive spectrum. The modification is accomplished through both thermal and photochemical initiation. However, side reactions, such as intramolecular cyclization, occur by adding the formed carbanion to the adjacent double bond (Scheme 2.30).[92, 93]

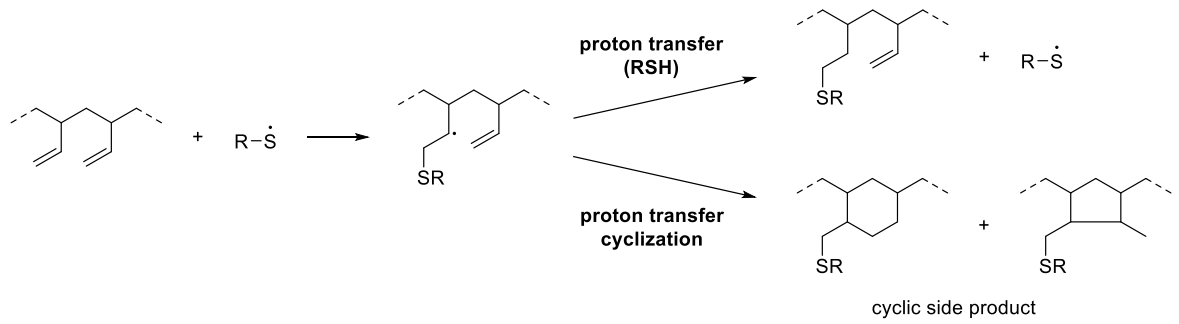

Scheme 2.30: Thiol-ene modification of 1,2-polybutadiene: regular addition and intramolecular cyclization.[92]

Achieving functionalization degree exceeding 80% with complete conversion is possible when photochemical thiol addition is conducted at high reactant concentrations and low temperatures.[108] However, radical thiol-ene reactions can also be applied to other polymer substrates, such as the initially developed poly(2-(3-butenyl)-2-oxazoline) homopolymers and copolymers (as illustrated in Scheme 2.31).[108] The post-polymerization modification of allyl side groups in these cases is accomplished quantitatively through photochemical initiation. Unlike polybutadiene, the greater distance between the radical intermediates and adjacent double bonds in these polymers prevents intramolecular cyclic side reactions.[92]

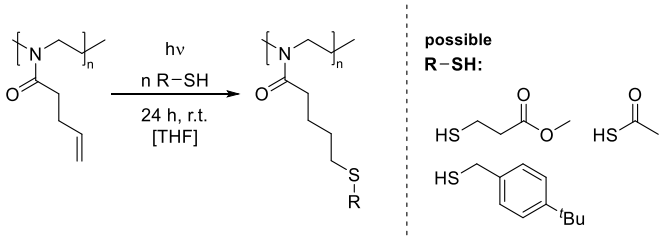

Scheme 2.31: Functionalization of poly(2-(3-butenyl)-2-oxazoline) *via* radical thiol-ene click reaction.[92]

As previously mentioned, polymer-analogous thiol-ene click reactions can be conducted photochemically and thermally. However, it has been observed that photochemical reactions yield significantly higher efficiency and shorter reaction times. Furthermore, they exhibit greater tolerance to functional groups and the polymer backbone compared to thermally activated reactions.[92, 109]

Double Click Reaction

Another promising characteristic of the thiol-ene click reaction is its orthogonality to AAC, which provides the opportunity to modify polymers with different groups. *Campos et al.* demonstrated this with a poly(styrene) polymer synthesized *via* ATRP, featuring two distinct end-group functionalities. After treatment with sodium azide, the group was able to generate an azide and a vinyl group as reactive moieties. Subsequently, the alkene was reacted *via* thiol-ene chemistry, followed by the addition of propargyl alcohol to the azide (Scheme 2.32).[109]

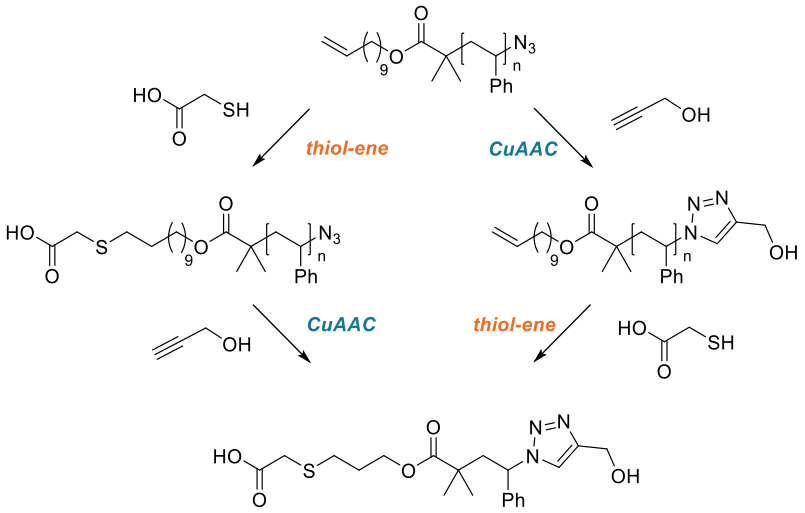

Scheme 2.32: Example of orthogonal functionalization *via* thiol-ene click chemistry and CuAAC.[110]

Another example of multifunctionalities *via* thiol-ene addition is published by *Javakhishvili*, who modified poly(*ε*-caprolactone) at both chain ends. After the CuAAC at the alkene group, this group added thiocholesterol to the polymer as a second functionalization using a photochemical thiol-ene reaction (Scheme 2.33).[111]

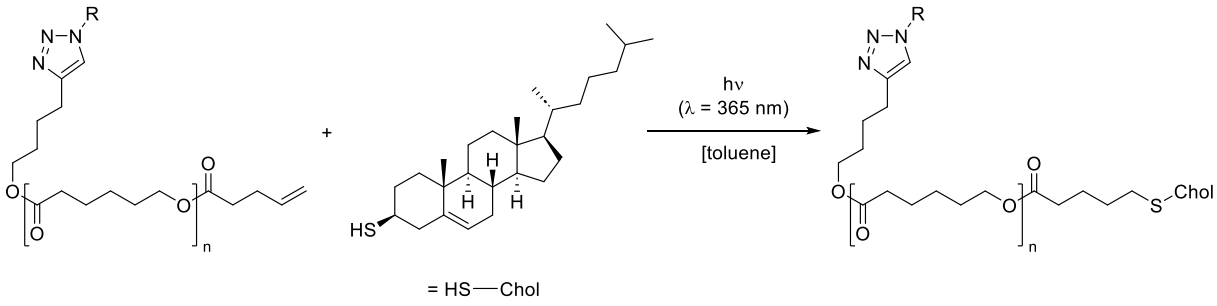

Scheme 2.33: End group functionalization of poly(ε-caprolactone) with thiocholesterol.[112]

This approach demonstrates that it is possible to conjugate sterically demanding biomolecules to polymers, opening a wide range of potential applications in macromolecular chemistry. In this way, it is possible to unite biochemistry with polymer chemistry and bridge various other chemical disciplines.

2.3 Potential Application

Polymers are versatile materials that find applications in various fields due to their exceptional design flexibility, modifiability, and ability to tailor a wide range of properties. Unsurprisingly, they attract substantial interest, particularly within the fields of biology and medicine.

2.3.1 Drug Delivery Systems

An interesting approach and a wide range of applications are presented by polymers in the context of drug delivery systems, which refer to methods for administering pharmaceuticals and various technologies for transporting active drugs through the body. These systems can lead to improved effectiveness and reduced toxicity of cancer medications. Long-circulating macromolecular carriers such as micelles, polymersomes, or liposomes can exploit the "enhanced permeability and retention" effect for preferential extravasation from tumor vessels.[113] Furthermore, these systems are expanded with molecular targeting, wherein the integration of various biological components capable of tumor recognition further enhances the targeted delivery of pharmaceutical agents.[114-116]

Polymeric Micelles

In the context of drug delivery systems, polymeric nanostructures constitute a significant area of research due to their capacity to achieve both enhanced bioavailability and site-specific delivery. Moreover, polymers can impart desired particle size, surface properties, permeation profiles, and flexibility to nanostructures. These advantages are in addition to the fundamental requirements of increased solubility and controlled drug release. The possibilities of bioengineering and functionalization further enhance the utility and applications of polymer nanostructures. All of this has led to their diverse use in the field of biomedicine. The key polymer nanostructures for drug delivery applications encompass polymersomes and polymeric micelles.[117-119]

Depending on the polymer and solution attributes, several ways exist to form different types of polymeric micelles. The type of polymer that is used influences the self-assembly process for polymeric micelles formation. Di-block, tri-block, multi-block copolymers, graft polymers, stimuli-responsive polymers, and others can generate different types of micelles (like spherical, reverse, or cylindrical/worm-like micelles) (Figure 2.3). Furthermore, the solvent, pH value, polymer concentration, and ratios, or co-solvent, can significantly influence the type formed.[120, 121] Based on the method of drug encapsulation, the drug carrier are mainly categorized into two groups: chemical covalent binding of drugs or physical encapsulation. The drug can be encapsulated in different regions of the micelles according to polarity: non-polar drugs in the

core, polar drugs in the shell, and drugs with intermediate polarity encapsulated between the core and the shell.[122]

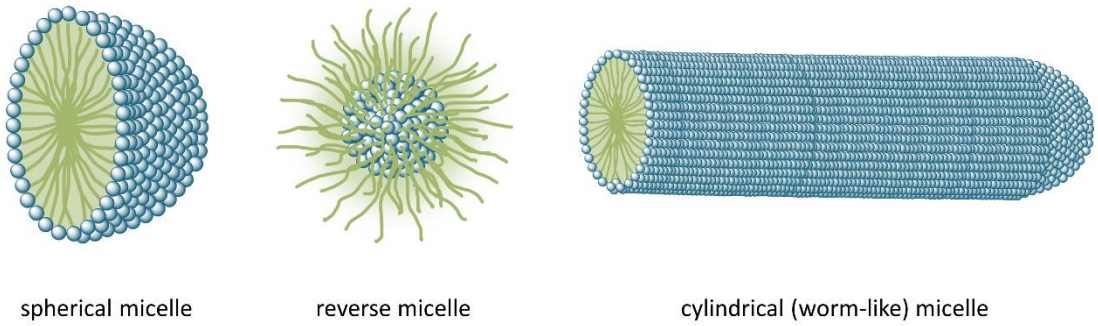

Figure 2.3: Conceptual illustration of selected micelle types.

For micelles in drug delivery systems, the most commonly used hydrophilic blocks are PEG, while the hydrophobic blocks typically are poly(ester)s, poly(ether)s, or poly(amino acid)s, such PLA, PCL, and poly(propylene oxide) (PPO).[123]

Moreover, micelles with a core-shell structure offer many advantages for targeted cancer drug delivery. They can enhance drug solubility by encapsulating water-insoluble drugs, and their effectiveness in medicines in solid tumors primarily depends on the enhanced permeability and retention (EPR) effect, which serves as a passive targeting strategy.[121, 124] In passive targeting, nanoparticles have to circulate in the bloodstream for an extended period to ensure adequate delivery of therapeutic agents to the tumor tissue, with their size being a critical factor. Nanoparticles smaller than 10 nm are readily excreted through renal glomeruli, while the liver and spleen can rapidly eliminate those larger than 100 nm from the bloodstream.[125, 126] Utilizing this knowledge, micelles with the size range of 10-100 nm can avoid swift removal from the body, allowing for their accumulation in tumor tissue through the EPR effect.[127]

The biocompatible polymeric corona surrounding micelles can also inhibit non-specific interactions with biological components. This reduces their recognition by the reticuloendothelial system (RES) and extends their circulation time in the bloodstream. However, it is essential to note that the EPR effect of polymeric micelles may not always be beneficial for treatments, particularly in clinical human studies, due to the diversity and complexity of the tumor microenvironment. Consequently, micelles can be further customized with ligands for active targeting to enhance their tumor selectivity and facilitate intracellular drug delivery, reducing systemic toxicity and other undesirable effects.[128] Numerous studies have shown the superior outcomes of actively targeted systems compared to non-targeted systems, including improved cellular uptake, cytotoxicity, and tumor regression. This positions the active targeting strategy as a critical complement to passive targeting systems. These

advantages underscore the potential of polymeric micelles as a promising and potent drug delivery platform for cancer therapy.[127]

Liposome and Polymersome Linker

In addition to micelles, polymersomes and liposomes are particularly intriguing carriers for drug delivery systems. These are spherical vesicles with a bilayer structure with hydrophilic and hydrophobic parts. Polymersomes are primarily constructed from block copolymers, while liposomes are based on lipids. The general physical properties of lipids and amphiphilic polymers are highly analogous.[129, 130] Liposomes were the first developed nanodrug carriers in the 1960s.[131] Due to their amphiphilic properties, it is possible to incorporate both lipophilic active substances into the phospholipid bilayer and encapsulate hydrophilic active substances inside the vesicles.[132] To enhance the stability of liposomes in vivo, their surfaces can be specially modified. This can be achieved by grafting hydrophilic polymers like PEG (PEGylation), leading to an extended circulation time of the carriers. Additionally, ligand-functionalized liposomes have shown remarkable efficiency in targeted drug delivery.[133] Through the targeted delivery of anticancer drugs, the localization of the site of action and the accumulation of drugs in tumor tissue can be achieved. This has dual advantages that improve effectiveness and reduce potential side effects. Numerous studies have explored the modification of liposome surfaces with active targeting ligands such as antibodies, peptides, or vitamins (Figure 2.4).[134]

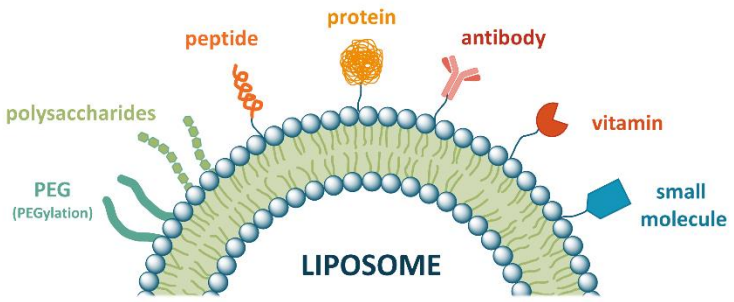

Figure 2.4: Modification of liposome surface with different ligands (targeted liposomes).

One of the most well-known and extensively researched targeting groups is folate. This water-soluble vitamin exhibits a high affinity for the folate receptor (FR) and, as a result, initiates receptor-mediated endocytosis. This system offers the advantage of the receptor being present in only minimal quantities in normal cells but being overexpressed in tumor cells, facilitating the possibility of selective targeting.[135] Folate-targeted liposomes can be produced by conjugating folate with lipids, cholesterol, or proteins. The essential concept behind developing folate-conjugated liposomal systems is to attach folate to the liposome using its lipophilic groups.[136]

One of the key constructs in the preparation of liposomes involves the combination of folic acid and cholesterol. Firstly, it can serve as an intercalator by interacting with the phospholipid molecules of the liposomes, thus acting as an anchor for the linkers. Secondly, it can function as a fluid buffer and a stabilizer for the lipid membrane against temperature fluctuations.[136-139] The cholesterol derivative 3*β*-Hydroxy-5-cholesten-3-hemisuccinate (CHEMS) is frequently employed in producing pH-sensitive liposomes.[140] *Xiang et al.* reported on the synthesis of FA-PEG-CHEMS and its application as a targeting ligand for liposomal doxorubicin (DOX) in FR-expressing cells. Liposomes containing FA-PEG-CHEMS exhibited remarkable colloidal stability and were selectively taken up by FR-overexpressing KB cells. Furthermore, these liposomes demonstrated enhanced vitro cytotoxicity and extended in vivo circulation compared to non-targeted liposomes.[141] *Chen et al.* also employed FA-PEG-CHEMS to develop FR-targeted pH-sensitive liposomes co-loaded with DOX and Imatinib to overcome multidrug resistance. These synthesized liposomes improved the anti-tumor effect and introduced a novel strategy for enhancing the efficacy of chemotherapy against multidrug-resistant tumors (Scheme 2.34).[136, 142]

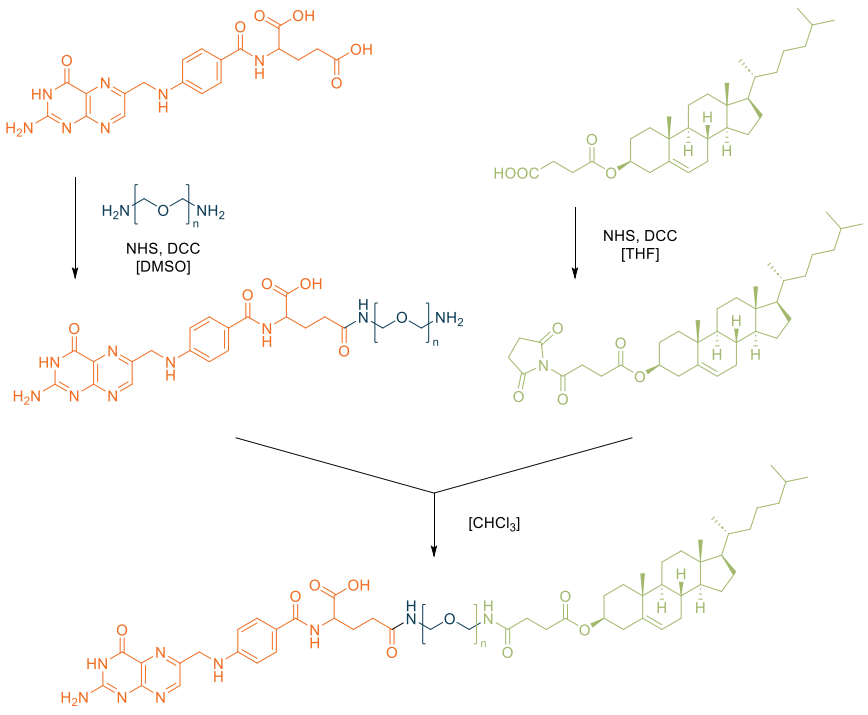

Scheme 2.34: Synthetic reaction cascade for FA-conjugated cholesterol (FA-PEG-CHEMS).[136]

Polymer-Drug-Conjugates

In addition to the incorporation of active substances into various carriers, using polymer-drug conjugates is of significant scientific interest. This is primarily attributed to the introduction of diverse functional groups, which pave the way for creating a versatile platform for modifications. Polymer-drug conjugates, or polymer-drug complexes, are nano-sized (1-100 nm) macromolecular structures with relatively low molecular weights. Typically, one or

more therapeutic agents, such as small molecules, proteins, or aptamers, are covalently attached to a polymeric carrier through a biodegradable linker.[143-145] Consequently, the general structure of a polymer-drug conjugate typically comprises three components: the polymer, the linker, and the therapeutic agent (Figure 2.5). Additionally, attaching targeting ligands to the polymer is possible, allowing the system to specifically target a particular biological objective.[146] The conjugation of bioactive substances to polymers offers numerous benefits, including improved drug solubility, enhanced effectiveness, and enhanced pharmacokinetics.[143]

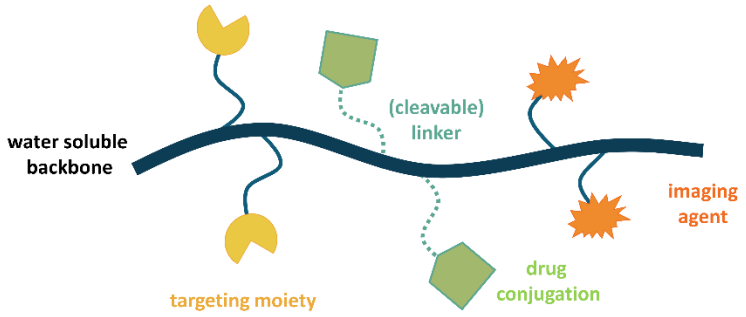

Figure 2.5: Schematic illustration of possible polymer-drug-complex.

In 1970, *Ringsdorf et al.* achieved a breakthrough with polymer-drug conjugates.[145] Since this pioneering achievement, polymer-drug conjugates have witnessed remarkable progress. Advances in synthetic polymer chemistry and construction techniques have expanded the repertoire of available materials, structures, and functionalities. Particularly, highly reactive and multifunctional carriers offer an exciting opportunity to control and optimize the administration of therapeutics. Many of these drug delivery systems have undergone clinical trials for anticancer therapies.[143] For instance, there are copolymers of N-(2-Hydroxypropyl)methacrylamide (N-(2-HPMA)) that bind various drugs through a Gly-Phe-Leu-Gly-peptide linker (Figure 2.6, a). One of the most well-known compounds in this category of drugs is the DOX conjugate PK 1 (FCE-28068), which exhibits significantly reduced toxicity compared to free Doxorubicin.[147, 148] In a more advanced approach for targeted tumor treatment, galactosamine was incorporated as a targeting group alongside the drug, coupling with the asialoglycoprotein, a receptor on tumor tissue (Figure 2.6,b).[148, 149]

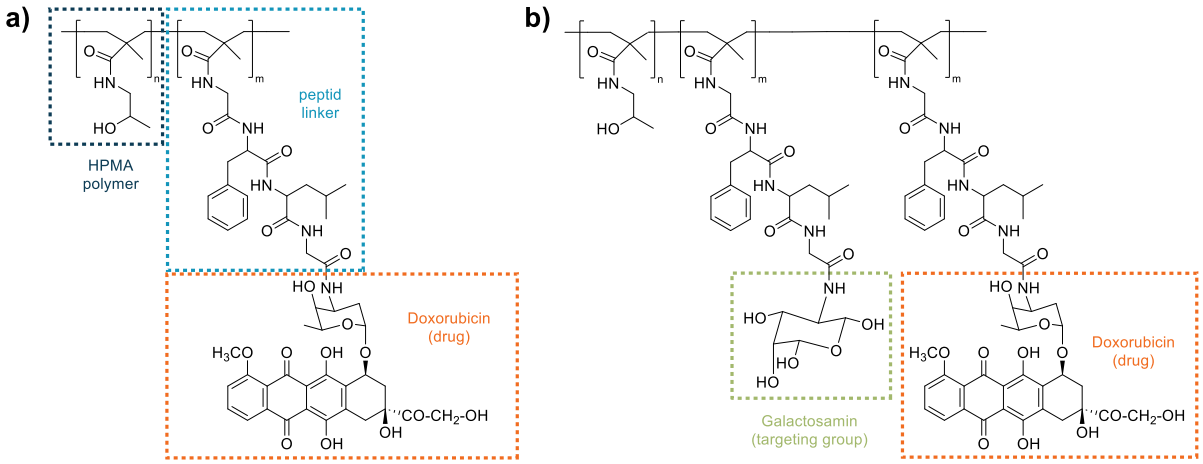

Figure 2.6: Illustration of a) PK-1(FCE-28068) and b) a polymer-drug conjugate with DOX and galactosamine.

In many cases, the multifunctionalization of polymers, allowing for the attachment of various molecules, presents a promising strategy for pharmaceutical manufacturing. To illustrate, the use of individual anticancer drugs has frequently been associated with the development of resistance. As a preventive measure, the administration of combination chemotherapy is a common practice in many types of cancer.[150, 151] The fundamental principle behind this approach is utilizing multiple cytotoxic drugs with orthogonal mechanisms of action to reduce the likelihood of resistant cancer cell emergence.[152] Therefore, it would be an intriguing approach for polymer-drug conjugates not only to conjugate a single type of therapeutic agent but also two different therapeutics to the macromolecule. Moreover, in addition to conjugating another drug, combining a radionuclide or a fluorescent label for polymer diagnostics or theragnostic is also a viable option.[153]

2.3.2 Functionalized Carbon Nanotubes

Apart from their utilization in vesicle-based drug delivery systems, polymers also find widespread applications in other (biomedical) fields. For instance, they offer a diverse range of opportunities for modifying carbon nanotubes (CNTs).[154]

CNTs are 1D nanomaterials based on carbon, characterized by a high length-to-diameter ratio (>1000), significant flexibility, low density (~1.9 g/cm3), and outstanding electromechanical and thermal properties.[155] Consequently, they are ideal candidates for various applications, including the development of multifunctional nanocomposites.[156] With an exceptional elasticity modulus (up to 1 TPa) and strength (up to 300 GPa), they rank among the most robust materials ever known, making them an excellent choice for reinforcing polymers.[157] Three main types of CNTs have been described: firstly, those consisting of a single graphite sheet rolled into a cylindrical form, with diameters ranging from 0.5-3 nm, known as single-walled carbon nanotubes (SWCNTs). Secondly, there are CNTs with a double-layered structure, containing two folded graphene layers, with diameters ranging from 1 to 4 nm, referred to as double-walled carbon nanotubes (DWCNTs). Additionally, there are multi-walled carbon nanotubes (MWCNTs) with diameters between 3 and 40 nm (Figure 2.7).[154, 158]

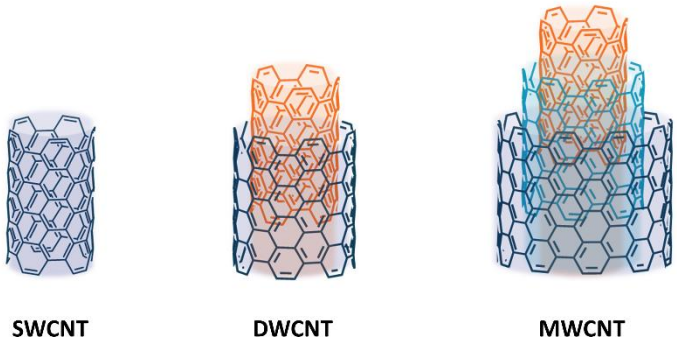

Figure 2.7: Nanostructures of SWCNTs, DWCNTs, and MWCNTs.

Unmodified CNTs exhibit extremely limited selectivity in their interactions with analytes due to their chemically inert outer walls. Through the chemical functionalization of CNTs, various properties, such as solubility and biocompatibility, can be enhanced.[159] Among the different possible approaches to surface modification, they can primarily be classified into two main categories. The first involves non-covalent modification, where polymer or biomolecule chains are wrapped around the surface of CNTs or various surfactants (often small molecules) bound to the nanotubes' surfaces using π-π interactions and *van der Waals* forces.[160] The second method is covalent functionalization, which allows functional molecules to be attached to the ends or conjugated surfaces of CNTs through chemical reactions. In this method, functional groups are attached to the side walls or ends of the nanotubes. This approach has the advantage of providing stable and fixed positions for functional groups on the nanotubes.

However, it results in a stronger sp^3 character due to the hybridization of sp^2 carbon atoms at the modified sites, reducing electronic delocalization and disrupting their intrinsic electronic and optical properties. Therefore, the extent of modification plays a crucial role in achieving an optimal balance between the covalent bonding of desired functional molecules and the disturbance of the π-surface.[160, 161]

In polymer nanocomposite production, two primary methods are employed: "grafting to" and "grafting from". In the "grafting from" approach, polymerization is initiated on the surface of CNTs by attaching initiator groups. A suitable initiator is covalently linked to the surface of the carbon nanotubes, depending on the chosen polymerization mechanism for grafting. In recent years, various successful synthesis techniques have been utilized, including radical atom transfer polymerization, reversible addition-fragmentations chain transfer polymerization, ring-opening metathesis polymerization, and free radical in-situ polymerization, to create polymer composite materials reinforced with carbon nanotubes.[162, 163] Conversely, in the "grafting to" method, end-functionalized polymer molecules react with complementary functional groups present on the surface of either pristine or pre-functionalized carbon nanotubes. Typically, additions to the CNT double bonds are employed, such as radical, carbanion or cycloaddition reactions, assuming their curvature makes them receptive to various addition reactions.[164] [2+1] Cycloadditions represent an intriguing approach in chemical reactions, as they make use of π-electrons for bonding without requiring free valence bonds. This allows for the restoration of the sp^2-π-conjugated system after the reaction.[165, 166] When functionalizing CNTs with azide-terminated polymers, a highly reactive azide group is transformed in situ into a nitrene through thermal or photochemical decomposition, releasing nitrogen. The biradical molecule can react with the π-system of the CNTs, leading to the attachment of the polymer to the CNT *via* an aziridine ring.[165, 167, 168] In their study, *Quin et al.* conducted a cycloaddition reaction between azide-terminated poly(styrene) and SWCNTs in an inert atmosphere. The degree of functionalization was estimated as one polymer chain per 48 CNT carbon atoms, calculated based on the molecular weight of polystyrene (PS) and the thermal gravimetric analysis (TGA) result (85% weight loss of the polymer) (Scheme 2.35).[163, 169]

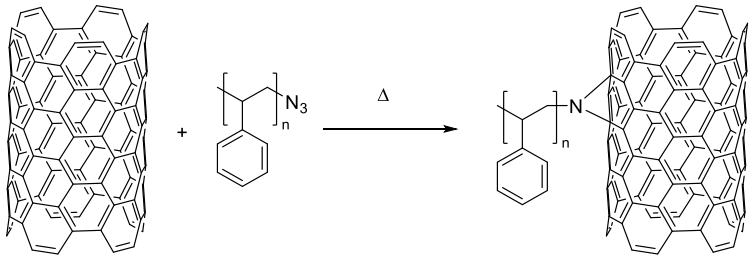

Scheme 2.35: Cycloaddition of azide-terminated polystyrene onto CNTs surface.[169]

Alternatively, defect sites, including open edges of oxidized CNTs with terminal COOH groups, enable the covalent attachment of segments or oligomers.[163] Polymers bearing terminal

hydroxyl or amino groups are often linked to the COOH groups on the nanotube's surface through esterification, anhydride formation, or amidation reactions. One advantage of this technique is using prefabricated commercial polymers with known mass. However, a limitation of this approach is that it yields only a limited number of grafting bonds and is restricted to polymers containing highly reactive groups.[154, 163, 170]

Despite some limitations, CNTs exhibit significant potential for various applications, including biomedical applications, biosensors, clinical diagnostics, energy storage, food safety, and environmental monitoring. They own their unique structure. Nevertheless, the limited solubility of CNTs in many solvents, particularly water, has constrained their application in fields like biomedicine, biomedical imaging, and cancer therapy. Consequently, several surface modifications are necessary to enhance their compatibility, solubility in common solvents, and selective binding ability to biotargets. This can be achieved by attaching hydrophilic polymers that improve solubility in aqueous media.[154, 171]

For instance, MWCNTs grafted with poly(amidoamine) (PAMAM) dendrimers have been developed for targeted delivery to cancer cells and imaging purposes.[172] Additionally, the use of conductive polymers such as poly(aniline) (PANI), grafted onto modified CNTs, has played a crucial role in developing biosensors due to their conductivity and selectivity for functional groups.[173] *Lay et al.* also investigated the potential of CNTs in delivering cancer drugs. In this study, PEG, which is widely known for its biocompatibility and dispersibility in aqueous solutions, was used for functionalization. CNTs loaded with cancer drugs such as doxorubicin and paclitaxel demonstrated promising results for the delivery system in both in vivo and in vitro studies.[174]

3. Aim – Functionalization of Poly (vinyl phosphonate)s with regard to (Bio)medical Applicability

In 2010, *Rieger et al*. successfully produced poly(vinyl phosphonate)s, a polymer that had previously been proven to be challenging or resistant to polymerization.[18] High-molecular-weight PDEVP was obtained via REM-GTP, using lanthanide-based catalysts.[43] This achievement marked the initiation of subsequent investigations into the polymerization process and material properties. The polymer exhibits thermoresponsive behavior and high biocompatibility, making poly (vinyl phosphonate) a promising candidate for various (bio)medical applications.[62, 63, 65, 67]

Building upon this foundation, this thesis focuses on the modification of poly(vinyl phosphonate)s to enhance their bio(chemical) applicability. The insertion of functional groups serves as an anchor point for attaching a variety of biologically active substrates or surface coatings and can be approached through various methods. Apart from connecting different end groups, it is feasible to incorporate the corresponding functional groups by designing new monomers or through polymer-analogous reactions (Figure 3.1). The resulting platform of functional groups and the ensuing possibilities for linking allow for the targeted and multiple modifications of polymers with diverse substrates. In general, the diversity of modification points and their adjustability give many opportunities for synthesizing advanced polymer structures, which will be explored in greater detail within the scope of this work.

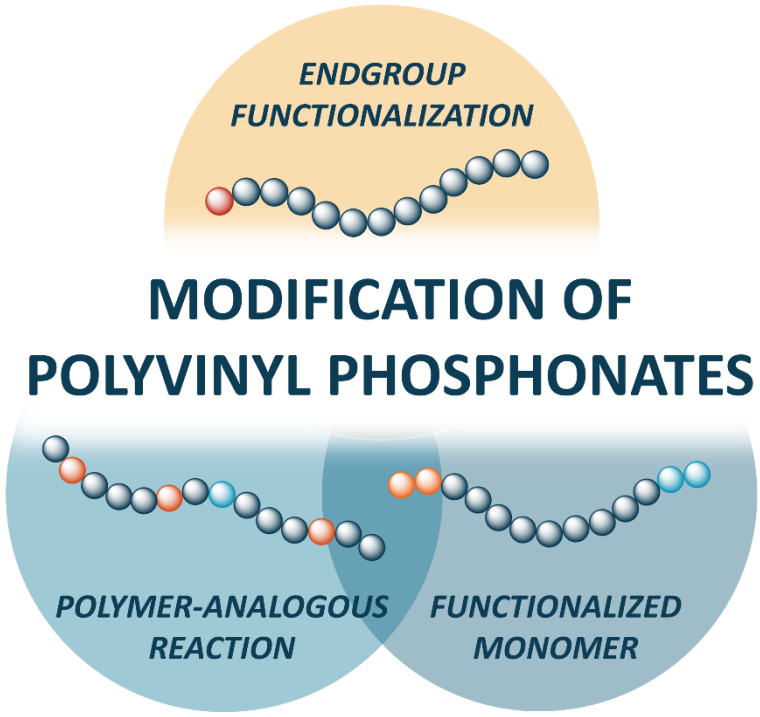

Figure 3.1: Overview of the various aims of this thesis.

3.1 End-group Functionalization

Initially, this research focuses on developing initiators with functionalized end groups for poly(vinyl phosphonate)s. By utilizing C-H activation with yttrium/lutetium catalysts, diverse α-methylpyridines featuring (protected) functional groups are incorporated as initiators into the polymer chain.[63, 64, 175] The choice of functional groups particularly prioritize azide and (protected) alkyne. Consequently, the initial step involves synthesizing the corresponding initiators, which is later used for the *in-situ* activation of $Cp_2Y(CH_2TMS)(thf)$ and $Cp_2Lu(CH2TMS)(thf)$ catalysts. The ensuing polymerization of DEVP is tested using the newly activated catalysts, and the presence of the incorporated functional group in the polymer is verified (Figure 3.2). Upon successful synthesis of end-group functionalized polymers, the research is progress to explore additional modifications. This may involve functionalizing MWCNT or attaching dyes through [2+1]-cycloaddition or AAC. This approach opens a broad spectrum of advanced materials, contributing to the development of innovative materials and applications by using the unique properties of the modified polymers.

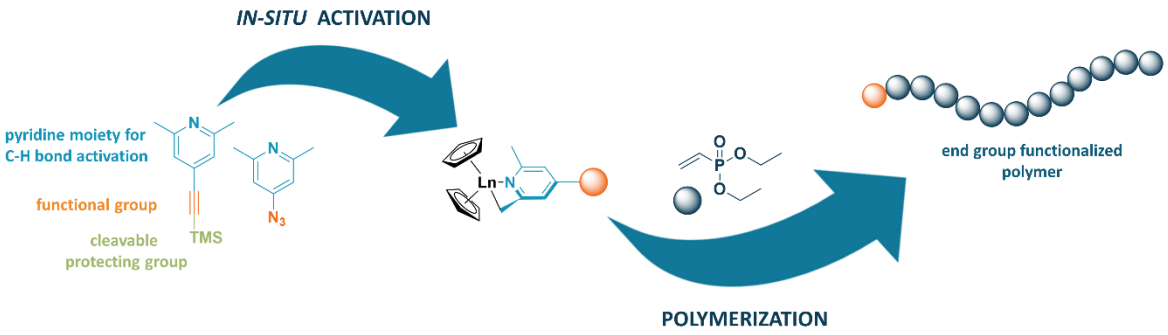

Figure 3.2: Introduction of functional groups to polyvinyl phosphonates by C-H bond activation with functionalized *α*-methylpyridines.

3.2 Incorporation of Functionality into the Polymer Chain

Besides end-group functionalization, the polymer chain itself presents a wide range of opportunities for functionalization. Polymer-analogous reactions can expand the repertoire of functional groups within the polymer. In this context, statistical copolymers, based on DEVP and the previously developed DAIVP, can be used as starting materials, distinguished by modifiable allyl groups in the monomer side chains.[67] The double bonds within the polymer chain resulting from this approach provide a strategic entry point for polymer-analogous reactions, such as bromination or epoxidation. These reactions, in turn, serve as excellent precursors for follow-up reactions, including the introduction of azide groups. Furthermore, additional functional groups through thiol-ene click reactions can be introduced. In this method, a linker comprising a thiol and the desired functional groups can be utilized to incorporate further functionalities under mild conditions and with quantitative conversion. The newly introduced functional groups can finally be attached to other substrates, including those relevant to bio(medical) application. This enables a broad range of polymer-substrate conjugates through an extensive pool of linking reactions. Additionally, selective modification of a fraction of the allyl bonds within the polymer, it becomes feasible to attach different substrates, facilitating the multiple functionalization of the polymers (Figure 3.3).

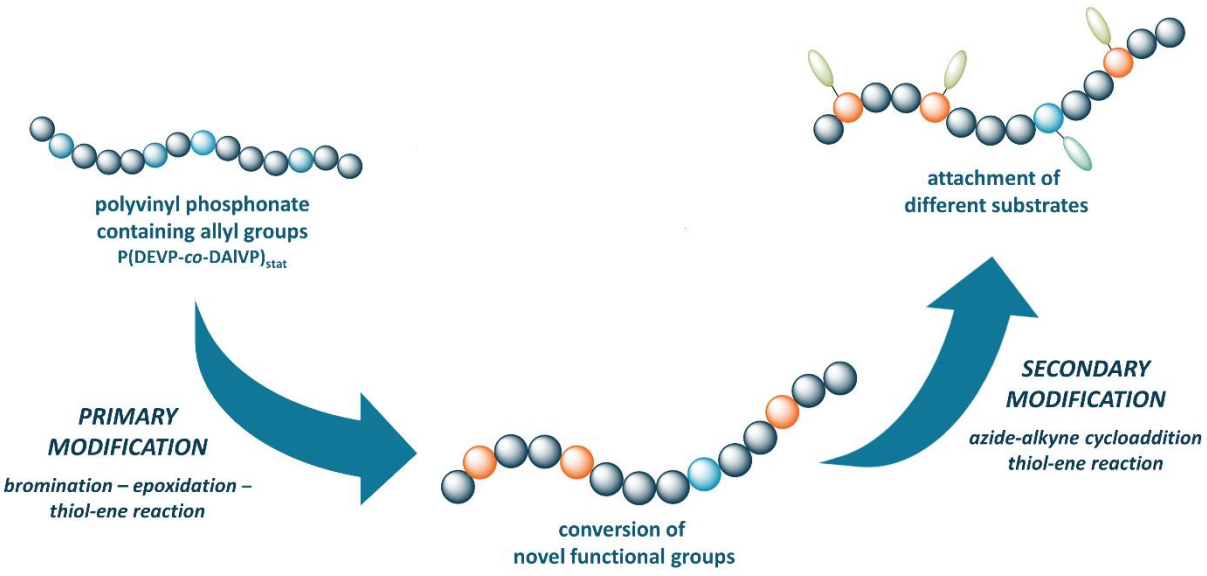

Figure 3.3: Expanding the spectrum of functional groups in the polymer chain through polymer-analogous reactions and subsequent modification.

While the multifunctionalization through polymer-analogous reactions inherently follows a statistical distribution, there is potential to design targeted multifunctionalization strategy via new monomers and orthogonal reactions. One can initially synthesize vinyl phosphonates with (protected) alkyl groups in the side chains to explore this possibility. This functional group is compatible with the yttrium catalysts typically employed for REM-GTP of poly(vinyl phosphonate)s and provides a potential prerequisite for AAC. Introducing these newly developed monomers allows for creating block copolymers/terpolymers and in this way the integrating of two distinct functional groups into the polymer alongside DEVP. Developing precisely designed polymer chains with adjustable ratios of functional groups precedes the targeted modification of poly(vinyl phosphonate)s through orthogonal functionalization. Sequential AAC and thiol-ene click reactions enable the selective and independent attachment of distinct substrates to the allyl and propargyl groups within the polymer (Figure 3.4). This approach enhances the versatility of the polymer structure, enabling a tailored and precise functionalization strategy that goes beyond the previously known modification possibilities. Moreover, it has a great potential for diverse applications, particularly in the (bio)medical field.

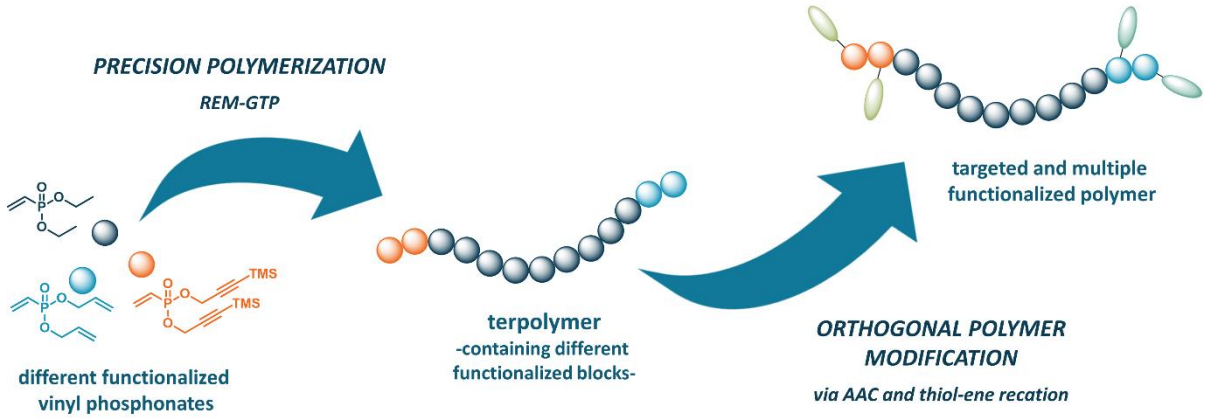

Figure 3.4: Precise introduction of functionalities through specific monomers and subsequent orthogonal modification.

4. End-group Modification

"Azide-Modified Poly(diethyl vinylphosphonate) for Straightforward Graft-to Carbon Nanotube Functionalization"

4.1 Bibliographic Data

Title: "Azide-Modified Poly(diethyl vinylphosphonate) for Straightforward Graft-to Carbon Nanotube Functionalization"

Status: Article, Publication Date: 22.12.2022

Journal: Macromolecular Materials and Engineering

DOI: 10.1002/mame.202200635

Authors: Moritz Kränzlein,‡ Thomas M. Pehl,‡ Kerstin Halama,‡ Paula F. Großmann, Tim Kratky, Amelie M. Mühlbach, and Bernhard Rieger*

4.2 Abstract Graphic (TOC)

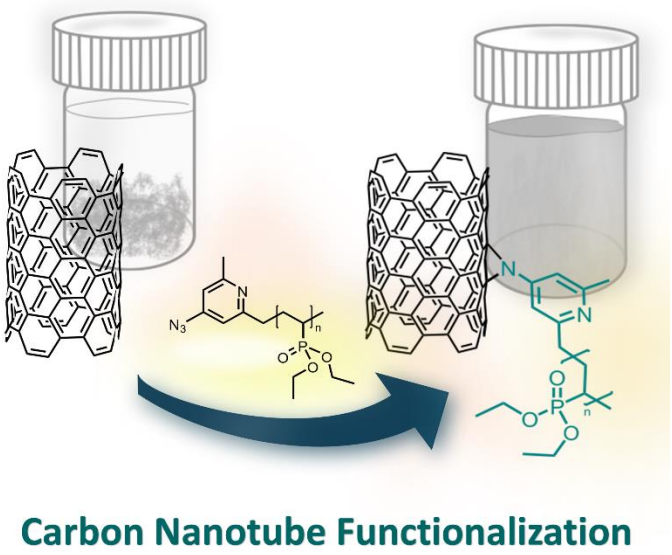

Figure 4.1: Table of content graphic for the manuscript titled "Azide-Modified Poly(diethyl vinylphosphonate) for Straightforward Graft-to Carbon Nanotube Functionalization".

4.3 Content

As highlighted in chapter 2.1.2, poly(vinyl phosphonate)s exhibit a high degree of functional ability and specific properties such as thermoresponsive behavior due to its LCST. Additionally, REM-GTP allows fast and convenient end-group functionalization of the synthesized polymers, serving as a valuable tool in synthesizing highly functionalized polymer structures. This approach can be employed in graft-to methods, enabling the attachment of specifically modified polymers to other functional materials, thereby providing a framework for the synthesis of further functional materials. Highly conductive carbon nanotubes, introduced in Chapter 2.3.2, present an intriguing option for such functionalizations, showcasing a wide range of potential applications, particularly in the biomedical field.

In this context, controlled C-H bond activation was employed, utilizing the catalysts $Cp_2Lu(CH_2TMS)$ and $Cp_2Y(CH_2TMS)$ activated with azide or protected alkyne functionalized α-methyl pyridines. During the C-H bond activation, the pyridine derivative is covalently bound to the metal center of the catalyst and transferred irreversibly during polymerization, as extensively described in Chapter 2.1.2. By attaching functional groups to the pyridine, it becomes feasible to anchor them to the end of the polymer chain, achieving quantitative end-group functionalization. In this case, an azide unit was introduced, and the polymerizability of PDEVP was examined at various chain lengths, confirming the subsequent presence of the azide group within the polymer chain. The synthesized azide-functionalized PDEVPs were attached to the surface of MWCNTs through [2+1]-cyclo-addition and the efficiency of the grafting process was demonstrated. Furthermore, through experiments on aqueous suspensions, the stabilizing effect of water-soluble polymers on MWCNTs was confirmed.

Moreover, the applicability of pyridines is extended by introducing an alkyne. In this case, it was necessary to protect it with TMS to prevent catalyst degradation and to ensure polymerizability and attachment of the alkyne group to the polymer. Following subsequent deprotection of the end group, the functionalization with 3-aziodo-7-hydroxycoumarin was additionally confirmed.

4.4 Manuscript

RESEARCH ARTICLE

Macromolecular Materials and Engineering
Open Access
www.mame-journal.de

Azide-Modified Poly(diethyl vinylphosphonate) for Straightforward Graft-to Carbon Nanotube Functionalization

*Moritz Kränzlein, Thomas M. Pehl, Kerstin Halama, Paula F. Großmann, Tim Kratky, Amelie M. Mühlbach, and Bernhard Rieger**

Rare-earth metal-mediated group-transfer polymerization (REM-GTP) offers distinctive features over common polymerization techniques, such as living character, a broad scope of functional monomers, high activity, excellent control of the polymeric parameters as well as inherent chain-end functionalization. Through the latter, polymers with reactive end-groups become feasible, opening the pathway for further post-polymerization functionalization. In this study, a straightforward graft-to immobilization of the Michael-type polymer poly(diethyl vinylphosphonate) (PDEVP) on multi-walled carbon nanotubes (MWCNT) is reported. Hence, a customized azide initiator is synthesized and studied in the C–H bond activation with various lanthanide-based catalysts and the subsequent polymerization of diethyl vinylphosphonate (DEVP). The successful attachment of the azide end-group is demonstrated via electrospray ionization mass spectrometry (ESI-MS) and the synthesized polymers are subjected to immobilization on multi-walled carbon nanotubes in a graft-to approach. The prepared MWCNT:PDEVP composites are analyzed via thermogravimetric analysis (TGA), elemental analysis (EA), Raman spectroscopy, X-Ray photoelectron spectroscopy (XPS), and transmission electron microscopy (TEM) and the versatility of this approach is shown via the stabilization of MWCNT dispersions in water.

1. Introduction

Poly(diethyl vinylphosphonate) (PDEVP) is an interesting candidate for functionalization of carbon nanotubes, as it is a water-soluble polymer with a tunable lower critical solution temperature (LCST) [1] and can act as a versatile platform as there are different structural derivatives of the vinylphosphonates reported, which are highly interesting for MWCNT functionalization. An allyl-containing PDEVP derivate has been introduced recently, allowing for sidechain modification of the polymers,[2] as well as an organic radical polymer obtained via attachment of 2,2,4,4-tetramethylpiperidinyloxyl (TEMPO)-units to the vinylphosphonate backbone.[3] Especially the latter would be highly interesting for the proposed functionalization, as it could offer a covalent attachment of a redox-active polymer to an highly electrical conductive carbon support, thus overcoming organic radical batteries main issues of low active mass and dissolution in the batteries electrolyte.[4] While generally non-covalent or covalent functionalization of carbon nanotubes can be applied, the latter offers the advantage of avoiding the use of an additional surfactant which might negatively influence material properties and does not rely on necessary non-covalent polymer-CNT interactions, ultimately allowing high versatility of the polymer used. Furthermore, covalently functionalized carbon nanotubes could be dispersed in a broad variety of solvents due to the solubility of PDEVP.[5] In order to attach the polymers covalently to the MWCNTs, a defined end-group with specific reactivity is necessary. In the context of carbon nanotube functionalization, azide-based functionalizations for graft-from and graft-to approaches have been investigated thoroughly, as azide moieties can be used either for azide-alkyne click chemistry functionalizations or link to the carbon nanotubes via [2+1] cycloaddition of an in situ formed nitrene.[6–11] Using these two methods, various different polymers like poly(*N*-isopropylacrylamide),[12] polycaprolactone,[13] poly(methyl methacrylate) (copolymers) [13,14] or polystyrene [13,15] have successfully been anchored to carbon nanotubes, for further functionalization examples a variety of comprehensive reviews exists in literature.[10,16] As a versatile functionalization technique for modifying group-transfer polymerization-based

M. Kränzlein, T. M. Pehl, K. Halama, P. F. Großmann, A. M. Mühlbach, B. Rieger
WACKER-Chair of Macromolecular Chemistry
Catalysis Research Center
School of Natural Sciences
Technical University of Munich
Lichtenbergstr. 4, 85748 Garching, Germany
E-mail: rieger@tum.de
T. Kratky
Associate Professorship of Physical Chemistry with Focus on Catalysis
Catalysis Research Center
TUM School of Natural Sciences
Technical University of Munich
Lichtenbergstr. 4, 85748 Garching, Germany

The ORCID identification number(s) for the author(s) of this article can be found under https://doi.org/10.1002/mame.202200635

DOI: 10.1002/mame.202200635

ADVANCED SCIENCE NEWS
www.advancedsciencenews.com

Macromolecular Materials and Engineering
Open Access
www.mame-journal.de

polymers, C–H bond activation of substituted α-methylpyridines has been utilized in literature, successfully introducing a variety of different moieties, including alcohols,[17,18] amines and thiols,[18] bipyridines,[19] di- and tripyridine initiators,[20,21] or double-bonds [22] as end-groups. In this approach, an azide-substituted α-methylpyridine is introduced to rare-earth metal-based pre-catalysts like $Cp_2Ln(CH_2TMS)(thf)$ or $[(ONOO)^{tBu}Ln(CH_2TMS)(thf)]$ (Ln = Y, Lu) by means of C–H bond activation. These azide-pyridines then act as initiating groups during polymerization initiation and are covalently linked to the polymer chain end via [2+1] cycloaddition of an in situ formed nitrene by nitrogen elimination, acting as functional anchoring groups.[6–9,18–20,22–24] While this method so far has primarily been used to attach functional moieties like biologically relevant molecules [18,22] or catalysts [19] to solvated polymers in a post-polymerization reaction, it could also be utilized to attach end-groups capable of binding to surface for graft-to approaches. PDEVP has successfully been used in a graft-from approach, but so far to the authors knowledge no graft-to methods are known.[25] Within this manuscript, such a functionalization is introduced in order to covalently couple PDEVP as highly functional REM-GTP-based polymer to multi-walled carbon nanotubes as a proof of principle study.

2. Results and Discussion

2.1. Catalyst Activation and DEVP Polymerization

To be able to introduce the desired azide-moiety to the polymers, a direct approach by C–H bond activation of a functionalized α-methylpyridine is chosen. Starting from 2,6-dimethylpyridine, a chloride is introduced in *para*-position via a literature-known substitution reaction.[22] The obtained 4-chloro-2,6-dimethylpyridine is reacted with hydrazine-hydrate to the corresponding 4-hydrazineyl-2,6-dimethylpyridine. Without prior isolation, the target molecule 4-azido-2,6-dimethylpyridine (PyN_3) is obtained from a diazotisation with sodium nitrite and 5% hydrochloric acid with a total yield of 20 % after purification by column chromatography.[26] Formation of the target compound has been confirmed using elemental analysis, gas-chromatography-(GC-MS), ^{1}H-nuclear magnetic resonance (^{1}H-NMR), and Fourier-transformed infrared spectroscopy (FT-IR) (see Figures S1 and S2, Supporting Information). To dry the pyridine azide for the subsequent C–H bond activation, it is filtered over activated aluminum oxide and a stock solution in dry benzene-d_6 is prepared (see ESI).

To generate the active polymerization catalyst, an in situ C–H bond activation protocol from literature is used, in which 1.0 equivalents of the functionalized pyridine are reacted with 1.0 equivalents of $Cp_2Y(CH_2TMS)(thf)$ at room temperature.[18,22] To assess the reactivity, a C–H bond activation kinetic is measured using ^{1}H-nuclear magnetic resonance spectroscopy at defined time intervals. Surprisingly, the reaction of PyN_3 with $Cp_2Y(CH_2TMS)(thf)$ led to immediate catalyst decomposition as indicated by ^{1}H-NMR and precipitation of a black solid within seconds. This behavior is attributed to the overall higher reactivity of the azide-pyridine. As the yttrium bis(phenolate) catalyst usually shows a lower reactivity toward C–H bond activation and requires higher activation temperatures of 60 °C,[23] in the next step the activation of $[(ONOO)^{tBu}Y(CH_2TMS)(thf)]$ with PyN_3 is tested. Similar to $Cp_2Y(CH_2TMS)(thf)$, upon mixing of the two compounds, the solution immediately turned black, and precipitate formed, indicating catalyst decomposition. This was confirmed using ^{1}H-NMR spectroscopy. As the last approach, lutetium-based pre-catalysts were tested, as lutetium is known to be less reactive toward C–H bond activation compared to yttrium.[23] The reaction of $Cp_2Lu(CH_2TMS)(thf)$ with PyN_3 under the same conditions led to the formation of a dark-green solution without precipitation upon mixing of the two reactants overnight at room temperature, indicating successful C–H bond activation. A kinetic investigation of the activation using ^{1}H-NMR showed complete consumption of PyN_3 within 4 h and formation of tetramethyl silane, revealing the formation of the desired polymerization catalyst (see ESI, Figure S3, Supporting Information). As indicated by the formation of multiple small ^{1}H-NMR signals in the range of the cyclopentadienyl ligand, some minor side products are formed during the C–H bond activation. These side products were separated by filtration of the catalyst mixture over a syringe filter. To ensure full activation PyN_3 and the lutetium pre-catalyst are reacted for 18 h at room temperature prior to polymerization. Unfortunately, all efforts to isolate the obtained catalyst $Cp_2Lu(PyN_3)(thf)$ to confirm its structure failed as they led to catalyst decomposition. To date, the in situ activation of the azidepyridine remains the only way of obtaining the desired catalyst.

Nevertheless, the in situ generated catalyst is used for the polymerization of diethyl vinylphosphonate (DEVP). The results from the polymerization experiments can be found in **Table 1**.

The polymerizations of DEVP with $Cp_2Lu(PyN_3)(thf)$ at various monomer:catalyst ratios of 25:1, 50:1, 100:1, and 200:1 have been performed in toluene at room temperature. All polymers are characterized regarding their conversion using aliquot-^{31}P-NMR, molecular structure using ^{1}H/^{31}P-NMR (Figures S4 and S5, Supporting Information) and molecular weight and polydispersity using size-exclusion chromatography multi-angle light scattering (SEC-MALS) (Figures S6 and S11, Supporting Information). The catalyst is capable of fully polymerizing the available monomer within 2 h for all monomer:catalyst ratios as indicated by ^{31}P-NMR. All polymers exhibit narrow polydispersity below 1.24, highlighting the controlled polymerization of DEVP by the in situ generated catalyst. Surprisingly, the absolute molecular weights of the polymers $M_{n,abs}$ are considerably higher than the calculated molecular weights at full initiator efficiency $M_{n,theo}$, revealing overall low initiator efficiencies of 8.6–14.5%. These initiator efficiencies are about half of the reported literature values for the structural similar lutetium catalyst $Cp_2Lu(sym\text{-}col)(thf)$ without azide functionalities of 21 %.[24] These low initiator efficiencies led to the formation of high molecular weight polymers with $M_{n,abs} > 35$ kg mol^{-1} even at low catalyst:monomer ratios of 25:1. Verification of whether the end-group is attached to the polymer is usually done by ^{1}H-NMR or diffusion ordered (DOSY)-NMR spectroscopy.[17,18] However for the herein prepared polymers this approach is not feasible due to the high molecular weight of the polymers and the overall low number of detectable protons of the PyN_3 end-group. Additionally, the intactness of the azide moiety cannot be ensured by means of NMR spectroscopy. Therefore, oligomers of PDEVP initiated by $Cp_2Lu(PyN_3)(thf)$ are prepared by reacting 1.0 equivalents of the catalyst with 5.0

ADVANCED SCIENCE NEWS
www.advancedsciencenews.com

Macromolecular Materials and Engineering
Open Access
www.mame-journal.de

Table 1. Results from DEVP polymerization with in situ generated $Cp_2Lu(PyN_3)$.

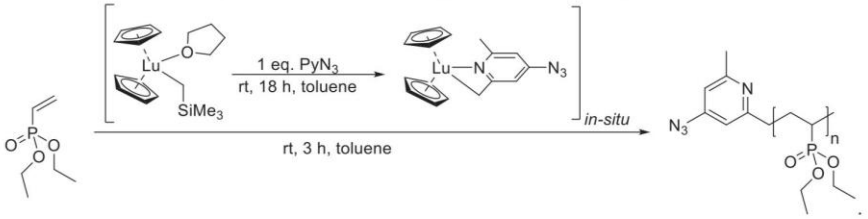

Entry	[DEVP]:[Lu] [a] [-]:[-]	$M_{n,theo}$ [b] [kg mol^{-1}]	$M_{n,abs}$ [c] [kg mol^{-1}]	$Đ$ [c] [-]	I.E. [d] [%]
1	25:1	4.3	36.7	1.17	11.7
2	50:1	8.4	86.7	1.24	9.7
3	50:1	8.4	58.0	1.19	14.5
4	100:1	16.6	185	1.18	9.0
5	100:1	16.6	192	1.24	8.6
6	200:1	33.0	293	1.14	11.3

[a] catalyst-monomer ratio as weighed, 13.5 µmol catalyst in 5 mL toluene, RT, 2 h. [b] theoretical molecular weight via $M_{n,theo} = M_{DEVP} \times X_{DEVP}$ x ([DEVP]/[Lu]). [c] absolute molecular weight $M_{n,abs}$ and polydispersity determined via SEC-MALS (40 °C, THF:H_2O = 1:1 with 9 g L^{-1} *tetra-n*-butyl ammonium bromide and 272 mg L^{-1} 2,6-di-*tert*-butyl-4-methylphenol) using dn/dc = 0.0922 mL g^{-1} for PDEVP. [d] initiator efficiency as, i.e., = $M_{n,theo}/M_{n,abs}$ x 100%.

equivalents of monomer and the oligomers are subjected to ESI-MS measurements directly from the reaction mixture (see ESI, Figure S12, Supporting Information). In the electron-spray ionization mass-spectrometry (ESI-MS), two series can be detected, corresponding to PDEVP oligomers initiated by PyN_3 with an intact azide moiety and one series of PDEVP oligomers with the pyridine lacking the azide moiety, presumably due to decomposition in the ESI-MS. While no quantitative functionalization of the polymers with the azide can be verified, still attachment of the azide via C–H bond activation functionalization is generally possible. The prepared polymers from Table 1 are used for further reactions with the multi-walled carbon nanotubes to assess the proposed functionalization pathway.

2.2. Polymer-Carbon Nanotube Coupling and Characterization

To covalently link the prepared polymers to the multi-walled carbon nanotubes, a [2+1] cycloaddition between the π-electrons of the carbon nanotubes and an in situ formed nitrene by thermally induced nitrogen extrusion of the polymers azide moiety is performed (see ESI).[6–9] Different weight-percent ratios of MWCNT:PDEVP of 1:1, 1:2, and 1:5 of PDEVP with a molecular weight of 192 kg mol^{-1} ($PDEVP_{100}$, Table 1, entry 5) are tested as well as additional 1:5 ratios with different polymer chain lengths of 58.0 kg mol^{-1} ($PDEVP_{50}$, Table 1, entry 3) and 293 kg mol^{-1} ($PDEVP_{200}$, Table 1, entry 6). To assess the loading of the nanotubes with the polymer, elemental analysis of the C, H, N, and P content of all prepared compounds is measured, and the loading is calculated based on the phosphorus percentage found (**Table 2**).

As an additional method of quantification, the prepared composites are subject to thermogravimetric analysis under an argon atmosphere, the corresponding graphs are shown in **Figure 1**.

Pure MWCNTs do not show any decomposition up to 850 °C under argon, while pure PDEVP starts to decompose by loss of its ethyl side chains at 260 °C as indicated by a weight loss of 38 wt.%. Starting at about 450 °C, a second decomposition onset can be detected, attributed to thermal fragmentation of the backbone, followed by a less defined decomposition step at about 800°C, leaving a carbon residue of 18%.[27] Using the first decomposition step of 38 wt.% for pure PDEVP, the relative content of PDEVP on the MWCNTs can be calculated by determining the weight percent difference before and after the first decomposition step and dividing it by 38 wt.%. The loadings determined from elemental analysis and from TGA are compared to each other, the corresponding results are listed in **Table 3**.

Comparison of the loadings determined from EA and TGA shows quite good agreement with deviations of only about 5 wt.%, which are attributed to measurement uncertainties. Overall, the compounds with the lowest initial MWCNT:PDEVP ratio of $PDEVP_{100}$ also show the lowest loading of ≈10 wt.% of polymer content. The two experiments with higher MWCNT:PDEVP ratio (1:2 and 1:5) of $PDEVP_{100}$ achieve about the same degree of functionalization with 21–22 wt.% of polymer. This might be due to steric blocking/coverage of the MWCNT surface by the polymers, impeding azide end-groups from reacting with the MWCNT surface, thus making a higher degree of functionalization impossible. When using shorter-chain $PDEVP_{50}$ in a 1:5 ratio, about the same wt.% of polymer can be detected, corresponding to a higher surface density of functionalized polymer on the carbon nanotubes. This might be due to an overall much shorter chain length of $PDEVP_{50}$ compared to $PDEVP_{100}$ and therefore less sterical hinderance during the graft-to functionalization. For the longest $PDEVP_{200}$, 42 wt.% of polymer loading were determined due to the overall higher molecular weight of the polymer with a similar degree of functionalization as for the MWCNT:PDEVP 1:2 and 1:5 loadings.

Additionally, the functionalization of the carbon nanotubes is investigated using Raman spectroscopy, XPS, and TEM. To access whether MWCNTs have successfully been functionalized, Raman spectra of pure MWCNTs and of MWCNT:$PDEVP_{100}$ = 1:2

ADVANCED SCIENCE NEWS
www.advancedsciencenews.com

Macromolecular Materials and Engineering
Open Access
www.mame-journal.de

Table 2. Elemental analysis results of the MWCNT:PDEVP composites prepared.

Entry	Compound	MWCNT:PDEVP [wt.%]:[wt.%]		C [%]	H [%]	N [%]	P [%]	Loading[a] [wt.%]:[wt.%]
1	pure MWCNTs	1:0	Calculated[b]	100	0.00	0.00	0.00	-
			Found[c]	95.77	0.04	0.00	0.00	-
2	pure PDEVP	0:1	Calculated[b]	43.90	7.98	0.00	18.87	-
			Found[c]	41.15	8.05	0.12	16.85	-
3	MWCNT:PDEVP$_{100}$	1:1	Calculated[b]	69.00	3.99	0.00	9.43	50:50
			Found[c]	87.65	1.23	0.20	2.58	85:15
4	MWCNT:PDEVP$_{100}$	1:2	Calculated[b]	61.47	5.19	0.00	12.27	35:65
			Found[c]	80.70	1.90	0.20	4.84	76:24
5	MWCNT:PDEVP$_{100}$	1:5	Calculated[b]	53.94	6.38	0.00	15.10	20:80
			Found[c]	80.06	1.99	0.00	4.80	75:25
6	MWCNT:PDEVP$_{50}$	1:5	Calculated	53.94	6.38	0.00	15.10	20:80
			Found	81.71	1.66	0.23	4.15	79:21
7	MWCNT:PDEVP$_{200}$	1:5	Calculated	53.94	6.38	0.00	15.10	20:80
			Found	70.81	3.40	0.15	7.33	57:43

[a] loading determined from the wt.% phosphorus found in elemental analysis. [b] expected elemental composition of C, H, N, and P based on the wt.%:wt.% ratios used in the experiments. [c] determined C, H, N, P content from single determination elemental analysis.

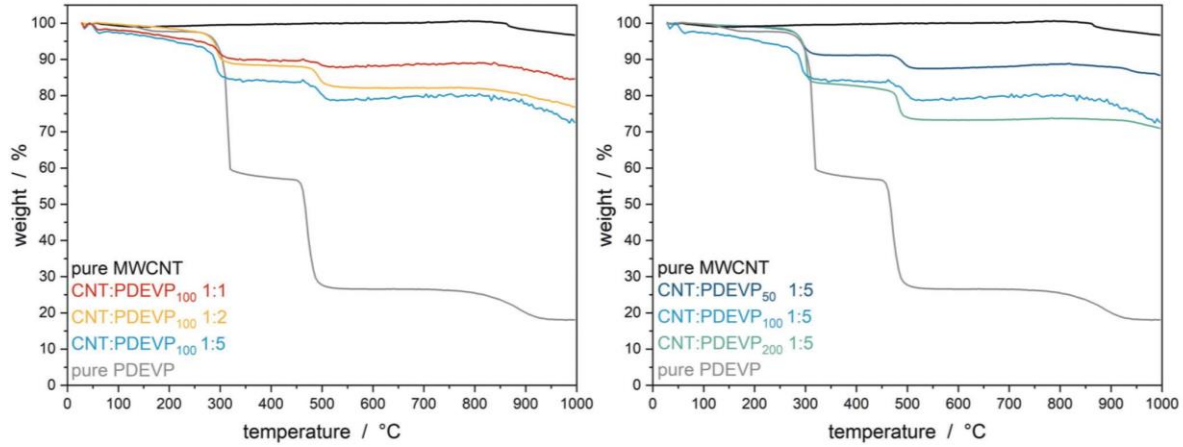

Figure 1. TGA measurements of PDEVP-MWCNT composite materials with varying polymer chain lengths at constant MWCNT:PDEVP ratio (left) and with varying MWCNT:PDEVP functionalization ratios of the same polymer (right).

Table 3. Comparison of MWCNT:PDEVP loading determined via elemental analysis and thermogravimetric analysis.

Entry	Compound	MWCNT:PDEVP [wt%]:[wt%.]	Loading from EA [wt%]:[wt%]	Loading from TGA [wt%]:[wt%]
1	MWCNT:PDEVP$_{100}$	1:1	85:15	90:10
2	MWCNT:PDEVP$_{100}$	1:2	76:24	79:21
3	MWCNT:PDEVP$_{100}$	1:5	75:25	78:22
4	MWCNT:PDEVP$_{50}$	1:5	79:21	78:22
5	MWCNT:PDEVP$_{200}$	1:5	57:43	58:42

(Table 2, entry 4) in the range of 1000–1800 cm^{-1} are measured (Figure S13, Supporting Information). In the Raman spectra, the band at around 1326 cm^{-1} can be assigned to the G band of the sp^2-bonded carbon atoms within the CNT surface layers, while the band between 1570–1610 cm^{-1} can be assigned to the D band of sp^3-hybridized carbon atoms of defects of the carbon nanotubes.[11,13,28] When comparing the D band of pristine MWCNTs with the MWCNT:PDEVP$_{100}$ = 1:2 D band, a slight shift of the band can be observed. While the pure MWCNTs exhibit a single D band with a slight shoulder at higher Raman shifts, for the hybrid material the emergence of an additional band can be observed. This is attributed to a covalent functionalization of the MWCNTs with the polymer via [2+1] cycloaddition, however, this has to be considered with care as the overall amount of new defects due to covalent bonding is

ADVANCED SCIENCE NEWS
www.advancedsciencenews.com

Macromolecular Materials and Engineering
Open Access
www.mame-journal.de

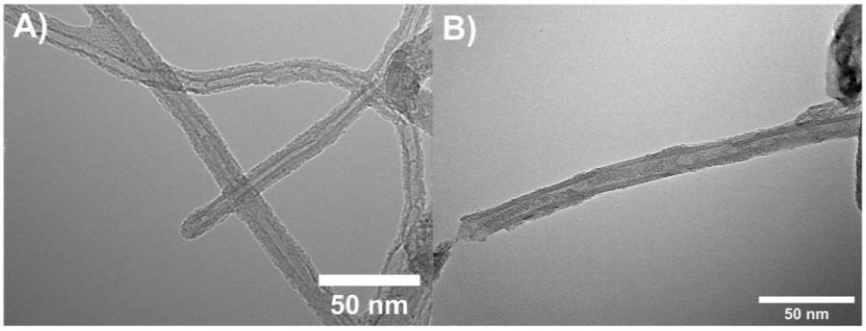

Figure 2. A). TEM images of pristine MWCNTs before functionalization and B) after functionalization with $PDEVP_{200}$ (Table 2, entry 7).

very low compared to the overall surface of the MWCNTs.[13] XPS analysis of pristine carbon nanotubes, pure PDEVP, and the MWCNT:$PDEVP_{100}$ = 1:5 compound material reveals the formation of a hybrid material (Figure S14, Supporting Information), while the attachment point via the nitrogen itself could not be found due to the small quantity of attachment units compared to the overall mass of the MWCNTs and the polymer. Quantification of the corresponding C 1s components gives an MWCNT:$PDEVP_{100}$ ratio of 40:60 ([at% C]:[at% C]) which is substantially lower compared to a ratio of 87:13 ([at% C]:[at% C]) as observed by elemental analysis. The higher fraction of polymer found in XPS evidences a structure of the composite material in which the polymer covers the MWCNT surface leading to an attenuation of the C 1s signal intensity of the MWCNT components. In the TEM pictures, the pristine MWCNT (**Figure 2**A) exhibits a typical homogeneous structure of multiwalled carbon nanotubes featuring a smooth surface with a diameter of 20 nm, for the MWCNT functionalized with $PDEVP_{200}$ (Table 2, entry 7) heterogeneous surface species can be observed (Figure 2B). The higher absorption of the TEM electron beam can be induced by higher adsorption of the phosphorous-containing PDEVP. In addition, TEM allows for a rough estimation of the surface species size, resulting in a diameter of 2 nm and a length of 30 nm, which is in good agreement with the hydrodynamic radius of $PDEVP_{200}$ derived via SEC-MALS. Thus, the authors conclude that the attached surface species is the grafted poly(diethyl vinylphosphonate). The overall high coverage of the MWCNT's surface with the polymer species is in good agreement with the previously observed limit for further polymer immobilization due to steric blocking of the MWCNT surface by, e.g., wrapping.[29]

2.3. Suspension Experiments

In the final step, the functionalized carbon nanotubes are suspended in water to assess the capability of the water-soluble PDEVP to stabilize the nanotubes against coagulation. Suspensions of 0.05 mg mL^{-1} of the MWCNT:PDEVP compound materials in Millipore water are prepared and pictures are taken immediately after suspension, 5 min, 3 h, and 24 h (**Figure 3**). The composites from the 1:5 MWCNT:PDEVP loadings at different chain lengths (A–C) and the composites from the 1:2 and the 1:1 loading with $PDEVP_{100}$ (D, E) are compared to the pure MWC-

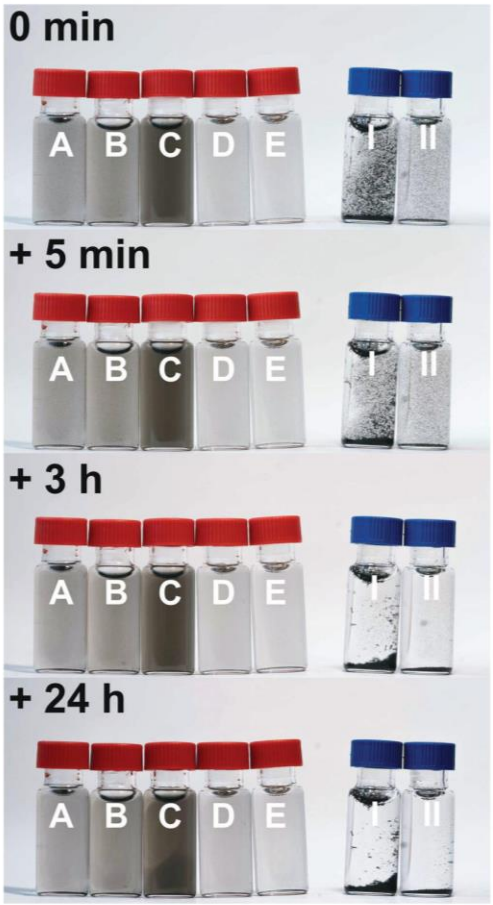

Figure 3. A) MWCNT:$PDEVP_{200}$ = 1:5 (Table 2, entry 7); B) MWCNT:$PDEVP_{100}$ = 1:5 (Table 2, entry 5); C) MWCNT:$PDEVP_{50}$ = 1:5 (Table 2, entry 6); D) MWCNT:$PDEVP_{100}$ = 1:2 (Table 2, entry 4); E) MWCNT:$PDEVP_{100}$ = 1:1 (Table 2, entry 3), I pure MWCNTs without polymer functionalization; II MWCNTs after functionalization with a non-azide functionalized PDEVP as control experiment.

ADVANCED SCIENCE NEWS
www.advancedsciencenews.com

Macromolecular Materials and Engineering
Open Access
www.mame-journal.de

NTs in water (I) and a mixture of carbon nanotubes with non-functionalized PDEVP ($M_{n,abs}$ = 121 kg mol^{-1}, $Đ$ = 1.09) of 1:5 (II) using the same functionalization protocol. Each of the control experiments I and II show immediate coagulation of the carbon nanotubes, forming unstable suspensions. The compounds from lower MWCNT:PDEVP ratios D and E show a lower stabilizing effect, while the compounds from the 1:5 loadings A–C show a good stabilization of the carbon nanotubes in water. This behavior is attributed to an overall higher degree of functionalization from the experiments where more polymer is used for the surface modification. Additionally, we tried triggering the LCST effect of the surface bound PDEVP by heating the samples to 60 °C. Unfortunately, no defined precipitation of the polymer-MWCNT composites could be observed. Overall, the attached PDEVP chains are capable of stabilizing the carbon nanotubes against coagulation, forming stable suspensions, yet the LCST effect of PDEVP is not retained.

3. Conclusion

By means of group-transfer polymerization of DEVP with an in situ generated C–H bond activation-based catalyst from $Cp_2Lu(CH_2TMS)(thf)$ and an azide-substituted pyridine, poly(diethyl vinylphosphonate) was successfully functionalized with an azide polymer end-group. By using a thermally induced nitrene [2+1] cycloaddition, the PDEVPs prepared were covalently linked to MWCNTs via the azide moiety in a graft-to approach. Different polymer chain lengths and polymer to carbon nanotubes have been tested in the functionalization and the loaded compounds were characterized using elemental analysis, thermogravimetric analysis, transmission electron microscopy, raman spectroscopy, and X-ray photoelectron spectroscopy. The polymer on the surface on the carbon nanotube is capable of stabilizing suspensions of MWCNTs in water against coagulation. The herein-presented pathway toward MWCNT functionalization with GTP-based polymers could provide a synthetic tool toward more advanced materials like organic radical polymers immobilized on carbon nanotubes to overcome one of the limiting components of organic radical batteries. Further, the azide functionality itself is an immensely useful building block in organic chemistry to further functionalize organic (macro)molecules via copper-mediated click chemistry, thus opening a feasible pathway for further research.

Supporting Information

Supporting Information is available from the Wiley Online Library or from the author.

Acknowledgements

The authors want to thank Maximilian Stierle for his help with preparing the pyridine azide. Funding Sources: M.K. is grateful for the Ph.D. scholarship from the Studienstiftung des Deutschen Volkes.

Open access funding enabled and organized by Projekt DEAL.

Conflict of Interest

The authors declare no conflict of interest.

Author Contributions

M.K., T.M.P., and K.H., contributed equally to this work. The manuscript was written through the contributions of all authors. All authors have given approval for the final version of the manuscript.

Data Availability Statement

The data that support the findings of this study are available from the corresponding author upon reasonable request.

Keywords

biscyclopentadienyl lutetium catalysts, carbon nanotubes, polymer-composites, polymer-functionalization, polymerization catalysis, rare-earth metal-mediated group-transfer polymerization

Received: November 3, 2022
Revised: December 9, 2022
Published online: December 22, 2022

[1] N. Zhang, S. Salzinger, B. Rieger, *Macromolecules*. **2012**, *45*, 9751.
[2] K. Halama, A. Schaffer, B. Rieger, *RSC Adv.* **2021**, *11*, 38555.
[3] T. M. Pehl, F. Adams, M. Kränzlein, B. Rieger, *Macromolecules*. **2021**, *54*, 4089
[4] C. Friebe, U. S. Schubert, *Top. Curr. Chem.* **2017**, *375*, 19.
[5] a) B. Vigolo, V. Mamane, F. Valsaque, T. N. H.a Le, J. Thabit, J. Ghanbaja, L. Aranda, Y. Fort, E. Mcrae, *Carbon.* **2009**, *47*, 411,; b) P. Bilalis, D. Katsigiannopoulos, A. Avgeropoulos, G. Sakellariou, *RSC Adv.* **2014**, *4*, 2911;
[6] M. Holzinger, J. Abraham, P. Whelan, R. Graupner, L. Ley, F. Hennrich, M. Kappes, A. Hirsch, *J. Am. Chem. Soc.* **2003**, *125*, 8566.
[7] J. Park, M. Yan, *Acc. Chem. Res.* **2013**, *46*, 181.
[8] S. J. Pastine, D. Okawa, B. Kessler, M. Rolandi, M. Llorente, A. Zettl, J. M. J. Fréchet, *J. Am. Chem. Soc.* **2008**, *130*, 4238.
[9] A. Setaro, M. Adeli, M. Glaeske, D. Przyrembel, T. Bisswanger, G. Gordeev, F. Maschietto, A. Faghani, B. Paulus, M. Weinelt, R. Arenal, R. Haag, S. Reich, *Nat. Commun.* **2017**, *8*, 14281.
[10] J. Han, C. Gao, *N.-M. Lett.* **2010**, *2*, 213.
[11] I. Kumar, S. Rana, C. V. Rode, J. W. Cho, *J. Nanosci. Nanotechnol.* **2008**, *8*, 3351.
[12] X. Su, Y.a Shuai, Z. Guo, Y. Feng, *Molecules* **2013**, *18*, 4599.
[13] C. Gao, H. He, L.i Zhou, X. Zheng, Y.u Zhang, *Chem. Mater.* **2009**, *21*, 360.
[14] G. Li, H.u Wang, H. Zheng, R. Bai, *Langmuir* **2010**, *26*, 7529.
[15] H. Li, F. Cheng, A. M. Duft, A. Adronov, *J. Am. Chem. Soc.* **2005**, *127*, 14518.
[16] a) N. G. Sahoo, S. Rana, J. W. Cho, L. Li, S. H. Chan, *Prog. Polym. Sci.* **2010**, *35*, 837; b) A. M. Díez-Pascual, *Macromol.* **2021**, *1*, 64; c) Z. Abousalman-Rezvani, P. Eskandari, H. Roghani-Mamaqani, M. Salami-Kalajahi, *Adv. Colloid. Interface. Sci.* **2020**, *278*, 102126; d) S. Campidelli, *COC.* **2011**, *15*, 1151;
[17] T. M. Pehl, M. Kränzlein, F. Adams, A. Schaffer, B. Rieger, *Catalysts* **2020**, *10*, 448.
[18] A. Schaffer, M. Kränzlein, B. Rieger, *Macromolecules*. **2020**, *53*, 4345.
[19] F. Adams, M. Pschenitza, B. Rieger, *ChemCatChem*. **2018**, *10*, 4309.
[20] P. Pahl, C. Schwarzenböck, F. A. D. Herz, B. S. Soller, C. Jandl, B. Rieger, *Macromolecules*. **2017**, *50*, 6569.
[21] a) A. Saurwein, A. Schaffer, C. Wieser, B. Rieger, *RSC Adv.* **2021**, *11*, 1586; b) P. T. Altenbuchner, P. D. L. Werz, P. Schöppner, F. Adams,

A. Kronast, C. Schwarzenböck, A. Pöthig, C. Jandl, M. Haslbeck, B. Rieger, *Chemistry* **2016**, *22*, 14576;
[22] C. Schwarzenböck, A. Schaffer, P. Pahl, P. J. Nelson, R. Huss, B. Rieger, *Polym. Chem.* **2018**, *9*, 284.
[23] F. Adams, M. R. Machat, P. T. Altenbuchner, J. Ehrmaier, A. Pöthig, T. N. V. Karsili, B. Rieger, *Inorg. Chem.* **2017**, *56*, 9754.
[24] B. S. Soller, S. Salzinger, C. Jandl, A. Pöthig, B. Rieger, *Organometallics* **2014**, *34*, 2703.
[25] N. Zhang, S. Salzinger, B. S. Soller, B. Rieger, *J. Am. Chem. Soc.* **2013**, *135*, 8810.
[26] H. Sawanishi, K. Tajima, T. Tsuchiya, *Chem. Pharm. Bull.* **1987**, *35*, 3175.
[27] D. Lanzinger, S. Salzinger, B. S. Soller, B. Rieger, *Ind. Eng. Chem. Res.* **2015**, *54*, 1703.
[28] M. S. Dresselhaus, G. Dresselhaus, R. Saito, A. Jorio, *Phys. Rep.* **2005**, *409*, 47.
[29] M. Raimondo, C. Naddeo, L. Vertuccio, L. Bonnaud, P. Dubois, W. H. Binder, A. Sorrentino, L. Guadagno, *Nanotechnology.* **2020**, *31*, 225708.

4.5 Addendum

4.5.1 Synthesis of Functionalized Pyridines

In conjunction with the end-group functionalization utilizing an azide, an alkyne-modified pyridine derivative is devised for the AAC complementary. This involves the transformation of 4-chloro-2,6-dimethylpyridine (**1**) into 4-iodo-2,6-dimethylpyridine (**2**) *via* nucleophilic aromatic substitution. By switching from column chromatography to sublimation as the purification method, the yield is increased to 45%. The final initiator, 4-trimethylsilylacetylene-2,6-dimethylpyridine (**3**), can be produced with a 67% yield through copper-catalyzed *Sonogashira* coupling with 1-trimethylsilyl acetylene (Scheme 4.1). To prevent the destruction of the catalyst used in REM-GTP during polymerization, protecting the alkyne by introducing a TMS group is necessary.

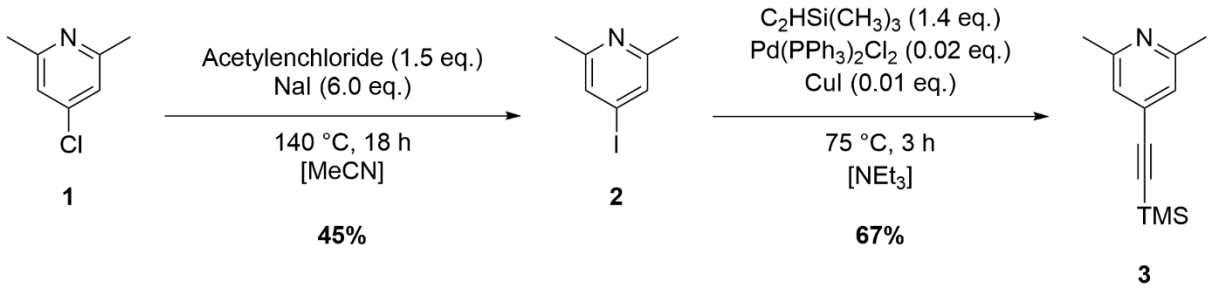

Scheme 4.1: Synthesis route to the alkyne-pyridine (**3**) *via* nucleophilic aromatic substitution and *Sonogashira* coupling.

4.5.2 C-H bond Activation

The pyridine derivative **3** is subsequently activated using the catalyst $Cp_2Y(CH_2TMS)(thf)$, enabling its activation and initiation behavior assessment. To study the kinetic activation of C-H bonds using ^{1}H-NMR, catalyst **4** and alkyne-pyridine **3** are dissolved in deuterated benzene, and regular ^{1}H-NMR analyses are performed at specific time intervals (Figure 4.2). During the reaction, signals from the TMS group (δ = 0.44 ppm) and the CH_2 group (δ = −0.65 ppm) (Figure 4.2, dark orange) of the CH_2TMS initiator, binding to the yttrium center, decrease. Simultaneously, a new signal emerged at δ = 0.00 ppm, indicating tetramethylsilane (Figure 4.2, light orange). The signal of the methyl groups in the α-position to the nitrogen atom of **3** (δ = 2.29 ppm) (Figure 4.2, dark blue) decreases over time, while two new signals at δ = 1.89 ppm and δ = 2.32 ppm are observed (Figure 4.2, light blue). The [2σ+2σ]-cycloaddition of one methyl group at the α-position of the pyridine with the CH_2TMS group of **4** resulted in the successful binding of **3** to the yttrium center. Furthermore, the signal from two protons adjacent to the methyl groups of **4** (δ = 6.83 ppm) (Figure 4.2, black) split during the reaction due to coordination-induced asymmetry to the yttrium complex, forming two new signals. Additionally, the ^{1}H-NMR kinetics indicate selective C-H bond activation without forming side products.

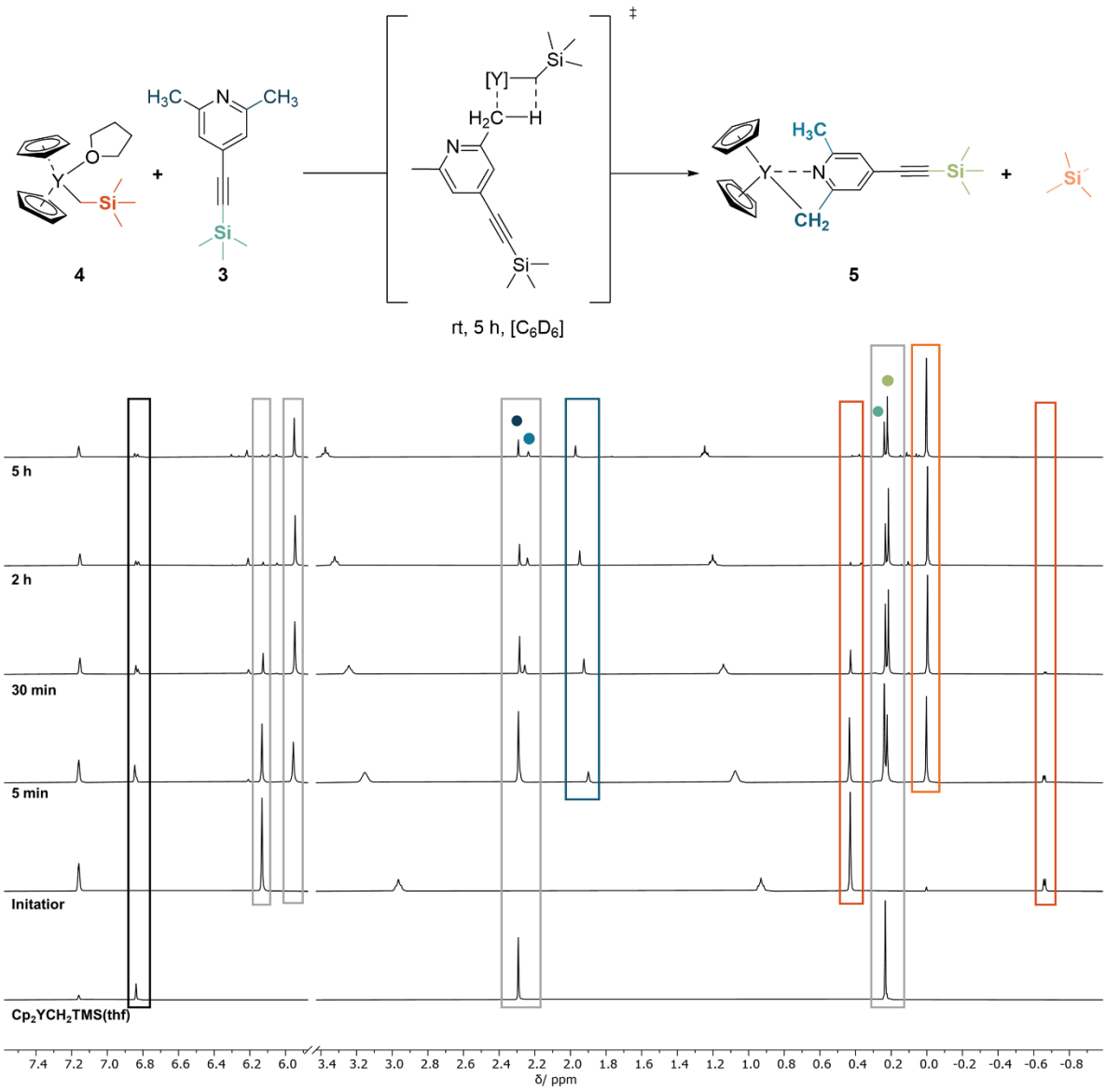

Figure 4.2: ^{1}H-NMR kinetic reaction of the σ-bond metathesis of catalyst **4** with the protected pyridine **3** in benzene-*d6*.

4.5.3 Polymerization

Following the successful demonstration of C-H activation, subsequent test polymerizations using DEVP are conducted. Initially, catalyst **4** is activated in situ with initiator **3**, followed by the addition of monomers (Scheme 4.1). Various monomer-catalyst ratios are tested and compared in Table 4.1.

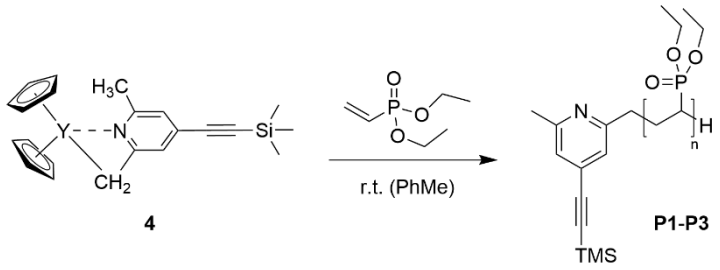

Scheme 4.2: Polymerization of DEVP with the *in-situ* activated catalyst **5**.

Table 4.1: Results from DEVP polymerization of activated catalyst **5** generated in-situ from alkyne-pyridine **3** with $Cp_2Y(CH_2TMS)(thf)$.

Entry	[DEVP]/ [Y][a]	X[b] [%]	$M_{n,theo}$[c] [kg/mol]	$M_{n,abs}$[d] [kg/mol]	$Đ$[d] [-]	I.E.[e] [%]
P1	50/1	99	8.7	19.6	1.09	44
P2	100/1	99	19.7	31.5	1.09	53
P3	200/1	99	33.7	66.1	1.05	50

[a] 13.5 µmol catalyst, 2 mL toluene, rt, 2 h; [b] conversion determined *via* integration of ^{31}P-NMR, [c] theoretical molecular weight determined as $M_{n,theo} = X \cdot M_{DEVP} \cdot [DEVP]/[Y] + M_{ini}$; [d] absolute molecular weight and polydispersity determined *via* SEC-MALS in THF:H_2O with added TBAF, 40 °C, dn/dc = 0.0922 mL/g; [e] initiator efficiency determined *via* I.E. = $M_{n,theo}/M_{n,abs} \cdot 100\%$.

All polymers, **P1-P3**, are analyzed using ^{1}H and ^{31}P-NMR spectroscopy as well as DOSY-NMR, demonstrating complete conversion. MALS-GPC analysis indicates narrow PDIs for all tested polymers, signifying highly controlled polymerization and initiator efficiency ranging between 44-53%. Furthermore, the attachment of the TMS-protected catalyst to the polymer is confirmed via ^{1}H-NMR (Figure 4.3, left). In the ^{1}H spectrum, the signals corresponding to the methyl groups (δ = 0.22 ppm) of the silyl-protecting group of the initiator can be identified. These exhibit identical diffusion coefficients to the polymer signals in the DOSY-NMR spectrum, suggesting that the initiator is attached to the PDEVP polymer and no free initiator **3** remains after purification. Furthermore, the attachment of the initiator **3** to the polymer is confirmed through ESI-MS measurements of DEVP oligomers generated by activated catalyst **5** (Figure 4.3, right). The ESI-MS spectrum reveals the presence of pyridine **3** attached to the oligomer, indicated by a 204 m/z mass shift (corresponding to the initiator **3**) in the DEVP oligomers ($m/z = ((M_{Ini} - H) + n \times M_{DEVP} + H)^+$, n = 2–9). Additionally, unreacted pyridine **3** (m/z = 204) was also detected. The visibility of the initiator groups in ESI-MS suggests a nucleophilic

transfer reaction of the initiator via a monomer insertion into an yttrium-carbon bond during initiation, leading to the desired end group.

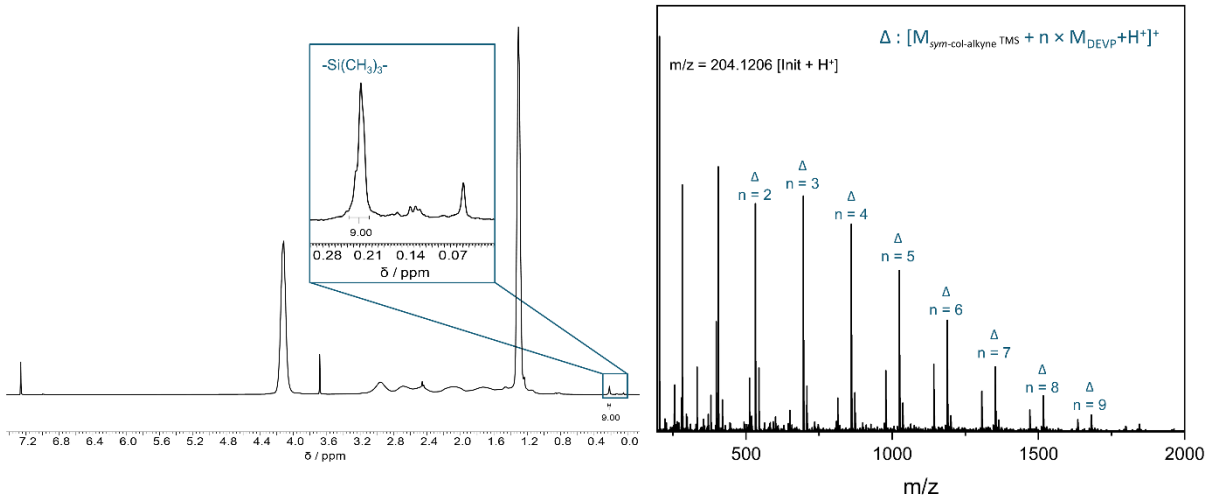

Figure 4.3: ^{1}H-NMR spectrum of PDEVP prepared with the activated **5** with a close-up of silyl region (left) and ESI-MS spectrum of PDEVP oligomers showing the series with the protected alkyne group attached.

4.5.4 End-Group Functionalization via AAC

To restore the reactivity of the alkynes, the TMS group is removed by stirring the polymer with potassium carbonate in methanol overnight at room temperature, leading to complete cleavage of the protecting group, as confirmed by ^{1}H-NMR (Figure 4.4, left). The signal assignable to the TMS-protecting group completely disappeared after the reaction. In addition to demonstrating the presence of the alkyne as the end group, a qualitative study is carried out using ruthenium-catalyzed azide-alkyne click conditions (RuAAC). This involves modifying the alkyne with water-soluble azide-containing dye, specifically 3-aziodo-7-hydroxycoumarin (**6**) (Scheme 4.3).

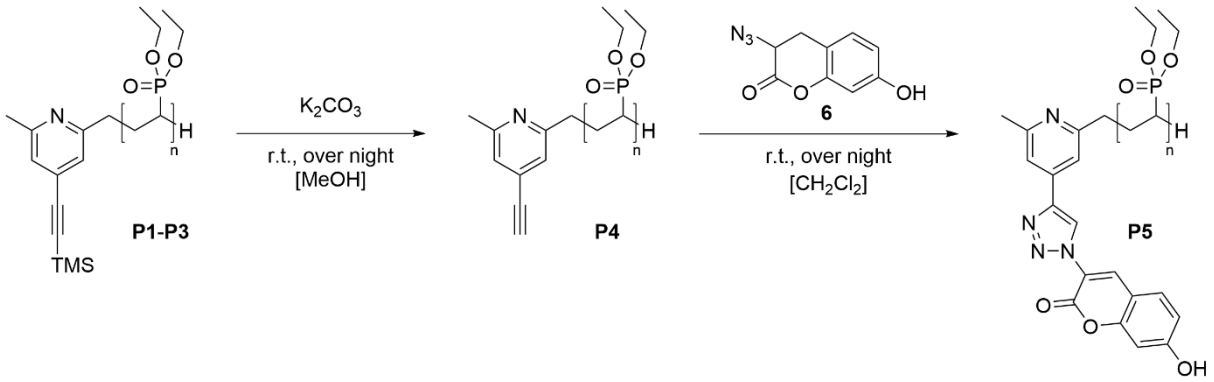

Scheme 4.3: Deprotection of the alkyne end group and functionalization with 3-Azido-7-hydroxycoumarin (**6**) via RuAAC.

After purifying the polymer through dialysis, the confirmation of functionalizing the alkyne end group with dye **6** is determined using fluorescence spectroscopy (Figure 4.4, right). The emission spectrum exhibits a prominent fluorescence band at 490 nm. Overall, this demonstrates both the successful bonding of dye **6** to the polymer chain and the previously successful introduction of an alkyne as an end group.

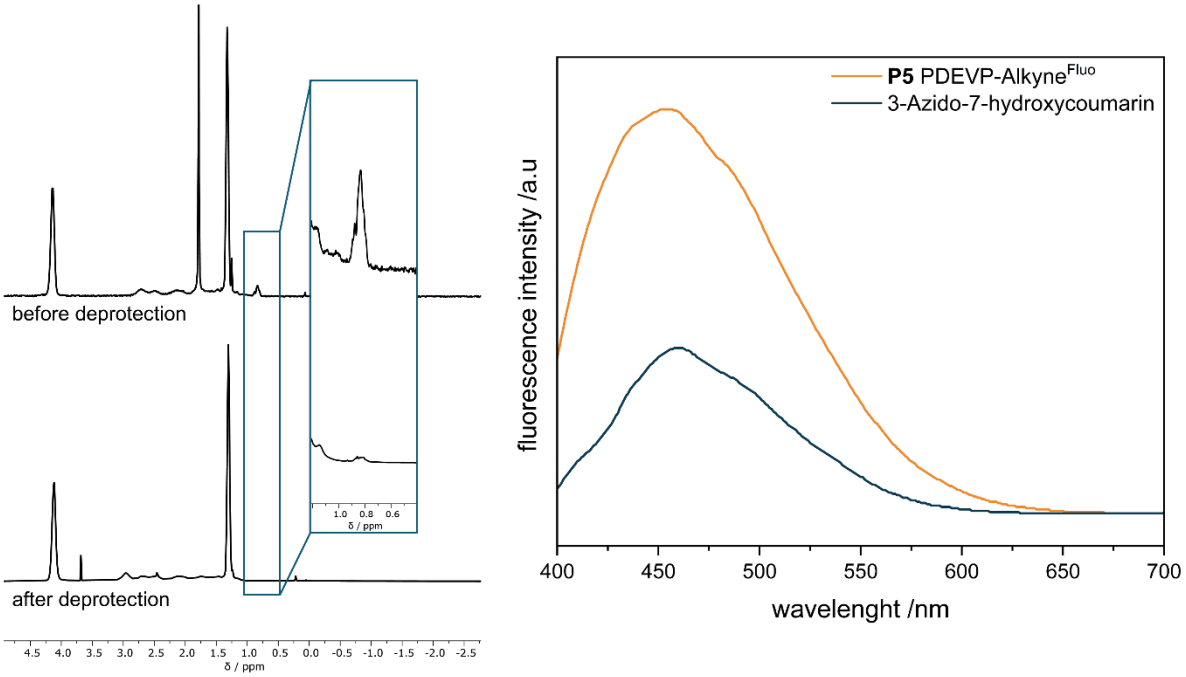

Scheme 4.4: Stacked ^{1}H-NMRs of alkyne-functionalized PDEVP before and after deprotection with a close-up of silyl region (left) and fluorescent spectrum (right) of with coumarin functionalized polymer **P5** (orange) and the dye **6** (blue).

5. Incorporation of Functional Groups into the Polymer Chain through Polymer-Analogous Reactions

"Allyl group-containing polyvinylphosphonates as a flexible platform for the selective introduction of functional groups via polymer-analogous transformations†"

5.1 Bibliographic Data

Title: "Allyl group-containing polyvinylphosphonates as a flexible platform for the selective introduction of functional groups via polymer-analogous transformations†"

Status: Article, Publication Date: 30.11.2021

Journal: RSC Advances

DOI: 10.1039/d1ra06452e

Authors: Kerstin Halama,‡ Andreas Schaffer‡ and Bernhard Rieger *

5.2 Abstract Graphic (TOC)

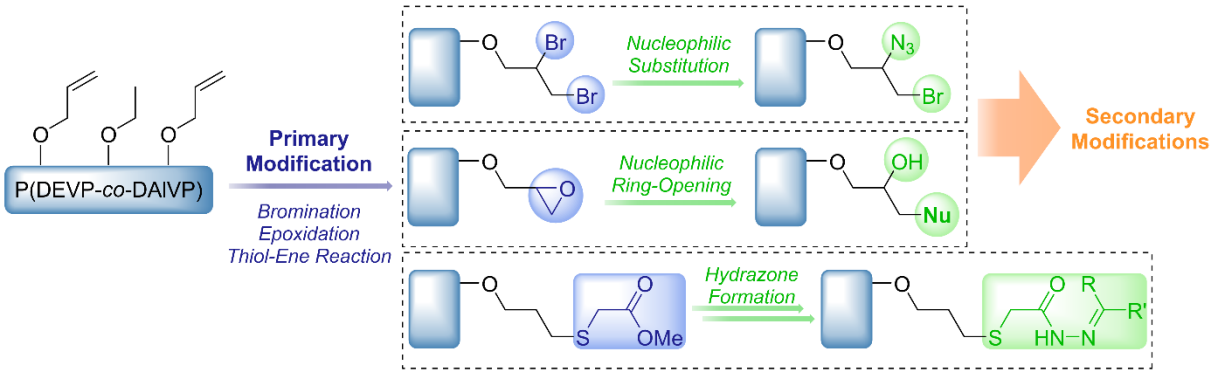

Figure 5.1: Table of content graphic for the manuscript titled "Allyl group-containing polyvinylphosphonates as a flexible platform for the selective introduction of functional groups via polymer-analogous transformations†".

5.3 Content

The task of incorporating functionality into the polymer chain of poly(vinyl phosphonate)s has been previously addressed through diverse approaches, as detailed in Chapter 2.1. In the context of polymer-drug conjugates (Chapter 2.3.1), the challenge extends beyond expanding the platform with novel functional groups to create new anchor points for attaching selected substrates. Equally important is the subsequent coupling of these substrates (or test substrates) is equally important.

In this study, the primary focus revolved around allyl group-containing poly(vinyl phosphonate)s, chosen for their distinctive chemical attributes that confer a high degree of flexibility. The allyl groups serve as reactive sites for subsequent polymer-analogous transformations, including bromination, epoxidation, and thiol-ene click chemistry, enabling precise and selective incorporation of various functional groups. To achieve this, azides were introduced into the brominated and epoxidized polymers for subsequent azide-alkyne couplings, with phenylacetylene as a model substrate. Additionally, the epoxides underwent ring-opening reactions with various organic nucleophiles (phenol, benzylamine, 4-amino-2,1,3-benzothiadiazol). Any unreacted allyl groups were subsequently saturated through orthogonal thiol-ene reactions. Furthermore, methyl thioglycolate was incorporated quantitatively during the basic thiol-ene click reaction and converted into the corresponding hydrazide. The resulting hydrazide was conjugated with 2-hydroxyacetophenone to form a hydrazone linkage between the polymer and small molecules. The selective introduction of functional groups offers the prospect of designing polymers with enhanced characteristics, including improved solubility, biocompatibility, and responsiveness to external stimuli.

5.4 Manuscript

RSC Advances

ROYAL SOCIETY OF CHEMISTRY

PAPER

View Article Online
View Journal | View Issue

Check for updates

Cite this: *RSC Adv.*, 2021, **11**, 38555

Allyl group-containing polyvinylphosphonates as a flexible platform for the selective introduction of functional groups *via* polymer-analogous transformations†

Kerstin Halama,‡ Andreas Schaffer‡ and Bernhard Rieger *

Received 26th August 2021
Accepted 23rd November 2021

DOI: 10.1039/d1ra06452e

rsc.li/rsc-advances

Polyvinylphosphonates are highly promising candidates for (bio)medical applications as they exhibit a tunable lower critical solution temperature, high biocompatibility of homo- and copolymers, and a broad foundation for post-synthetic modifications. In this work we explored polymer-analogous transformations with statistical polyvinylphosphonates comprising diethyl vinylphosphonate (DEVP) and diallyl vinylphosphonate (DAlVP). The C=C double bonds were used as a starting point for a cascade of organic transformations. Initially, the reactive moieties were successfully introduced *via* bromination, epoxidations with *OXONE* and *m*CPBA, or thiol–ene click chemistry with methyl thioglycolate (**6**). The obtained substrates were then employed in a variety of consecutive reactions depending on the introduced functional motif: (1) the brominated substrates were converted with sodium azide to enable the copper-mediated alkyne–azide coupling with phenylacetylene (**1**). (2) The epoxides were reacted with sodium azide for an alkyne–azide click coupling with 1 as well as small nucleophilic compounds (phenol (**2**), benzylamine (**3**), and 4-amino-2,1,3-benzothiadiazol (**4**)). Afterwards the non-converted allyl groups were reacted with thiochloesterol (**5**) to form complex polymer conjugates. (3) An acid-labile hydrazone-linked conjugate was formed in a two-step approach. The polymeric substrates were characterized by NMR, FTIR, and UV/Vis spectroscopy as well as elemental analysis and gel permeation chromatography to monitor the structural changes of the polymeric substrates and to prove the success of these modification approaches.

Introduction

The history of polymer-analogous reactions reaches back to the 19th century, but their actual use was first established by H. Staudinger in 1939.[1] By definition these reactions involve a part of the polymer, but while the degree of polymerization does not change, the molecular weight does not remain necessarily constant throughout the reaction.[2] These reactions differ fundamentally from organic transformations with small molecules. As a result, purification processes are more complex, kinetic parameters can be affected, or the polymer solubility can change during the reaction.[2] Prominent examples are the formation of poly(vinyl alcohol) (PVA) *via* saponification of poly(vinyl acetate)[3] or the synthesis of linear polyethylenimine.[4,5] In addition, polymer-analogous reactions are also used to form derivatives of cellulose and starch or to refine the material properties of polyolefins.[6–8]

Such organic transformations also allow the application of modified polymers in biomedical fields, *i.e.* for (bio)imaging through the conjugation of fluorescent probes,[9] or radiolabeling of polymers for positron emission tomography,[10] which allows advances in cancer diagnostics and monitoring of the therapeutic progress. Yet, the best known are polymer–drug conjugates, which were conceptualized by H. Ringsdorf in 1975.[11,12] This rational design combines a water-soluble polymer backbone that is covalently linked to the targeting moiety and the (pro)drug motif.[12] This concept was extensively used for the synthesis of a plethora of linear polymer conjugates. A broad variety of polymers was investigated ranging from poly(vinyl pyrrolidine),[13,14] PVA,[15] poly(ethylene glycol) (PEG),[16] which is already clinically established due to its high biocompatibility,[17] and *N*-(2-hydoxypropyl)methyl-acrylamide (HPMA).[18] In the case of PEG reactive chain end-groups allow a simple and fast conjugation of small molecules. However, this approach also results in low drug loadings.[19,20] Hence, branched and multi-arm PEGs were developed to overcome this limitation.[21–23] In

WACKER-Chair of Macromolecular Chemistry, Catalysis Research Center, Technical University of Munich, Lichtenbergstraße 4, 85748 Garching near Munich, Germany. E-mail: rieger@tum.de

† Electronic supplementary information (ESI) available: Detailed synthetic procedures of the follow-up functionalisations. Detailed characterisation data (^{1}H-, ^{13}C-, ^{31}P-, and DOSY-NMR spectra, FTIR spectra, UV/Vis spectra, elemental analysis, as well as GPC traces). See DOI: 10.1039/d1ra06452e

‡ These authors contributed equally.

this context, dendrimeric systems are also of great interest, since the synthesis of these types of polymers can be performed with high precision and provide a high density of functional groups at the surface, thus enabling the conjugation of drugs, targeting moieties and imaging agents.[12,24–26] In recent years, researchers also focused on the application of stimuli-responsive polymers, which respond to changes of external stimuli such as pH or temperatures.[12] In exemplary studies doxorubicin was either linked to a HPMA-based polymer[27] or to poly(ethylene oxide)[28] *via* a pH-sensitive hydrazone linkage. In another study thermoresponsive elastin-like polypeptides were labeled with derivatives of rhodamine and were able to show an increased accumulation of polymer aggregates within the tumor tissue by exploiting hyperthermia conditions.[9] The class of polyvinylphosphonates offers interesting properties for biomedical applications, *e.g.* a high biocompatibility[29–32] and tunable cloud points between 5–92 °C.[33–35] The successful synthesis of defined, high-molecular weight poly(diethyl vinylphosphonate) (PDEVP) was performed *via* rare earth metal-mediated group transfer polymerization (REM-GTP) for the first time in 2010 with Cp_2YbMe.[36] Coming from a simple homopolymerization we constantly aimed to push the boundaries of the REM-GTP by expanding the monomer scope towards new functional monomers and (co)polymer and architectures. Initial studies with these polymers also included polymer-analogous reactions such as the saponification and the transesterification of the phosphonate esters. Moreover, REM-GTP facilitated the efficient incorporation of tailor-made end-groups in these polymers at the initial step of the polymerisation.[29,37–39] In this context a bipyridine-based initiator enabled the selective complexation of $Re(CO)_5Cl$ in a copolymer comprising 2-vinylpyridine (2VP) and diethyl vinylphosphonate (DEVP) for the photoreduction of carbon dioxide.[40] An initiator consisting of a vinyl group allowed the precise formation of polymer–biomolecule conjugates with cholesterol and folic acid.[29] Both polymer conjugates were also successfully used in localization studies with HMEC-1 cells.[41] The detection of the conjugates by confocal microscopy required the presence of a fluorescent moiety and was achieved by the introduction of pyrene groups *via* a partial transesterification of the ethyl esters. In addition, block copolymers of 2VP, DEVP, and diallyl vinylphosphonate (DAlVP) were used in the formation of nanoparticular drug carriers.[31] Introduction of this small DAlVP block in the outer shell facilitated the covalent cross-linking *via* thiol–ene click chemistry.

As shown in the literature allyl moieties represent flexible anchors to selectively incorporate biological moieties.[42] In addition, DAlVP-containing polymers are advantageous as two ester per monomer unit can double the loading capacity compared to other copolymer systems (polyethers[28,43] or polylactides[44]). Additionally, the water-solubility can be easily tuned by the DEVP amount. Therefore, no solubilizing motifs such as PEG or zwitterions are required.[44–46] In combination with their intrinsic biocompatibility and a polymerization technique, which enables predictable and reproducible polymerization results, these copolymer types emerge as model candidates for biomedical applications. In this study, we took advantage of the allylic groups introduced through DAlVP and explored a variety of organic transformations of unsaturated carbon–carbon bonds in form of polymer-analogous reactions with statistical P(DEVP-*co*-DAlVP). Starting with basic transformations (bromination, epoxidation, thiol–ene click chemistry), consecutive reactions were performed to investigate the accessibility of the newly introduced, reactive groups and advanced to more complex polymeric structures. Moreover, unreacted allyl groups were converted *via* thiol–ene reactions to form dual-functionalized polymers and mimic the basic architecture of polymer–drug conjugates.

Experimental section

Materials and methods

General. All reactions with air- and moisture-sensitive substances were carried out under an argon atmosphere using standard Schlenk techniques or in a glovebox. Prior to use, all glassware was heat dried under a vacuum. Unless otherwise stated, all chemicals were purchased from Sigma-Aldrich, *ABCR*, or *TCI Europe* and used without further purification. Toluene, THF and DCM were dried using a *MBraun* SPS-800 solvent purification system and stored over 3 Å molecular sieves. The precursor complexes $Y(CH_2Si(CH_3)_3)_3(THF)_2$ and $LiCH_2TMS$ and the catalyst $Cp_2Y(CH_2TMS)(THF)$ were prepared according to procedures found in the literature.[47–50] Diethyl vinylphosphonate (DEVP) was synthesized according to procedures from the literature, dried over calcium hydride, and distilled prior to use.[51] Likewise, diallyl vinylphosphonate (DAlVP) was prepared according to a published procedure.[31,52]

Nuclear magnetic resonance spectroscopy. NMR spectra were recorded on a Bruker AV-400HD and an AVIII-500 Cryo spectrometer. ^{1}H- and ^{13}C-NMR spectroscopic chemical shifts δ were reported in ppm relative to the residual proton signal of the solvent. δ (^{1}H) was calibrated to the residual proton signal, and δ (^{13}C) to the carbon signal of the solvent. Unless otherwise stated, coupling constants J were averaged values and refer to couplings between two protons. All deuterated solvents (C_6D_6, MeOD-d_4) were obtained from Sigma-Aldrich. For the analysis of C–H bond activation products, C_6D_6 was dried and stored over 3 Å molecular sieves in a glovebox. DOSY-NMR measurements were performed for the characterization of polymer conjugates.

Elemental analysis. Elemental analyses were measured on a Vario EL (Elementar) at the Laboratory for Microanalysis of the Institute of Inorganic Chemistry at the Technical University of Munich.

Infrared spectroscopy. FTIR spectra were recorded with a Vertex 70 FTIR (Bruker) using a Platinum ATR from Bruker.

UV/Vis spectroscopy. UV/Vis spectra were recorded on a *Varian* Cary 50 UV/Vis spectrophotometer in 40 mm × 10 mm × 2 mm quartz glass cuvettes. Methanol (HPLC grade) was used as solvent.

Dialysis. Purification *via* dialysis was performed with Spectra/Por 1 dialysis membranes (regenerated cellulose) with a molecular weight cut-off (MWCO) of 6–8 kDa (Spectrumlabs). Prior to use the membranes were treated with deionized water

over night and then rinsed with deionized water. A 100 : 1 ratio of a dialysis fluid to sample volume was applied. Specific solvents used as dialysis fluid were given for the corresponding procedures.

Molecular weight distribution. Gel permeation chromatography was performed with samples of 5 mg mL^{-1} on a combination of a Shimadzu LC-10ADVP with a DGU-3A as degasser (Shimadzu) and a column thermostat CTO-10A (Shimadzu) equipped with two PL Polargel-M columns (Agilent). The eluent used was a mixture of 50% THF and 50% water, treated with tetrabutylammonium bromide (TBAB) (9 g L^{-1}), and 340 mg L^{-1} 3,5-di-*tert*-butyl-4-hydroxytoluene (BHT) as a stabilizing agent. The samples were analyzed *via* multiangle light scattering (MALS) using a Wyatt Dawn Heleos II in combination with a Wyatt Optilab rEX as RI detector unit.

Main synthetic procedures

Synthesis of P(DEVP-*co*-DAlVP) P1. A solution of *sym*-collidine (73.8 mg, 609 μmol, 1.00 equiv.) in absolute toluene (5.00 mL) was added to a solution of $Cp_2Y(CH_2TMS)(THF)$ (23.1 mg, 60.9 μmol, 1.00 equiv.) in absolute toluene (5.00 mL), resulting in the instant yellow coloration of the reaction mixture. After stirring at room temperature overnight, full conversion was verified by proton NMR, and the mixture was diluted with additional toluene (80.0 mL). A mixture of DEVP (9.00 g, 54.8 mmol, 90 equiv.) and DAlVP (1.15 g, 6.09 mmol, 10 equiv.) in absolute toluene (5.00 mL) was then added to the solution in one portion. After four hours, the completion of the polymerization was detected by ^{31}P-NMR spectroscopy. The reaction was quenched by the addition of MeOH (5 mL), and the polymer was precipitated in pentane. The supernatant solvent was decanted off, and the residual polymer was dissolved in water and freeze-dried to yield the pure polymer as a colorless solid.

Procedure for the bromination of P1. Bromine (50.3 mg, 315 μmol, 3.00 equiv. per allyl group) was carefully added to a solution of 100 mg of polymer **P1** ($n_{polymer}$ = 5.00 μmol; n_{allyl} = 105 μmol,[53] 1.00 equiv.) in methylene chloride (8.00 mL). After two hours of stirring at room temperature, proton NMR showed the full conversion of the allyl motifs. The brominated polymer was precipitated in ice cold hexane and washed several times with hexane to remove excess bromine.

General procedure for the epoxidation of P1 with *OXONE*. A solution of **P1** (100 mg, $n_{polymer}$ = 5.00 μmol; n_{allyl} = 105 μmol, 1.00 equiv.) in acetone (5.00 mL) was treated with sodium bicarbonate (74.1 mg, 882 μmol, 8.40 equiv. per allyl group). A solution of *OXONE* (220 mg, 357 μmol, 3.40 equiv. per allyl group) in deionized water (5.00 mL) was added slowly to this suspension. The suspension was stirred for 24 hours at room temperature and the conversion was determined by ^{1}H-NMR (65%). The solids were filtrated off and the resulting polymer solution was used for further transformations.

General procedure for the epoxidation of P1 with *meta*-chloroperbenzoic (*m*CPBA). *m*CPBA (145 mg, 840 μmol, 8.00 equiv. per allyl group) was added to a solution of 100 mg of polymer **P1** ($n_{polymer}$ = 5.00 μmol; n_{allyl} = 105 μmol, 1.00 equiv.) in methylene chloride (6.00 mL). This solution was stirred for 48 hours at room temperature. The conversion (23%) of the allyl groups was checked by proton NMR and excess *m*CPBA was removed by filtration from the ice-cooled reaction mixture. The solution was concentrated *in vacuo* to half its volume and used without further purification for the consecutive modifications.

General procedure for the thermally induced thiol–ene click reaction. The polymer was dissolved in tetrahydrofuran (10 mL THF per 100 mg polymer) and treated with the respective thiol (5.00 equiv. per allyl group) as well as catalytic amounts of azobisisobutyronitrile (AIBN). The mixture was degassed *via* repeated evacuation and filling with argon (20 iterations) and stirred for 24 hours at 60 °C. After quantitative conversion of the allyl motifs was confirmed by ^{1}H-NMR, volatiles were removed under reduced pressure and the residue was dissolved in water. The aqueous solution was purified by dialysis against water and freeze dried to yield the functionalized substrates.

General procedure for the photochemically induced thiol–ene click reaction. The polymer was dissolved in a mixture of tetrahydrofuran and methanol (THF/MeOH = 5/1) (10 mL solvent per 100 mg polymer) and was treated with the respective thiol (5.00 equiv. per allyl group and catalytic amounts of 2,2-dimethoxy-2-phenylacetophenone (DMPA) (0.1 equiv. per allyl group). The mixture was degassed *via* repeated evacuation and filling with argon (15 iterations) and irradiated (λ = 365 nm) for 18 hours. After quantitative conversion of the allyl motifs was confirmed by ^{1}H-NMR, the volatiles were removed under reduced pressure and the residue was dissolved in water. The aqueous solution was purified by dialysis against water and freeze-dried to yield the functionalized substrates.

Results and discussion

Bromination and consecutive modifications of copolymer P1

The first modification route started with the bromination of the allyl groups of **P1** ($M_{n,NMR}$ = 20.0 kg mol^{-1}, n_{DEVP} : n_{DAlVP} = 10 : 1,[54] $Đ$ = 1.04) and was followed by a nucleophilic substitution with NaN_3, to later facilitate an alkyne–azide click reaction between the polymer and a model compound (Scheme 1).

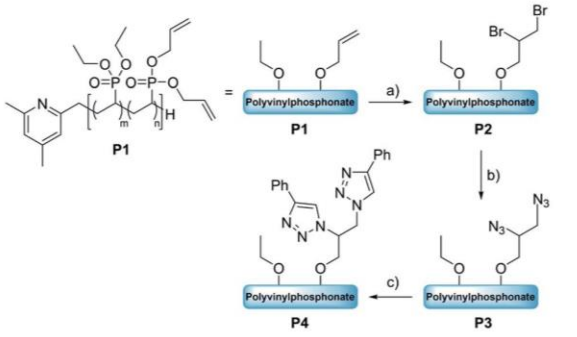

Scheme 1 Transformation of polyvinylphosphonate **P1** to the click adduct **P4** *via* bromination and conversion to the azide. Reaction conditions: (a) Br_2, RT, 2 h [DCM], (b) NaN_3, NH_4Cl, 50 °C, 24 h [DCM/DMF], (c) phenylacetylene (**1**), $CuSO_4 \cdot H_2O$ (cat.), Na ascorbate, RT, 18 h [THF/H_2O].

In the present case copolymer **P1** was treated with bromine and the reaction was monitored by ^{1}H-NMR spectroscopy. After only two hours full conversion of the allyl groups was observed *via* ^{1}H-NMR, since the signals of the allyl groups between 4.50 and 6.20 ppm fully disappeared (Fig. 1, left). A comparison of the integral ratios verified the integrity of **P2**. The section from 1.15 to 2.91 ppm (polymer backbone and $POCH_2CH_3$) was normalized to a value of $I = 1036$ (**P1**: $I = 1036$). Hence, an integral of 547 was determined for the section between 3.44 and 4.79 ppm ($POCH_2$, CHBr and CH_2Br). This value is equivalent to the integral of **P1** between 4.50 and 6.20 ppm ($I = 543$). In addition to the polymer-related bands, an absorption band was found at 594 cm^{-1} (C–Br stretching mode) in the FTIR spectrum (Fig. 1, right). Moreover, analysis *via* GPC-MALS confirmed a defined copolymer with a narrow polydispersity ($M_{n,NMR}$ = 23.4 kg mol^{-1}, $Đ = 1.02$). **P2** was then reacted with NaN_3 in the presence of NH_4Cl at 50 °C for 18 hours (Scheme 1) and dialyzed against water. A qualitative analysis done by IR spectroscopy provided evidence for the presence of the azide group at 2111 cm^{-1} (N=N=N stretching mode) (Fig. S8†). Approximately 53% of the bromide groups were converted during the substitution reaction. These newly introduced azide moieties were investigated in the coupling of phenylacetylene (Scheme 1). Initially, the coupling of phenylacetylene (**1**) to **P3** was performed at 90 °C for 20 to avoid the use of a copper species as catalyst.[55] Unfortunately, the analysis of **P4** done by diffusion ordered spectroscopy (DOSY) revealed two distinct diffusion coefficients for the copolymer and phenylacetylene (**1**). Consequently, the copper-catalyzed click reaction was tested with model compound **1**. Here, the use of $CuSO_4 \cdot H_2O$ in the presence of sodium ascorbate presumably yielded the coupling product as a corresponding DOSY spectrum of the crude product had shown. However, the polymer remained insoluble in a variety of solvents after the work-up, preventing further characterizations. This behavior was explained with the high degree of aromaticity in the polymer side chains reducing the flexibility of the polymer chain by intra- and intermolecular interactions of the aromatic groups.

Epoxidation and follow-up modifications of copolymer P1

Due to the inconveniences with the alkyne–azide click reactions after the bromination of precursor **P1**, the synthetic strategy was focused on the epoxidation of the allyl groups (Scheme 2). Starting from the epoxide-containing polymer a variety of consecutive reactions were performed, namely the ring-opening of the epoxide motif with model nucleophilic reagents (amines, alcohols) and the investigation of the alkyne–azide click reaction after a ring-opening with sodium azide.

Epoxidation of the allyl motifs of P1. In a first attempt the conversion of **P1** was tested with hydrogen peroxide and catalytic amounts of 2,2,2-trifluoroacetophenone.[56] However, no consumption of the allyl groups was observed using these reagents. The epoxidation with *OXONE* as oxidizing agent in water and acetone turned out to be successful. In the corresponding ^{1}H-NMR spectrum of **P5a**, new signals at 2.71 (epoxide), 2.84 (epoxide), 3.94 (PO*CH*), and 4.48 ppm (PO*CH*) corroborated the phosphonate-bound epoxide groups (Fig. 2, green). In comparison to precursor **P1** (Fig. 2, blue) the signal intensities of the allyl groups were clearly reduced and exhibited a conversion of 65% after comparison of the integrals before and after the reaction. However, dialysis against water and lyophilization resulted in an insoluble solid. Presumably, a cross-linking process was initiated *via* the epoxide groups during work-up. Therefore, the reaction media containing the *in situ* generated epoxides were directly used in the consecutive reactions after filtration. Due to the limitation to water/acetone as solvent, the epoxidation of **P1** was also investigated in the presence of *meta*-chloroperbenzoic acid (*m*CPBA) as oxidizing agent. The reaction was performed in DCM over a period of two days. Solid side products were then removed by filtration from

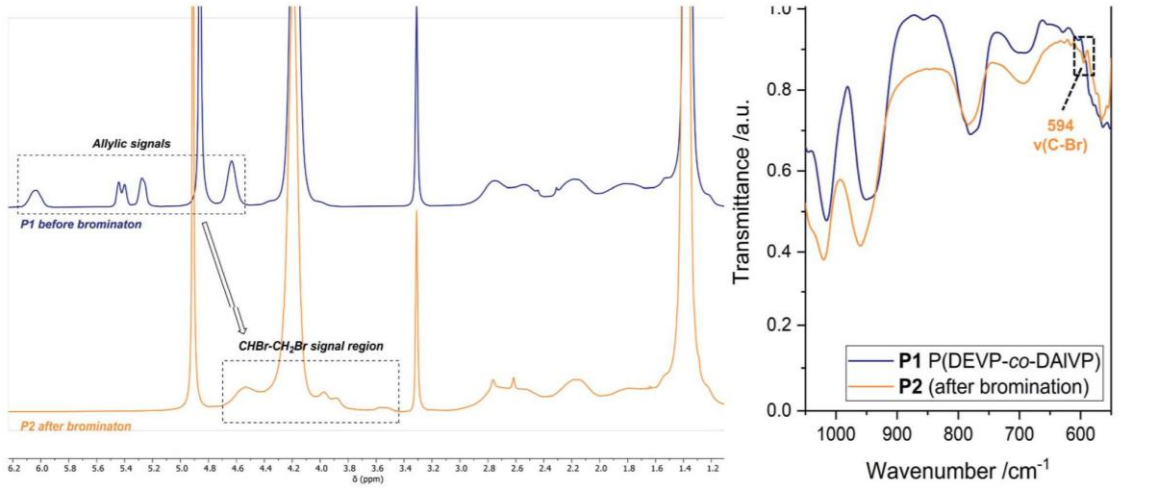

Fig. 1 Left: Comparison of the ^{1}H-NMR spectra before (blue) and after (orange) the bromination reaction measured in MeOD-d_4. Right: Section of the IR spectra of **P1** (blue) and **P2** (orange).

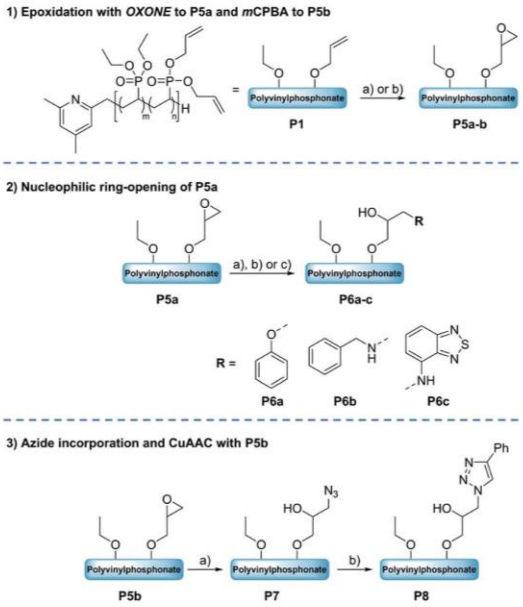

Scheme 2 Top: Epoxidation of **P1** to **P5a–b**: (a) *OXONE*, $NaHCO_3$, RT, 24 h [H_2O/acetone], (b) *m*CPBA, RT, 48 h [DCM]. Middle: Ring-opening of the *OXONE*-derived substrate **P5a** to **P6a–c** with phenol (**2**), benzylamine (**3**) or 4-amino-2,1,3-benzothiadiazol (**4**). Reaction conditions: (a) **2**, NaOH, 50 °C, 24 h [H_2O/acetone], (b) **3**, 50 °C, 24 h [H_2O/acetone], (c) **4**, 50 °C, 24 h [H_2O/acetone]. Bottom: Ring-opening of **P5b** with NaN_3 and subsequent CuAAC to click adduct**P8**. Reaction conditions: (a) NaN_3, NH_4Cl, 50 °C, 24 h [DCM/DMF], (b) **1**, 90 °C, 21 h [Tol].

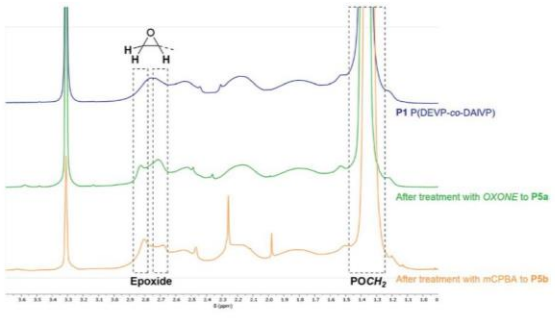

Fig. 2 Comparison of the significant shift regions of polymer **P1** after epoxidation with *OXONE* (**P5a**, green) or *m*CPBA (**P5b**, orange).

an ice-cooled solution. A comparative analysis of the oxidized substrate with the precursor **P1** by means of ^{1}H-NMR spectroscopy showed a consumption of the allyl groups and the occurrence of the epoxide-related signals at 2.68, 2.81, 4.01 and 4.49 ppm (Fig. 2, orange). Compared to the conversion with *OXONE* the reaction with *m*CPBA was less efficient and reached a conversion of 23% with respect to the corresponding amount of allyl groups. The low conversion might be a result of the presence of random coils in solution which can hinder the oxidant from reaching the allyl groups. Moreover, *m*CPBA might be sterically repulsed from the polymer chains due to its bulkiness of the rigid aromatic framework.

Ring-opening of the epoxide motifs. The *OXONE*-derived derivative of **P1** was applied in the nucleophilic ring-opening with phenol (**2**), benzylamine (**3**), and 4-amino-2,1,3-benzothiadiazol (**4**) (Scheme 2, middle) as test substrates. Phenol was reacted with the polyvinylphosphonate-bound epoxide in the presence of sodium hydroxide using the solution with the *in situ*-generated epoxides (*vide supra*). ^{1}H-NMR spectroscopy confirmed the vanishing of the epoxide-related signals, while the phenyl group was able to be assigned to the signals at 6.93 and 7.26 ppm (Fig. 3, blue). According to NMR 34% of the allyl groups are functionalized with phenyl ethers. DOSY-NMR further corroborated the presence of one species exclusively since the aromatic and the phosphonate signals (1.36 and 4.18 ppm) shared the same diffusion coefficient ($D = 4.94 \times 10^{-7}$ cm^2 s^{-1}; Fig. S13†). In addition, two absorption bands at 1497 and 1600 cm^{-1} (C=C bending mode) corroborated the presence of the aromatic groups (Fig. 3, right; Fig. S14†). Likewise, benzylamine (**3**) was coupled to the epoxidized polyvinylphosphonate. The crude solution of the epoxidized copolymer **P1** was treated with the amine and stirred for 24 hours at 50 °C. ^{1}H-NMR confirmed the complete conversion of the epoxide groups and revealed the methylene at 3.65 ppm as well as the benzylic motif between 7.07 and 7.77 ppm (Fig. 3, green) which again shared the same diffusion coefficient ($D = 4.94 \times 10^{-7}$ cm^2 s^{-1}) as the phosphonate esters (Fig. S17†). According to a comparison of the integral values approximately 65% of the original allyl groups are bearing amine groups. However, IR spectroscopy only showed a very weak shoulder at 1495 cm^{-1} that can be assigned to the δ(C=C) mode (Fig. 3, green). In a similar fashion, dye **4** was conjugated to the polyvinylphosphonate. Here, too, the signals of the aromatic framework (6.63, 7.20, 7.41 ppm) could be assigned in the ^{1}H-NMR spectrum (Fig. S20†) with 26% of the allyl groups being conjugated to **4**. The corresponding DOSY spectrum confirmed a covalent conjugation of the dye to the phosphonate framework ($D = 1.13 \times 10^{-6}$ cm^2 s^{-1}, Fig. S21†). A decisive IR band at 1556 cm^{-1} was able to be assigned to C=N vibrations. Moreover, UV/Vis measurements featured changes in the absorption behavior of 4-amino-2,1,3-benzothiadiazol (**4**) since the absorption maximum shifted from 413 nm (free dye) to 422 nm (polymer conjugate). The bathochromic shift can be a result of the interaction of the aromatic motifs due to their spatial proximity, hydrogen bonding between the benzothiadiazole and the newly generated hydroxyl groups, as well as a polarity change of the surrounding environment upon conjugation.[57–59] The introduction of the azide groups was performed with the crude solution containing the copolymer epoxidized by *m*CPBA. Similarly, sodium azide was dissolved in DMF and added to the epoxide-containing solution. The mixture was stirred at 50 °C for 24 hours (Scheme 2). As proven by ^{1}H-NMR spectroscopy the characteristic epoxide signals (compare Fig. 2) vanished during the reaction indicating a quantitative conversion. Analysis by IR supported the success of the reaction by revealing the stretching mode of the azide at 2109 cm^{-1} (Fig. 4). This transformation was followed by the copper-free alkyne–azide coupling with

View Article Online
RSC Advances Paper

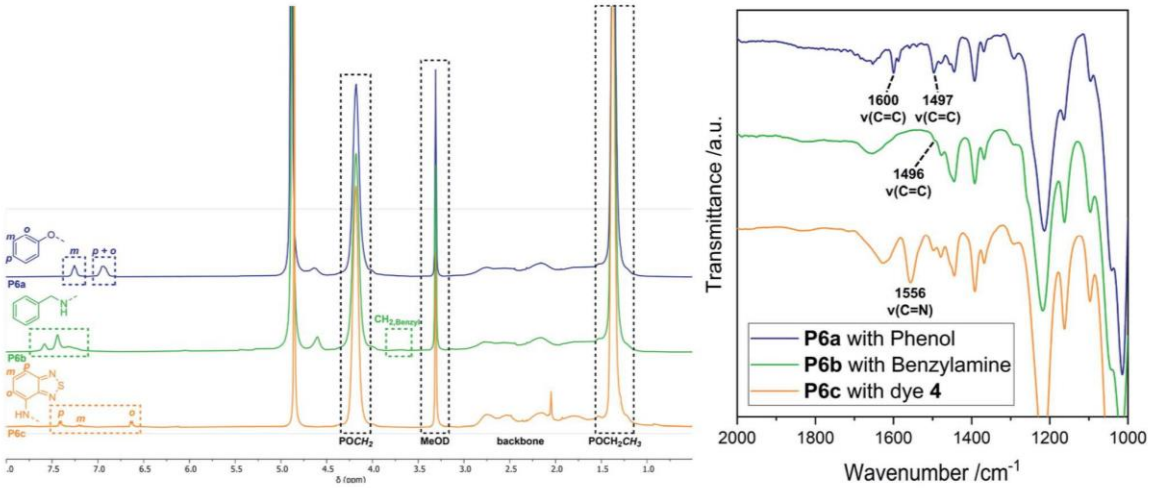

Fig. 3 Left: Comparison of the ^{1}H-NMR spectra of the conjugation products **P6a** (blue), **P6b** (green), and **P6c** (orange) in MeOD-d_4. Exact integral values can be found in the ESI† for each reaction. Right: Zoomed-in view of the IR spectra of the conjugation products **P6a** (blue), **P6b** (green), and **P6c** (orange).

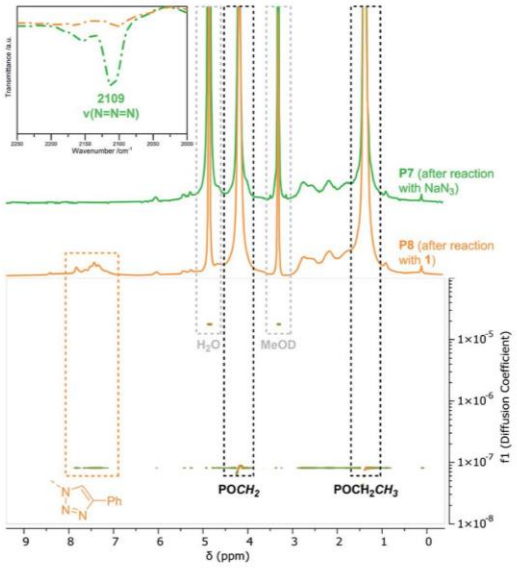

Fig. 4 Comparison of the ^{1}H-NMR spectra recorded in MeOD-d_4 of **P7** (green) and **P8** (orange) and corresponding region of the DOSY-NMR of **P8**. Top left: IR section of the azide vibration before and after azide–alkyne reaction.

phenylacetylene (**1**) at 90 °C. In contrast to the analogue reaction with copolymer **P3** ^{1}H-NMR revealed a successful coupling to **P7**. Two new signal groups emerged between 7.28 and 7.68 ppm corresponding to the triazole motif (49% of all allyl groups). Again, DOSY corroborated a covalent incorporation of aromatic compound **1** since it shared the same diffusion coefficient as the signals of the polyvinylphosphonate (Fig. 4).

Synthesis of dual-functionalized copolymers. As presented, approximately 35% of the allyl groups remained unreacted after treatment with *OXONE* and 77% after using *m*CBPBA. These free allyl groups are easily accessible by mercaptans through the efficient thiol–ene click chemistry. This reaction enabled the introduction of additional functionalities and an imitation of the basic framework of polymer–drug conjugates. Therefore, polymers **P6b** (benzylamine side groups) and **P8** (alkyne–azide coupling adduct) were reacted with thiocholesterol (**5**) (Scheme 3). All modifications were carried out under irradiation of UV light with a wavelength of 365 nm, since light-mediated thiol–ene reactions are known to be more efficient than their temperature-induced equivalents.[60] The modifications of **P6b** were performed in a mixture of tetrahydrofuran and methanol with 2,2-dimethoxy-2-phenylacetophenone (DMPA). A comparison of the ^{1}H-NMR spectra of **P6b** and the functionalized **P9** provided evidence for the conversion of the remaining allyl

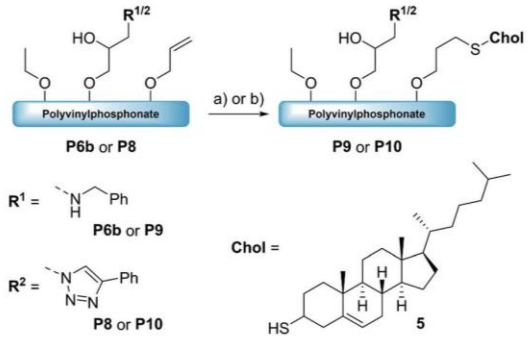

Scheme 3 Formation of the dual-functionalized polymers **P9**and**P10** with thiocholesterol (**5**) *via* thiol–ene chemistry. Reaction conditions: **5**, DMPA, λ = 365 nm, RT, 18 h [THF/MeOH].

groups (Fig. 5). A comparison of the aromatic motif and the isolated methyl group of cholesterol at 0.72 ppm gave a functionalization ratio of 77% (benzylamine) to 23% (cholesterol). The same observation was made for the conversion of **P8** with thiocholesterol to **P10** (Fig. 5). Moreover, DOSY measurements confirm the incorporation of **5** in the polymer chain as the cholesterol-related methyl groups between 0.80 and 1.20 ppm shared the same diffusion level as the polymer signals (Fig. 5). Similarly, a functionalization ratio of 75% (aromatic group) to 25% (cholesterol) was determined.

Introduction of acid-labile hydrazone linkages. In contrast to the previous functionalization strategies, which ought to insert the new, functional groups irreversibly, we also explored the introduction of a reversible hydrazone motif. Due to its pH-sensitivity, pharmaceutically active agents are frequently linked *via* hydrazones, which allows the pH-triggered release of the cargo from the conjugate. In this context, polyvinylphosphonates appear to be promising candidates because each phosphonate repeating unit carries two ester groups, which potentially double the drug-payload compared to other systems. Inspired by the work of Zhong *et al.*,[28] 2-hydroxyacetophenone (**7**) was conjugated to the polymer side chains in a three-step process (Scheme 4). In the first reaction methyl thioglycolate (**6**) was conjugated to **P1** by a thiol–ene click reaction to yield **P11**, which was followed by the conversion to the respective hydrazide **P12**. In a last step, the formation of the hydrazone was studied with ketone **7** (Scheme 4). As visible in the corresponding ^{1}H-NMR spectrum, the allyl groups of **P1** between 4.50 and 6.20 ppm were consumed, while new signals appeared at 2.04 and 2.79 ppm (CH_2 groups adjacent to the thioether bridge) as well as at 3.71 ppm (methyl ester) (Fig. 6A, green). Analysis by DOSY confirmed the presence of one single polymeric species (Fig. S38†). The corresponding IR spectrum corroborates a successful thiol–ene reaction. Compared to the spectrum of **P1**, which exhibits the characteristic absorption bands at 1016 and 1045 cm^{-1} (P–O stretching mode) and 1223 cm^{-1} (P=O stretching mode),[61,62] most decisive is the band at 1736 cm^{-1} that represents the C=O stretching mode of the newly introduced ester (Fig. 6B, green). The addition of hydrazine enabled the conversion of the methyl ester to the respective hydrazide. In the corresponding proton NMR, the signal at 3.71 ppm vanished completely, while the signal structure of the polymer backbone remained untouched (Fig. 6A, orange). DOSY measurements were performed to

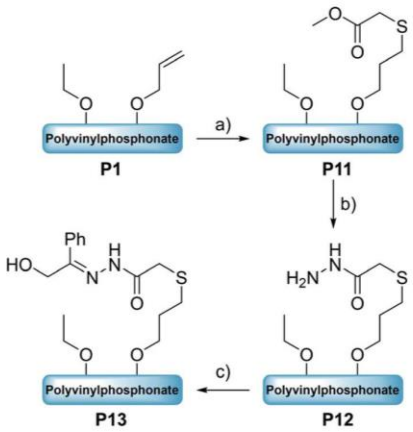

Scheme 4 Transformation of polyvinylphosphonate **P1** to the hydrazine-bearing adduct **P13** *via* a thiol–ene click reaction. Reaction conditions: (a) methyl thioglycolate (**6**), AIBN, 60 °C, 18 h [THF], (b) $H_4N_2 \cdot H_2O$, reflux, 16 h [THF], (c) 2-hydroxyacetophenone (**7**), 4 Å molecular sieves, RT, 24 h [DMF].

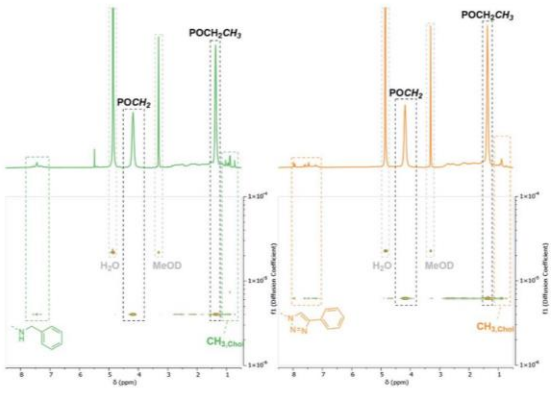

Fig. 5 Respective section of the ^{1}H- and DOSY-NMR of **P6b** (green) and **P8** (orange) after conversion with thiocholesterol (**5**) recorded in MeOD-d_4.

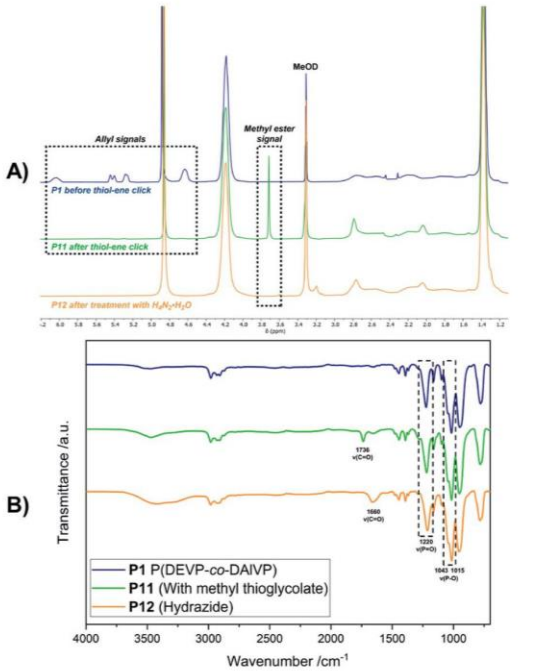

Fig. 6 ^{1}H-NMR spectra in MeOD of polymer **P1**, after conversion with **6**, and after conversion with $H_4N_2 \cdot H_2O$ (A). Respective IR spectra of the polymeric species before and after the transformations (B).

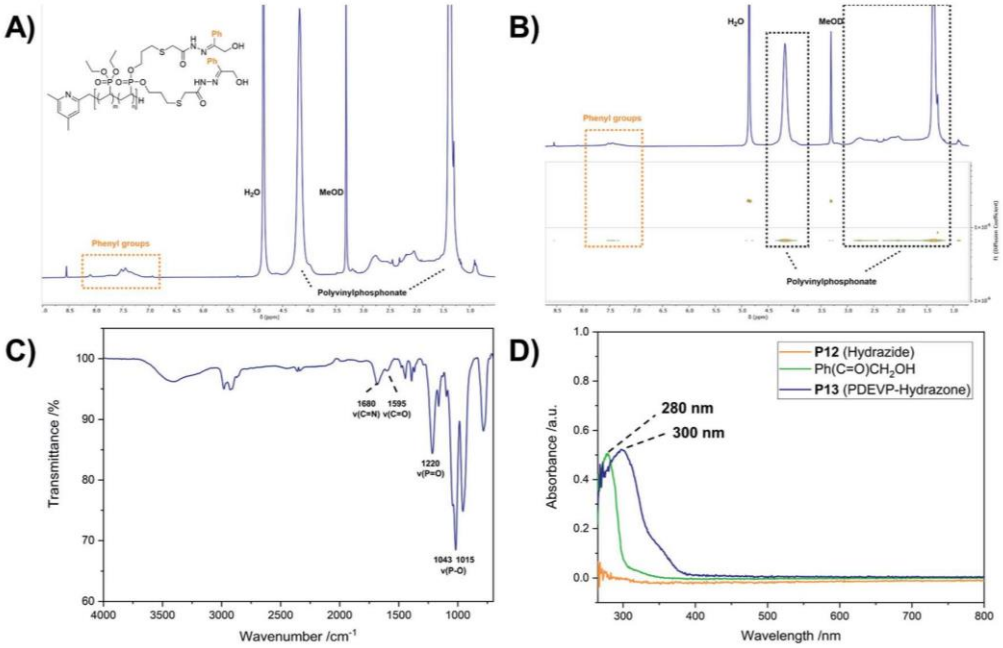

Fig. 7 ^{1}H-NMR spectrum of **P13** in MeOD (A) and corresponding DOSY (B) as well as IR spectrum of **P13** (C). UV/Vis spectra of the hydrazide **P12** (100 μM with respect to the allyl groups), 2-hydroxyacetophenone (**7**) (500 μM) and the hydrazone conjugate **P13** (100 μM with respect to the phenyl groups) in methanol (D).

further confirm the integrity of the polymer (Fig. S42†). The related IR spectrum supports the conclusions made by NMR analysis. The carbonyl-related stretching band shifted from 1736 cm^{-1} to 1660 cm^{-1} (Fig. 6B, orange), which can be explained by the formation of an amide motif. Moreover, the absorption at 3100 to 3600 cm^{-1} is more pronounced, which was accounted for by the N–H stretching mode of the hydrazide motif. However, the O–H stretching mode must also be considered, since the introduction of the polar hydrazides might cause a higher water content after freeze-drying. The hydrazone formation with 2-hydroxyacetophenone (**7**) revealed a new signal pattern in the aromatic region between 6.86 and 8.20 ppm. In comparison to the free ketone **7**, which shows three defined multiplets at 7.54, 7.65 and 7.98 ppm (Fig. S45†), a signal broadening can be observed for the phenyl signals found in the ^{1}H-NMR spectrum of **P13** (Fig. 7A). This concluded the successful conjugation of **7** to the polymer, since the phenyl groups are now statistically distributed along the polymer chain. Again, the presence of a single polymeric species in the respective DOSY spectrum clearly corroborated the successful conjugation (Fig. 7B). A comparison of the integrals of the phenyl signals (I = 62.0) and the phosphonate signal at 4.18 ppm (I = 502) resulted in a coupling efficiency of approximately 60%. Alongside NMR analysis, FTIR measurements revealed two bands at 1595 cm^{-1} and 1680 cm^{-1}, which were referred to the C=O and C=N stretching modes, substantiated the presence of the hydrazone motif (Fig. 7C).[63,64] UV/Vis measurements of **P13** in methanolic solution confirmed a peak at 300 nm, which was not observed for precursor **P12** (Fig. 7D), and exhibits a bathochromic shift of approximately 20 nm compared to the peak of the free compound **7** at 280 nm.

Conclusions

In this study, we explored several synthetic routes to functionalize statistical P(DEVP-*co*-DAlVP) selectively at the position of the allyl groups. Three basic transformations (bromination, epoxidation, and thiol–ene click chemistry) were selected to insert reactive groups for the follow-up modifications. The addition of bromine was found to proceed quantitatively and was transferred into the azide with NaN_3. However, solubility issues rendered the conversion of these azides *via* CuAAC problematic. The epoxidation of the olefines was possible using *OXONE* and *m*CPBA. In the case of *OXONE*, a conversion of 65% of the allyl groups was detected whereas the reaction with *m*CPBA was limited to 23%. The *OXONE*-derived substrate **P5a** was functionalized with phenol, benzylamine or dye **4**. **P5b** was reacted with NaN_3 followed by the conjugation of **1** in a copper-free azide–alkyne cyclization to form species **P8**. In all cases DOSY-NMR confirmed a successful coupling of the model substrates. Moreover, **P6b** and **P8** were converted with thiocholesterol (**5**) and proved that the remaining allyl groups are still accessible to form complex polymer-conjugates potentially mimicking polymer–drug conjugates. This study was concluded by the introduction of an acid-labile hydrazone motif. Therefore, **P1** was subsequently reacted with thiol **6** and hydrazine-hydrate, which was monitored *via* NMR and IR spectroscopy.

Eventually, NMR, IR, and UV/Vis spectroscopy corroborated the successful formation of the hydrazone **P13** from ketone **7**.

Clearly, the polymer-bound allyl groups give access to a rich functionalization chemistry. Combined with the power of the REM-GTP, which allows the production of defined (co)polymers with predictable compositions and architectures, and our experience on their end-group modification, we established a highly flexible and versatile synthetic toolbox for the generation of smart materials. In the future this toolbox allows even more sophisticated conjugates which can comprise a variety of functional agents and are precisely attuned to their intended applications.

Conflicts of interest

There are no conflicts to declare.

Acknowledgements

The authors are grateful to Fabian Späth, Moritz Kränzlein and Jonas Bruckmoser for revising the manuscript.

References

1 H. Staudinger, *Rubber Chem. Technol.*, 1939, **12**, 117–118.
2 S. Koltzenburg, M. Maskos and O. Nuyken, in *Polymer Chemistry*, Springer Berlin Heidelberg, Berlin, Heidelberg, 2017, pp. 407–424, DOI: 10.1007/978-3-662-49279-6_15.
3 L. S. Peixoto, F. M. Silva, M. A. L. Niemeyer, G. Espinosa, P. A. Melo, M. Nele and J. C. Pinto, *Macromol. Symp.*, 2006, **243**, 190–199.
4 B. Brissault, A. Kichler, C. Guis, C. Leborgne, O. Danos and H. Cheradame, *Bioconjugate Chem.*, 2003, **14**, 581–587.
5 R. Tanaka, I. Ueoka, Y. Takaki, K. Kataoka and S. Saito, *Macromolecules*, 1983, **16**, 849–853.
6 Z. Söyler and M. A. R. Meier, *Green Chem.*, 2017, **19**, 3899–3907.
7 T. Heinze, O. A. El Seoud and A. Koschella, in *Cellulose Derivatives: Synthesis, Structure, and Properties*, Springer International Publishing, Cham, 2018, pp. 259–292, DOI: 10.1007/978-3-319-73168-1_4.
8 K. Jedvert and T. Heinze, *J. Polym. Eng.*, 2017, **37**, 845.
9 M. R. Dreher, W. Liu, C. R. Michelich, M. W. Dewhirst and A. Chilkoti, *Cancer Res.*, 2007, **67**, 4418.
10 K. Stockhofe, J. M. Postema, H. Schieferstein and T. L. Ross, *Pharmaceuticals*, 2014, **7**, 392–418.
11 H. Ringsdorf, *J. Polym. Sci., Polym. Symp.*, 1975, **51**, 135–153.
12 N. Larson and H. Ghandehari, *Chem. Mater.*, 2012, **24**, 840–853.
13 H. Kamada, Y. Tsutsumi, Y. Yamamoto, T. Kihira, Y. Kaneda, Y. Mu, H. Kodaira, S.-i. Tsunoda, S. Nakagawa and T. Mayumi, *Cancer Res.*, 2000, **60**, 6416–6420.
14 Y. Kaneda, Y. Tsutsumi, Y. Yoshioka, H. Kamada, Y. Yamamoto, H. Kodaira, S.-i. Tsunoda, T. Okamoto, Y. Mukai, H. Shibata, S. Nakagawa and T. Mayumi, *Biomaterials*, 2004, **25**, 3259–3266.
15 T. Yasukawa, H. Kimura, Y. Tabata, H. Miyamoto, Y. Honda, Y. Ikada and Y. Ogura, *Invest. Ophthalmol. Visual Sci.*, 1999, **40**, 2690–2696.
16 G. Pasut and F. M. Veronese, *Adv. Drug Delivery Rev.*, 2009, **61**, 1177–1188.
17 S. Jevševar, M. Kunstelj and V. G. Porekar, *Biotechnol. J.*, 2010, **5**, 113–128.
18 J. Kopeček and P. Kopečková, *Adv. Drug Delivery Rev.*, 2010, **62**, 122–149.
19 H. Zhao, C. Lee, P. Sai, Y. H. Choe, M. Boro, A. Pendri, S. Guan and R. B. Greenwald, *J. Org. Chem.*, 2000, **65**, 4601–4606.
20 E. K. Rowinsky, J. Rizzo, L. Ochoa, C. H. Takimoto, B. Forouzesh, G. Schwartz, L. A. Hammond, A. Patnaik, J. Kwiatek, A. Goetz, L. Denis, J. McGuire and A. W. Tolcher, *J. Clin. Oncol.*, 2003, **21**, 148–157.
21 Y. Nojima, Y. Suzuki, K. Yoshida, F. Abe, T. Shiga, T. Takeuchi, A. Sugiyama, H. Shimizu and A. Sato, *Pharm. Res.*, 2009, **26**, 2125–2132.
22 G. Prencipe, S. M. Tabakman, K. Welsher, Z. Liu, A. P. Goodwin, L. Zhang, J. Henry and H. Dai, *J. Am. Chem. Soc.*, 2009, **131**, 4783–4787.
23 H. Zhao, B. Rubio, P. Sapra, D. Wu, P. Reddy, P. Sai, A. Martinez, Y. Gao, Y. Lozanguiez, C. Longley, L. M. Greenberger and I. D. Horak, *Bioconjugate Chem.*, 2008, **19**, 849–859.
24 N. Vijayalakshmi, A. Ray, A. Malugin and H. Ghandehari, *Bioconjugate Chem.*, 2010, **21**, 1804–1810.
25 A. R. Menjoge, R. M. Kannan and D. A. Tomalia, *Drug Discovery Today*, 2010, **15**, 171–185.
26 I. J. Majoros, C. R. Williams, A. Becker and J. R. Baker Jr, *Wiley Interdiscip. Rev.: Nanomed. Nanobiotechnol.*, 2009, **1**, 502–510.
27 K. Ulbrich, T. Etrych, P. Chytil, M. Jelínková and B. Říhová, *J. Controlled Release*, 2003, **87**, 33–47.
28 L. Zhou, R. Cheng, H. Tao, S. Ma, W. Guo, F. Meng, H. Liu, Z. Liu and Z. Zhong, *Biomacromolecules*, 2011, **12**, 1460–1467.
29 C. Schwarzenböck, A. Schaffer, P. Pahl, P. J. Nelson, R. Huss and B. Rieger, *Polym. Chem.*, 2018, **9**, 284–290.
30 C. Schwarzenböck, S. I. Vagin, W. R. Heinz, P. J. Nelson and B. Rieger, *Macromol. Rapid Commun.*, 2018, **39**, 1800259.
31 C. Schwarzenböck, P. J. Nelson, R. Huss and B. Rieger, *Nanoscale*, 2018, **10**, 16062–16068.
32 P. T. Altenbuchner, P. D. L. Werz, P. Schöppner, F. Adams, A. Kronast, C. Schwarzenböck, A. Pöthig, C. Jandl, M. Haslbeck and B. Rieger, *Chem.–Eur. J.*, 2016, **22**, 14576–14584.
33 F. Adams, P. T. Altenbuchner, P. D. L. Werz and B. Rieger, *RSC Adv.*, 2016, **6**, 78750–78754.
34 N. Zhang, S. Salzinger and B. Rieger, *Macromolecules*, 2012, **45**, 9751–9758.
35 S. Salzinger, U. B. Seemann, A. Plikhta and B. Rieger, *Macromolecules*, 2011, **44**, 5920–5927.
36 U. B. Seemann, J. E. Dengler and B. Rieger, *Angew. Chem.*, 2010, **122**, 3567–3569.

37 B. S. Soller, S. Salzinger, C. Jandl, A. Pöthig and B. Rieger, *Organometallics*, 2015, **34**, 2703–2706.
38 P. Pahl, C. Schwarzenböck, F. A. D. Herz, B. S. Soller, C. Jandl and B. Rieger, *Macromolecules*, 2017, **50**, 6569–6576.
39 A. Schaffer, M. Kränzlein and B. Rieger, *Macromolecules*, 2020, **53**, 4345–4354.
40 F. Adams, M. Pschenitza and B. Rieger, *ChemCatChem*, 2018, **10**, 4309–4316.
41 C. Schwarzenböck, A. Schaffer, E. Nößner, P. J. Nelson, R. Huss and B. Rieger, *Chem.–Eur. J.*, 2018, **24**, 2584–2587.
42 H. Yang, A. Sun, C. Chai, W. Huang, X. Xue, J. Chen and B. Jiang, *Polymer*, 2017, **121**, 256–261.
43 X. Guan, X. Hu, S. Liu, Y. Huang, X. Jing and Z. Xie, *RSC Adv.*, 2014, **4**, 55187–55194.
44 H. Sun, L. Yan, M. Y. Z. Chang, K. A. Carter, R. Zhang, L. Slyker, J. F. Lovell, Y. Wu and C. Cheng, *Nanoscale Adv.*, 2019, **1**, 2761–2771.
45 H. Sun, M. Y. Z. Chang, W.-I. Cheng, Q. Wang, A. Commisso, M. Capeling, Y. Wu and C. Cheng, *Acta Biomater.*, 2017, **64**, 290–300.
46 H. Sun, L. Yan, R. Zhang, J. F. Lovell, Y. Wu and C. Cheng, *Biomater. Sci.*, 2021, **9**, 5000–5010.
47 K. C. Hultzsch, P. Voth, K. Beckerle, T. P. Spaniol and J. Okuda, *Organometallics*, 2000, **19**, 228–243.
48 G. D. Vaughn, K. A. Krein and J. A. Gladysz, *Organometallics*, 1986, **5**, 936–942.
49 C.-X. Cai, L. Toupet, C. W. Lehmann and J.-F. Carpentier, *J. Organomet. Chem.*, 2003, **683**, 131–136.
50 S. Salzinger, B. S. Soller, A. Plikhta, U. B. Seemann, E. Herdtweck and B. Rieger, *J. Am. Chem. Soc.*, 2013, **135**, 13030–13040.
51 S. Salzinger, PhD thesis, Technical University of Munich, 2013.
52 L. Rigger, R. L. Schmidt, K. M. Holman, M. Simonović and R. Micura, *Chem.–Eur. J.*, 2013, **19**, 15872–15878.
53 The uneven number of allyl groups is a result of their calculation. On a molecular level each individual chain contributes an even number of allyl groups. However, the number mean of the copolymer composition averaged out to be an uneven number on a macroscopic level.
54 Compared to the feed ration the polymer composition tended slightly in favour of DEVP. The propagation rate is dependent from the bulkiness of the phosphonate ester. Here, DEVP is slightly less bulky than DAlVP leading to a faster consumption which is represented by a slightly higher content in the resulting copolymer. Same observations can be found in the literature for the conversion of methacrylates derivatives with zirconocenes.
55 R. Huisgen, *Angew. Chem., Int. Ed.*, 1963, **2**, 565–598.
56 D. Limnios and C. G. Kokotos, *J. Org. Chem.*, 2014, **79**, 4270–4276.
57 D. Seo, J. Park, T. J. Shin, P. J. Yoo, J. Park and K. Kwak, *Macromol. Res.*, 2015, **23**, 574–577.
58 K. K. Bansal, E. Özliseli, A. Rosling and J. M. Rosenholm, *Adv. Funct. Mater.*, 2021, **31**, 2101998.
59 K. Takagi, H. Takao and T. Nakagawa, *Polym. J.*, 2013, **45**, 396–400.
60 L. M. Campos, K. L. Killops, R. Sakai, J. M. J. Paulusse, D. Damiron, E. Drockenmuller, B. W. Messmore and C. J. Hawker, *Macromolecules*, 2008, **41**, 7063–7070.
61 N. Zhang, S. Salzinger, F. Deubel, R. Jordan and B. Rieger, *J. Am. Chem. Soc.*, 2012, **134**, 7333–7336.
62 Q. Wang, S. Chen, Y. Liang, D. Dong and N. Zhang, *Macromolecules*, 2017, **50**, 8456–8463.
63 D. Sadhukhan, A. Ray, G. Pilet, G. M. Rosair, E. Garribba, A. Nonat, L. J. Charbonnière and S. Mitra, *Bull. Chem. Soc. Jpn.*, 2011, **84**, 764–777.
64 Z.-Y. Yin, J.-H. Hu, Q.-Q. Fu, K. Gui and Y. Yao, *Soft Matter*, 2019, **15**, 4187–4191.

6. Orthogonally Functionalization of Poly(vinyl phosphonate)s by Developing New Monomers

"Cytocompatible Triblock Copolymers with Controlled Microstructure enabling Orthogonally Functionalized Bio-Polymer-Conjugates"

6.1 Bibliographic Data

Title: **"**Cytocompatible Triblock Copolymers with Controlled Microstructure Enabling Orthogonally Functionalized Bio-Polymer-Conjugates"

Status: Article, Publication Date: 06.02.2024

Journal: Macromolecules

DOI: 10.1021/acs.macromol.3c02238

Authors: Kerstin Halama, Molly Tzu-Yu Lin, Andreas Schaffer, Marvin Foith, Friederike Adams, Bernhard Rieger*

6.2 Abstract Graphic (TOC)

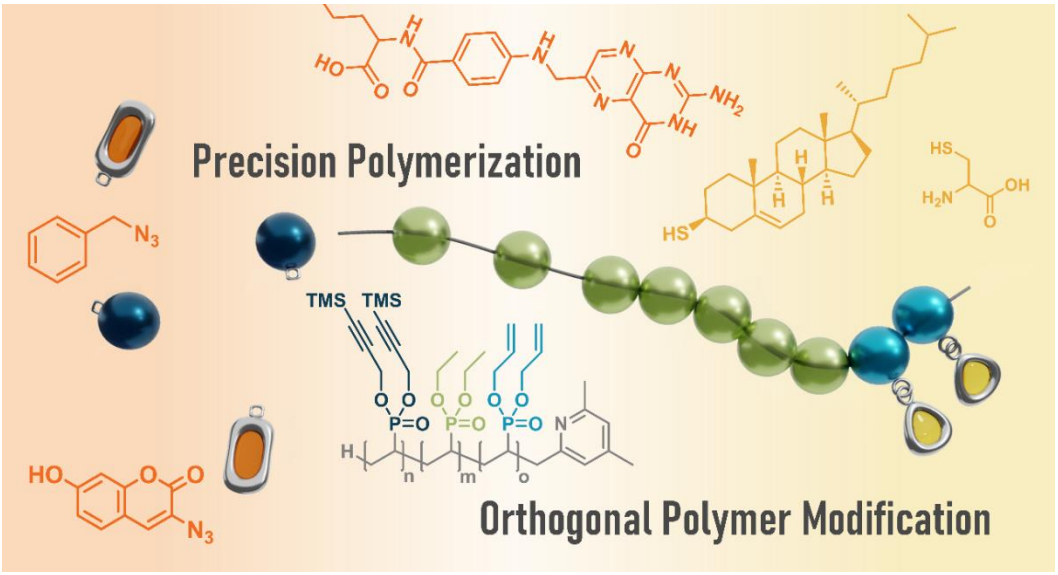

Figure 6.1: Table of Content graphic for the manuscript titled **"**Cytocompatible Triblock Copolymers with Controlled Microstructure Enabling Orthogonally Functionalized Bio-Polymer-Conjugates".

6.3 Content

Copolymerization with poly(vinyl phosphonate)s provide a targeted approach to adjusting polymer properties (Chapter 2.1.3). Additionally, incorporating functional groups into monomers allows a high level of control over their location and number. This aspect is crucial in producing liposome linkers (Chapter 2.3.1), making the development of new functionalized monomers essential for achieving site-specific multiple functionalization.

Precision polymerization via REM-GTP was applied to selectively introduce allyl and propargyl groups into poly(vinyl phosphonate)s, using their specific advantages. These functional groups are adaptable anchors for the subsequent selective incorporation of various biological substrates. To achieve this, poly(vinyl phosphonate)e monomers with compatible functional side groups were selected, and they were paired with diethyl vinyl phosphonate (DEVP), renowned for its heightened water solubility and excellent biocompatibility. The efforts resulted in the synthesis of α,ω-block copolymers, facilitating orthogonal functionalization through azide-alkyne cycloaddition (AAC) followed by a thiol-ene click reaction. This method allowed for the precise introduction of various model substrates at specific sites within the polymers. The success of post-polymerization functionalization and sequential modification of propargyl groups was confirmed using aromatic benzyl azide and the dye 3-azido-7-hydroxycoumarin. Additionally, the functionalization of allyl groups with cysteamine was realized. In the context of potential biomedical applications, the synthesis of polymer conjugates incorporating cholesterol, a vital component of cell membranes, and folic acid, a targeting moiety known for its specific binding to the folic acid receptor (FR-α), was explored. Notably, these conjugates and α-allyl-ω-propargyl-block-co-poly(vinyl phosphonate) demonstrated exceptional cell viability.

6.4 Manuscript

Macromolecules

Open Access

pubs.acs.org/Macromolecules

Article

Cytocompatible Triblock Copolymers with Controlled Microstructure Enabling Orthogonally Functionalized Bio-polymer Conjugates

Kerstin Halama, Molly Tzu-Yu Lin, Andreas Schaffer, Marvin Foith, Friederike Adams, and Bernhard Rieger*

Cite This: *Macromolecules* 2024, 57, 1438–1447

Read Online

ACCESS | Metrics & More | Article Recommendations | Supporting Information

ABSTRACT: α,ω-Functionalized block copolymers create various opportunities across myriads of applications such as linkers for targeted drug delivery systems. Combining them with the exceptional properties of polyvinyl phosphonates, such as high control over polymer architecture and biocompatibility, further reinforces their benefits. This study focuses on synthesizing the α-allyl-ω-TMSpropargyl-*block-co*-polymer P(DAlVP-DEVP-DPrTMSVP) by rare-earth metal-mediated group transfer polymerization. The monomers involved in this process are functionalized diallyl vinyl phosphonate (DAlVP) and dipropargyl vinyl phosphonate (DPrTMSVP), as well as hydrophilic diethyl vinyl phosphonate (DEVP), enabling the incorporation of diverse functionalities into the polymer structure. Click chemistry, including azide-alkyne cycloaddition (AAC) and thiol-ene reactions, facilitates specific and controlled modifications of polymer side chains. Various model substrates, such as benzyl azide, 3-azido-7-hydroxycoumarin, and cysteamine, show the scope of these modifications. The potential in (bio)medical applications is proven with the polymer−biomolecule conjugate α-cholesteryl-ω-folate-*block-co*-polyvinyl phosphonate, exhibiting remarkable biocompatibility. Our versatile approach also establishes a synthetic platform for drug delivery systems, for instance, in targeted therapy.

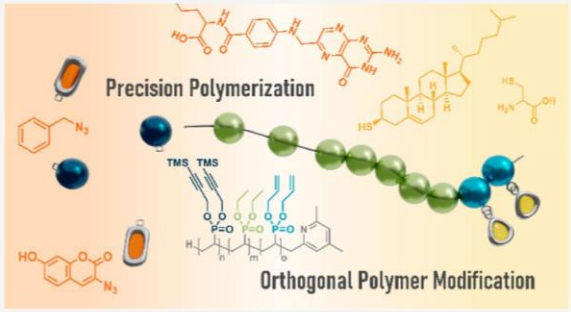

1. INTRODUCTION

Precisely defined and highly functionalized polymers exhibit a high potential in various applications, including biomedical administrations and delivery systems.[1−3] In addition to forming amphiphilic block copolymer-based systems such as micelles and polymersomes, there is great interest in the surface modification of liposomes and polymersomes using specially designed polymer substrate conjugates.[3−7]

One extensively utilized polymer for these purposes is poly(ethylene glycol) (PEG), which is well established as a precursor for therapeutic agents and highly valuable in designing targeted drug delivery systems. PEGylation, the covalent and noncovalent attachment of PEG to different biologically relevant motifs, offers several advantages, such as increasing half-life, reducing immunology, improving solubility, and enhancing stability.[8] PEG also plays a crucial role in site-specific targeting therapeutics and enables the modification of nanoparticles.[9,10] Functionalized macromolecule conjugates are often based on precursor polymers with (different) functional end groups, including both homo (same functional groups on both chain ends) and hetero bifunctional (different functional moieties) systems achieved through initiator/terminating agents or by postpolymerization approaches.[11,12]

Another option for equipping linear polymers with multifunctional units is using triblock copolymers of the ABC type, allowing the incorporation of three different blocks with distinct functionalities and properties.[13] This structure provides a broad range of synthetic options for the sequential, orthogonal functionalization of the blocks with varying functional groups and the potential to access self-assembled nanostructures.[14,15] Achieving precise control over the distribution and placement of functional moieties along the macromolecular backbone offers the opportunity for well-defined polymer conjugates through targeted orthogonal modification.

"Click" chemistry, introduced by Sharpless and co-workers in 2001, shows a valuable concept for subsequent functionalization of various polymeric materials.[15,16] It provides high

Received: November 2, 2023
Revised: January 18, 2024
Accepted: January 24, 2024
Published: February 6, 2024

https://doi.org/10.1021/acs.macromol.3c02238
Macromolecules 2024, 57, 1438−1447

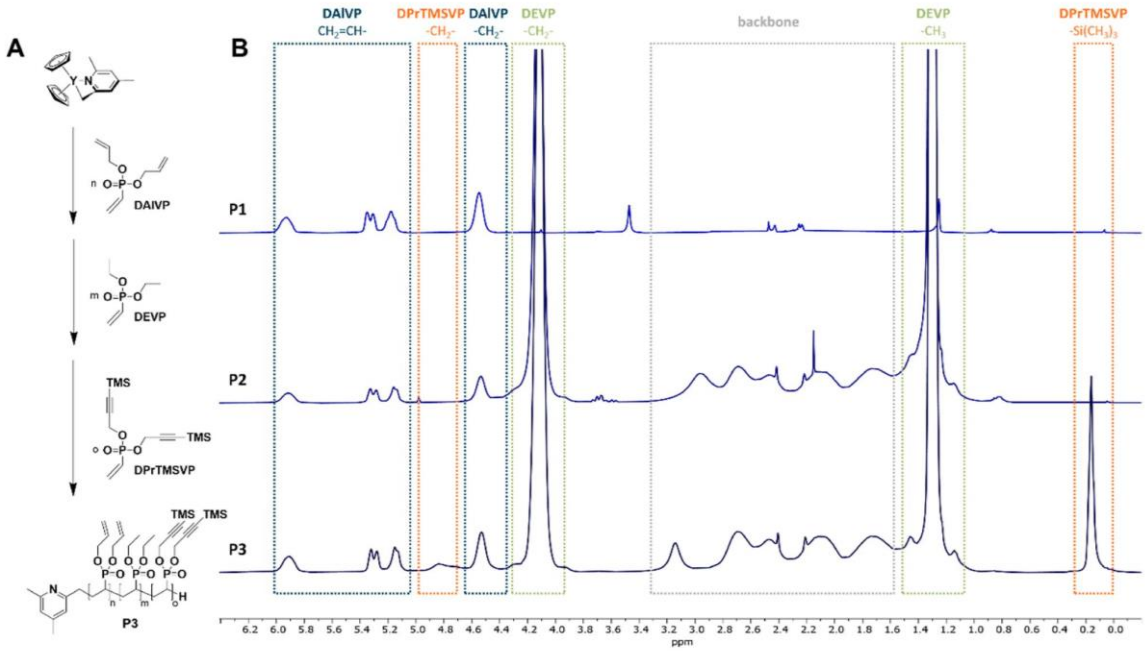

Figure 1. Sequential REM-GTP of DAlVP, DEVP, and DPrTMSVP with the CH-bond activated species of $Cp_2YCH_2TMS(thf)$ at room temperature (A). Comparison of ^1H NMR spectra (B) for P(DAlVP) **P1**, P(DAlVP-DEVP) **P2**, and P(DAlVP-DEVP-DPrTMSVP) **P3**. ^1H NMR signals of monomers DAlVP (blue), DEVP (green), and DPrTMSVP (orange) are highlighted.

regio- and stereoselectivity, excellent yields under mild reaction conditions, and the possibility to obtain the final structure in few simple steps in a high-yield and reasonable time scale.[15,17] "Double click reactions" enable the orthogonal functionalization of macromolecules by utilizing two chemically and mechanistically different click reactions to ensure the targeted modification of the polymer side chains.[17−19] One promising strategy is the combination of a thiol-ene click reaction and azide-alkyne cycloaddition (AAC).

Polyvinyl phosphonates also provide a versatile platform for functionalized polymers and enhance properties in new and smart materials. These macromolecules possess notable characteristics, including high biocompatibility,[20−24] good solubility in water, and a tunable lower critical solution temperature (LCST).[25] Moreover, the presence of two functionalizable motifs per monomer unit allows doubling of the attached molecules per repeating unit, resulting in a higher loading capacity. Our group has successfully achieved well-defined, high molecular-weight polyvinyl phosphonates via living rare-earth metal-mediated group transfer polymerization (REM-GTP).[25−30] This method enables excellent control over the polymer microstructure in terms of copolymer composition and the creation of block structures with various functional monomers while maintaining a narrow polydispersity. Besides, various modification options are available, including end-group functionalization with different initiators functionalized with azides, allyl groups, or other protected reactive groups.[21,31−34] Moreover, modifying polymers through postpolymerization functionalization or incorporating diverse functional monomer units is feasible.[35,36] Furthermore, amphiphilic block copolymers containing polyvinyl phosphonates have been studied for their micellar formation, loading and release behavior, and modification options.[20,23,37−39] Postpolymerization functionalization also allows the attachment of different biologically active substrates to the polymer. The successful synthesis of a polymer−biomolecule conjugate involving folic acid or cholesterol has been achieved via thiol-ene click chemistry on a vinyl-containing polymer end group, followed by investigations on the localization of these polyvinyl phosphonate conjugates in HMEC-1 cells.[21,40]

This study capitalizes on the advantages of precision polymerization via REM-GTP for the selective introduction of allyl and propargyl moieties into terpolymers, which serve as flexible anchors for the selective incorporation of (biological) substrates.[41] To this end, monomers containing functional groups, such as diallyl vinyl phosphonate (DAlVP, **1**) and di trimethylsilyl propargyl vinyl phosphonate (DPrTMSVP, **3**), are chosen. By combining these monomers with diethyl vinyl phosphonate (DEVP, **2**), which contributes to the enhanced water solubility of the final polymer structure, the *block-co*-polyvinyl phosphonate P(DAlVP-DEVP-DPrTMSVP) **P3** is synthesized.

These α,ω-block copolymers enable orthogonal functionalization through AAC followed by a thiol-ene click reaction, opening the pathway for site-specific introduction of different model substrates. The postpolymerization functionalization and sequential modification of the propargyl groups containing polyvinyl phosphonate **P4** is tested using aromatic benzyl azide and the dye 3-azido-7-hydroxycoumarin as model substrates. Furthermore, the functionalization of the allyl groups with cysteamine is confirmed. To advance toward a biological application of these polymers, modification with cholesterol, an essential compound of the cell membrane,[42,43] and folic acid, which specifically targets the folic-acid receptor (FR-α) and is a well-known drug-delivery targeting group, are investigated.[44−46]

https://doi.org/10.1021/acs.macromol.3c02238
Macromolecules 2024, 57, 1438−1447

2. RESULTS AND DISCUSSION

2.1. Synthesis of α-Allyl-ω-TMSpropargyl-*block-co*-polyvinyl Phosphonate P(DAlVP-DEVP-DPrTMSVP). The controlled incorporation of allyl and propargyl functionalized monomers to form the hetero terpolymer is facilitated by the living character of REM-GTP, allowing a sequential addition of different monomers due to the constant coordination of the growing polymer chain at the catalyst center. After quantitative C−H bond activation of $Cp_2YCH_2TMS(thf)$ with 2,4,6-trimethylpyridine in toluene is confirmed via nuclear magnetic resonance (NMR) spectroscopy, the initial monomer DAlVP is introduced.[47] A limited number of five monomer units is employed to maintain the water solubility of the final polymer. Consequently, the hydrophilic DEVP core is polymerized before introducing the newly developed vinyl phosphonate DPrTMSVP (Figure 1A). To avoid catalyst decomposition by the acidic proton of the propargyl group upon polymerization, the monomer is previously protected with a trimethylsilyl (TMS) group. This enables the polymerization of a third short polymer block, consisting of propargyl-functionalized vinyl phosphonate **3**, thereby introducing a second modification handle and, finally, the synthesis of α-allyl-ω-TMSpropargyl-*block-co*-polymer **P3**.

To verify the block structure of polymer **P3**, the conversion of each monomer is assessed via NMR after every polymerization step (Figure 1B). The disappearance of the vinyl group in the ^{1}H NMR spectra and the absence of the monomer signal in the ^{31}P NMR spectra indicate complete monomer conversion (Figure S5). This allows for the addition of the following monomer. While the first monomers, DAlVP and DEVP, exhibit living character and achieve full conversion, the polymerization of DPrTMSVP does not proceed to full conversion. It is assumed that although the polymerization is the preferred reaction, the trimethylsilyl-1-properyl side chain of DPrTMSVP can also interact with the catalyst through C−H activation at the CH_2-position, thereby terminating the polymerization process.[48] Nonetheless, incorporating an adequate amount of propargylic-modified monomer **3** into the terpolymer **P3** is possible. The ^{1}H NMR spectra display signals indicative of the allylic side groups in the range of 5.04 to 5.87 ppm (DAlVP), as well as the trimethylsilyl protecting group at 0.13 ppm (DPrTMSVP). Furthermore, the CH_2 group of the respective monomers in **P3** can be observed at 4.08 (DEVP), 4.49 (DAlVP), and 4.79 ppm (DPrTMSVP), enabling the precise determination of the exact monomer composition.

By correlating the above signals with those from the trimethylpyridine initiator, it becomes feasible to determine the monomer composition of DAlVP/DEVP/DPrTMSVP = 5:110:2 through spectral analysis. Additionally, successful polymerization toward **P3** and the absence of homopolymers are confirmed using diffusion-ordered NMR spectroscopy (DOSY-NMR) (Figure S6). Furthermore, the determination of the number-average molecular weight (M_n) and narrow polydispersity (PDI) for the polymers **P2** and **P3** is carried out via size-exclusion chromatography multiangle light scattering (SEC-MALS) (Figures S7 and S8). Dynamic light scattering (DLS) determines that terpolymer **P3** undergoes self-aggregation into micelles due to the hydrophobic nature of the trimethylsilyl group (Figure S9). Comparing DLS measurements between polymers **P2** and **P3** reveals that the diblock copolymer **P2** does not exhibit self-assembly behavior, whereas **P3** forms micelles with an approximate size of 100 nm (Figure 2B).

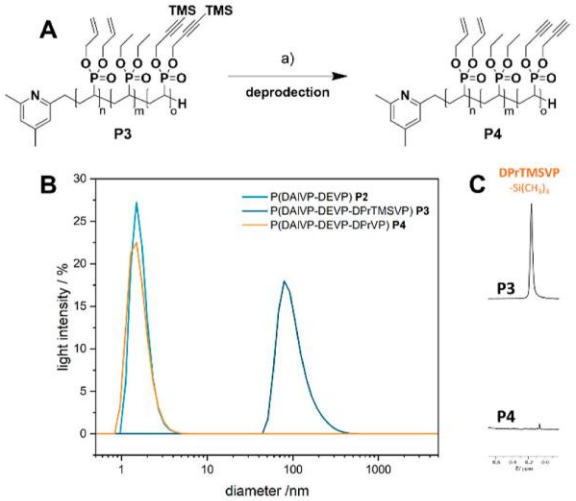

Figure 2. Overview of deprotection of DPrTMSVP in terpolymer **P3**. Conditions (A): (a) K_2CO_3, rt, and overnight [MeOH]. DLS measurements (B) of the polymers **P2** (light blue), **P3** (dark blue), and **P4** (orange) and the extract of the ^{1}H NMR spectra (C) of **P3** and **P4**.

2.2. Deprotection. Before functionalization, the removal of the trimethylsilyl group from the PDPrTMSVP block is required to give access to the desired polymer−substrate conjugates. For the deprotection of the propargyl groups, **P3** is dissolved in methanol, followed by the addition of potassium carbonate. The reaction mixture is stirred at room temperature overnight. The reaction demonstrates full conversion, as confirmed by ^{1}H NMR analysis, where the signals of the TMS group at 0.13 ppm and the CH_2 group at 4.79 ppm disappear entirely (Figures 2C and S10). The SEC-MALS analysis of polymer **P4** provides evidence that the polymer backbone remains unaffected by the reaction conditions and is fully preserved (Figure S13). The DLS measurements confirm no micelle formation in polyvinyl phosphonate **P4** (Figure 2B). To sum up, the results indicate the successful and complete deprotection of the propargyl groups.

2.3. Orthogonal Functionalization of α-Allyl-ω-propargyl-*block-co*-polyvinyl Phosphonate. After successfully synthesizing polyvinyl phosphonate **P4** as an unmodified polymer with well-defined quantities of functionalized monomers, the subsequent step involves testing the orthogonal functionalization of **P4**. To ensure the targeted introduction of diverse substrates, modifying the propargyl groups through AAC is beneficial before performing thiol-ene click reactions on the allyl groups (Figure 3). This approach prevents unwanted thiolyne click reactions between the propargyl groups and the utilized thiols. To screen the AAC, benzyl azide (**4**) is employed as a model substrate due to its distinct aromatic signals in ^{1}H NMR spectroscopy.

The modification of the alkyne groups of the polymer **P4** through AAC is achieved via thermal activation following the Huisgen method.[49] The thermal activation approach successfully eliminates the need to deal with potential metal catalyst contaminations, which would be particularly crucial for later

https://doi.org/10.1021/acs.macromol.3c02238
Macromolecules 2024, 57, 1438−1447

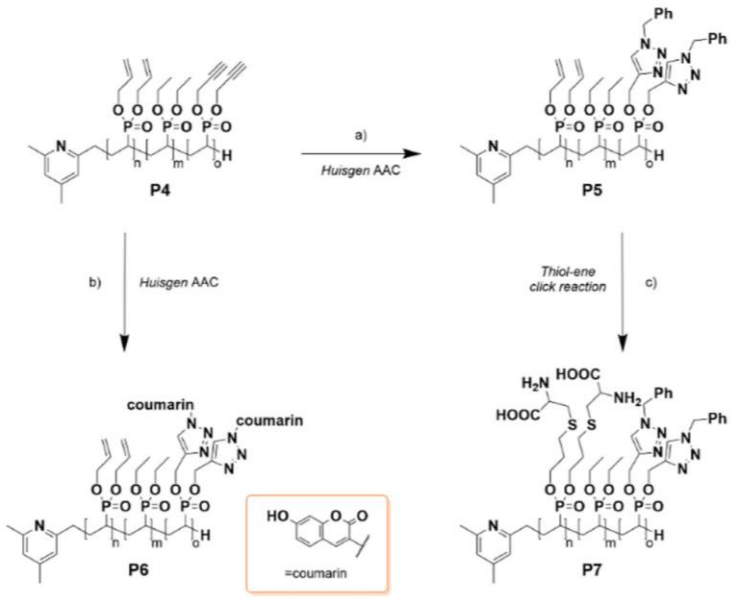

Figure 3. Overview of the synthetic pathway of postpolymerization functionalization of polyvinyl phosphonate **P4**. (a) Benzyl azide (**4**), 110 °C, overnight [DMF], (b) 3-azido-7-hydroxycoumarin (**5**), 110 °C, overnight [DMF], and (c) cysteine (**6**), ACPA, 70 °C, overnight [THF/MeOH].

biomedical applications. Consequently, the polymer and azide derivative **4** are heated overnight to facilitate the reaction. Upon purification, the ^{1}H NMR spectrum reveals a signal ranging from 7.24 to 7.69 ppm, indicating the presence of aromatic protons from the conjugated benzylic group. Furthermore, the effectiveness of the postpolymerization functionalization can be assessed by the weak signal at 8.57 ppm, corresponding to the newly formed triazole (Figure S19). However, due to the low proportion of substrate molecules attached to the polymer and their weak signals, a quantitative analysis of the reaction is not feasible. Nevertheless, the confirmation of successful side-chain functionalization can be inferred based on additional evidence from DOSY-NMR experiments (Figure 4A). It can also be shown that modifying the polymer by the method above did not lead to decomposition of the parent block copolymer (Figures S20–S22). Additionally, the cycloaddition of propargyl groups in polyvinyl phosphonate is confirmed by coupling a water-soluble azide-containing dye, specifically 3-azido-7-hydroxy-coumarin (**5**). This verification is conducted under reaction conditions identical to those of the previous Huisgen click reaction with benzyl azide **4**, and the resulting product is purified via dialysis against water. The successful synthesis of polyvinyl phosphonate **P6** is demonstrated using ^{1}H NMR spectroscopy, wherein the spectrum exhibited aromatic signals ranging from 6.62 to 7.79 ppm, as well as the newly formed triazole signal around 8.47 ppm (Figure S23). Additionally, the DOSY-NMR spectrum confirms the successful conjugation by presenting identical diffusion coefficients for the signals corresponding to the polymer and substrate **5** (Figure 4B). Furthermore, the dye-functionalized polymer **P6** is subjected to absorption (Figure 4C) and fluorescence (Figure 4D) spectroscopy. The absorption spectrum unveils an absorption band at approximately 250 nm and another band at 320 nm, which indicates the conjugate dye **5**. The emission spectrum exhibits a prominent fluorescence band at 490 nm. Collectively, these spectra provide further evidence supporting the presence of the dye within the polymer. To conclude, the functionalization of the propargyl group via Huisgen cyclo-addition is achieved on the block copolymer backbone.

Following the introduction of substrates through azide-alkyne cycloaddition, the allyl groups undergo targeted modification by a second structural motif via the thiol-ene click reaction. For this purpose, the amino acid L-cysteine (**6**) is chosen as a thiol, which can also be used for coupling different modified amino acid sequences and thus opens the possibility of peptide functionalization of polyvinyl phosphonates.[50,51] For the modification, the radical reaction of polyvinyl phosphonate **P5** and substrate **6** is initiated by the water-soluble initiator 4,4′-azobis(4-cyanopentanoic acid) (ACPA). In contrast to previous studies,[35] only 1.2 equiv of cysteine is used for each allyl group present in the polymer to prevent thiol-yne click side reactions with unreacted propargyl groups. The success of the synthesis is determined by the NMR analysis of the purified polymer after dialysis. In the ^{1}H NMR spectrum, the signals assigned to the allyl groups at 4.60, 5.46−5.20, and 6.01 ppm have disappeared completely, suggesting quantitative conversion of the allyl groups (Figure S10).

2.4. Application-Oriented Approach—*α*-Cholesteryl-*ω*-folate-*block*-*co*-polyvinyl Phosphonate. Drawing inspiration from the successful end-group postpolymerization functionalization of PDEVP with folic acid (FA) and cholesterol and considering the diverse applications of PEG-modified biomolecules, we synthesize an *α*-cholesteryl-*ω*-folate-*block*-*co*-polyvinyl phosphonate (Figure 5).[21,52,53] This novel copolymer confirms the sequential functionalization strategy based on orthogonal click reactions for the creation of biologically active systems. In this context, coupling of folic acid to the polymer through the radical thiol-ene click reaction is not possible due to the role of FA as a free radical scavenger.[54] Alternatively, attachment of the folic acid

https://doi.org/10.1021/acs.macromol.3c02238
Macromolecules 2024, 57, 1438−1447

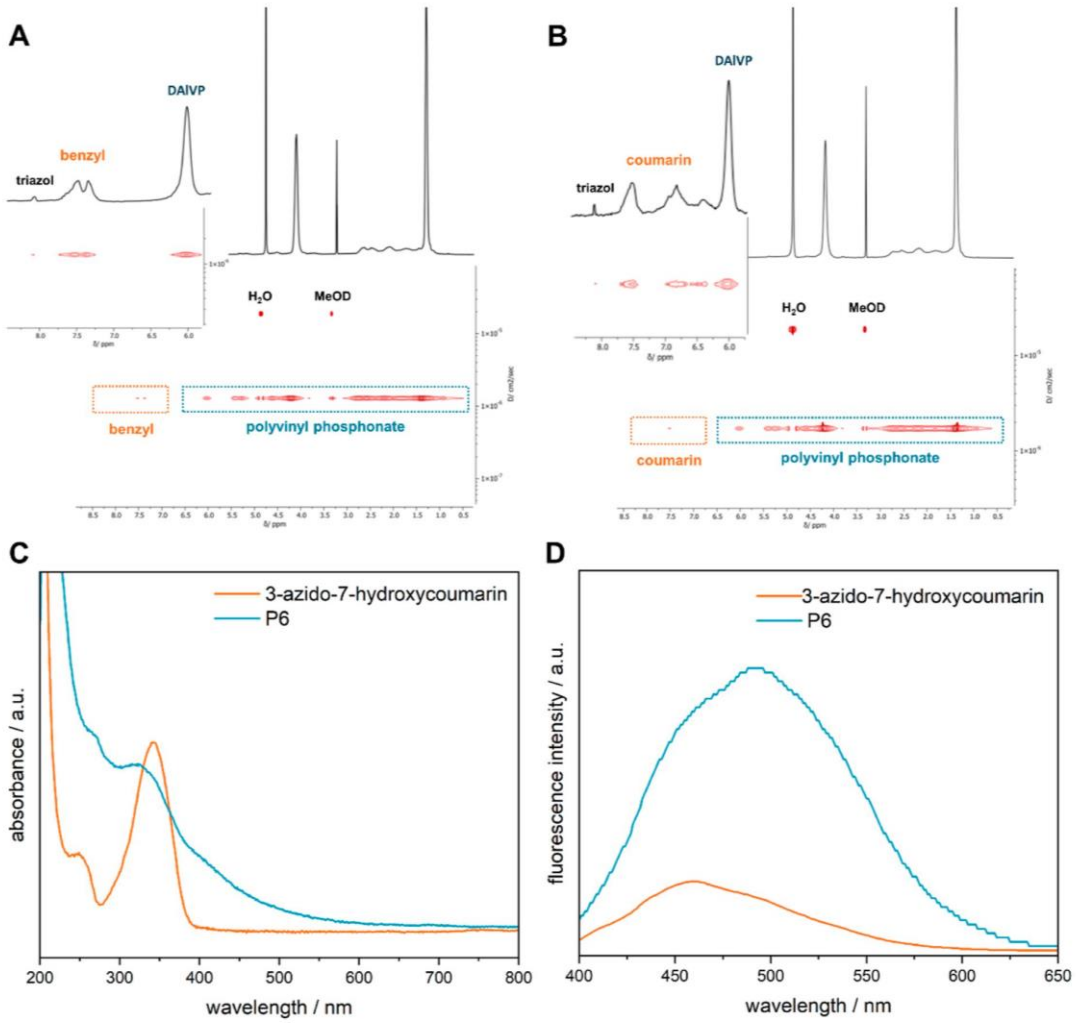

Figure 4. DOSY-NMR spectra of polyvinyl phosphonate **P5** (A) and **P6** (B). Polyvinyl phosphonate (blue) and substrates (orange) are highlighted. UV−vis (C) and fluorescence (D) spectra of **P6** (blue) and 3-azido-7-hydroxycoumarin (orange).

derivative to the polymer does not exhibit a modification of the allyl groups with a second substrate in subsequent thiol-ene click reactions due to the above-mentioned reasons.

Therefore, we initiated the functionalization process by modifying the protected terpolymer **P3** through a thiol-ene click reaction with thiocholesterol (Chol-SH, **7**). To prevent thiol-ene click reactions with the propargyl groups present in the polymer, we apply the protected terpolymer **P3**, in which TMS groups still shield the mentioned functional groups.[55−57] Deprotection of these moieties is performed after functionalization of the allyl bonds. Additionally, we use only 0.9 equiv of cholesterol **7** relative to the allylic groups in the polyvinyl phosphonate during the thiol-ene click reaction. This approach avoids excessive thiols that can react with the alkyne groups. Moreover, a high degree of functionalization negatively affects the solubility of the polymer−biomolecule conjugate and hinders further applications. In the experiment, terpolymer **P3** reacts with thiocholesterol in the presence of the photoinitiator 2,2-dimethoxy-2-phenylacetophenone (DMPA). ^{1}H NMR spectroscopy of polyvinyl phosphonate **P8** demonstrates 75% conversion of the allylic side groups by comparing the spectrum with polymer **P3**. This conversion is confirmed by the decrease in signals corresponding to the allyl groups in the range of 5.04 to 5.87 ppm and the prominent signals of the cholesterol methyl groups from 0.81 to 0.99 ppm (Figure 6).

Additionally, DOSY-NMR investigations of polyvinyl phosphonate **P8** demonstrate that the cholesterol moiety, as well as the polymer signals, exhibits the same diffusion coefficient (Figure S38). The cholesterol-functionalized polyvinyl phosphonate **P8** is not soluble in water due to the presence of two hydrophobic functionalized polymer chain ends, namely, the TMS groups on one side and the lipophilic cholesterol conjugates on the other.

Before the modification with folic acid, the propargyl groups of the polymer **P8** are subjected to deprotection of the TMS groups, following the same procedure as that for polyvinyl phosphonate **P3**. The complete conversion is confirmed for polymer **P9** via ^{1}H NMR spectroscopy (Figure 6). Additionally, the DLS analysis demonstrated that upon the removal of the hydrophobic TMS groups, the polyvinyl phosphonate

https://doi.org/10.1021/acs.macromol.3c02238
Macromolecules 2024, 57, 1438−1447

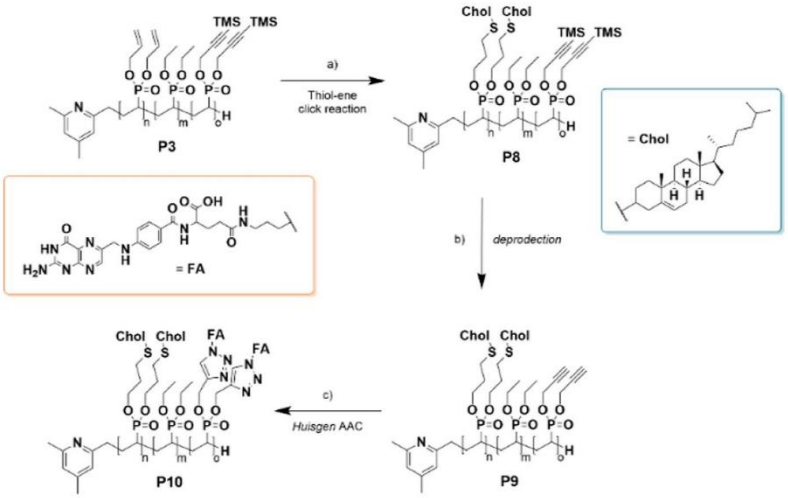

Figure 5. Overview of the synthetic pathway of orthogonal functionalization of terpolymer **P3**. (a) Thiocholesterol (7), DMPA, rt, λ = 365 nm, overnight [THF/MeOH], (b) K_2CO_3, rt, overnight [MeOH], and (c) folic acid azide (**8**), 110 °C, overnight [DMF].

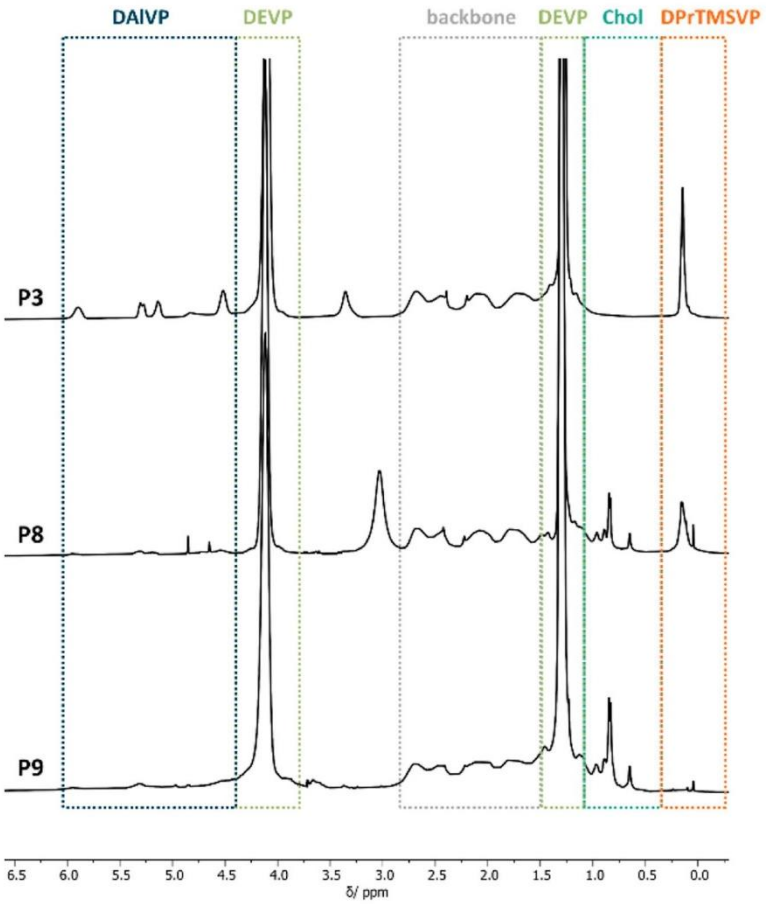

Figure 6. Comparison of ^{1}H NMR spectra of the polymers **P3**, **P8**, and **P9**. Monomers DAlVP (blue), DEVP (light green), DPrTMSVP (orange), as well as cholesterol (dark green), are highlighted.

regained its amphiphilic nature, forming micelles. Notably, the core of the micelles is constituted by the cholesterol-modified block of the polymer (Figure S18). Following the deprotection of the propargyl groups, azido folate **8** needs to be attached to

https://doi.org/10.1021/acs.macromol.3c02238
Macromolecules 2024, 57, 1438−1447

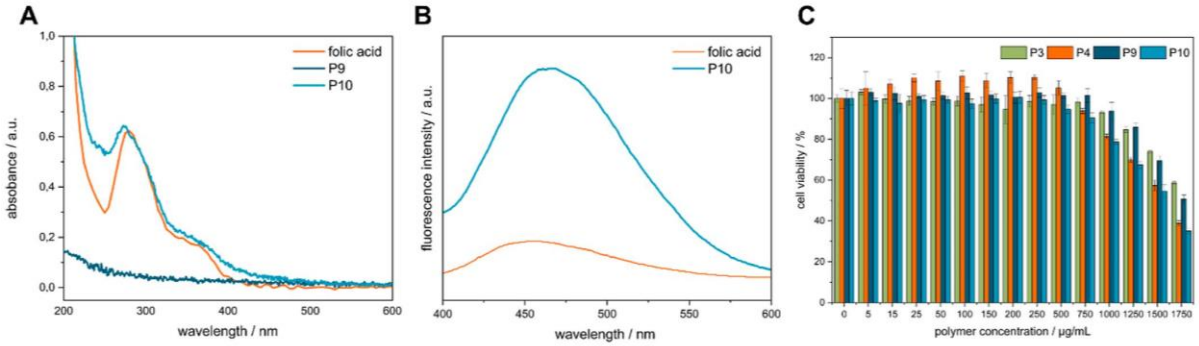

Figure 7. UV−vis (A) and fluorescence (B) spectra of polyvinyl phosphonate **P9** (dark blue), **P10** (light blue), and folic acid (orange). Cell viability (C) of MIO-M1 cells after 24 h with the polymers **P3** (green), **P4** (orange), **P9** (dark blue), and **P10** (light blue).

them in a manner orthogonal to the cholesterol moieties. Considering the previously mentioned reasons, the terminally initiated Huisgen cycloaddition is selected as the preferred method and executes under the same reaction conditions as those used for **P5** and **P6**. The synthesis of the azido-functionalized folic acid derivative **8** follows an established procedure described in the literature.[45] After complete purification of the polymer−biomolecule conjugate **P10**, confirmation of the successful coupling of the folic acid is achieved through meticulous ^{1}H NMR analysis. In the aromatic region of the NMR spectrum, distinct signals are observed at chemical shifts between 6.64 and 8.37 ppm, corresponding to characteristic resonances of folic acid. A signal attributed to the triazole moiety formed during the cycloaddition reaction is also identified at 7.56 ppm (Figure S28). However, owing to the relatively low proportion of folic acid within the polymer conjugate **P10** and the significantly reduced signal intensity of the functional groups in the NMR spectrum, a quantitative analysis of the functionalization degree is impossible. The covalent incorporation of the folic acid derivative **8** into the polymer is further confirmed by DOSY-NMR, as evidenced by its similar diffusion coefficient to that of the polyvinyl phosphonate (Figure S30). This observation not only indicates successful integration but also ensures the purity of the sample. Moreover, the polymer−biomolecule conjugate **P10** is analyzed using UV−vis and fluorescence spectroscopy. The UV−vis spectrum revealed two characteristic absorption bands in the range of 250−300 and 300−400 nm, corresponding to the $\pi-\pi^*$ and $n-\pi^*$ electronic transitions, respectively, of the pterin and *p*-amino benzoyl acid moieties of the folic acid (Figure 7A).[58] Moreover, the fluorescence spectra displayed an emission maximum at 465 nm, exhibiting a noticeable shift compared with the pure folic acid ($\lambda_{max} \approx 451$ nm) (Figure 7B). Notably, the exclusively cholesterol-functionalized polyvinyl phosphonate **P9** shows no signals in the fluorescence and UV−vis spectra. Furthermore, DLS determines that the polymer is capable of self-assembly and forms micelles with a cholesterol core (Figure S32).

Finally, the cytotoxicity of the unmodified polymers **P3** and **P4**, along with the cholesterol and folic acid-functionalized polyvinyl phosphonates **P9** and **P10**, is examined on cells. This assessment stands as a crucial determinant for the potential biomedical applications of these materials. Cell viability assays are performed using a spontaneously immortalized human Müller cell line (MIO-M1) by exposing the cells to different concentrations of the polymers (ranging from 5 to 1750 μg/mL) after 24 h. The resulting values of the assay are presented in Figure 7C. Up to a 500 μg/mL concentration, a cell viability of over 90% is observed for all polymers. Results show that TMS-protected terpolymer **P3** has a higher viability than 100%, but the cell viability decreases as the polymer concentration increases. Upon deprotection, the resulting polymer P(DAlVP-DEVP-DPrVP) **P4** demonstrates a significantly higher viability level of around 100% compared to **P3**, indicating the absence of toxicity. The cell viability of the cholesterol-functionalized polyvinyl phosphonate **P9** remains above 100% across the tested concentration range, indicating high biocompatibility. However, the addition of folic acid (**P10**) as an additional functionalized compound slightly decreases the obtained viability values. From a concentration of 1000 μg/mL onward, there is a noticeable decrease in the cell viability across all polymers. This decline is observed to be more dynamic in the case of polymers **P4** and **P10** compared to **P3** and **P9**. This can probably be attributed to the fact that higher molecular masses lead to an increase in cell membrane damage.[59] Nevertheless, it is evident that both deprotection from **P3** to **P4** and the functionalization of **P9** with folic acid to generate **P10** leads to a marked reduction in the cell viability in their respective cell tests (Figure S39). Preceding tests of polyvinyl phosphonates yielded promising results, with cell viability surpassing 50% in MTT assays.[21] However, the recent findings show that all four polymers exhibited a minimum of 78% cell viability following a 24 h treatment with a polymer concentration of 1 mg/mL. This finding provides valuable insights into subsequent cellular experiments. This further emphasizes the positive potential of these materials for biomedical applications. Additionally, a noteworthy observation emerges where data points surpassed 100%. These instances are construed as compelling evidence showcasing the favorable influence of the polymers on cell growth, imparting an intriguing dimension to their potential utility in the field of biomedicine. Overall, it can be concluded that all evaluated polyvinyl phosphonates (**P3**, **P4**, **P9**, and **P10**) display low toxicity. These findings suggest that these polymers are promising platforms for biological and medical applications.

3. CONCLUSIONS

In summary, the presented study reports the successful synthesis of α-allyl-ω-TMSpropargyl-*block*-*co*-polyvinyl phosphonate P(DAlVP-DEVP-DPrTMSVP) **P3**, employing the newly developed vinyl phosphonate DPrTMSVP via REM-

https://doi.org/10.1021/acs.macromol.3c02238
Macromolecules 2024, 57, 1438−1447

GTP. The sequential polymerization of the terpolymer is monitored via ^{1}H- and ^{31}P NMR spectroscopy, and the targeted structure is confirmed via DOSY-NMR spectroscopy as well as SEC-MALS. Additionally, the amphiphilic nature and self-assembly of the block copolymer are studied via DLS, revealing the formation of micelles of 100 nm size.

The modification of propargyl groups after quantitative cleavage of the TMS groups via the Huisgen click reaction with benzyl azide and 3-azido-7-hydroxy-coumarin is achieved and qualitatively demonstrated (Figure 8) via ^{1}H NMR spectroscopy. The attachment of the fluorescent dye to the polymer is further confirmed through UV−vis and fluorescence measurements of polymer **P6**. Moreover, a subsequent thiol-ene click reaction enabled almost quantitative conversion in functionalizing the allyl groups with the amino acid cysteine, opening the possibility of modifying the polymers with various peptide sequences. As a proof of concept for the functionalization approach using sequential, orthogonal click reactions on polyvinyl phosphonates toward potential biomedical applications, the terpolymer **P3** is modified through a thiol-ene click reaction with cholesterol, converting 75% of the allyl bonds in the polyvinyl phosphonate. Subsequent deprotection of the propargyl groups allows for the attachment of folic acid via AAC, which is confirmed through fluorescence and UV−vis measurements. Notably, the lipophilic character of cholesterol contributed to the formation of micelles in modified polymers **P9** and **P10**. Furthermore, unfunctionalized polymers **P3** and **P4** and biologically functionalized polymers **P9** and **P10** exhibit no cytotoxic behavior. Therefore, the investigated polyvinyl phosphonates exhibit essential fundamental characteristics. On the one hand, there is potential for further exploration through orthogonal modifications of *α*-allyl-*ω*-propargyl-*block-co*-polyvinyl phosphonate **P4**, allowing for the incorporation of diverse targeting groups, dyes, peptides, nucleobases, and other functionalities in various fields of application. On the other hand, research efforts can be dedicated to assess the suitability of the modified *α*-cholesteryl-*ω*-folate-*block-co*-polyvinyl phosphonate **P10**, for instance, as a linker for liposome-based drug delivery systems, comparing its performance with the well-established PEG variant.[60]

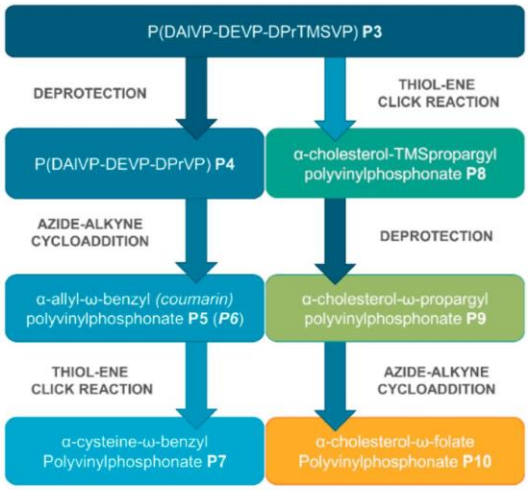

Figure 8. Schematic overview of synthesis cascades.

■ ASSOCIATED CONTENT

Supporting Information

The Supporting Information is available free of charge at https://pubs.acs.org/doi/10.1021/acs.macromol.3c02238.

Synthetic procedures of the synthesis, polymerization, and follow-up functionalization; and detailed characterization data (^{1}H-, ^{13}C-, ^{31}P-, and DOSY-NMR spectra, fluorescence spectra, UV−vis spectra, DLS measurements, elemental analysis, SEC-MALS traces, as well as cell viability assays) (PDF)

■ AUTHOR INFORMATION

Corresponding Author

Bernhard Rieger − *WACKER-Chair of Macromolecular Chemistry, Catalysis Research Center, Department of Chemistry, Technical University of Munich, 85748 Garching, Germany;* orcid.org/0000-0002-0023-884X; Email: rieger@tum.de

Authors

Kerstin Halama − *WACKER-Chair of Macromolecular Chemistry, Catalysis Research Center, Department of Chemistry, Technical University of Munich, 85748 Garching, Germany*

Molly Tzu-Yu Lin − *Institute for Ophthalmic Research, University of Tübingen, 72076 Tübingen, Germany*

Andreas Schaffer − *WACKER-Chair of Macromolecular Chemistry, Catalysis Research Center, Department of Chemistry, Technical University of Munich, 85748 Garching, Germany*

Marvin Foith − *WACKER-Chair of Macromolecular Chemistry, Catalysis Research Center, Department of Chemistry, Technical University of Munich, 85748 Garching, Germany*

Friederike Adams − *Institute for Ophthalmic Research, University of Tübingen, 72076 Tübingen, Germany; Chair of Macromolecular Materials and Fiber Chemistry, Institute of Polymer Chemistry, University of Stuttgart, 70569 Stuttgart, Germany;* orcid.org/0000-0002-4362-0387

Complete contact information is available at: https://pubs.acs.org/10.1021/acs.macromol.3c02238

Author Contributions

The manuscript was written through contributions of all authors. All authors have given approval for the final version of the manuscript.

Notes

The authors declare no competing financial interest.

■ ACKNOWLEDGMENTS

The authors are grateful to Fabian Späth, Anton Maier, and Marina Wittig for revising the manuscript. Furthermore, they thank Johanna Haimerl for her assistance in creating the graphical abstract and Brigita Bratić. F.A. and M.T.Y.L. are grateful for the funding received from the Federal Ministry of Education and Research (BMBF) and the Baden-Württemberg Ministry of Science, Research and Art, as part of the Excellence Strategy of the German Federal and State Governments.

■ REFERENCES

(1) Yen, S. K.; Jańczewski, D.; Lakshmi, J. L.; Dolmanan, S. B.; Tripathy, S.; Ho, V. H. B.; Vijayaragavan, V.; Hariharan, A.;

Padmanabhan, P.; Bhakoo, K. K.; et al. Design and Synthesis of Polymer-Functionalized NIR Fluorescent Dyes-Magnetic Nanoparticles for Bioimaging. *ACS Nano* **2013**, *7* (8), 6796−6805.
(2) Nicolas, J.; Mura, S.; Brambilla, D.; Mackiewicz, N.; Couvreur, P. Design, functionalization strategies and biomedical applications of targeted biodegradable/biocompatible polymer-based nanocarriers for drug delivery. *Chem. Soc. Rev.* **2013**, *42* (3), 1147−1235.
(3) Gai, M.; Simon, J.; Lieberwirth, I.; Mailänder, V.; Morsbach, S.; Landfester, K. A bio-orthogonal functionalization strategy for site-specific coupling of antibodies on vesicle surfaces after self-assembly. *Polym. Chem.* **2020**, *11* (2), 527−540.
(4) Cao, Y.; Dong, X.; Chen, X. Polymer-Modified Liposomes for Drug Delivery: From Fundamentals to Applications. *Pharmaceutics* **2022**, *14* (4), 778.
(5) Ghezzi, M.; Pescina, S.; Padula, C.; Santi, P.; Del Favero, E.; Cantù, L.; Nicoli, S. Polymeric micelles in drug delivery: An insight of the techniques for their characterization and assessment in biorelevant conditions. *J. Controlled Release* **2021**, *332*, 312−336.
(6) Hari, S. K.; Gauba, A.; Shrivastava, N.; Tripathi, R. M.; Jain, S. K.; Pandey, A. K. Polymeric micelles and cancer therapy: an ingenious multimodal tumor-targeted drug delivery system. *Drug Delivery Transl. Res.* **2023**, *13* (1), 135−163.
(7) Moulahoum, H.; Ghorbanizamani, F.; Zihnioglu, F.; Timur, S. Surface Biomodification of Liposomes and Polymersomes for Efficient Targeted Drug Delivery. *Bioconjugate Chem.* **2021**, *32* (8), 1491−1502.
(8) Veronese, F. M. Peptide and protein PEGylation: a review of problems and solutions. *Biomaterials* **2001**, *22* (5), 405−417.
(9) Mishra, P.; Nayak, B.; Dey, R. K. PEGylation in anti-cancer therapy: An overview. *Asian J. Pharm. Sci.* **2016**, *11* (3), 337−348.
(10) Dhiman, S.; Mishra, N.; Sharma, S. Development of PEGylated solid lipid nanoparticles of pentoxifylline for their beneficial pharmacological potential in pathological cardiac hypertrophy. *Artif. Cells, Nanomed., Biotechnol.* **2016**, *44* (8), 1901−1908.
(11) Gupta, V.; Bhavanasi, S.; Quadir, M.; Singh, K.; Ghosh, G.; Vasamreddy, K.; Ghosh, A.; Siahaan, T. J.; Banerjee, S.; Banerjee, S. K. Protein PEGylation for cancer therapy: bench to bedside. *J. Cell Commun. Signaling* **2019**, *13* (3), 319−330.
(12) Loiseau, F. A.; Hii, K. K.; Hill, A. M. Multigram Synthesis of Well-Defined Extended Bifunctional Polyethylene Glycol (PEG) Chains. *J. Org. Chem.* **2004**, *69* (3), 639−647.
(13) Hadjichristidis, N.; Iatrou, H.; Pitsikalis, M.; Pispas, S.; Avgeropoulos, A. Linear and non-linear triblock terpolymers. Synthesis, self-assembly in selective solvents and in bulk. *Prog. Polym. Sci.* **2005**, *30* (7), 725−782.
(14) Konishcheva, E.; Daubian, D.; Gaitzsch, J.; Meier, W. Synthesis of Linear ABC Triblock Copolymers and Their Self-Assembly in Solution. *Helv. Chim. Acta* **2018**, *101* (2), No. e1700287.
(15) Skandalis, A.; Sentoukas, T.; Giaouzi, D.; Kafetzi, M.; Pispas, S. Latest Advances on the Synthesis of Linear ABC-Type Triblock Terpolymers and Star-Shaped Polymers by RAFT Polymerization. *Polymers* **2021**, *13* (11), 1698.
(16) Kolb, H. C.; Finn, M. G.; Sharpless, K. B. Click Chemistry: Diverse Chemical Function from a Few Good Reactions. *Angew. Chem., Int. Ed.* **2001**, *40* (11), 2004−2021.
(17) Durmaz, H.; Sanyal, A.; Hizal, G.; Tunca, U. Double click reaction strategies for polymer conjugation and post-functionalization of polymers. *Polym. Chem.* **2012**, *3* (4), 825−835.
(18) Campos, L. M.; Killops, K. L.; Sakai, R.; Paulusse, J. M. J.; Damiron, D.; Drockenmuller, E.; Messmore, B. W.; Hawker, C. J. Development of Thermal and Photochemical Strategies for Thiol-Ene Click Polymer Functionalization. *Macromolecules* **2008**, *41* (19), 7063−7070.
(19) Javakhishvili, I.; Binder, W. H.; Tanner, S.; Hvilsted, S. Facile synthesis of linear-dendritic cholesteryl-poly(ϵ-caprolactone)-b-(l-lysine)G2 by thiol-ene and azide-alkyne "click" reactions. *Polym. Chem.* **2010**, *1* (4), 506−513.
(20) Schwarzenböck, C.; Nelson, P. J.; Huss, R.; Rieger, B. Synthesis of next generation dual-responsive cross-linked nanoparticles and their application to anti-cancer drug delivery. *Nanoscale* **2018**, *10* (34), 16062−16068.
(21) Schwarzenböck, C.; Schaffer, A.; Pahl, P.; Nelson, P. J.; Huss, R.; Rieger, B. Precise synthesis of thermoresponsive polyvinylphosphonate-biomolecule conjugates via thiol-ene click chemistry. *Polym. Chem.* **2018**, *9* (3), 284−290.
(22) Schwarzenböck, C.; Vagin, S. I.; Heinz, W. R.; Nelson, P. J.; Rieger, B. Studies on the Biocompatibility of Poly(diethyl vinylphosphonate) with a New Fluorescent Marker. *Macromol. Rapid Commun.* **2018**, *39* (15), 1800259.
(23) Altenbuchner, P. T.; Werz, P. D. L.; Schöppner, P.; Adams, F.; Kronast, A.; Schwarzenböck, C.; Pöthig, A.; Jandl, C.; Haslbeck, M.; Rieger, B. Next Generation Multiresponsive Nanocarriers for Targeted Drug Delivery to Cancer Cells. *Chem.—Eur. J.* **2016**, *22* (41), 14576−14584.
(24) Schaffer, A.; Weger, M.; Rieger, B. From lanthanide-mediated, high-precision group transfer polymerization of Michael-type monomers, to intelligent, functional materials. *Eur. Polym. J.* **2020**, *122*, 109385.
(25) Zhang, N.; Salzinger, S.; Rieger, B. Poly(vinylphosphonate)s with Widely Tunable LCST: A Promising Alternative to Conventional Thermoresponsive Polymers. *Macromolecules* **2012**, *45* (24), 9751−9758.
(26) Adams, F.; Pahl, P.; Rieger, B. Metal-Catalyzed Group-Transfer Polymerization: A Versatile Tool for Tailor-Made Functional (Co)Polymers. *Chem.—Eur. J.* **2018**, *24* (3), 509−518.
(27) Kränzlein, M.; Pehl, T. M.; Adams, F.; Rieger, B. Uniting Group-Transfer and Ring-Opening Polymerization-Block Copolymers from Functional Michael-Type Monomers and Lactones. *Macromolecules* **2021**, *54* (23), 10860−10869.
(28) Lanzinger, D.; Salzinger, S.; Soller, B. S.; Rieger, B. Poly(vinylphosphonate)s as Macromolecular Flame Retardants for Polycarbonate. *Ind. Eng. Chem. Res.* **2015**, *54* (6), 1703−1712.
(29) Adams, F.; Machat, M. R.; Altenbuchner, P. T.; Ehrmaier, J.; Pöthig, A.; Karsili, T. N. V.; Rieger, B. Toolbox of Nonmetallocene Lanthanides: Multifunctional Catalysts in Group-Transfer Polymerization. *Inorg. Chem.* **2017**, *56* (16), 9754−9764.
(30) Pahl, P.; Schwarzenböck, C.; Herz, F. A. D.; Soller, B. S.; Jandl, C.; Rieger, B. Core-First Synthesis of Three-Armed Star-Shaped Polymers by Rare Earth Metal-Mediated Group Transfer Polymerization. *Macromolecules* **2017**, *50* (17), 6569−6576.
(31) Kränzlein, M.; Pehl, T. M.; Halama, K.; Großmann, P. F.; Kratky, T.; Mühlbach, A. M.; Rieger, B. Azide-Modified Poly(diethyl vinylphosphonate) for Straightforward Graft-to Carbon Nanotube Functionalization. *Macromol. Mater. Eng.* **2023**, *308* (6), 2200635.
(32) Adams, F.; Pschenitza, M.; Rieger, B. Yttrium-Catalyzed Synthesis of Bipyridine-Functionalized AB-Block Copolymers: Micellar Support for Photocatalytic Active Rhenium-Complexes. *ChemCatChem* **2018**, *10* (19), 4309−4316.
(33) Schaffer, A.; Kränzlein, M.; Rieger, B. Synthesis and Application of Functional Group-Bearing Pyridyl-Based Initiators in Rare Earth Metal-Mediated Group Transfer Polymerization. *Macromolecules* **2020**, *53* (11), 4345−4354.
(34) Pehl, T. M.; Kränzlein, M.; Adams, F.; Schaffer, A.; Rieger, B. C-H Bond Activation of Silyl-Substituted Pyridines with Bis(Phenolate)Yttrium Catalysts as a Facile Tool towards Hydroxyl-Terminated Michael-Type Polymers. *Catalysts* **2020**, *10* (4), 448.
(35) Halama, K.; Schaffer, A.; Rieger, B. Allyl group-containing polyvinylphosphonates as a flexible platform for the selective introduction of functional groups via polymer-analogous transformations. *RSC Adv.* **2021**, *11* (61), 38555−38564.
(36) Pehl, T. M.; Adams, F.; Kränzlein, M.; Rieger, B. Expanding the Scope of Organic Radical Polymers to Polyvinylphosphonates Synthesized via Rare-Earth Metal-Mediated Group-Transfer Polymerization. *Macromolecules* **2021**, *54* (9), 4089−4100.
(37) Saurwein, A.; Schaffer, A.; Wieser, C.; Rieger, B. Synthesis, characterisation and functionalisation of BAB-type dual-responsive nanocarriers for targeted drug delivery: evolution of nanoparticles

https://doi.org/10.1021/acs.macromol.3c02238
Macromolecules 2024, 57, 1438−1447

based on 2-vinylpyridine and diethyl vinylphosphonate. *RSC Adv.* **2021**, *11* (3), 1586−1594.
(38) Schaffer, A.; Kränzlein, M.; Rieger, B. Precise Synthesis of Poly(dimethylsiloxane) Copolymers through C-H Bond-Activated Macroinitiators via Yttrium-Mediated Group Transfer Polymerization and Ring-Opening Polymerization. *Macromolecules* **2020**, *53* (19), 8382−8392.
(39) Adams, F.; Altenbuchner, P. T.; Werz, P. D. L.; Rieger, B. Multiresponsive micellar block copolymers from 2-vinylpyridine and dialkylvinylphosphonates with a tunable lower critical solution temperature. *RSC Adv.* **2016**, *6* (82), 78750−78754.
(40) Schwarzenböck, C.; Schaffer, A.; Nößner, E.; Nelson, P. J.; Huss, R.; Rieger, B. Fluorescent Polyvinylphosphonate Bioconjugates for Selective Cellular Delivery. *Chem.—Eur. J.* **2018**, *24* (11), 2584−2587.
(41) Yang, H.; Sun, A.; Chai, C.; Huang, W.; Xue, X.; Chen, J.; Jiang, B. Synthesis and post-functionalization of a degradable aliphatic polyester containing allyl pendent groups. *Polymer* **2017**, *121*, 256−261.
(42) Ruwizhi, N.; Aderibigbe, B. A. The Efficacy of Cholesterol-Based Carriers in Drug Delivery. *Molecules* **2020**, *25* (18), 4330.
(43) Misiak, P.; Markiewicz, K. H.; Szymczuk, D.; Wilczewska, A. Z. Polymeric Drug Delivery Systems Bearing Cholesterol Moieties: A Review. *Polymers* **2020**, *12* (11), 2620.
(44) Wang, W.-Y.; Cao, Y.-X.; Zhou, X.; Wei, B. Delivery of folic acid-modified liposomal curcumin for targeted cervical carcinoma therapy. *Drug Des., Dev. Ther.* **2019**, *13*, 2205−2213.
(45) Liu, L.; Zheng, M.; Renette, T.; Kissel, T. Modular Synthesis of Folate Conjugated Ternary Copolymers: Polyethylenimine-graft-Polycaprolactone-block-Poly(ethylene glycol)-Folate for Targeted Gene Delivery. *Bioconjugate Chem.* **2012**, *23* (6), 1211−1220.
(46) Kumar, P.; Huo, P.; Liu, B. Formulation Strategies for Folate-Targeted Liposomes and Their Biomedical Applications. *Pharmaceutics* **2019**, *11* (8), 381.
(47) Soller, B. S.; Salzinger, S.; Jandl, C.; Pöthig, A.; Rieger, B. C-H Bond Activation by σ-Bond Metathesis as a Versatile Route toward Highly Efficient Initiators for the Catalytic Precision Polymerization of Polar Monomers. *Organometallics* **2015**, *34* (11), 2703−2706.
(48) Kaneko, H.; Nagae, H.; Tsurugi, H.; Mashima, K. End-Functionalized Polymerization of 2-Vinylpyridine through Initial C-H Bond Activation of N-Heteroaromatics and Internal Alkynes by Yttrium Ene-Diamido Complexes. *J. Am. Chem. Soc.* **2011**, *133* (49), 19626−19629.
(49) Huisgen, R. 1.3-Dipolare Cycloadditionen Rückschau und Ausblick. *Angew. Chem.* **1963**, *75* (13), 604−637.
(50) Tsurkan, M. V.; Chwalek, K.; Prokoph, S.; Zieris, A.; Levental, K. R.; Freudenberg, U.; Werner, C. Defined Polymer-Peptide Conjugates to Form Cell-Instructive starPEG-Heparin Matrices In Situ. *Adv. Mater.* **2013**, *25* (18), 2606−2610.
(51) Colak, B.; Wu, L.; Cozens, E. J.; Gautrot, J. E. Modulation of Thiol-Ene Coupling by the Molecular Environment of Polymer Backbones for Hydrogel Formation and Cell Encapsulation. *ACS Appl. Bio Mater* **2020**, *3* (9), 6497−6509.
(52) Sharma, S.; Pukale, S. S.; Sahel, D. K.; Agarwal, D. S.; Dalela, M.; Mohanty, S.; Sakhuja, R.; Mittal, A.; Chitkara, D. Folate-Targeted Cholesterol-Grafted Lipo-Polymeric Nanoparticles for Chemotherapeutic Agent Delivery. *AAPS PharmSciTech* **2020**, *21* (7), 280.
(53) Wang, H.; Zhao, P.; Liang, X.; Gong, X.; Song, T.; Niu, R.; Chang, J. Folate-PEG coated cationic modified chitosan - Cholesterol liposomes for tumor-targeted drug delivery. *Biomaterials* **2010**, *31* (14), 4129−4138.
(54) Joshi, R.; Adhikari, S.; Patro, B. S.; Chattopadhyay, S.; Mukherjee, T. Free radical scavenging behavior of folic acid: evidence for possible antioxidant activity. *Free Radical Biol. Med.* **2001**, *30* (12), 1390−1399.
(55) Fairbanks, B. D.; Sims, E. A.; Anseth, K. S.; Bowman, C. N. Reaction Rates and Mechanisms for Radical, Photoinitated Addition of Thiols to Alkynes, and Implications for Thiol-Yne Photopolymerizations and Click Reactions. *Macromolecules* **2010**, *43* (9), 4113−4119.
(56) Lowe, A. B.; Hoyle, C. E.; Bowman, C. N. Thiol-yne click chemistry: A powerful and versatile methodology for materials synthesis. *J. Mater. Chem.* **2010**, *20* (23), 4745−4750.
(57) Stolz, R. M.; Northrop, B. H. Experimental and Theoretical Studies of Selective Thiol-Ene and Thiol-Yne Click Reactions Involving N-Substituted Maleimides. *J. Org. Chem.* **2013**, *78* (16), 8105−8116.
(58) Baibarac, M.; Smaranda, I.; Nila, A.; Serbschi, C. Optical properties of folic acid in phosphate buffer solutions: the influence of pH and UV irradiation on the UV-VIS absorption spectra and photoluminescence. *Sci. Rep.* **2019**, *9* (1), 14278.
(59) Correia, J. S.; Mirón-Barroso, S.; Hutchings, C.; Ottaviani, S.; Somuncuoğlu, B.; Castellano, L.; Porter, A. E.; Krell, J.; Georgiou, T. K. How does the polymer architecture and position of cationic charges affect cell viability? *Polym. Chem.* **2023**, *14* (3), 303−317.
(60) Zhao, X. B.; Muthusamy, N.; Byrd, J. C.; Lee, R. J. Cholesterol as a bilayer anchor for PEGylation and targeting ligand in folate receptor targeted liposomes. *J. Pharm. Sci.* **2007**, *96* (9), 2424−2435.

https://doi.org/10.1021/acs.macromol.3c02238
Macromolecules 2024, 57, 1438−1447

7. Excursus I: Micellformation of New Block-*co*-Polymers

7.1 Polymerization

The previously mentioned terpolymers P(DAIVP-DEVP-DPrTMSVP) synthesis process uncovered their capacity to form micelles. As a result, this behavior and the ensuing properties should be further investigated in a supplementary project. To explore this, P(DEVP-co-DPrTMSVP) block copolymers with varying monomer ratios are synthesized (Scheme 7.1). The polymerization challenge arises from termination reactions during DPrTMSVP polymerization due to the coordination of the monomer side chain to the catalyst, making the precise formation of longer PDPrTMSVP blocks challenging.[56] Consequently, the primary focus centered on investigating the impact of DEVP block on micelle behavior, with monomer ratios of DEVP-DPrTMSVP set at 50-10 (**P6**), 100-10 (**P7**), 200-10 (**P8**), and 400-10 (**P9**).

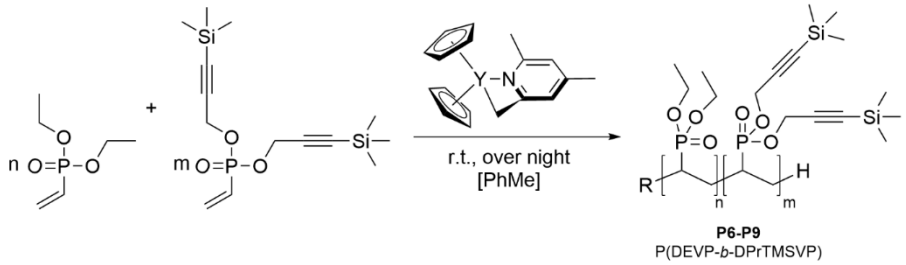

Scheme 7.1: Polymerization of P(DEVP-b-DPrTMSVP) **P6**-**P9**.

The polymerization process starts by adding the appropriate quantity of DEVP to the *sym*-collidine-activated catalyst $Cp_2Y(CH_2TMS)(thf)$, followed by monitoring the complete conversion of the first monomer block using proton and phosphorous NMR to validate the subsequent block structure. After the polymerization with the respective quantity of DPrTMSVP, the monomer ratio within the polymer is calculated using ^{1}H and ^{31}P-NMR. This determination relies on the signals derived from the CH_2 groups of the side chains of DEVP (4.13 ppm) and DPrTMSVP (4.84 ppm). Additionally, confirming the presence of a copolymer and the absence of homopolymers is achieved through DOSY-NMR. During the analysis of the block copolymers using MALS-GPC, precise polymer molar masses, and a narrow polydispersity are determined (refer to Table 7.1). Similar to previous examinations of terpolymers, a bimodal distribution is observed, indicating the presence of micelles. However, it is noteworthy that an increasing DEVP content in the polymer resulted in a shift in the ratio of the two signals in favor of the associated monomer signal. This shift indicates a diminishing tendency for micelle formation with a higher DEVP content, suggesting a reduction in the size of the hydrophilic block.

Table 7.1: Monomer feed, polymer composition, molecular weight, and *Đ* of block copolymer substrates

Entry	[DEVP]/[DPrTMSVP] feed	[DEVP]/[DPrTMSVP][a] composition	$M_{n,abs}$[b] [kg/mol]	*Đ*[b] [-]
P6	50:10	50:2	28.0	1.1
P7	100:10	100:7	40.8	1.1
P8	200:10	200:4	101.2	1.1
P9	400:10	400:2	253.0	1.1

[a] ratio of DEVP to DPrTMSVP determined via ^{1}H-NMR [b] absolute molecular weight and polydispersity determined via SEC-GPC in THF:H_2O with added TBAF, 40 °C, dn/dc = 0.0922 mL/g.

7.2 Characterization of Micelles

Upon a more detailed investigation into micelle properties, this hypothesis is confirmed. In determining the critical micelle concentration (CMC) using nile red, an increasing DEVP content in Polymers **P6**-**P8** correlate with a higher CMC. However, for **P9,** the copolymer with the highest hydrophilic component, determining a CMC is impossible, indicating the absence of micelle formation due to insufficient amphiphilic character. This is also reflected in the conducted DLS measurements (Table 7.2, Figure 1, left). For **P9**, only a diameter of 12.3 nm is measured, indicating a tendency toward a polymer coil rather than a micelle structure. Diameters ranging from 67.2 to 83.3 nm can be determined for polymers **P6** to **P7**, suggesting the presence of micelles. An interesting observation is that as the DEVP content increases, resulting in larger polymer chains, the micelle radius decreases. In prior research involving block copolymers using 2VP and DEVP, a consistent hydrodynamic micelle diameter is observed despite maintaining an unchanged hydrophilic block size and varying DEVP chain lengths.[60, 67] This suggests that the DEVP content does not exert a significant influence on the size of the micelles. However, in this case, there is not just stability but also a decrease in diameter by up to 9.00 nm. Due to this phenomenon and the notably wide distribution of micelle sizes, additional transmission electron microscopy (TEM) measurements are conducted (Tabel 7.2, Figure 7.1, right). These reveal notably smaller micelle diameters, attributed to the drying process during TEM sample preparation. Notably, unlike findings from DLS, micelle size increases with higher DEVP content. This observation can be traced back to a detailed examination of the TEM images, which indicates that **P6** particularly tends to form road-shaped and worm-like micelles. These variations in morphology are weighted differently across these analysis methods, consequently influencing the statistical outcomes of each method differently. Overall, it suggests that the tendency to form wormlike micelles diminishes with the larger DEVP blocks. This not only explains the relatively larger diameter in **P6** and the reduced hydrodynamic diameter (from **P6** to **P8**) in DLS measurements but also accounts for the

decrease in polydispersity (in both analysis methods) with increased hydrophilic components. During TEM measurements, no micelles are observed for polymer **P9**, confirming the assumption that this polymer is also incapable of forming micelles.

Table 7.2: Critical micelle concentration, diameter, and polydispersity of the micelles

Entry	CMC [mg/mL]	d_{DLS} [a] [nm]	PDI_{DLS} [a] [%]	d_{TEM} [b] [nm]	PDI_{TEM} [b] [%]
P6	0.40	83.3	20.3	26.3	27.7
P7	0.41	74.9	15.6	55.8	25.9
P8	0.48	67.2	11.8	72.3	15.5
P9	-	12.3	9.0	-	-

[a] measured by DLS in millipore water (c = 2.5 mg/mL). The micelle size is given as the average hydrodynamic diameter. [b] analyzed by TEM in millipore water (c = 0.5 mg/mL).

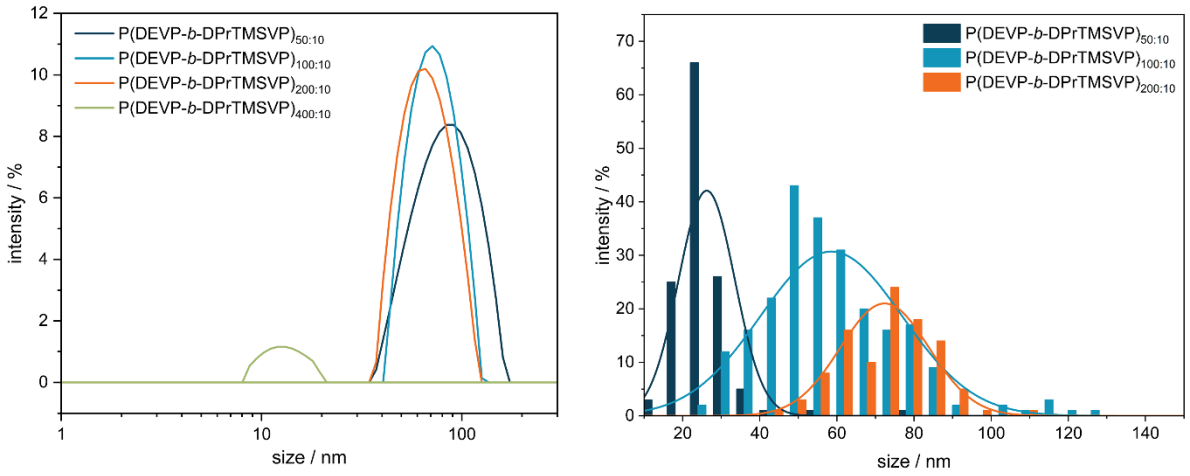

Figure 7.1: Size distribution of **P6** (dark blue), **P7** (light blue), **P8** (orange), and **P9** (green) determined via DLS measurements at a concentration of 2.5 mg/mL in water (left); histogram plot with a Gaussian regression fit (right).

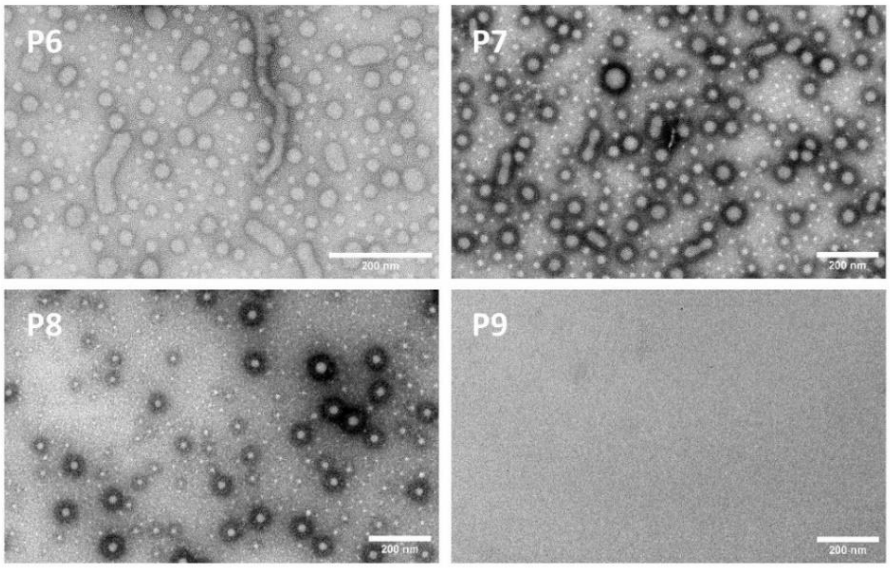

Figure 7.2: TEM images of **P6**, **P7**, **P8** and **P9**. Scale bar = 200 nm.

In addition to characterizing the size and shape of the formed micelles, the thermoresponsive behavior characteristic of polyvinyl phosphonates is investigated. This study reveals the expected reversible thermoresponsive behavior and identified an increase in the cloud temperature from 36 °C to 42 °C corresponding to the growing DEVP content in polymers **P6**-**P9** (Figure 7.3). This capacity allows the tailoring of the LCST of the polymers based on chain length. Moreover, DLS measurements conducted within a 25 °C to 50 °C temperature range validate the transferability of previously acquired temperature data to the micellar system. This also proofs the reversibility of the polymers and the reformation of micelles upon falling below the LCST. Additionally, the UV/vis-derived cloud temperatures are reflected, exhibiting minor deviations compared to the cloud points derived from DLS analysis.

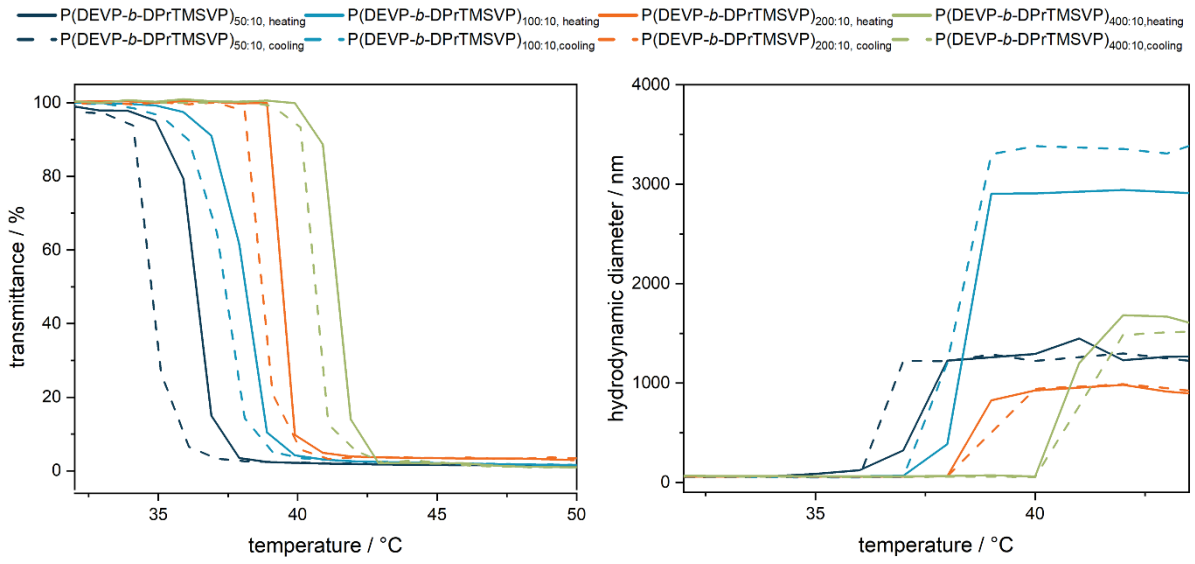

Figure 7.3: Determination of cloud point (left) of poly(vinyl phosphonate)s **P6** (dark blue), **P7** (light blue), **P8** (orange), and **P9** (green) and temperature-dependent behavior of their micelles (right).

Building upon the findings from the investigations into the thermoresponsive behavior of the block copolymers, subsequent studies are conducted with **P6**-**P8** to explore potential applications in drug delivery systems (Figure 7.4). These studies involve loading micelles with fluorescein and investigating the release of the dye over 48 hours at various temperatures: room temperature, 37°C, 42°C, and 44°C. Generally, the highest release of fluorescein is observed at a medium temperature of 44°C, closely followed by conditions at 42°C. Comparatively, the release at 37°C and room temperature showed notably lower values, which are quite similar. Polymer **P6** demonstrates nearly complete release at 44°C and 42°C, promising for drug delivery systems. However, substantial release is also observed at 37°C and room temperature, indicating the need for further improvement. **P7** and **P8** show slightly reduced releases at lower temperatures, but higher temperatures result in lower release rates. Overall, a trend is evident where the release increases with the rise in medium temperature at the selected measuring points. Nevertheless, no correlation is observed concerning the polymer composition

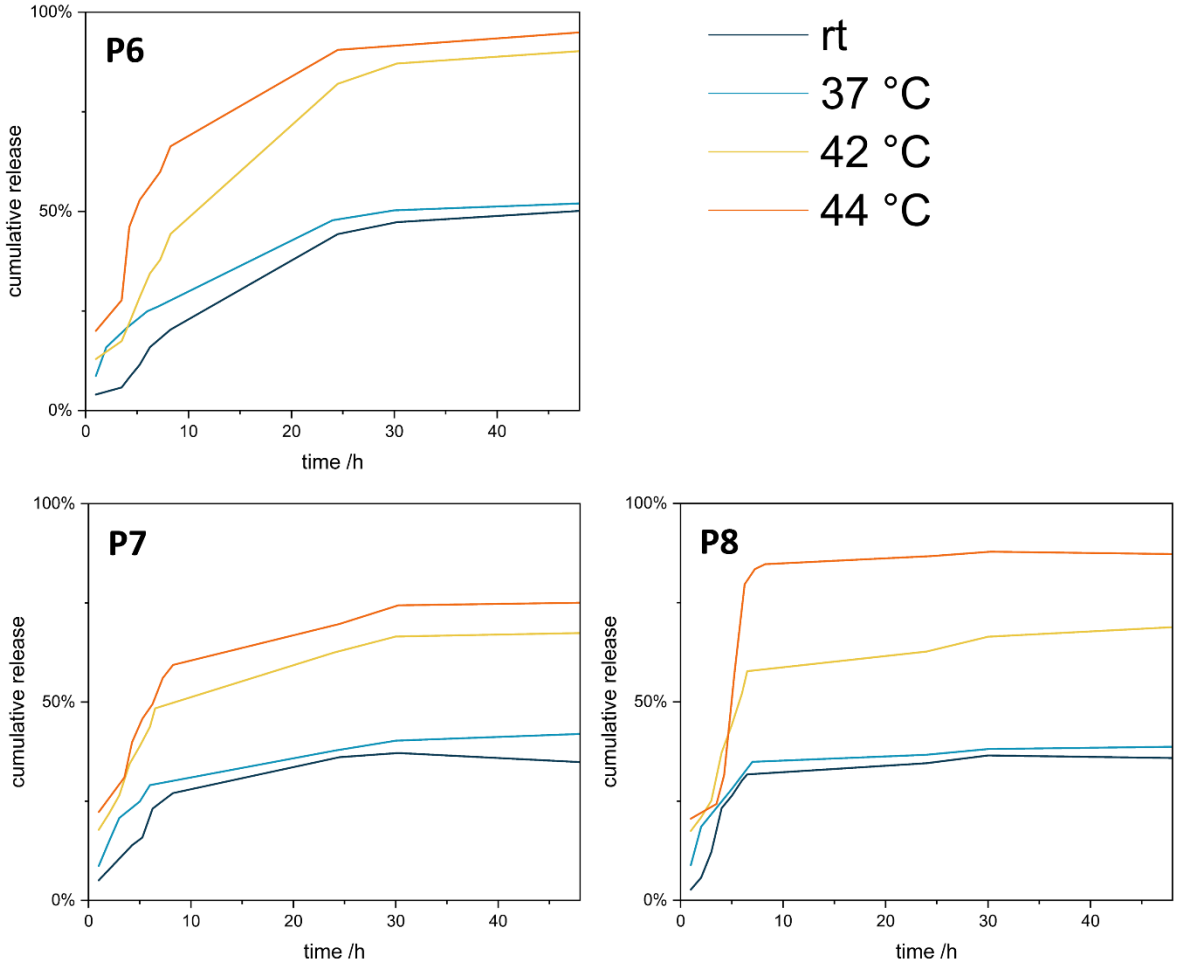

Figure 7.4: Cumulative fluorescein release from **P6** (left top), **P7** (left bottom), and **P8** (right bottom) under varying conditions.

Besides exploring the release behavior, the biocompatibility of the polymers is assessed with the spontaneously immortalized human *Müller* cell line (MIO-M1) (Figure 7.5). The cells are treated with varying polymer concentrations for 24 hours. Notably, all tested polymers demonstrated cell viability exceeding 93% up to a concentration of 500 µg/mL, comparing with the trends observed in the previously discussed terpolymers and affirming their performance. However, a further increase in polymer concentration led to a significant reduction in cell viability for all tested polymers. Specifically, **P6** exhibits a viability of only 60% at 1000 µg/mL. Comparing individual polymers, it is noted that **P6**, containing the highest percentage of DPrTMSVP, exhibited markedly higher toxicity compared to **P9**, which has the lowest DPrTMSVP content. **P7** and **P8** fall between these extremes, showing no distinct trend. Generally, all polymers demonstrate promising biocompatibility. It is conjectured that the toxicity of the polymers correlates with the proportion of DPrTMSVP, but this hypothesis requires validation through further exploration of different polymer compositions and additional cell tests.

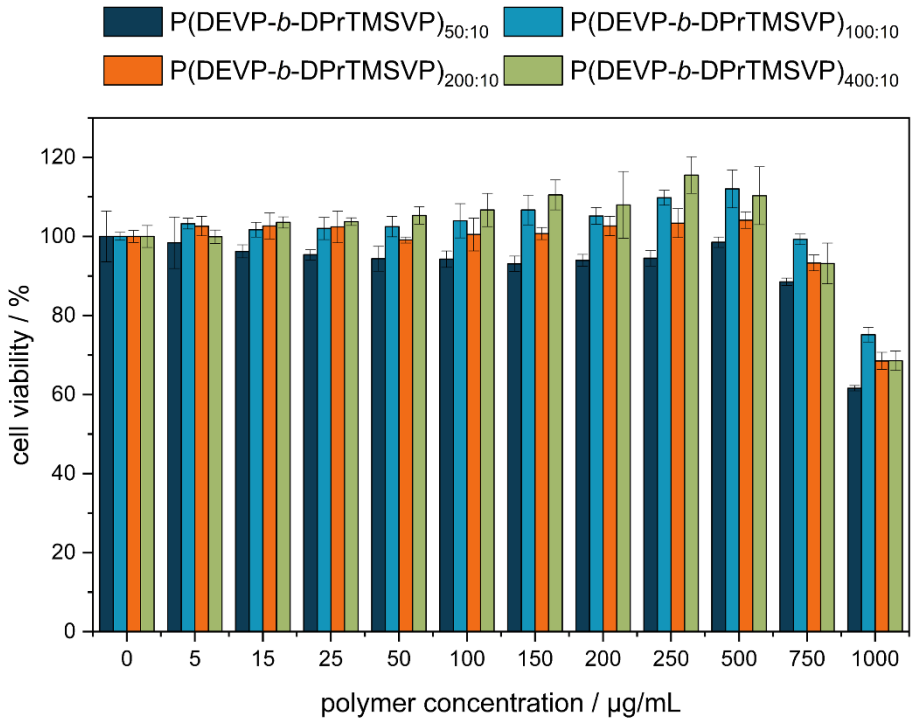

Figure 7.5: Analysis of the cell viability of *Müller* cell line (MIO-M1) as a function of increasing **P6** (dark blue), **P7** (light blue), **P8** (orange), and **P9** (green) polymer concentration.

8. Excursus II: Functionalization with Nucleobase Derivates

Apart from investigating the self-assembly behavior of P(DEVP-*co*-DPrTMSVP) copolymers, an additional examination of potential functionalization with nucleobases is conducted, considering their potential for further promising biological applications.

8.1 Polymerization

As a model system, the statistical copolymer P(DEVP-*co*-DPrTMSVP)$_{90/10,stat}$ **P10**, based on a monomer ration DEVP: DPrTMSVP = 90:10, is selected to enhance accessibility to the modifiable propargyl groups (Scheme 8.1, left). The polymerization is carried out and characterized under nearly analogous conditions to the preceding block copolymers **P6**-**P9**. The successful completion of the polymerization is validated using ^{1}H, ^{31}P, and DOSY-NMR spectroscopy.

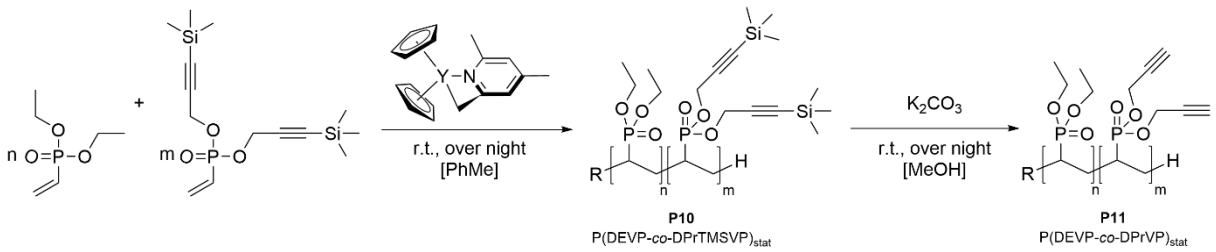

Scheme 8.1: Polymerization of statistical P(DEVP-b-DPrTMSVP)$_{90/10,stat}$ **P10**, followed by deprotection of propargyl groups gainig **P11**.

Before functionalizing the polymer **P10** through AAC, it is necessary to deprotect the propargyl groups (Scheme 8.1, right). To remove the TMS group, the polymer **P10** is dissolved in methanol and stirred overnight at room temperature with potassium carbonate, following the deprotection methods previously mentioned. Quantitative deprotection is confirmed via ^{1}H-NMR analysis, where the signal attributed to the TMS group at 0.13 ppm and the CH_2 group at 4.79 ppm completely disappeared (Figure 8.1). Additionally, DOSY-NMR reveals that all signals associated with the polymer exhibited identical diffusion coefficients, indicating intact polymer chains and the absence of polymer degradation.

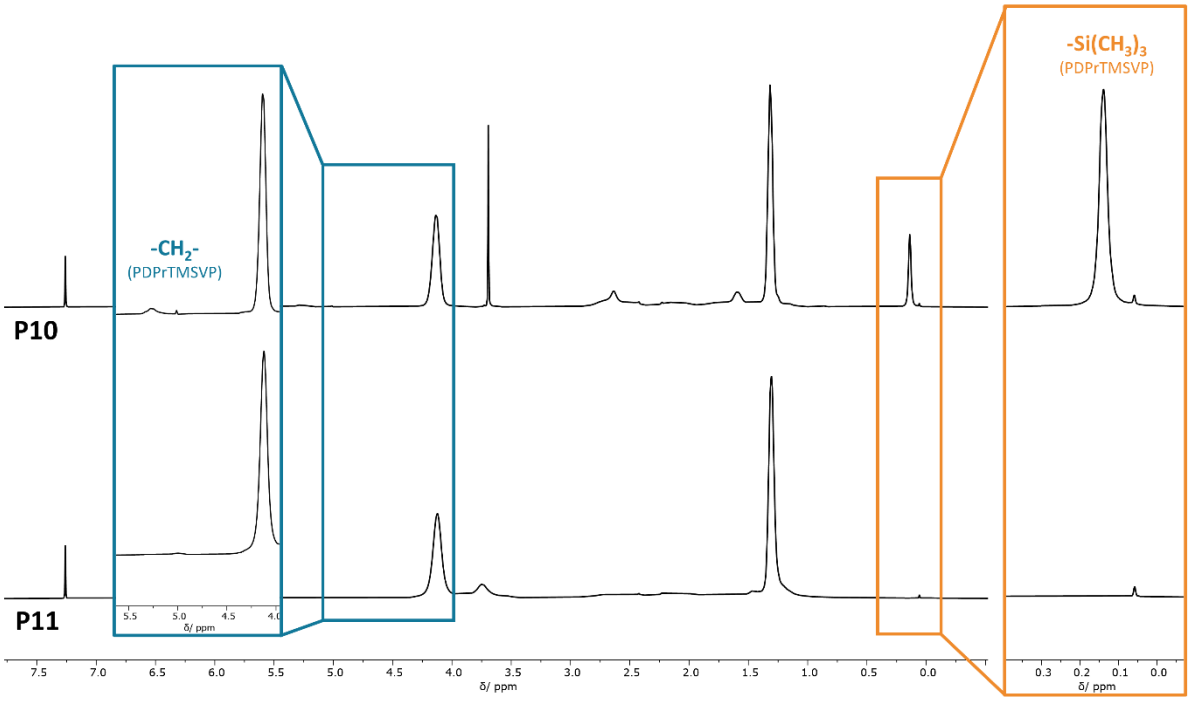

Figure 8.1: Stacked ^{1}H-NMRs of the statistical polyvinyl phosphonate before (**P10**) and after (**P11**) deprotection with a close-up of the -CH_2-groups region of the monomer side chains (blue) and the silyl region (orange).

8.2 Functionalization with Adenine and Thymine

Following this, the post-polymerization functionalization of the obtained model polymer P(DEVP-*co*-DPrVP)$_{stat}$ **P11** with adenine and thymine derivatives is investigated (Scheme 8.2). The azide derivatives of the nucleobases essential for the AAC are synthesized analogously in the literature. The modification through copper-catalyzed AAC (CuAAC) is initially compared to the thermally activated *Huisgen* method. In CuAAC, Cu^{II+} sourced from copper sulfate is reduced to the catalytically active CuI^{+} *via* sodium ascorbate, while the *Huisgen* method achieves reaction activation through an increase in temperature.

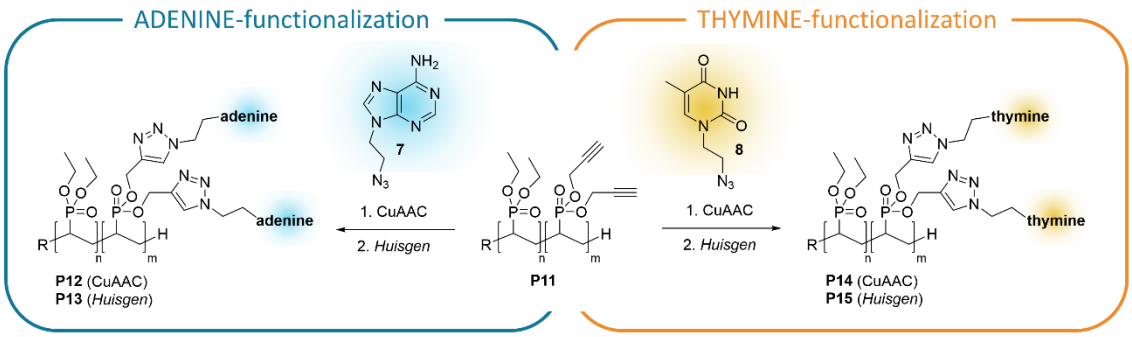

Scheme 8.2: Conjugation of the adenine (blue)- and thymine (orange)-derivates to polymer **P11**.

The initial focus involves exploring the functionalization process of poly(vinyl phosphonate) **P11** using the adenine derivative **7**. The success of the modification can be assessed through analysis using ^{1}H-NMR spectroscopy (Figure 8.2). In this case, polymer **P13**, modified through

CuAAC, shows a signal at 8.29 ppm, while polymer **P14**, functionalized *via* the Huisgen method, presents a signal at 8.30 ppm. These correspond to the aromatic protons of adenine derivative **7**, which are found at 8.14 ppm. Moreover, the broadening of the signal compared to the uncoupled substance **7** indicates coordination of the nucleobase to the polymer. Additionally, DOSY-NMR analysis shows that the signal attributed to azide **7** shares the same diffusion coefficient with signals stemming from the poly(vinyl phosphonate), confirming the binding of azide **7** to poly(vinyl phosphonate) **P11**. Both CuAAC and *Huisgen* reactions demonstrated successful qualitative modification of the polymer, as evidenced by ^{1}H- and DOSY-NMR. However, due to the low intensity of these signals, the exact degree of functionalization could not be determined, thereby hindering the comparison of different reaction conditions using NMR analytics.

Nevertheless, the functionalization with the nucleobase thymine, complementary to adenine in DNA, is qualitatively examined for both reactions, CuAAC (**P14**) and *Huisgen* methode (**P15**), using ^{1}H-NMR. During this analysis, the presence of an aromatic signal at 7.25 ppm (**P14**)/ 7.20 ppm (**P15**) is associated with the aromatic proton of thymine. Additionally, an observed signal at 11.2 ppm (**P14**)/ 11.3 ppm (**P15)** corresponds to the acidic proton of the amide group. Moreover, the shift and broadening of these signals compared to the utilized thymine derivative **8** further support the successful post-polymerization functionalization *via* CuAAC and *Huisgen* reactions. However, a quantitative assessment of the functionalization in this reaction remains unfeasible. Additionally, in both cases, the coupling of thymine to the polymer is demonstrated.

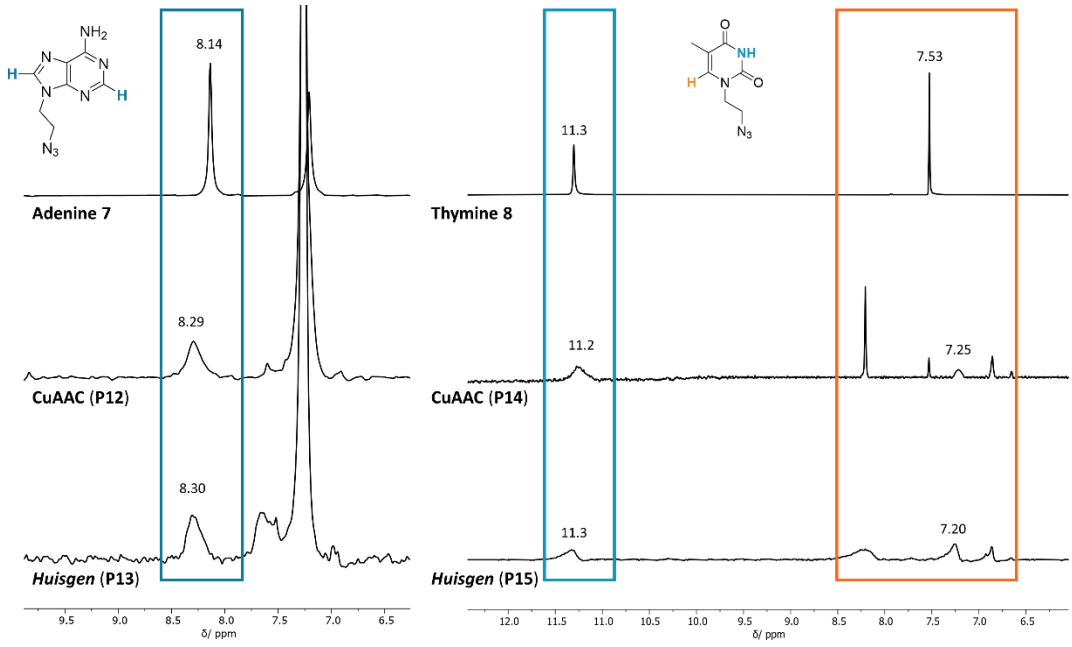

Figure 8.2: Stacked ^{1}H-NMRs of adenine (left)- and thymine (right) functionalization via CuACC (middle) and *Huisgen* method (bottom) compared with the nucleobase substrate (top).

To facilitate comparing different variations of the cycloaddition process, the detectability of nucleobases is utilized through UV/vis spectroscopy (Figure 8.3). All purified, with adenine and thymine functionalized, polymers, **P12**, **P13, P14,** and **P15** are measured in methanol. The adenine-functionalized polymers **P12** and **P13** exhibit an absorption band at approximately 260 nm, corresponding to adenine.[176] Additionally, the absorption around 210 nm indicates the presence of 1,2,3-triazole formed during the cycloaddition, further confirming the successful modification through AAC. A comparison between polymers **P12** and **P13** reveals a display of a very similar intensity of absorption bands, suggesting a comparable effectiveness of both cycloaddition reactions. Subsequently, the polymers functionalized with thymine, **P14**, and **P15**, are also examined. At a wavelength of 262 nm, a distinct absorption band indicative of thymine is observed.[177] Considering the similar intensity of signals in both polymers, it suggests a comparable degree of functionalization achieved by both methods.

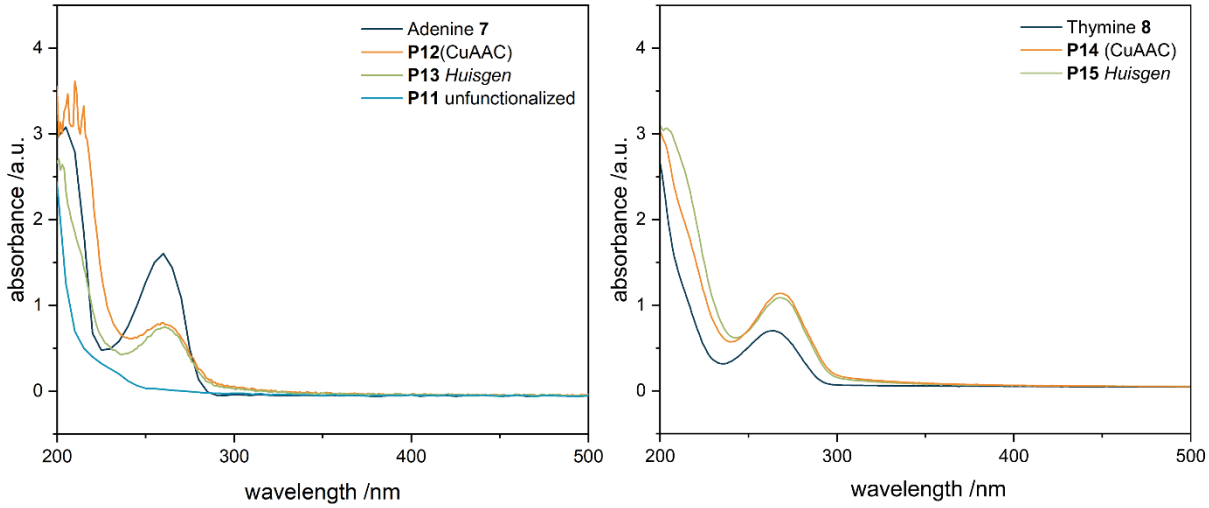

Figure 8.3: UV/vis spectra of adenine (**P12**, **P13**, left)- and thymine (**P14**, **P15**, right) functionalized polymers. Comparison of the nucleobases (dark blue), the modification *via* CuAAC (orange) and *Huisgen* (green), as well as the unfunctionalized polymer **P11** (light blue).

The comparison between the CuAAC and *Huisgen* methods did not show a clear preference because both approaches produced highly similar results. However, the tendency of copper to coordinate with phosphonate groups complicates the purification of polymers and makes the CuAAC variant challenging, especially in biomedical applications. Consequently, further research efforts have prioritized the *Huisgen* method. To optimize it, analogous reactions are conducted at various temperatures ranging from 90°C to 150°C. Different solvents are chosen considering the temperatures applied and their boiling points.

Table 8.1: Post-polymerization functionalization of P(DEVP-*co*-DPrVP) **P11** with adenine **7** at different temperatures

Entry	nucleobase	solvent	T [°C]
P12	adenine **7**	H_2O:DMSO (2:5)	90
P16	adenine **7**	DMF	130
P17	adenine **7**	DMAc	150

The functionalization of the polymers is qualitatively confirmed for all modification approaches by ^{1}H and DOSY-NMR spectroscopy. However, analysis of the ^{31}P NMR spectra revealed significant observations. Treatment at 150°C (**P17**) results in the disappearance of the typical polymer signal at 33.1 ppm, replaced by signals at 30.7 ppm and 22.5 ppm, indicating potential polymer chain degradation. The newly formed signals can likely be attributed to the degradation products of the previous compound. At 130°C (**P16**), additional signals at 29.3 ppm and 20.0 ppm are observed alongside the expected polymer signal, suggesting the beginning degradation of the polymer chain, although with low signal intensity. Identifying the precise nature of these degradation products necessitates further experimental investigation. Interestingly, at 90°C, no supplementary signal is detected beyond the anticipated polymer signal at 33.1 ppm, indicating an absence of polymer chain degradation under these conditions (Figure 8.4).

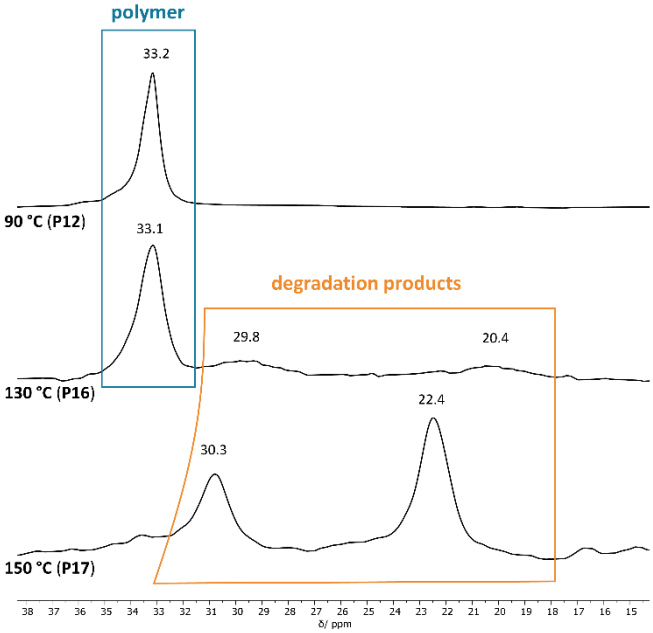

Figure 8.4: Cutout of ^{31}P-NMR spectra of adenine-functionalized poly(vinyl phosphinates) synthesized *via Huisgen* at 90°C (**P12**), 130°C (**P16**) and 150°C (**P17**). Polymer (blue) and degradation products (orange) are highlighted.

Nevertheless, UV/vis spectroscopy is utilized to examine the functionalized polymers. Polymer **P17** is disregarded due to the suspected degradation reaction. As polymer **P16** exhibited only a minor proportion of degradation reactions, it is nonetheless used for comparative analysis. By comparing polymers **P12** and **P16** at equal concentrations, a relative assessment based on the intensity of the absorption band is made possible. Initially, it is noted that both polymers exhibited an absorption band at the anticipated wavelength of 260 nm (Figure 8.5). However, a significantly higher intensity is observed at 130°C, suggesting a higher degree of functionalization. This implies that the reaction at higher temperatures leads to better functionalization, albeit limited in this case due to polymer chain degradation. Although further investigation between 100°C and 120°C is essential for making clear statements, such studies are not conducted as part of this research.

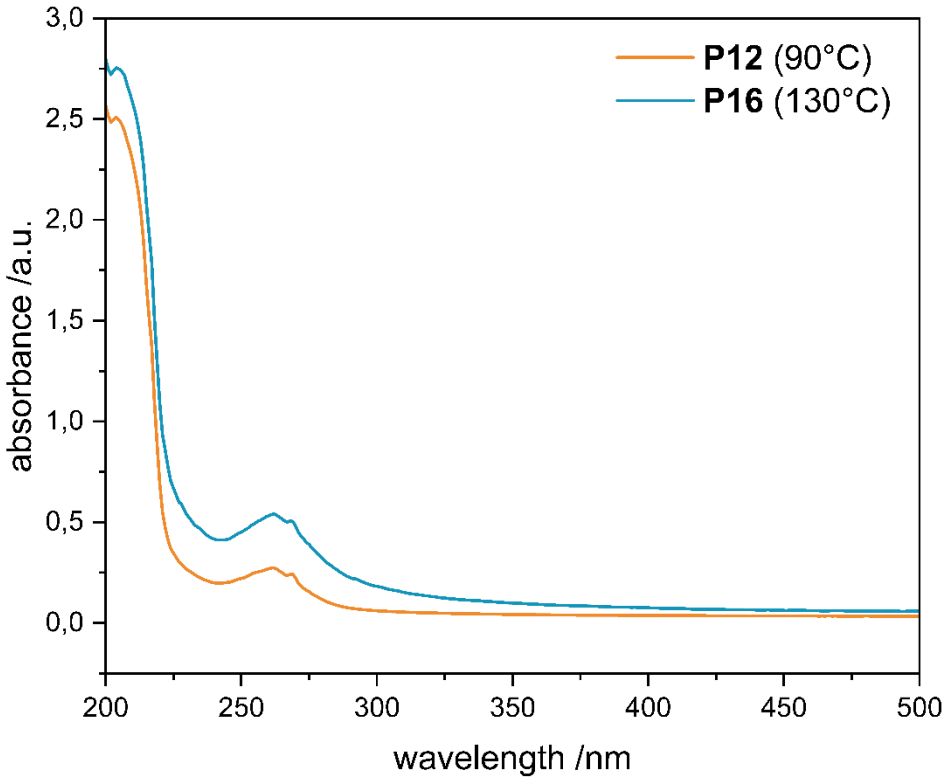

Figure 8.5: UV/vis spectra of adenine functionalization via *Huisgen* method at 90°C (**P12**, orange) and 130 °C (**P16**, blue).

9. Summary and Outlook

Within the scope of this thesis, the previous achievements, such as the precise polymerization of poly(vinyl phosphonate)s *via* REM-GTP and the already implemented modifications, were utilized as a foundation to develop polymers with a broad potential for functionalization and applications across various fields, particularly in the biomedical field.[18, 27, 61, 62, 67]

One aspect involved the expansion of available end-groups for poly(vinyl phosphonate)s by incorporating (protected) alkynes and azides. This, in conjunction with previously reported functional groups such as double bonds, bipyridines, multifunctional pyridines, amines, and thiols, resulted in a diverse spectrum of anchor points for subsequent linking reactions.[48, 63, 64, 175] The quantitative *in-situ* activation and integration of initiators based on pyridine derivatives enable the dependable attachment of functional groups. This type of modification is especially relevant when only one linking site or specifically one substrate per polymer chain is required, as is often the case for labeling or surface modifications. DEVP was chosen as the monomer for polymerization screening. Future research endeavors could explore alternative alkyl vinyl phosphonates, vinylpyridines, or IPOx as highly functional monomers. Strategic combinations of these monomers in copolymers make it possible to selectively tune polymer properties in alignment with the targeted objectives of developing advanced materials (Figure 9.1).

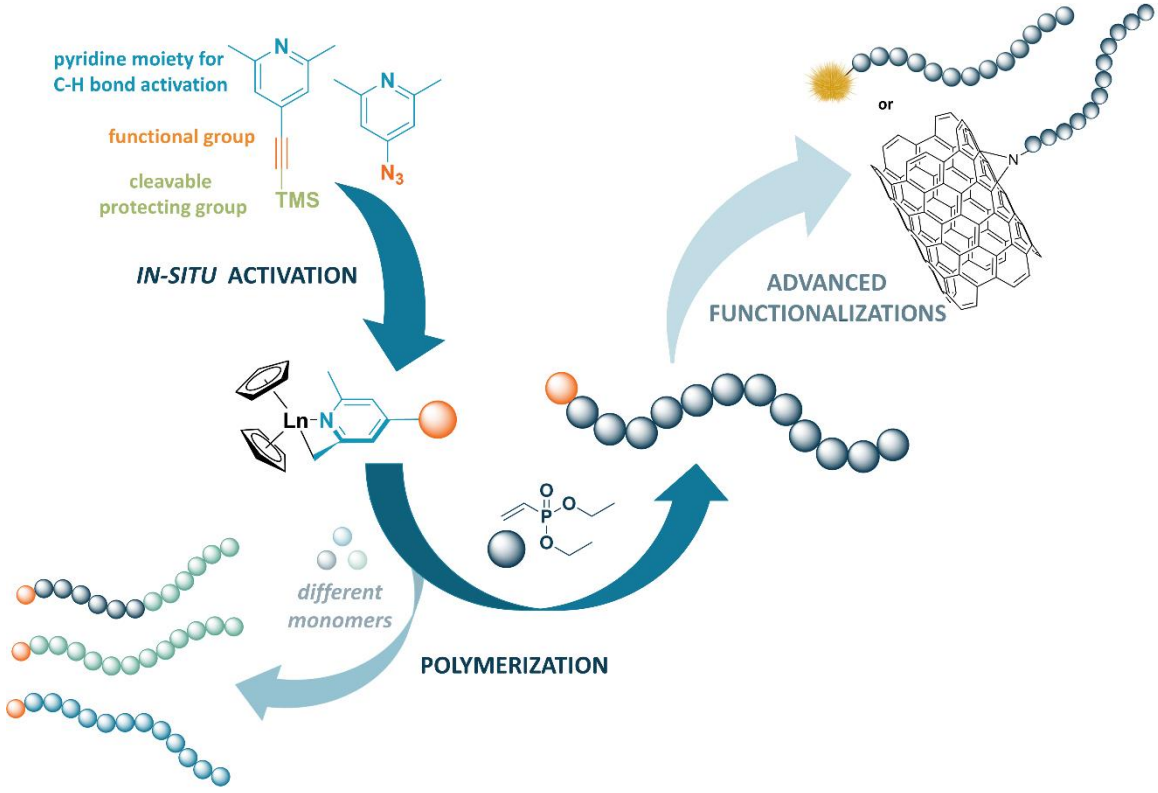

Figure 9.1: Graphical overview of end-group functionalization in poly(vinyl phosphonates) within the scope of this thesis and prospective approaches.

In addition to incorporating diverse end groups, it is also possible to enhance functionalities within the polymer chain by choosing suitable monomers. This approach was addressed by *Rieger et al.* via the monomer DAIVP, a vinyl phosphonate with pending allyl groups.[67]This monomer was also applied in the context of this work, whereby the double bonds are functionalized further through polymer-analogous reactions. This allowed the integration of novel functionalities like azides after reactions like brominations, epoxidations, thiol-ene reactions, subsequent nucleophilic substitutions, nucleophilic ring-openings, and hydrazone formation. Moreover, various test substrates were coupled to the polymers through AAC, further expanding the plaform via multifunctionalization. This serves as the foundation to create new poly(vinyl phosphonate) conjugates. Subsequent investigations could explore the polymeric materials with biologically active units, such as drugs, peptides, targeting groups, or other active substrates attached to them. This, in turn, could help to develop polymer-drug conjugates and subsequently application-oriented testing (Figure 9.2).

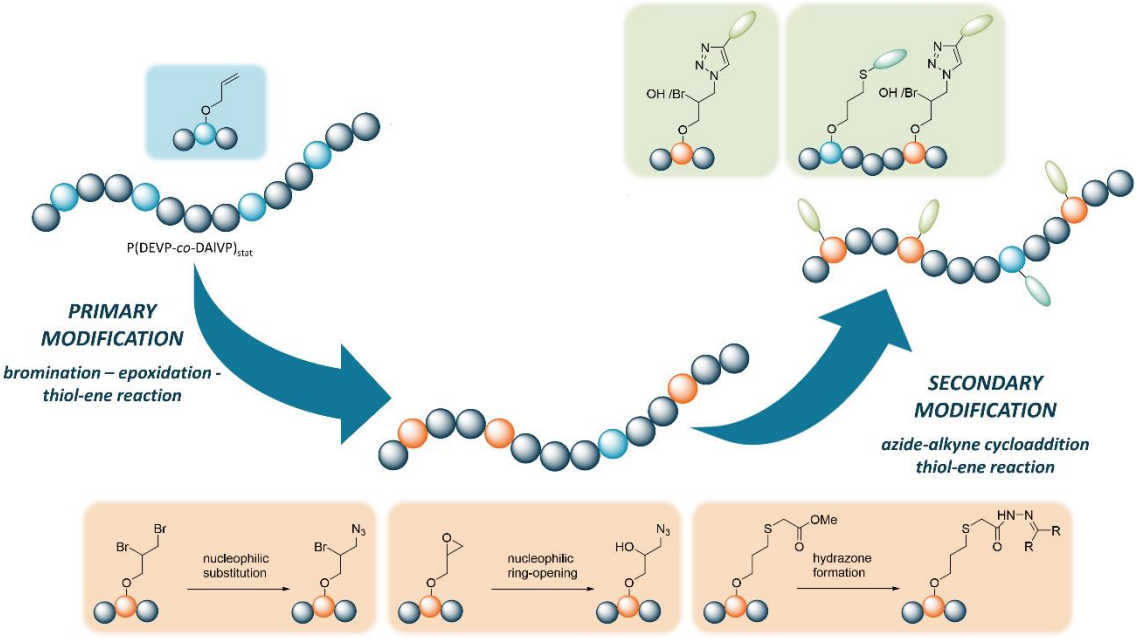

Figure 9.2: Visual Representation of polymer-analogous reactions on P(DEVP-*co*-DAIVP)$_{stat}$ for expanding the spectrum of polymer functionalization within the scope of this thesis.

Especially concerning the targeted multifunctionalization of poly(vinyl phosphonate)s, this study has achieved significant progress by introducing the new monomer DPrTMSVP. This monomer features TMS-protected propargyl groups as side chains. With two available monomers classes equipped with functional groups, it is possible to selectively introduce functionalities into the terpolymer P(DAIVP-DEVP-DPrTMSVP). A thoughtful selection of these functionalities enables subsequent orthogonal modification of poly(vinyl phosphonate)e through AAC and thiol-ene click reactions with diverse test substrates. This once again establish a concept for the precise multifunctionalization of phosphorus-containing polymers. Furthermore, strategically attaching biologically active substrates, such as cholesterol and folic acid, demonstrates the promising utility of the polymers. Their low toxicity further reinforces their potential. In addition to further investigations regarding the applicability of these polymer conjugates, for example, in liposomal drug delivery systems, there is the potential for extensive variation of selected substrates over a wide range and testing in different combinations (Figure 9.3).

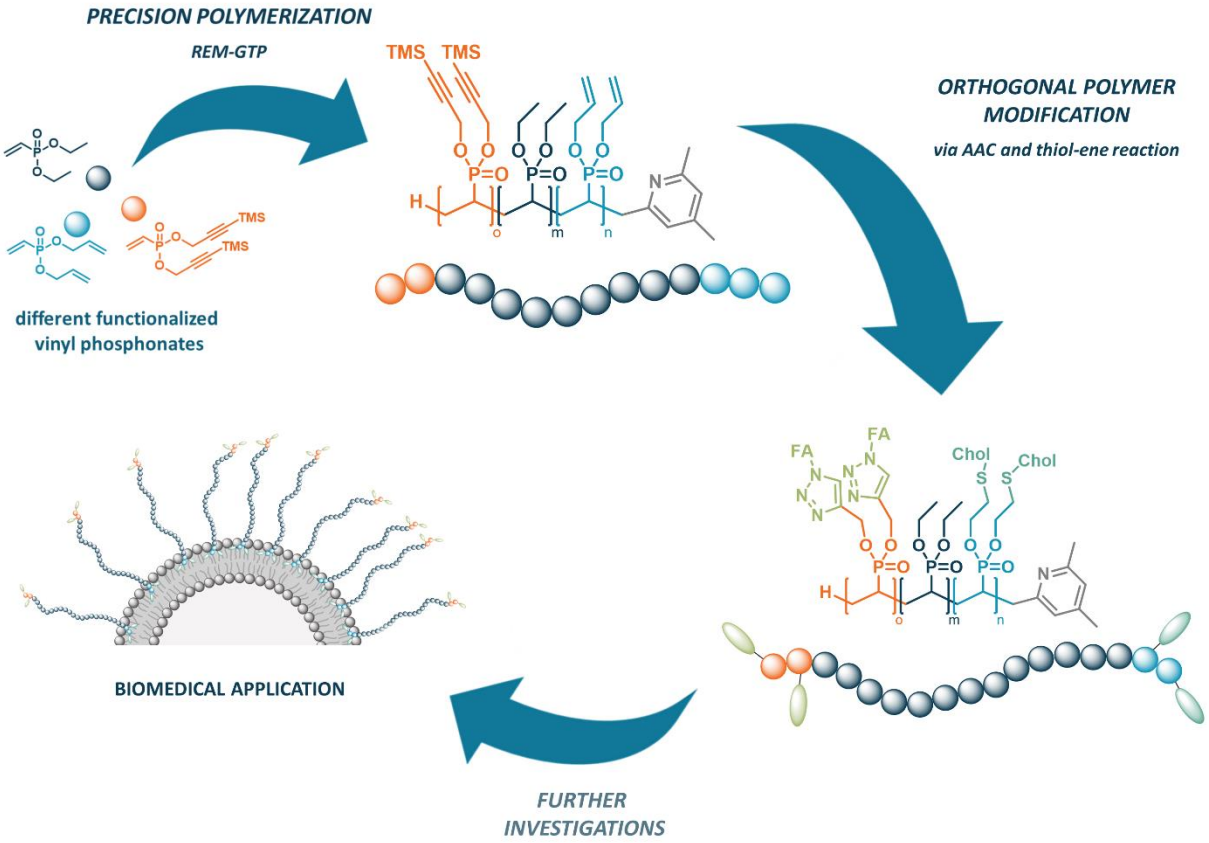

Figure 9.3: Graphic summary of the polymerization of dual functionalized terpolymers and subsequent orthogonal modification in the context of this thesis, as well as potential future approaches.

In summary, various pathways to integrate functional anchor points into poly(vinyl phosphonates) were investigated. While the present study focused on end-group functionalization, polymer-analogous reactions, and functionality in individual monomers, a future approach could consolidate all achieved modification methods (Figure 9.4). This comprehensive perspective could focus on biomedical applications like drug delivery systems.

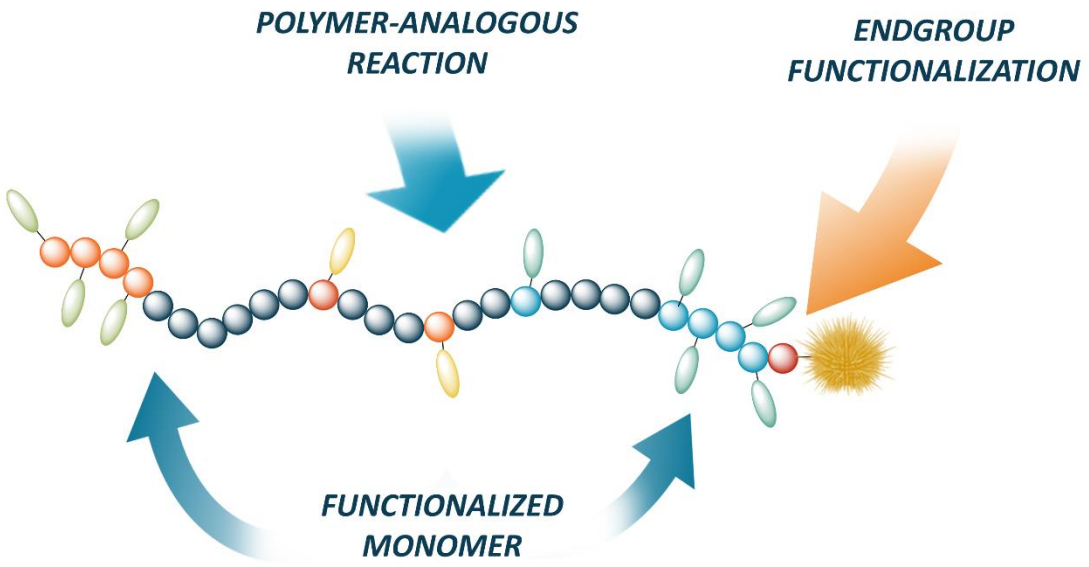

Figure 9.4: Graphical outlook for integration of the investigated modification options explored in this thesis into a unified approach.

10. Literature

(1) Jagur-Grodzinski, J. Biomedical application of functional polymers. *Reactive and Functional Polymers* **1999**, *39* (2), 99-138.

(2) Chen, W.-H.; Chen, Q.-W.; Chen, Q.; Cui, C.; Duan, S.; Kang, Y.; Liu, Y.; Liu, Y.; Muhammad, W.; Shao, S.; et al. Biomedical polymers: synthesis, properties, and applications. *Science China Chemistry* **2022**, *65* (6), 1010-1075.

(3) Kalirajan, C.; Dukle, A.; Nathanael, A. J.; Oh, T.-H.; Manivasagam, G. A Critical Review on Polymeric Biomaterials for Biomedical Applications. *Polymers* **2021**, *13* (17), 3015.

(4) Van de Velde, K.; Kiekens, P. Biopolymers: overview of several properties and consequences on their applications. *Polymer testing* **2002**, *21* (4), 433-442.

(5) Endres, H.-J.; Siebert-Raths, A. Engineering biopolymers. *Eng. Biopolym* **2011**, *71148*, 3-15.

(6) Gunatillake, P. A.; Adhikari, R.; Gadegaard, N. Biodegradable synthetic polymers for tissue engineering. *Eur Cell Mater* **2003**, *5* (1), 1-16.

(7) Liechty, W. B.; Kryscio, D. R.; Slaughter, B. V.; Peppas, N. A. Polymers for drug delivery systems. *Annual review of chemical and biomolecular engineering* **2010**, *1*, 149-173.

(8) Xu, L.; Yu, C.; Wang, D.; Pang, J.; Shi, L.; Su, Y.; Gong, L.; Yan, D.; Zhu, X. Endogenous nucleotide as drug carrier: base-paired guanosine-5′-monophosphate: pemetrexed vesicles with enhanced anticancer capability. *Science China Chemistry* **2020**, *63*, 244-253.

(9) Premkumar, J.; SonicaSree, K.; Sudhakar, T. Polymers in Biomedical Use. In *Handbook of Polymer and Ceramic Nanotechnology*, Hussain, C. M., Thomas, S. Eds.; Springer International Publishing, 2020; pp 1-28.

(10) Li, Y.; Zheng, X.; Chu, Q. Bio-based nanomaterials for cancer therapy. *Nano Today* **2021**, *38*, 101134.

(11) Aguilar, M. R.; San Román, J. *Smart polymers and their applications*; Woodhead publishing, 2019.

(12) Zhu, M.; Song, X. Z.; Song, S. Y.; Zhao, S. N.; Meng, X.; Wu, L. L.; Wang, C.; Zhang, H. J. A Temperature-Responsive Smart Europium Metal-Organic Framework Switch for Reversible Capture and Release of Intrinsic Eu3+ Ions. *Advanced Science* **2015**, *2* (4), 1500012.

(13) Verma, R.; Adhikary, R. R.; Banerjee, R. Smart material platforms for miniaturized devices: implications in disease models and diagnostics. *Lab on a Chip* **2016**, *16* (11), 1978-1992.

(14) Hollingshead, S.; Lin, C. Y.; Liu, J. C. Designing smart materials with recombinant proteins. *Macromolecular bioscience* **2017**, *17* (7), 1600554.

(15) Hsiao, S.-H.; Hsu, S.-h. Synthesis and characterization of dual stimuli-sensitive biodegradable polyurethane soft hydrogels for 3D cell-laden bioprinting. *ACS applied materials & interfaces* **2018**, *10* (35), 29273-29287.

(16) Kamerlin, S. C. L.; Sharma, P. K.; Prasad, R. B.; Warshel, A. Why nature really chose phosphate. *Quarterly Reviews of Biophysics* **2013**, *46* (1), 1-132.
(17) Westheimer, F. H. Why Nature Chose Phosphates. *Science* **1987**, *235* (4793), 1173-1178. DOI: doi:10.1126/science.2434996.

(18) Soller, B. S.; Salzinger, S.; Rieger, B. Rare Earth Metal-Mediated Precision Polymerization of Vinylphosphonates and Conjugated Nitrogen-Containing Vinyl Monomers. *Chemical Reviews* **2016**, *116* (4), 1993-2022.

(19) Chaubal, M. V.; Gupta, A. S.; Lopina, S. T.; Bruley, D. F. Polyphosphates and Other Phosphorus-Containing Polymers for Drug Delivery Applications. **2003**, *20* (4), 22.

(20) Tian, H.; Tang, Z.; Zhuang, X.; Chen, X.; Jing, X. Biodegradable synthetic polymers: Preparation, functionalization and biomedical application. *Progress in Polymer Science* **2012**, *37* (2), 237-280.

(21) Zhang, S.; Zou, J.; Zhang, F.; Elsabahy, M.; Felder, S. E.; Zhu, J.; Pochan, D. J.; Wooley, K. L. Rapid and Versatile Construction of Diverse and Functional Nanostructures Derived from a Polyphosphoester-Based Biomimetic Block Copolymer System. *Journal of the American Chemical Society* **2012**, *134* (44), 18467-18474.

(22) Macarie, L.; Ilia, G. Poly(vinylphosphonic acid) and its derivatives. *Progress in Polymer Science* **2010**, *35* (8), 1078-1092.

(23) Pike, R. M.; Cohen, R. A. Organophosphorus polymers. I. Peroxide-initiated polymerization of diethyl and diisopropyl vinylphosphonate. *Journal of Polymer Science* **1960**, *44* (144), 531-538.

(24) Ford-Moore, A. H.; Williams, J. H. 278. The reaction between trialkyl phosphites and alkyl halides. *Journal of the Chemical Society (Resumed)* **1947**, (0), 1465-1467, 10.1039/JR9470001465.

(25) Kalek, M.; Ziadi, A.; Stawinski, J. Microwave-Assisted Palladium-Catalyzed Cross-Coupling of Aryl and Vinyl Halides with H-Phosphonate Diesters. *Organic Letters* **2008**, *10* (20), 4637-4640.

(26) Lee, H.-S.; Pai, S.-H.; Liao, W.-T.; Yang, X.-J.; Tsai, F.-Y. Mono and double Mizoroki–Heck reaction of aryl halides with dialkyl vinylphosphonates using a reusable palladium catalyst under aqueous medium. *RSC Advances* **2017**, *7* (54), 34293-34299.

(27) Pehl, T. M.; Adams, F.; Kränzlein, M.; Rieger, B. Expanding the Scope of Organic Radical Polymers to Polyvinylphosphonates Synthesized via Rare-Earth Metal-Mediated Group-Transfer Polymerization. *Macromolecules* **2021**, *54* (9), 4089-4100. DOI: 10.1021/acs.macromol.1c00217.

(28) Herpel, R. H.; Vedantham, P.; Flynn, D. L.; Hanson, P. R. High-load, oligomeric phosphonyl dichloride: facile generation via ROM polymerization and application to scavenging amines. *Tetrahedron Letters* **2006**, *47* (36), 6429-6432.

(29) Maity, P. K.; Faisal, S.; Rolfe, A.; Stoianova, D.; Hanson, P. R. Silica-Supported Oligomeric Benzyl Phosphate (Si-OBP) and Triazole Phosphate (Si-OTP) Alkylating Reagents. *The Journal of Organic Chemistry* **2015**, *80* (20), 9942-9950.

(30) Bordoni, A. V.; Zalduendo, M. M.; Escobar, A.; Amenitsch, H.; Moya, S. E.; Angelomé, P. C. Phosphonate mesoporous hybrid thin films: Synthesis of organophosphosilane by thiol-ene click chemistry and applications in formation and stabilization of silver nanoparticles. *Microporous and Mesoporous Materials* **2020**, *295*, 109958.

(31) Matveeva, E. V.; Shipov, A. E.; Petrovskii, P. V.; Odinets, I. L. Amino acids as suitable N-nucleophiles for the aza-Michael reaction of vinylphosphoryl compounds in water. *Tetrahedron Letters* **2011**, *52* (49), 6562-6565.

(32) Fang, Y.; Zhang, L.; Jin, X.; Li, J.; Yuan, M.; Li, R.; Wang, T.; Wang, T.; Hu, H.; Gu, J. α-Phosphonovinyl Arylsulfonates: An Attractive Partner for the Synthesis of α-Substituted Vinylphosphonates through Palladium-Catalyzed Suzuki Reactions. *European Journal of Organic Chemistry* **2016**, *2016* (8), 1577-1587.

(33) Bingöl, B.; Hart-Smith, G.; Barner-Kowollik, C.; Wegner, G. Characterization of Oligo(vinyl phosphonate)s by High-Resolution Electrospray Ionization Mass Spectrometry: Implications for the Mechanism of Polymerization. *Macromolecules* **2008**, *41* (5), 1634-1639.

(34) Sato, T.; Hasegawa, M.; Seno, M.; Hirano, T. Radical polymerization behavior of dimethyl vinylphosphonate: Homopolymerization and copolymerization with trimethoxyvinylsilane. *Journal of Applied Polymer Science* **2008**, *109* (6), 3746-3752.

(35) Wagner, T.; Manhart, A.; Deniz, N.; Kaltbeitzel, A.; Wagner, M.; Brunklaus, G.; Meyer, W. H. Vinylphosphonic Acid Homo- and Block Copolymers. *Macromolecular Chemistry and Physics* **2009**, *210* (22), 1903-1914.

(36) Salzinger, S.; Rieger, B. Rare Earth Metal-Mediated Group Transfer Polymerization of Vinylphosphonates. *Macromolecular Rapid Communications* **2012**, *33* (16), 1327-1345.

(37) Chen, E. Y. X. Coordination Polymerization of Polar Vinyl Monomers by Single-Site Metal Catalysts. *Chemical Reviews* **2009**, *109* (11), 5157-5214.

(38) Webster, O. W.; Hertler, W. R.; Sogah, D. Y.; Farnham, W. B.; RajanBabu, T. V. Group-transfer polymerization. 1. A new concept for addition polymerization with organosilicon initiators. *Journal of the American Chemical Society* **1983**, *105* (17), 5706-5708.

(39) Yasuda, H.; Yamamoto, H.; Yokota, K.; Miyake, S.; Nakamura, A. Synthesis of monodispersed high molecular weight polymers and isolation of an organolanthanide(III) intermediate coordinated by a penultimate poly(MMA) unit. *Journal of the American Chemical Society* **1992**, *114* (12), 4908-4910.

(40) Collins, S.; Ward, D. G. Group-transfer polymerization using cationic zirconocene compounds. *Journal of the American Chemical Society* **1992**, *114* (13), 5460-5462.

(41) Yasuda, H.; Yamamoto, H.; Yamashita, M.; Yokota, K.; Nakamura, A.; Miyake, S.; Kai, Y.; Kanehisa, N. Synthesis of high molecular weight poly(methyl methacrylate) with extremely low polydispersity by the unique function of organolanthanide(III) complexes. *Macromolecules* **1993**, *26* (26), 7134-7143.

(42) Leute, M. *Macromolecules with phosphorus functionalities*; Universität Ulm und Technischen Hochschule Ulm, 2007.

(43) Seemann, U. B.; Dengler, J. E.; Rieger, B. High-Molecular-Weight Poly(vinylphosphonate)s by Single-Component Living Polymerization Initiated by Rare-Earth-Metal Complexes. *Angewandte Chemie International Edition* **2010**, *49* (20), 3489-3491.

(44) Salzinger, S.; Seemann, U. B.; Plikhta, A.; Rieger, B. Poly(vinylphosphonate)s Synthesized by Trivalent Cyclopentadienyl Lanthanide-Induced Group Transfer Polymerization. *Macromolecules* **2011**, *44* (15), 5920-5927.

(45) Salzinger, S.; Soller, B. S.; Plikhta, A.; Seemann, U. B.; Herdtweck, E.; Rieger, B. Mechanistic Studies on Initiation and Propagation of Rare Earth Metal-Mediated Group Transfer Polymerization of Vinylphosphonates. *Journal of the American Chemical Society* **2013**, *135* (35), 13030-13040.

(46) Yasuda, H.; Yamamoto, H.; Yokota, K.; Miyake, S.; Nakamura, A. Synthesis of monodispersed high molecular weight polymers and isolation of an organolanthanide (III) intermediate coordinated by a penultimate poly (MMA) unit. *Journal of the American Chemical Society* **1992**, *114* (12), 4908-4910.

(47) Nguyen, H.; Jarvis, A. P.; Lesley, M. J. G.; Kelly, W. M.; Reddy, S. S.; Taylor, N. J.; Collins, S. Isotactic Polymerization of Methyl Methacrylate Using a Prochiral, Zirconium Enolate Initiator. *Macromolecules* **2000**, *33* (5), 1508-1510.

(48) Soller, B. S.; Salzinger, S.; Jandl, C.; Pöthig, A.; Rieger, B. C–H Bond Activation by σ-Bond Metathesis as a Versatile Route toward Highly Efficient Initiators for the Catalytic Precision Polymerization of Polar Monomers. *Organometallics* **2015**, *34* (11), 2703-2706.

(49) Keiter, E.; Huheey, J.; Steudel, R.; Keiter, R. Anorganische Chemie: Prinzipien von Struktur und Reaktivität. De Gruyter Berlin/Boston: 2012.

(50) Goldberg, K. I.; Goldman, A. S. *Activation and Functionalization of C—H Bonds*; ACS Publications, 2004.

(51) Steinborn, D. *Grundlagen der metallorganischen Komplexkatalyse*; Springer, 2007.
(52) Waterman, R. σ-Bond metathesis: a 30-year retrospective. *Organometallics* **2013**, *32* (24), 7249-7263.

(53) Deelman, B.-J.; Stevels, W. M.; Teuben, J. H.; Lakin, M. T.; Spek, A. L. Insertion Chemistry of Yttrium Complex Cp* 2Y (2-pyridyl) and Molecular Structure of an Unexpected CO Insertion Product (Cp* 2Y) 2 (. mu.-. eta. 2:. eta. 2-OC (NC5H4) 2). *Organometallics* **1994**, *13* (10), 3881-3891.

(54) Duchateau, R.; van Wee, C. T.; Teuben, J. H. Insertion and C− H Bond Activation of Unsaturated Substrates by Bis (benzamidinato) yttrium Alkyl,[PhC (NSiMe3) 2] 2YR (R= CH2Ph⊙ THF, CH (SiMe3) 2), and Hydrido,{[PhC (NSiMe3) 2] 2Y (μ-H)} 2, Compounds. *Organometallics* **1996**, *15* (9), 2291-2302.

(55) Duchateau, R.; Brussee, E. A.; Meetsma, A.; Teuben, J. H. Synthesis and Reactivity of Bis (alkoxysilylamido) yttrium η2-Pyridyl and η2-α-Picolyl Compounds. *Organometallics* **1997**, *16* (25), 5506-5516.

(56) Kaneko, H.; Nagae, H.; Tsurugi, H.; Mashima, K. End-Functionalized Polymerization of 2-Vinylpyridine through Initial C–H Bond Activation of N-Heteroaromatics and Internal Alkynes by Yttrium Ene–Diamido Complexes. *Journal of the American Chemical Society* **2011**, *133* (49), 19626-19629.

(57) Schaffer, A.; Weger, M.; Rieger, B. From lanthanide-mediated, high-precision group transfer polymerization of Michael-type monomers, to intelligent, functional materials. *European Polymer Journal* **2020**, *122*, 109385.

(58) Adams, F.; Pahl, P.; Rieger, B. Metal-Catalyzed Group-Transfer Polymerization: A Versatile Tool for Tailor-Made Functional (Co)Polymers. *Chemistry – A European Journal* **2018**, *24* (3), 509-518.

(59) Pahl, P.; Schwarzenböck, C.; Herz, F. A. D.; Soller, B. S.; Jandl, C.; Rieger, B. Core-First Synthesis of Three-Armed Star-Shaped Polymers by Rare Earth Metal-Mediated Group Transfer Polymerization. *Macromolecules* **2017**, *50* (17), 6569-6576.

(60) Altenbuchner, P. T.; Werz, P. D. L.; Schöppner, P.; Adams, F.; Kronast, A.; Schwarzenböck, C.; Pöthig, A.; Jandl, C.; Haslbeck, M.; Rieger, B. Next Generation Multiresponsive Nanocarriers for Targeted Drug Delivery to Cancer Cells. *Chemistry – A European Journal* **2016**, *22* (41), 14576-14584.

(61) Schwarzenböck, C.; Vagin, S. I.; Heinz, W. R.; Nelson, P. J.; Rieger, B. Studies on the Biocompatibility of Poly(diethyl vinyl-phosphonate) with a New Fluorescent Marker. *Macromolecular Rapid Communications* **2018**, *39* (15), 1800259.

(62) Schwarzenböck, C.; Schaffer, A.; Nößner, E.; Nelson, P. J.; Huss, R.; Rieger, B. Fluorescent Polyvinylphosphonate Bioconjugates for Selective Cellular Delivery. *Chemistry – A European Journal* **2018**, *24* (11), 2584-2587.

(63) Schwarzenböck, C.; Schaffer, A.; Pahl, P.; Nelson, P. J.; Huss, R.; Rieger, B. Precise synthesis of thermoresponsive polyvinylphosphonate-biomolecule conjugates via thiol–ene click chemistry. *Polymer Chemistry* **2018**, *9* (3), 284-290.

(64) Schaffer, A.; Kränzlein, M.; Rieger, B. Synthesis and Application of Functional Group-Bearing Pyridyl-Based Initiators in Rare Earth Metal-Mediated Group Transfer Polymerization. *Macromolecules* **2020**, *53* (11), 4345-4354.

(65) Zhang, N.; Salzinger, S.; Rieger, B. Poly(vinylphosphonate)s with Widely Tunable LCST: A Promising Alternative to Conventional Thermoresponsive Polymers. *Macromolecules* **2012**, *45* (24), 9751-9758.

(66) Adams, F.; Altenbuchner, P. T.; Werz, P. D. L.; Rieger, B. Multiresponsive micellar block copolymers from 2-vinylpyridine and dialkylvinylphosphonates with a tunable lower critical solution temperature. *RSC Advances* **2016**, *6* (82), 78750-78754.

(67) Schwarzenböck, C.; Nelson, P. J.; Huss, R.; Rieger, B. Synthesis of next generation dual-responsive cross-linked nanoparticles and their application to anti-cancer drug delivery. *Nanoscale* **2018**, *10* (34), 16062-16068.

(68) Kim, Y.-J.; Matsunaga, Y. T. Thermo-responsive polymers and their application as smart biomaterials. *Journal of Materials Chemistry B* **2017**, *5* (23), 4307-4321.

(69) Clark, E. A.; Lipson, J. E. G. LCST and UCST behavior in polymer solutions and blends. *Polymer* **2012**, *53* (2), 536-545.

(70) Weber, C.; Hoogenboom, R.; Schubert, U. S. Temperature responsive bio-compatible polymers based on poly(ethylene oxide) and poly(2-oxazoline)s. *Progress in Polymer Science* **2012**, *37* (5), 686-714.

(71) Ayano, E.; Kanazawa, H. Aqueous chromatography system using temperature-responsive polymer-modified stationary phases. *Journal of Separation Science* **2006**, *29* (6), 738-749.

(72) Tan, J.; Gemeinhart, R. A.; Ma, M.; Mark Saltzman, W. Improved cell adhesion and proliferation on synthetic phosphonic acid-containing hydrogels. *Biomaterials* **2005**, *26* (17), 3663-3671.

(73) Ghag, A. K.; Gough, J. E.; Downes, S. The osteoblast and osteoclast responses to phosphonic acid containing poly(ε-caprolactone) electrospun scaffolds. *Biomaterials Science* **2014**, *2* (2), 233-241.

(74) Dey, R. E.; Zhong, X.; Youle, P. J.; Wang, Q. G.; Wimpenny, I.; Downes, S.; Hoyland, J. A.; Watts, D. C.; Gough, J. E.; Budd, P. M. Synthesis and Characterization of Poly(vinylphosphonic acid-co-acrylic acid) Copolymers for Application in Bone Tissue Scaffolds. *Macromolecules* **2016**, *49* (7), 2656-2662.

(75) Wang, Q. G.; Wimpenny, I.; Dey, R. E.; Zhong, X.; Youle, P. J.; Downes, S.; Watts, D. C.; Budd, P. M.; Hoyland, J. A.; Gough, J. E. The unique calcium chelation property of poly(vinyl phosphonic acid-co-acrylic acid) and effects on osteogenesis in vitro. *Journal of Biomedical Materials Research Part A* **2018**, *106* (1), 168-179.

.

(76) Adden, N.; Hoffmann, A.; Gross, G.; Windhagen, H.; Thorey, F.; Menzel, H. Screening of photochemically grafted polymer films for compatibility with osteogenic precursor cells. *Journal of Biomaterials Science, Polymer Edition* **2007**, *18* (3), 303-316.

(77) Schwarzenböck, C.; Schaffer, A.; Nößner, E.; Nelson, P. J.; Huss, R.; Rieger, B. Fluorescent Polyvinylphosphonate Bioconjugates for Selective Cellular Delivery. *Chemistry–A European Journal* **2018**, *24* (11), 2584-2587.

(78) Gauthier, M. A.; Gibson, M. I.; Klok, H.-A. Synthesis of Functional Polymers by Post-Polymerization Modification. *Angewandte Chemie International Edition* **2009**, *48* (1), 48-58.

(79) Kolb, H. C.; Finn, M.; Sharpless, K. B. Click chemistry: diverse chemical function from a few good reactions. *Angewandte Chemie International Edition* **2001**, *40* (11), 2004-2021.

(80) Sumerlin, B. S.; Vogt, A. P. Macromolecular engineering through click chemistry and other efficient transformations. *Macromolecules* **2010**, *43* (1), 1-13.

(81) Iha, R. K.; Wooley, K. L.; Nystrom, A. M.; Burke, D. J.; Kade, M. J.; Hawker, C. J. Applications of orthogonal “click” chemistries in the synthesis of functional soft materials. *Chemical reviews* **2009**, *109* (11), 5620-5686.

(82) Tiwari, V. K.; Mishra, B. B.; Mishra, K. B.; Mishra, N.; Singh, A. S.; Chen, X. Cu-catalyzed click reaction in carbohydrate chemistry. *Chemical Reviews* **2016**, *116* (5), 3086-3240.

(83) van Steenis, D. J. V.; David, O. R.; van Strijdonck, G. P.; van Maarseveen, J. H.; Reek, J. N. Click-chemistry as an efficient synthetic tool for the preparation of novel conjugated polymers. *Chemical communications* **2005**, (34), 4333-4335.

(84) Rostovtsev, V. V.; Green, L. G.; Fokin, V. V.; Sharpless, K. B. A stepwise huisgen cycloaddition process: copper (I)-catalyzed regioselective “ligation” of azides and terminal alkynes. *Angewandte Chemie* **2002**, *114* (14), 2708-2711.

(85) Tornøe, C. W.; Christensen, C.; Meldal, M. Peptidotriazoles on solid phase:[1, 2, 3]-triazoles by regiospecific copper (I)-catalyzed 1, 3-dipolar cycloadditions of terminal alkynes to azides. *The Journal of organic chemistry* **2002**, *67* (9), 3057-3064.

(86) Durmaz, H.; Sanyal, A.; Hizal, G.; Tunca, U. Double click reaction strategies for polymer conjugation and post-functionalization of polymers. *Polymer Chemistry* **2012**, *3* (4), 825-835.

(87) Binauld, S.; Fleury, E.; Drockenmuller, E. Solving the loss of orthogonality during the polyaddition of α-azide-ω-alkyne monomers catalyzed by Cu (PPh3) 3Br: Application to the synthesis of high-molar mass polytriazoles. *Journal of Polymer Science Part A: Polymer Chemistry* **2010**, *48* (11), 2470-2476.

(88) Kushwaha, D.; Dwivedi, P.; K Kuanar, S.; K Tiwari, V. Click reaction in carbohydrate chemistry: recent developments and future perspective. *Current Organic Synthesis* **2013**, *10* (1), 90-135.

(89) Worrell, B. T.; Malik, J. A.; Fokin, V. V. Direct Evidence of a Dinuclear Copper Intermediate in Cu(I)-Catalyzed Azide-Alkyne Cycloadditions. *Science* **2013**, *340* (6131), 457-460.

(90) Geng, Z.; Shin, J. J.; Xi, Y.; Hawker, C. J. Click chemistry strategies for the accelerated synthesis of functional macromolecules. *Journal of Polymer Science* **2021**, *59* (11), 963-1042.

(91) Hoyle, C. E.; Bowman, C. N. Thiol–ene click chemistry. *Angewandte Chemie International Edition* **2010**, *49* (9), 1540-1573.

(92) Singha, N. K.; Schlaad, H. Thiol–ene Based Functionalization of Polymers. In *Functional Polymers by Post-Polymerization Modification*, 2012; 65-86.

(93) Lowe, A. B. Thiol-ene “click” reactions and recent applications in polymer and materials synthesis. *Polymer Chemistry* **2010**, *1* (1), 17-36.

(94) Huo, J.; Lin, C.; Liang, J. A brief minireview of poly-triazole: Alkyne and azide substrate selective, metal-catalyst expansion. *Reactive and Functional Polymers* **2020**, *152*, 104531.

(95) Song, H. B.; Sowan, N.; Shah, P. K.; Baranek, A.; Flores, A.; Stansbury, J. W.; Bowman, C. N. Reduced shrinkage stress via photo-initiated copper (I)-catalyzed cycloaddition polymerizations of azide-alkyne resins. *Dental Materials* **2016**, *32* (11), 1332-1342.

(96) Song, H. B.; Baranek, A.; Bowman, C. N. Kinetics of bulk photo-initiated copper (I)-catalyzed azide–alkyne cycloaddition (CuAAC) polymerizations. *Polymer chemistry* **2016**, *7* (3), 603-612.

(97) Baranek, A.; Song, H. B.; McBride, M.; Finnegan, P.; Bowman, C. N. Thermomechanical formation–structure–property relationships in photopolymerized copper-catalyzed azide–alkyne (CuAAC) networks. *Macromolecules* **2016**, *49* (4), 1191-1200.

(98) Zhao, E.; Li, H.; Ling, J.; Wu, H.; Wang, J.; Zhang, S.; Lam, J. W.; Sun, J. Z.; Qin, A.; Tang, B. Z. Structure-dependent emission of polytriazoles. *Polymer Chemistry* **2014**, *5* (7), 2301-2308.

(99) Huang, D.; Liu, Y.; Qin, A.; Tang, B. Z. Structure–property relationship of regioregular polytriazoles produced by ligand-controlled regiodivergent Ru (II)-catalyzed azide–alkyne click polymerization. *Macromolecules* **2019**, *52* (5), 1985-1992.

(100) Sumerlin, B.; Tsarevsky, N.; Louche, G.; Lee, R.; Matyjaszewski, K. Macromolecules2005, 38, 7540− 7545.

(101) Ladmiral, V.; Legge, T. M.; Zhao, Y.; Perrier, S. b. “Click” chemistry and radical polymerization: Potential loss of orthogonality. *Macromolecules* **2008**, *41* (18), 6728-6732.

(102) Parrish, B.; Breitenkamp, R. B.; Emrick, T. PEG-and peptide-grafted aliphatic polyesters by click chemistry. *Journal of the American Chemical Society* **2005**, *127* (20), 7404-7410.

(103) Coumes, F.; Darcos, V.; Domurado, D.; Li, S.; Coudane, J. Synthesis and ring-opening polymerisation of a new alkyne-functionalised glycolide towards biocompatible amphiphilic graft copolymers. *Polymer Chemistry* **2013**, *4* (13), 3705-3713.

(104) Cao, Y.; Lai, Z.; Feng, J.; Wu, P. Graphene oxide sheets covalently functionalized with block copolymers via click chemistry as reinforcing fillers. *Journal of Materials Chemistry* **2011**, *21* (25), 9271-9278.

(105) Arslan, M.; Acik, G.; Tasdelen, M. A. The emerging applications of click chemistry reactions in the modification of industrial polymers. *Polymer Chemistry* **2019**, *10* (28), 3806-3821.

(106) Muzammil, E. M.; Khan, A.; Stuparu, M. C. Post-polymerization modification reactions of poly (glycidyl methacrylate) s. *RSC advances* **2017**, *7* (88), 55874-55884.

(107) Stadermann, J.; Erber, M.; Komber, H.; Brandt, J.; Eichhorn, K.-J.; Bönsch, M.; Mertig, M.; Voit, B. Photopatternable films of block copolymers prepared through double-click reaction. *Macromolecules* **2010**, *43* (7), 3136.

(108) Ten Brummelhuis, N.; Diehl, C.; Schlaad, H. Thiol-ene modification of 1, 2-polybutadiene using UV light or sunlight. *Macromolecules* **2008**, *41* (24), 9946-9947.

(109) Campos, L. M.; Killops, K. L.; Sakai, R.; Paulusse, J. M.; Damiron, D.; Drockenmuller, E.; Messmore, B. W.; Hawker, C. J. Development of thermal and photochemical strategies for thiol− ene click polymer functionalization. *Macromolecules* **2008**, *41* (19), 7063-7070.

(110) Campos, L. M.; Killops, K. L.; Sakai, R.; Paulusse, J. M. J.; Damiron, D.; Drockenmuller, E.; Messmore, B. W.; Hawker, C. J. Development of Thermal and Photochemical Strategies for Thiol−Ene Click Polymer Functionalization. *Macromolecules* **2008**, *41* (19), 7063-7070.

(111) Javakhishvili, I.; Binder, W. H.; Tanner, S.; Hvilsted, S. Facile synthesis of linear-dendritic cholesteryl-poly (ε-caprolactone)-b-(l-lysine) G2 by thiol-ene and azide-alkyne “click” reactions. *Polymer Chemistry* **2010**, *1* (4), 506-513.

(112) Javakhishvili, I.; Binder, W. H.; Tanner, S.; Hvilsted, S. Facile synthesis of linear-dendritic cholesteryl-poly(ε-caprolactone)-b-(l-lysine)G2 by thiol-ene and azide-alkyne “click” reactions. *Polymer Chemistry* **2010**, *1* (4), 506-513.

(113) Thacharodi, D.; Rao, K. P. Development and in vitro evaluation of chitosan-based transdermal drug delivery systems for the controlled delivery of propranolol hydrochloride. *Biomaterials* **1995**, *16* (2), 145-148.

(114) Tiwari, G.; Tiwari, R.; Sriwastawa, B.; Bhati, L.; Pandey, S.; Pandey, P.; Bannerjee, S. K. Drug delivery systems: An updated review. *Int J Pharm Investig* **2012**, *2* (1), 2-11.

(115) Krishna, R.; Pandit, J. Carboxymethylcellulose-sodium based transdermal drug delivery system for propranolol. *Journal of pharmacy and pharmacology* **1996**, *48* (4), 367-370.

(116) Vargason, A. M.; Anselmo, A. C.; Mitragotri, S. The evolution of commercial drug delivery technologies. *Nature Biomedical Engineering* **2021**, *5* (9), 951-967.

(117) Begines, B.; Ortiz, T.; Pérez-Aranda, M.; Martínez, G.; Merinero, M.; Argüelles-Arias, F.; Alcudia, A. Polymeric nanoparticles for drug delivery: Recent developments and future prospects. *Nanomaterials* **2020**, *10* (7), 1403.

(118) Paul, D. R.; Robeson, L. M. Polymer nanotechnology: nanocomposites. *Polymer* **2008**, *49* (15), 3187-3204.
(119) Kotta, S.; Aldawsari, H. M.; Badr-Eldin, S. M.; Nair, A. B.; Yt, K. Progress in Polymeric Micelles for Drug Delivery Applications. *Pharmaceutics* **2022**, *14* (8).

(120) Almgren, M. Mixed micelles and other structures in the solubilization of bilayer lipid membranes by surfactants. *Biochimica et biophysica acta (BBA)-biomembranes* **2000**, *1508* (1-2), 146-163.

(121) Peer, D.; Karp, J. M.; Hong, S.; Farokhzad, O. C.; Margalit, R.; Langer, R. Nanocarriers as an emerging platform for cancer therapy. *Nano-enabled medical applications* **2020**, 61-91.

(122) Yadav, H. K.; Almokdad, A. A.; Sumia, I.; Debe, M. S. Polymer-based nanomaterials for drug-delivery carriers. In *Nanocarriers for drug delivery*, Elsevier, 2019; 531-556.

(123) Sutton, D.; Nasongkla, N.; Blanco, E.; Gao, J. Functionalized micellar systems for cancer targeted drug delivery. *Pharmaceutical research* **2007**, *24*, 1029-1046.

(124) Greish, K. Enhanced permeability and retention (EPR) effect for anticancer nanomedicine drug targeting. *Cancer nanotechnology: Methods and protocols* **2010**, 25-37.

(125) Cabral, H.; Matsumoto, Y.; Mizuno, K.; Chen, Q.; Murakami, M.; Kimura, M.; Terada, Y.; Kano, M.; Miyazono, K.; Uesaka, M. Accumulation of sub-100 nm polymeric micelles in poorly permeable tumours depends on size. *Nature nanotechnology* **2011**, *6* (12), 815-823.

(126) Huang, K.; Ma, H.; Liu, J.; Huo, S.; Kumar, A.; Wei, T.; Zhang, X.; Jin, S.; Gan, Y.; Wang, P. C. Size-dependent localization and penetration of ultrasmall gold nanoparticles in cancer cells, multicellular spheroids, and tumors in vivo. *ACS nano* **2012**, *6* (5), 4483-4493.

(127) Zhou, Q.; Zhang, L.; Yang, T.; Wu, H. Stimuli-responsive polymeric micelles for drug delivery and cancer therapy. *Int J Nanomedicine* **2018**, *13*, 2921-2942.

(128) Mahmud, A.; Xiong, X.-B.; Aliabadi, H. M.; Lavasanifar, A. Polymeric micelles for drug targeting. *Journal of drug targeting* **2007**, *15* (9), 553-584.

(129) Cao, Y.; Dong, X.; Chen, X. Polymer-Modified Liposomes for Drug Delivery: From Fundamentals to Applications. *Pharmaceutics* **2022**, *14* (4).

(130) Rideau, E.; Dimova, R.; Schwille, P.; Wurm, F. R.; Landfester, K. Liposomes and polymersomes: a comparative review towards cell mimicking. *Chemical Society Reviews* **2018**, *47* (23), 8572-8610.

(131) Bangham, A. D.; Standish, M. M.; Watkins, J. C. Diffusion of univalent ions across the lamellae of swollen phospholipids. *Journal of Molecular Biology* **1965**, *13* (1), 238-IN227.

(132) Sabir, F.; Barani, M.; Rahdar, A.; Bilal, M.; Nadeem, M. How to face skin cancer with nanomaterials: A review. *Biointerface Res. Appl. Chem* **2021**, *11* (4), 11931-11955.

(133) Immordino, M. L.; Dosio, F.; Cattel, L. Stealth liposomes: review of the basic science, rationale, and clinical applications, existing and potential. *International journal of nanomedicine* **2006**, *1* (3), 297.

(134) Wang, S.; Chen, Y.; Guo, J.; Huang, Q. Liposomes for Tumor Targeted Therapy: A Review. *International Journal of Molecular Sciences* **2023**, *24* (3), 2643.

(135) O'Shannessy, D. J.; Somers, E. B.; Wang, L.-c.; Wang, H.; Hsu, R. Expression of folate receptors alpha and beta in normal and cancerous gynecologic tissues: correlation of expression of the beta isoform with macrophage markers. *Journal of ovarian research* **2015**, *8*, 1-9.

(136) Kumar, P.; Huo, P.; Liu, B. Formulation Strategies for Folate-Targeted Liposomes and Their Biomedical Applications. *Pharmaceutics* **2019**, *11* (8), 381.

(137) Liu, D.; Huang, L. Role of cholesterol in the stability of pH-sensitive, large unilamellar liposomes prepared by the detergent-dialysis method. *Biochimica et Biophysica Acta (BBA)-Biomembranes* **1989**, *981* (2), 254-260.

(138) Briuglia, M.-L.; Rotella, C.; McFarlane, A.; Lamprou, D. A. Influence of cholesterol on liposome stability and on in vitro drug release. *Drug delivery and translational research* **2015**, *5*, 231-242.

(139) Samad, A.; Sultana, Y.; Aqil, M. Liposomal drug delivery systems: an update review. *Current drug delivery* **2007**, *4* (4), 297-305.

(140) Ishida, T.; Kirchmeier, M.; Moase, E.; Zalipsky, S.; Allen, T. Targeted delivery and triggered release of liposomal doxorubicin enhances cytotoxicity against human B lymphoma cells. *Biochimica et Biophysica Acta (BBA)-Biomembranes* **2001**, *1515* (2), 144-158.

(141) Xiang, G.; Wu, J.; Lu, Y.; Liu, Z.; Lee, R. J. Synthesis and evaluation of a novel ligand for folate-mediated targeting liposomes. *International journal of pharmaceutics* **2008**, *356* (1-2), 29-36.

(142) Chen, Y.; Cheng, Y.; Zhao, P.; Zhang, S.; Li, M.; He, C.; Zhang, X.; Yang, T.; Yan, R.; Ye, P. Co-delivery of doxorubicin and imatinib by pH sensitive cleavable PEGylated nanoliposomes with folate-mediated targeting to overcome multidrug resistance. *International journal of pharmaceutics* **2018**, *542* (1-2), 266-279.

(143) Ekladious, I.; Colson, Y. L.; Grinstaff, M. W. Polymer–drug conjugate therapeutics: advances, insights and prospects. *Nature reviews Drug discovery* **2019**, *18* (4), 273-294.

(144) Duncan, R. Polymer conjugates as anticancer nanomedicines. *Nature reviews cancer* **2006**, *6* (9), 688-701.

(145) Ringsdorf, H. Structure and properties of pharmacologically active polymers. In *Journal of Polymer Science: Polymer Symposia*, 1975; Wiley Online Library: Vol. 51, 135-153.

(146) Uchegbu, I. F.; Schätzlein, A. G.; Cheng, W. P.; Lalatsa, A. *Fundamentals of pharmaceutical nanoscience*; Springer, 2013.

(147) Vasey, P. A.; Kaye, S. B.; Morrison, R.; Twelves, C.; Wilson, P.; Duncan, R.; Thomson, A. H.; Murray, L. S.; Hilditch, T. E.; Murray, T. Phase I clinical and pharmacokinetic study of PK1 [N-(2-hydroxypropyl) methacrylamide copolymer doxorubicin]: first member of a new class of chemotherapeutic agents—drug-polymer conjugates. *Clinical cancer research* **1999**, *5* (1), 83-94.

(148) Avendaño, C.; Menendez, J. C. *Medicinal chemistry of anticancer drugs*; Elsevier, 2015.

(149) Seymour, L. W.; Ferry, D. R.; Anderson, D.; Hesslewood, S.; Julyan, P. J.; Poyner, R.; Doran, J.; Young, A. M.; Burtles, S.; Kerr, D. J. Hepatic drug targeting: phase I evaluation of polymer-bound doxorubicin. *Journal of clinical oncology* **2002**, *20* (6), 1668-1676.

(150) Woodcock, J.; Griffin, J. P.; Behrman, R. E. Development of novel combination therapies. *New England Journal of Medicine* **2011**, *364* (11), 985-987.

(151) Devita Jr, V. T.; Young, R. C.; Canellos, G. P. Combination versus single agent chemotherapy: a review of the basis for selection of drug treatment of cancer. *Cancer* **1975**, *35* (1), 98-110.

(152) Hu, C.-M. J.; Zhang, L. Nanoparticle-based combination therapy toward overcoming drug resistance in cancer. *Biochemical pharmacology* **2012**, *83* (8), 1104-1111.

(153) Ulbrich, K.; Hola, K.; Subr, V.; Bakandritsos, A.; Tucek, J.; Zboril, R. Targeted drug delivery with polymers and magnetic nanoparticles: covalent and noncovalent approaches, release control, and clinical studies. *Chemical reviews* **2016**, *116* (9), 5338-5431.

(154) Díez-Pascual, A. M. Chemical Functionalization of Carbon Nanotubes with Polymers: A Brief Overview. *Macromol* **2021**, *1* (2), 64-83.

(155) Eatemadi, A.; Daraee, H.; Karimkhanloo, H.; Kouhi, M.; Zarghami, N.; Akbarzadeh, A.; Abasi, M.; Hanifehpour, Y.; Joo, S. W. Carbon nanotubes: properties, synthesis, purification, and medical applications. *Nanoscale research letters* **2014**, *9*, 1-13.

(156) Díez-Pascual, A. M.; Diez-Vicente, A. L. Development of nanocomposites reinforced with carboxylated poly (ether ether ketone) grafted to zinc oxide with superior antibacterial properties. *ACS Applied Materials & Interfaces* **2014**, *6* (5), 3729-3741.

(157) Bugatti, V.; Viscusi, G.; Di Bartolomeo, A.; Iemmo, L.; Zampino, D. C.; Vittoria, V.; Gorrasi, G. Ionic liquid as dispersing agent of LDH-carbon nanotubes into a biodegradable vinyl alcohol polymer. *Polymers* **2020**, *12* (2), 495.

(158) Dervishi, E.; Li, Z.; Xu, Y.; Saini, V.; Biris, A. R.; Lupu, D.; Biris, A. S. Carbon nanotubes: synthesis, properties, and applications. *Particulate Science and Technology* **2009**, *27* (2), 107-125.

(159) Merum, S.; Veluru, J. B.; Seeram, R. Functionalized carbon nanotubes in bio-world: Applications, limitations and future directions. *Materials Science and Engineering: B* **2017**, *223*, 43-63.

(160) Khan, A.; Alamry, K. A. Surface Modified Carbon Nanotubes: An Introduction. In *Surface Modified Carbon Nanotubes Volume 1: Fundamentals, Synthesis and Recent Trends*, ACS Symposium Series, Vol. 1424; American Chemical Society, 2022; 1-25.

(161) Avilés, F.; Cauich-Rodríguez, J. V.; Toro-Estay, P.; Yazdani-Pedram, M.; Aguilar-Bolados, H. 5 - Improving Carbon Nanotube/Polymer Interactions in Nanocomposites. In *Carbon Nanotube-Reinforced Polymers*, Rafiee, R. Ed.; Elsevier, 2018; 83-115.

(162) Chen, J.; Liu, B.; Gao, X.; Xu, D. A review of the interfacial characteristics of polymer nanocomposites containing carbon nanotubes. *RSC Advances* **2018**, *8* (49), 28048-28085.

(163) Spitalsky, Z.; Tasis, D.; Papagelis, K.; Galiotis, C. Carbon nanotube–polymer composites: Chemistry, processing, mechanical and electrical properties. *Progress in Polymer Science* **2010**, *35* (3), 357-401.

(164) González-Domínguez, J. M.; Castell, P.; Bespín-Gascón, S.; Ansón-Casaos, A.; Díez-Pascual, A. M.; Gómez-Fatou, M. A.; Benito, A. M.; Maser, W. K.; Martínez, M. T. Covalent functionalization of MWCNTs with poly(p-phenylene sulphide) oligomers: a route to the efficient integration through a chemical approach. *Journal of Materials Chemistry* **2012**, *22* (39), 21285-21297.
ske, M.; Przyrembel, D.; Bisswanger, T.; Gordeev, G.; Maschietto, F.; Faghani, A.; Paulus, B.; Weinelt, M.; et al. Preserving π-conjugation in covalently functionalized carbon nanotubes for optoelectronic applications. *Nature Communications* **2017**, *8* (1), 14281.

(166) Gao, C.; He, H.; Zhou, L.; Zheng, X.; Zhang, Y. Scalable Functional Group Engineering of Carbon Nanotubes by Improved One-Step Nitrene Chemistry. *Chemistry of Materials* **2009**, *21* (2), 360-370.

(167) Mendoza, J. J.; Ledezma, R.; Gallardo, C. A.; Elias, A.; Elizalde, L. E. Covalent surface functionalization of carbon nanostructures via [2 + 1] cycloaddition microwave-assisted reactions. *Journal of Materials Science* **2021**, *56* (24), 13524-13539.

(168) Leinonen, H.; Rintala, J.; Siitonen, A.; Lajunen, M.; Pettersson, M. New nitrene functionalizations onto sidewalls of carbon nanotubes and their spectroscopic analysis. *Carbon* **2010**, *48* (9), 2425-2434.

(169) Qin, S.; Qin, D.; Ford, W. T.; Resasco, D. E.; Herrera, J. E. Functionalization of Single-Walled Carbon Nanotubes with Polystyrene via Grafting to and Grafting from Methods. *Macromolecules* **2004**, *37* (3), 752-757.

(170) Nish, A.; Hwang, J.-Y.; Doig, J.; Nicholas, R. J. Highly selective dispersion of single-walled carbon nanotubes using aromatic polymers. *Nature Nanotechnology* **2007**, *2* (10), 640-646.

(171) Soleyman, R.; Hirbod, S.; Adeli, M. Advances in the biomedical application of polymer-functionalized carbon nanotubes. *Biomaterials Science* **2015**, *3* (5), 695-711.

(172) Zhang, B.; Chen, Q.; Tang, H.; Xie, Q.; Ma, M.; Tan, L.; Zhang, Y.; Yao, S. Characterization of and biomolecule immobilization on the biocompatible multi-walled carbon nanotubes generated by functionalization with polyamidoamine dendrimers. *Colloids and Surfaces B: Biointerfaces* **2010**, *80* (1), 18-25.

(173) El-Said, W. A.; Abdelshakour, M.; Choi, J.-H.; Choi, J.-W. Application of Conducting Polymer Nanostructures to Electrochemical Biosensors. *Molecules* **2020**, *25* (2), 307.

(174) Lay, C. L.; Liu, J.; Liu, Y. Functionalized carbon nanotubes for anticancer drug delivery. *Expert Review of Medical Devices* **2011**, *8* (5), 561-566.

(175) Pehl, T. M.; Kränzlein, M.; Adams, F.; Schaffer, A.; Rieger, B. C–H Bond Activation of Silyl-Substituted Pyridines with Bis(Phenolate)Yttrium Catalysts as a Facile Tool towards Hydroxyl-Terminated Michael-Type Polymers. *Catalysts* **2020**, *10* (4), 448.

(176) Biris, A. R.; Pruneanu, S.; Pogacean, F.; Lazar, M. D.; Borodi, G.; Ardelean, S.; Dervishi, E.; Watanabe, F.; Biris, A. S. Few-layer graphene sheets with embedded gold nanoparticles for electrochemical analysis of adenine. *International Journal of Nanomedicine* **2013**, 1429-1438.

(177) Ishikawa, N.; Furutani, M.; Arimitsu, K. Adhesive materials utilizing a thymine–adenine interaction and thymine photodimerization. *ACS Macro Letters* **2015**, *4* (7), 741-744.

(178) Zhang, X.; Zhang, Q.; Xie, C.; Gao, A.; Chang, Z.; Kwon Oh, J.; Yang, P.; Li, P. Phosphonated homopolymers and copolymers via ring opening metathesis polymerization: Tg tuning, flame resistance, and photolithography. *Journal of Polymer Science Part A: Polymer Chemistry* **2016**, *54* (10), 1396-1408.

(179) Vaughn, G. D.; Krein, K. A.; Gladysz, J. Synthesis and reactivity of metallacyclic manganese. alpha.-(silyloxy) alkyl complexes [cyclic](CO) 4MnC (R)(OSi (CH3) 3) P (C6H5) 2. A new thermodynamic driving force for carbonyl insertion. *Organometallics* **1986**, *5* (5), 936-942.

(180) Hultzsch, K. C.; Voth, P.; Beckerle, K.; Spaniol, T. P.; Okuda, J. Single-Component Polymerization Catalysts for Ethylene and Styrene: Synthesis, Characterization, and Reactivity of Alkyl and Hydrido Yttrium Complexes Containing a Linked Amido− Cyclopentadienyl Ligand. *Organometallics* **2000**, *19* (3), 228-243.

(181) Winkelhaus, D.; Neumann, B.; Stammler, H.-G.; Mitzel, N. W. Intramolecular Lewis acid–base pairs based on 4-ethynyl-2, 6-lutidine. *Dalton Transactions* **2012**, *41* (30), 9143-9150.

(182) Yang, Q.; Draghici, C.; Njardarson, J. T.; Li, F.; Smith, B. R.; Das, P. Evolution of an oxidative dearomatization enabled total synthesis of vinigrol. *Organic & biomolecular chemistry* **2014**, *12* (2), 330-344.

11. Appendix

11.1 List of Figures

11.2 List of Schemes

11.3 List of Tables

11.4 Supporting Information

11.4.1 Supporting Information Chapter 4

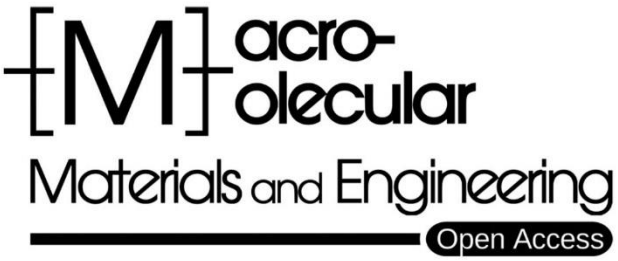

Supporting Information

for *Macromol. Mater. Eng.*, DOI 10.1002/mame.202200635

Azide-Modified Poly(diethyl vinylphosphonate) for Straightforward Graft-to Carbon Nanotube Functionalization

*Moritz Kränzlein, Thomas M. Pehl, Kerstin Halama, Paula F. Großmann, Tim Kratky, Amelie M. Mühlbach and Bernhard Rieger**

Azide-modified poly(diethyl vinylphosphonate) for straight-forward *graft-to* carbon nanotube functionalization

Moritz Kränzlein[⊥,‡], Thomas M. Pehl[⊥,‡], Kerstin Halama[⊥,‡], Paula F. Großmann[⊥], Tim Kratky[§], Amelie M. Mühlbach[⊥] and Bernhard Rieger[⊥,]*

[⊥] WACKER-Chair of Macromolecular Chemistry, Catalysis Research Center, School of Natural Sciences, Technical University of Munich, Lichtenbergstr. 4, 85748 Garching (Germany)

[§] Associate Professorship of Physical Chemistry with Focus on Catalysis, Catalysis Research Center, TUM School of Natural Sciences, Technical University of Munich, Lichtenbergstr. 4, 85748 Garching (Germany)

Corresponding Authors

* rieger@tum.de

TABLE OF CONTENTS

1. GENERAL EXPERIMENTAL

All reactions and polymerizations with moisture and air-sensitive reactants were carried out in a MBraun LabMaster120 glovebox filled with argon 4.6 from Westfalen or using standard Schlenk techniques. All glassware was heat-dried prior to use. All chemicals were purchased from Sigma-Aldrich, ABCR, or TCI Europe and used without further purification unless otherwise stated. Dichloromethane, tetrahydrofuran, toluene, and pentane were dried using an MBraun SPS-800 solvent purification system and stored over 3 Å molecular sieve. Diethyl vinylphosphonate was dried over CaH_2 for several days and distilled prior to use. $Y(CH_2TMS)_3(thf)$[1], the precursor catalyst $Cp_2Y(CH_2TMS)(thf)$[2], $Cp_2LuCH_2TMS(thf)$[2], $[(ONOO)^{tBu}Y(CH_2TMS)(thf)]$[3] and 4-chloro-2,6-dimethylpyridine[4] were prepared according to literature procedures.

Nuclear magnetic resonance (NMR) spectra were recorded on a Bruker AV-400HD spectrometer at 400 MHz (^1H), 125 MHz (^{13}C) and 162 MHz (^{31}P). NMR spectroscopical shifts δ were reported in ppm relative to the residual proton or carbon signal of the deuterated solvent. Deuterated solvents ($CDCl_3$, benzene-d_6) were purchased from Sigma-Aldrich or Deutero and dried over 3 Å molecular sieves prior to use. **Size-exclusion chromatography multi angle light scattering (SEC-MALS)** was used to determine molecular weights and polydispersity of the polymers (c = 2 mg/mL) with a Wyatt Dawn Heleos II MALS light scattering unit and a Wyatt Optilab rEX 536 RI unit in THF:H_2O = 1:1 (with 9 g/L *tetra-n*-butyl-ammonium bromide and 272 mg/L 2,6-di-*tert*-butyl-4-methylphenol added) as eluent at 40 °C on two Agilent PolarGel-M columns; for absolute molecular weight (triple detection) determination of DEVP the refractive index increment dn/dc = 0.0922 mL/g[5] was used. **Lyophilization** was performed on a VaCO 5-II-D at a pressure of 2 mbar and -90 °C condenser temperature from either 1,4-dioxane or benzene. **Elemental analysis (EA)** was performed by the Laboratory of Microanalytics at the Institute of Inorganic Chemistry at the Technical University of Munich, Department of Chemistry, Catalysis Research Center. **Electronspray Ionization Mass Spectrometry (ESI-MS)** was measured using a Thermo Fisher Scientific Exactive Plus Orbitrap in positive mode in HPLC acetonitrile straight from the reaction mixture without quenching. **Thermogravimetric analysis (TGA)** was measured inside a glovebox with argon atmosphere on a Netsch TG 209 F 1 Libra with a heating rate of 10 °C/min from 30-1000 °C under argon flow of 20 mL/min. Data

analysis was performed using the Netzsch Proteus 6 software. **Fourier-transformed infrared spectroscopy (FT-IR)** measurements were conducted on a nitrogen-cooled Bruker Vertex 70A on an attenuated total reflection module. The measurement resolution was 4 cm^{-1}, transmission mode, collected with Opus software. **Gas chromatography mass spectrometry (GC-MS)** analysis is performed on an Agilent GC 7890B equipped with a MS 5977A (single quadrupole mass detector), a 7693A Automatic Liquid Sampler and a G4513A Autoinjector. Separation is done with a HP-5MS UI column (30 m length, 0.25 mm internal diameter, 0.25 µm film) in a temperature range of 60-300 °C and the mass spectrometry was done using full scan in a mass range of 40 to 500 amu. Interpretation of the recorded data is done using the MassHunter software. **Transmission electron microscopy (TEM)** measurements were performed on a JEOL JEM 1400 plus instrument at an acceleration voltage of 120 kV. Before analysis, the samples were suspended in HPLC-grade ethanol and dispersed ultrasonically before being deposited on a carbon-coated copper mesh. **Raman** spectra of pristine MWCNTs and functionalized composites were acquired using a Renishaw inVia Raman spectrometer with a Leica DM/LM microscope. As excitation source a 622 nm (He) laser was used, the laser was focused on the surface using a 50x microscope objective. **X-ray photoelectron spectra (XPS)** were recorded on a Leybold-Heraeus LHS 10 spectrometer using a non-monochromatized Al K_α source (1486.7 eV). Samples were pressed into cavities and measured as pellets. All spectra were recorded in an ultra-high vacuum chamber at a pressure below 5×10^{-8} mbar. The analyzer was operated at a constant pass energy of 100 eV leading to an energy resolution with a full width at half-maximum (fwhm) of ~1.1 eV. High resolution-C 1s spectra were additionally acquired at a pass energy of 20 eV leading to an energy resolution of ~0.8 eV. The energy scale of the MWCNT:$PDEVP_{100}$ spectra was corrected for sample charging by using the C 1s main component of the MWCNT assuming the absence of charging in latter spectra. The energy scale of $PDEVP_{100}$ was corrected considering the P 2p core level of the MWCNT:$PDEVP_{100}$ composite. The intensity of all spectra was scaled to the total peak area of C 1s. Core level spectra were deconvoluted by using Doniach Sunjic functions after linear background subtraction.

2. SYNTHESIS PROCEDURES

((TRIMETHYLSILYL)METHYL)LITHIUM

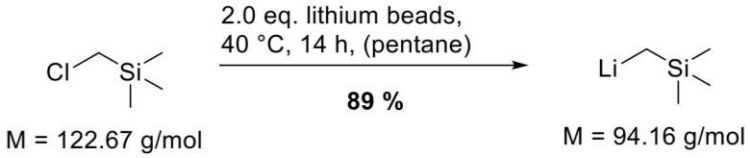

M = 122.67 g/mol

M = 94.16 g/mol

1.44 g (207 mmol, 3.35 eq.) lithium beads are added to a pressure Schlenk vessel and 70 mL of dry pentane are added. Under vigorous stirring, 8.8 mL (7.73 g, 63.0 mmol, 1 eq.) (chloromethyl)trimethylsilane are added and the suspension is heated to 35 °C. After 30 min the flask is put in an ultrasonic bath for 10 min to remove the passivating layer around the lithium beads. This procedure is repeated until a slight purple color appears. Afterwards the reaction mixture is heated to 35 °C for 14 hours. The purple suspension is filtered, and the residue washed with 3×15 mL hexane, the organic phases are combined, and the solvent is removed *in vacuo*. 5.27 g (56.0 mmol, 89%) ((Trimethylsilyl)methyl)lithium are obtained as white powder.

^{1}H-NMR (400 MHz, C_6D_6, 300 K): δ (ppm) = -2.07 (s, 2H, CH_2), 0.15 (s, 9H, $Si(CH_3)_3$).

^{13}C-NMR (100 MHz, C_6D_6, 300K): δ (ppm) = -4.67, 3.58.

^{29}Si-NMR (80 MHz, C_6D_6, 300K): δ (ppm) = -0.39.

4-AZIDO-2,6-DIMETHYLPYRIDINE[3]

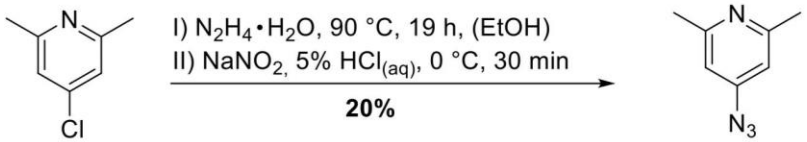

C_7H_8ClN
M = 141.03 g/mol

$C_7H_8N_4$
M = 148.07 g/mol

4-Chloro-2,6-dimethylpyridine (2.00 g, 14.1 mmol, 1.0 eq.) and a solution of 64% hydrazine-hydrate in water (3.4 mL, 44.5 mmol, 3.2 eq.) were heated in 6 mL ethanol under reflux for 19 hours. The solvent was removed under reduced pressure and the resulting white solid was dissolved in 35 mL 5% $HCl_{(aq)}$. The solution was cooled to 0 °C in an ice-bath and a solution of

sodium nitrite (1.46 g, 21.2 mmol, 1.5 eq.) in 18 mL water was slowly added. The yellow reaction solution was stirred at 0 °C for 30 min before adjusting an alkaline pH by addition of solid potassium carbonate. 50 mL dichloromethane were added and the organic layer was separated, the remaining aqueous phase is additionally extracted with 3x50 mL dichloromethane. The combined organic phases were washed with 50 mL water and dried over sodium sulphate before the solvent is removed in vacuo. Purification via column chromatography (gradient, 3%-5%MeOH/DCM, silica as stationary phase) yielded 0.38 g (2.54 mmol, 18%) 4-azido-2,6-dimethylpyridine as orange oil. Two combined experiments are dried together by filtration over aluminum oxide in benzene-d_6 and a stock solution with 3.72 mg azide/10 µL C_6D_6 is prepared for further reactions.

^{1}H-NMR (400 MHz, CDCl3, 300K): δ (ppm) = 2.50 (s, 6H, CH_3), 6.62 (s, 2H, H_{Ar}).

TLC: R_f = 0.41 (5 vol% MeOH in DCM) [UV].

IR: $\tilde{\upsilon}$ (cm^{-1}) = 2150 ($-N_3$)

GC-MS: t_R = 12.1 min, m/z = 240.2 [$2xM_{PyN3}$-$2xN_2$, dimeric species].

EA: calc: C 56.74%, H 5.44%, N 37.81%.

found: C 56.97%, H 5.73%, N 35.85%.

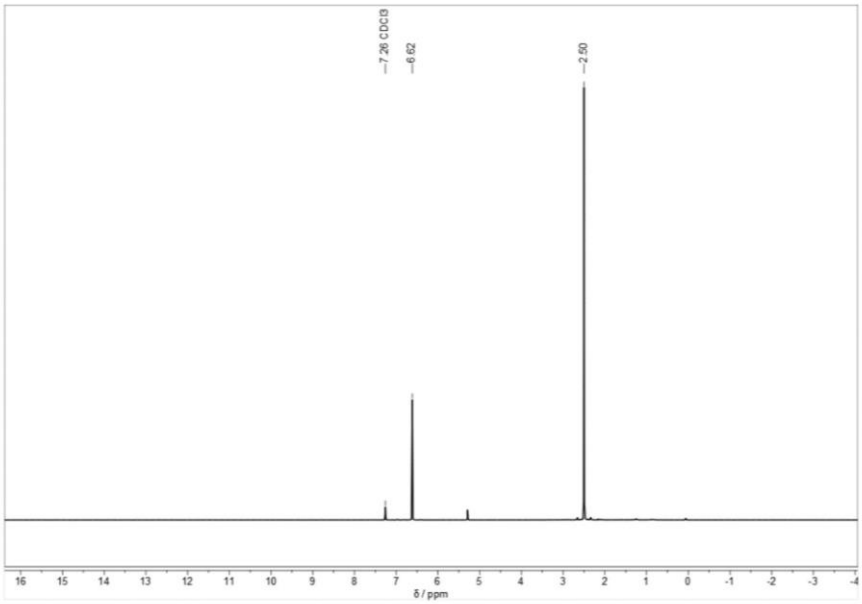

Figure S1: ^{1}H-NMR (400 MHz, $CDCl_3$, 300K) of 4-azido-2,6-dimethylpyridine.

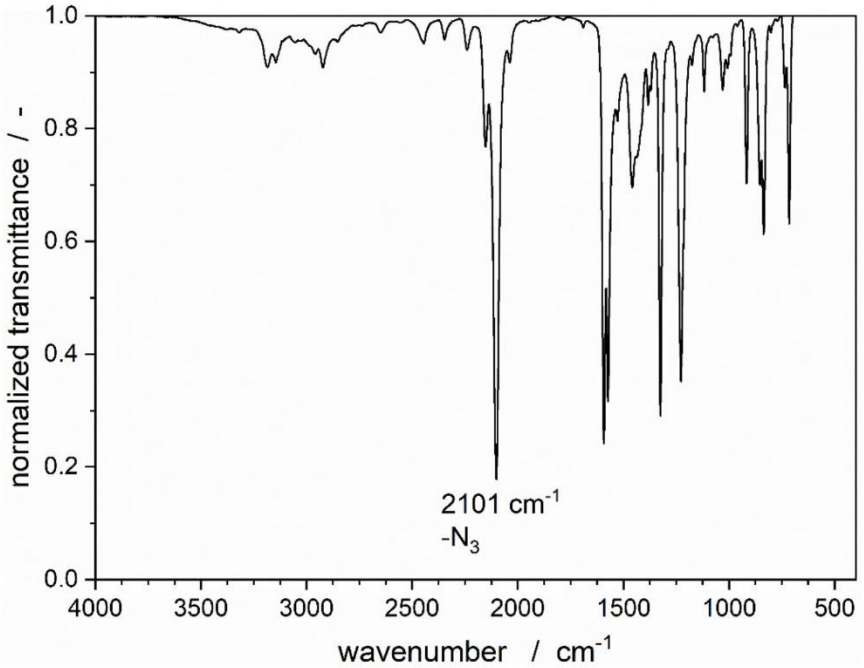

Figure S2: FT-IR spectrum of 4-azido-2,6-dimethylpyridine.

3. C-H BOND ACTIVATION

The *in-situ* CH-bond activation of the methyl pyridine compound is monitored via kinetic ^{1}H-NMR experiment in a *J-Young* NMR tube. 11.66 mg (0.0251 mmol, 1.0 eq.) $Cp_2Lu(CH_2TMS)thf$ are dissolved in 0.3 mL dry benzene-d_6 and 3.72 mg (0.0251 mmol, 1.0 eq.) 4-azido-2,6-dimethylpyridine in 0.3 mL dry benzene-d_6 are added at room temperature. ^{1}H-NMR spectra are measured immediately after addition, after 10 min and every 2 hours for 24 hours. Subsequently the mixture is filtered to remove any decomposition products and an additional ^{1}H-NMR is measured.

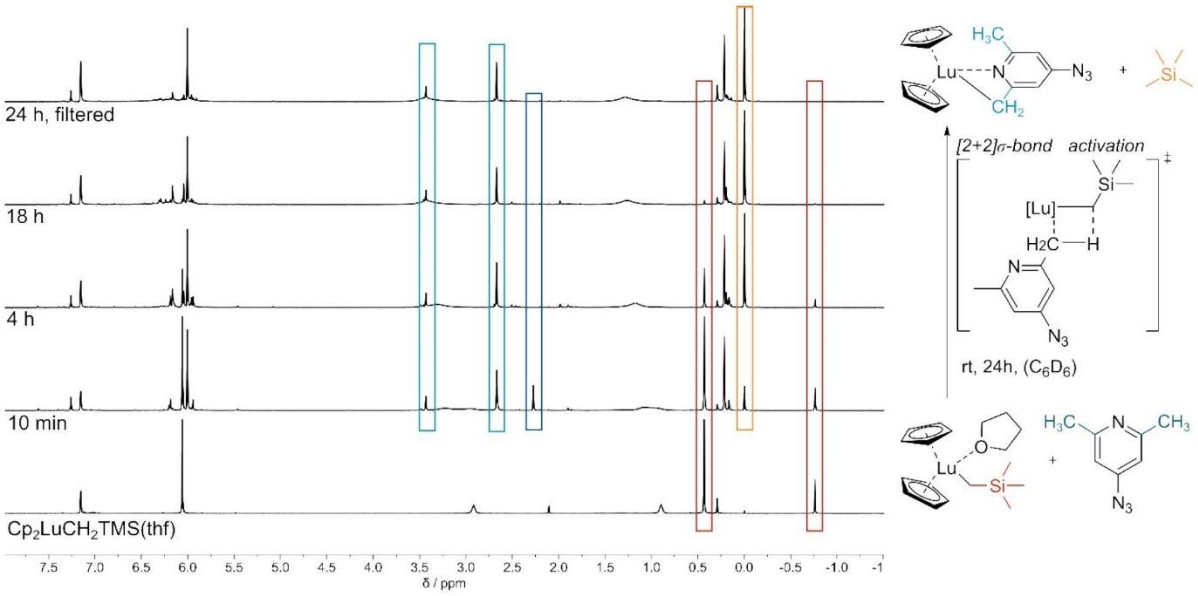

Figure S3: *in-Situ* ^{1}H-NMR (400 MHz, C6D6, 300 K) kinetic experiment of the CH-bond activation of 4-azido-2,6-dimethylpyridine with $Cp_2Lu(CH_2TMS)(thf)$ at room temperature.

4. POLYMERIZATION PROCEDURE

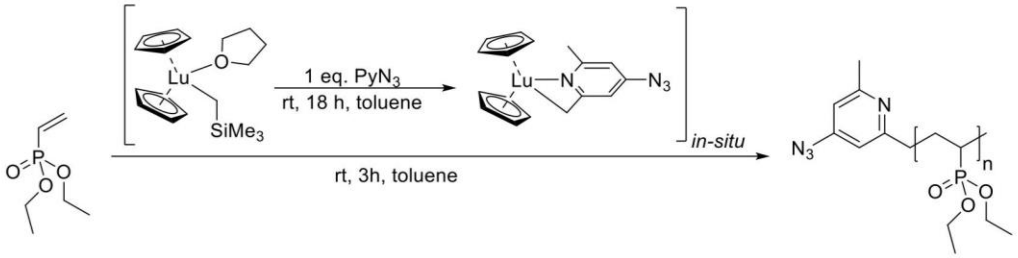

In a screw-cap vial, 10.6 mg (22.8 µmol, 1.0 eq.) $Cp_2Lu(CH_2TMS)(thf)$ are dissolved in 5 mL dry toluene and the corresponding amount of the prepared stock solution of 4-azido-2,6-dimethylpyridine (50.2 µmol, 1.1 eq.) are added. The *in-situ* activation of the catalyst is performed at room temperature over night before adding 374.6 mg (2.28 mmol, 100 eq.) diethyl vinylphosphonate. The polymerization is stirred at room temperature for 3 hours before an aliquot is withdrawn and the reaction is quenched by addition of wet methanol. The polymer is precipitated from pentane, subject to centrifugation and the supernatant is decanted of. The residual polymer is dissolved in 1,4-dioxane before being freeze-dried. The purified polymer is analyzed using $^{1}H/^{31}P$-NMR and SEC-MALS.

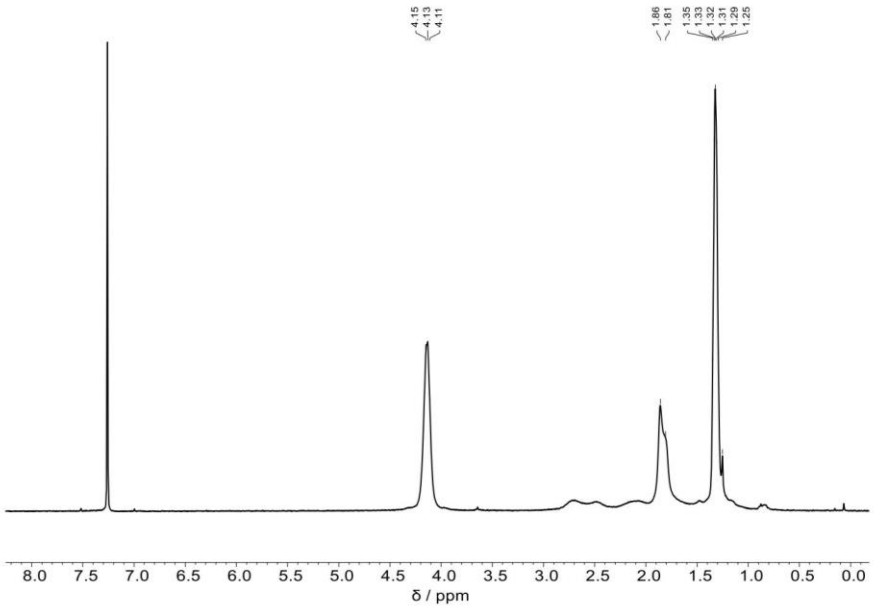

Figure S4: ^{1}H-NMR (400 MHz, $CDCl_3$, 300 K) of PDEVP prepared with $Cp_2Lu(PyN_3)(thf)$ (Table 1, entry 2).

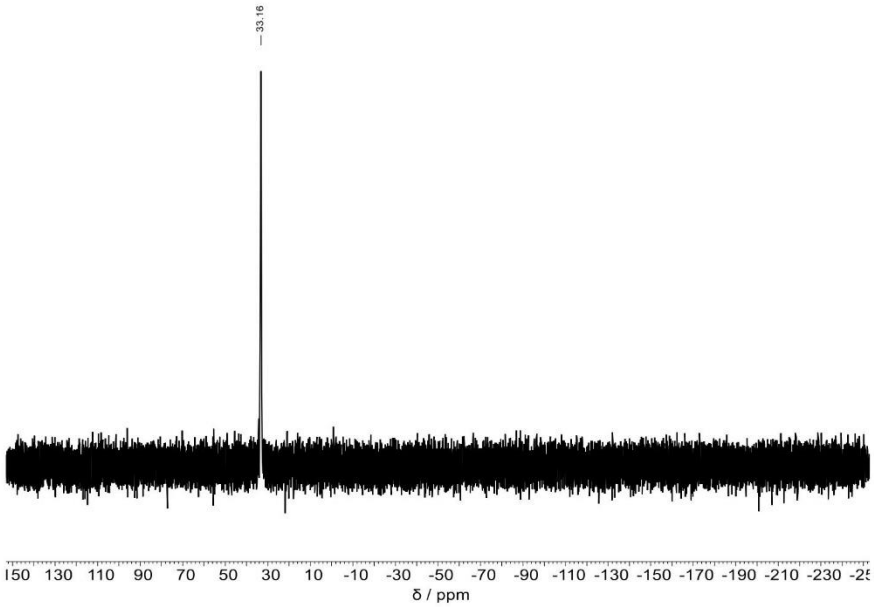

Figure S5: ^{31}P-NMR (162 MHz, $CDCl_3$, 300K) of PDEVP prepared with $Cp_2Lu(PyN_3)(thf)$ (Table 1, entry 2).

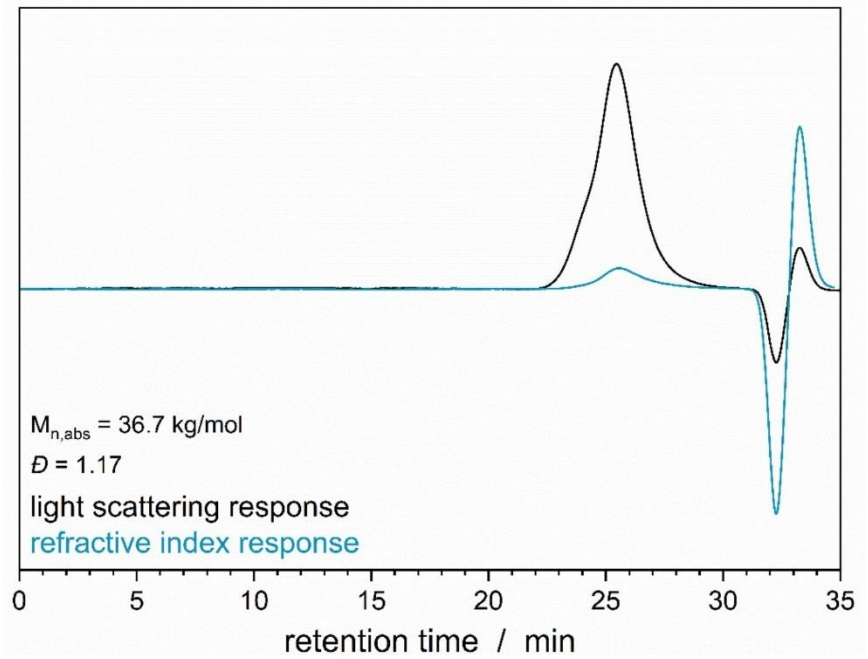

Figure S6: SEC-MALS of PDEVP prepared with $Cp_2Lu(PyN_3)(thf)$ (Table 1, entry 1).

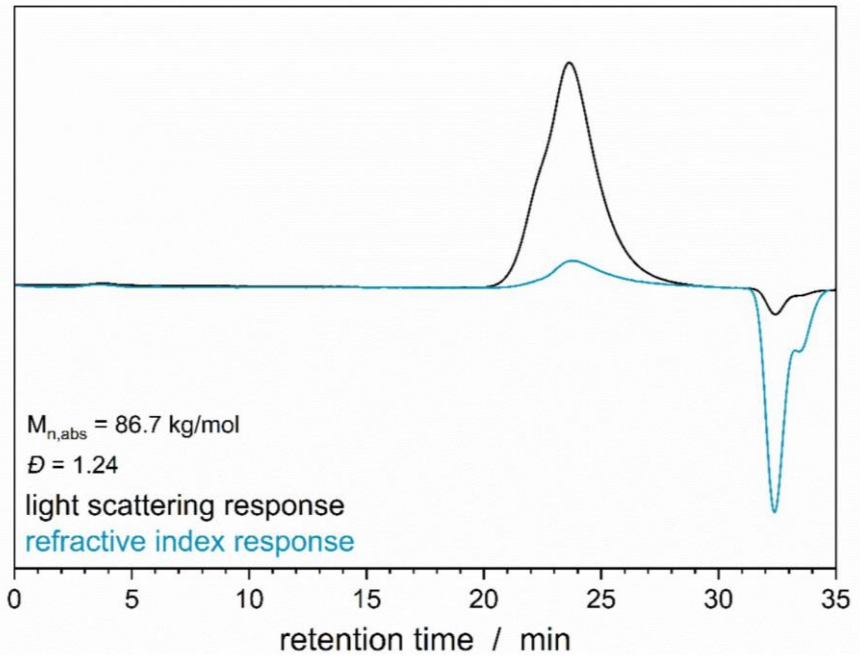

Figure S7: SEC-MALS of PDEVP prepared with $Cp_2Lu(PyN_3)(thf)$ (Table 1, entry 2).

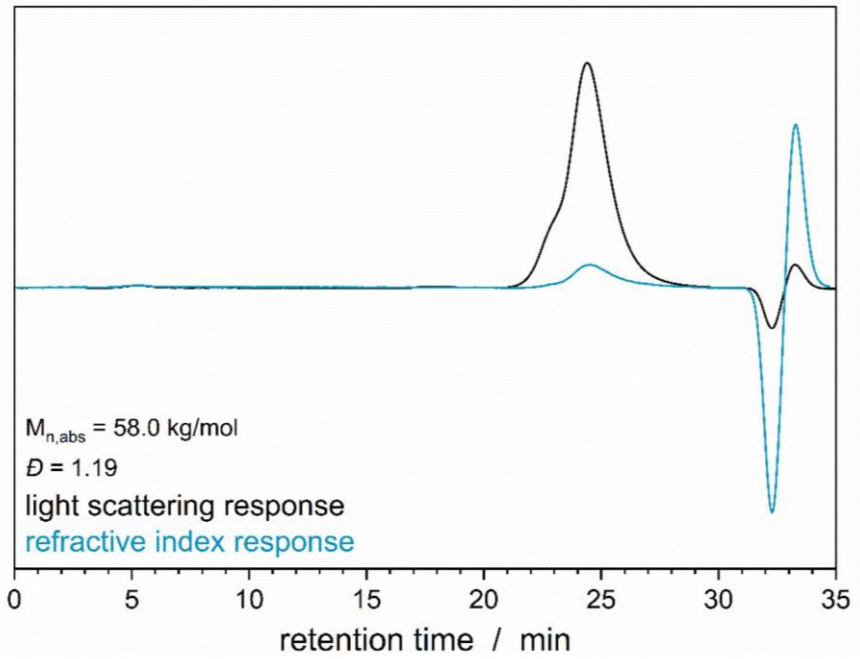

Figure S8: SEC-MALS of PDEVP prepared with $Cp_2Lu(PyN_3)(thf)$ (Table 1, entry 3).

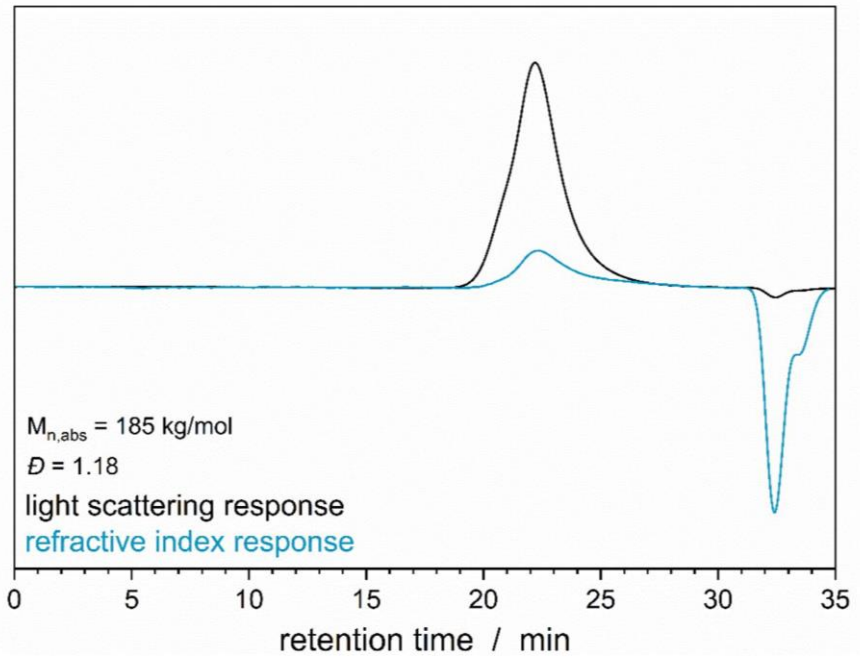

Figure S9: SEC-MALS of PDEVP prepared with $Cp_2Lu(PyN_3)(thf)$ (Table 1, entry 4).

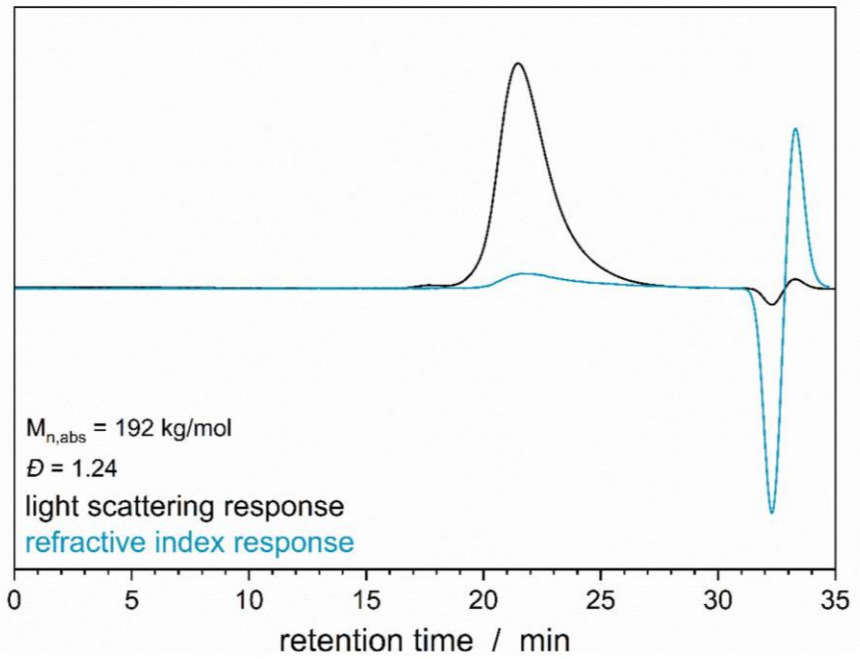

Figure S10: SEC-MALS of PDEVP prepared with $Cp_2Lu(PyN_3)(thf)$ (Table 1, entry 5)

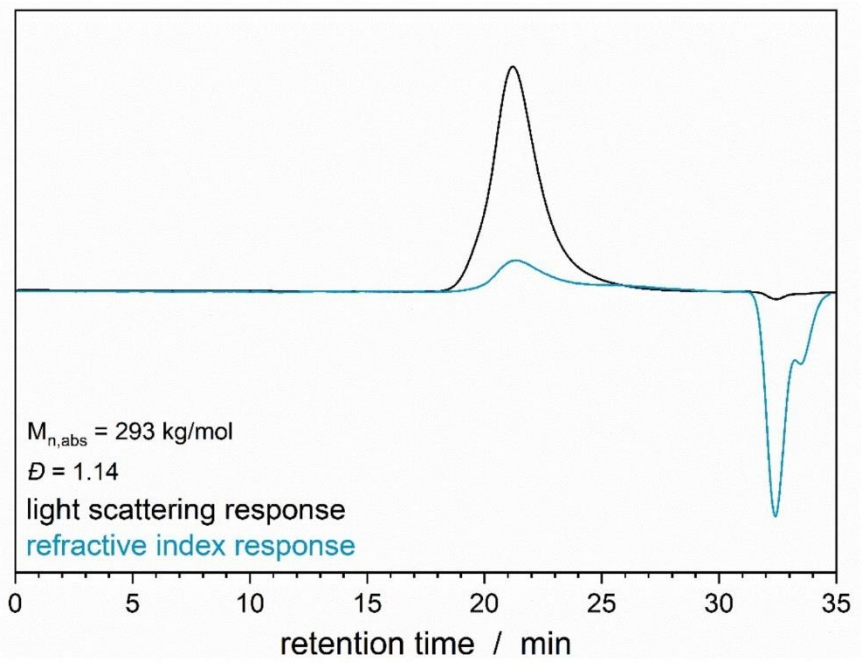

Figure S11: SEC-MALS of PDEVP prepared with $Cp_2Lu(PyN_3)(thf)$ (Table 1, entry 6).

5. END-GROUP ANALYSIS

To determine the attachment of the pyridine initiator and ensure functionalization with the desired azide moiety, oligomers of PDEVP are prepared as described for the polymerization with 5 equivalents of DEVP. 10 µL of the reaction mixture are withdrawn after 5 minutes and

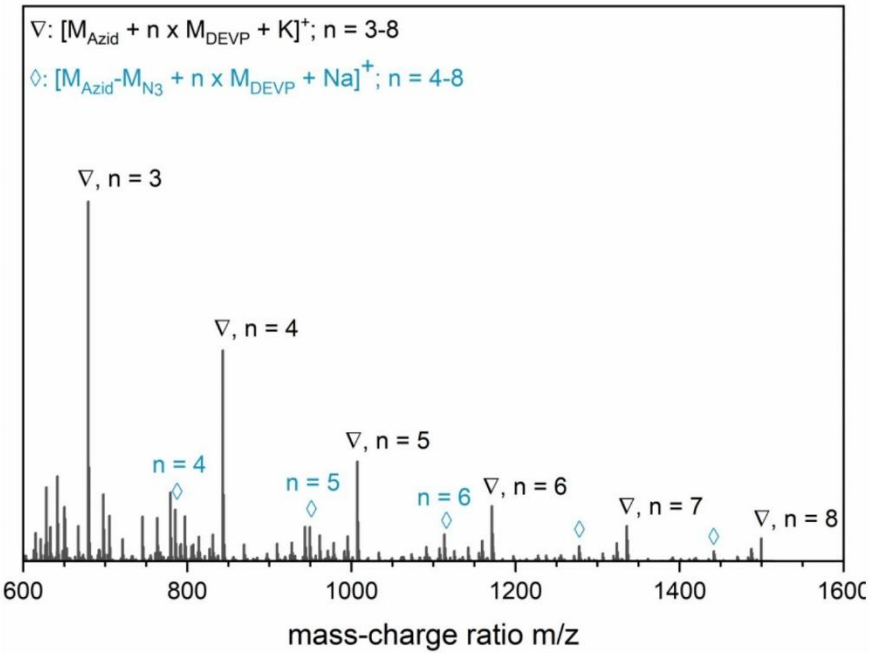

Figure S12: ESI-MS spectrum of short-chain PDEVP prepared with the catalyst $Cp_2Lu(PyN_3)$ showing a main series corresponding to $[n \times M_{DEVP} + M_{PyN3} + K]^+$ (black) and a parallel series corresponding to $[n \times MDEVP + M_{PyN3} - M_{N3} + Na]^+$ (blue) indicating successful attachment of the azido-pyridine to the PDEVP chain.

dissolved in HPLC-grade acetonitrile (100 µg/mL) immediately before ESI-MS measurement.

6. FUNCTIONALIZATION OF MWCNTS

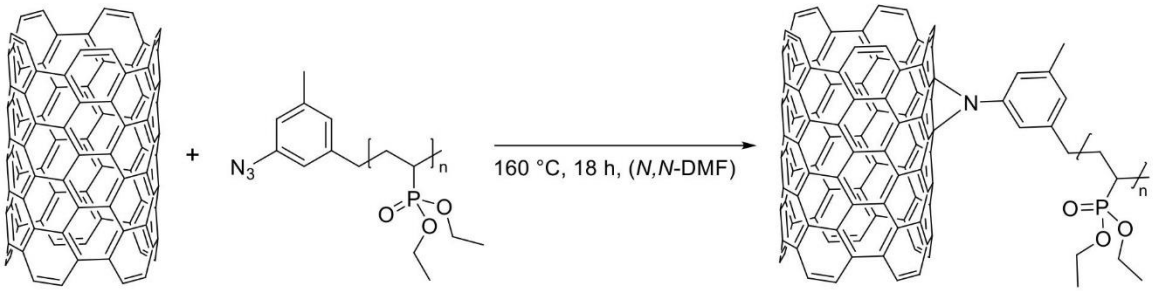

For the functionalization of the carbon nanotubes, 50 mg of MWCNTs are suspended in 25 mL of *N,N*-dimethylformamide by ultra-sonification and afterwards the corresponding amount of functionalized PDEVP (50 mg / 150 mg / 250 mg, based on desired wt%/wt% ratio) is added. The mixture is stirred at 160 °C over night to facilitate the thermal nitrene formation and subsequent [2+1] cycloaddition. The mixture is transferred into a centrifugation vial and centrifuged for 5 min at 9000 rpm. The supernatant is decanted off and the black residue is washed with *N,N*-dimethylformamide, ethanol and dichloromethane two times each. Afterwards, the residue is dried under vacuum at 60 °C over night before being analyzed by thermogravimetric analysis and elemental analysis.[6]

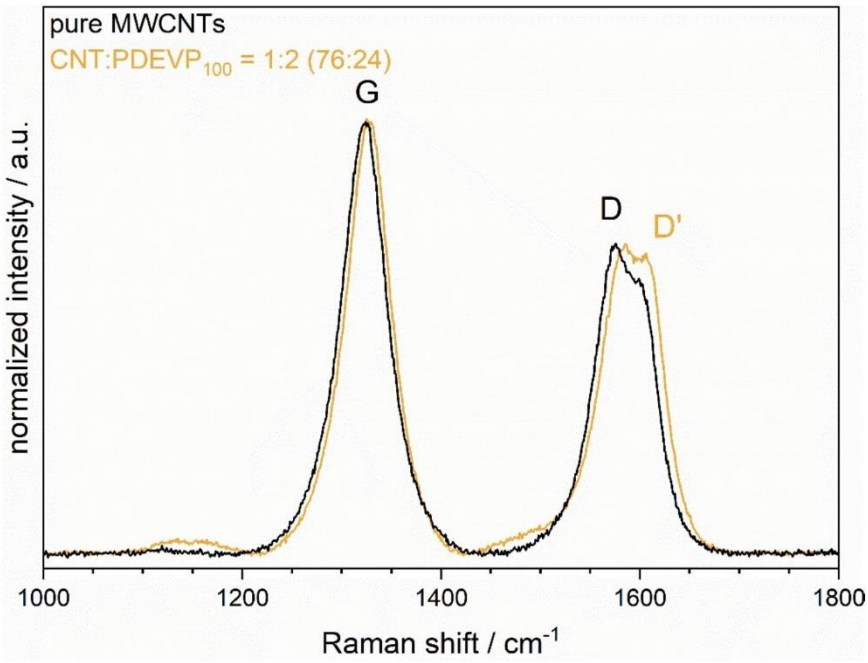

Figure S13: Raman spectra of pristine MWCNTs without polymer (black) and after functionalization with $PDEVP_{100}$ (Table 2, entry 4 / Table 3, entry 2) in the range of 1000 – 1800 cm^{-1} with the G band of sp^2-hybridized carbon bonds of the MWCNTs and D bands of sp^3-hybridized carbon bonds due to surface defects and functionalization.[7]

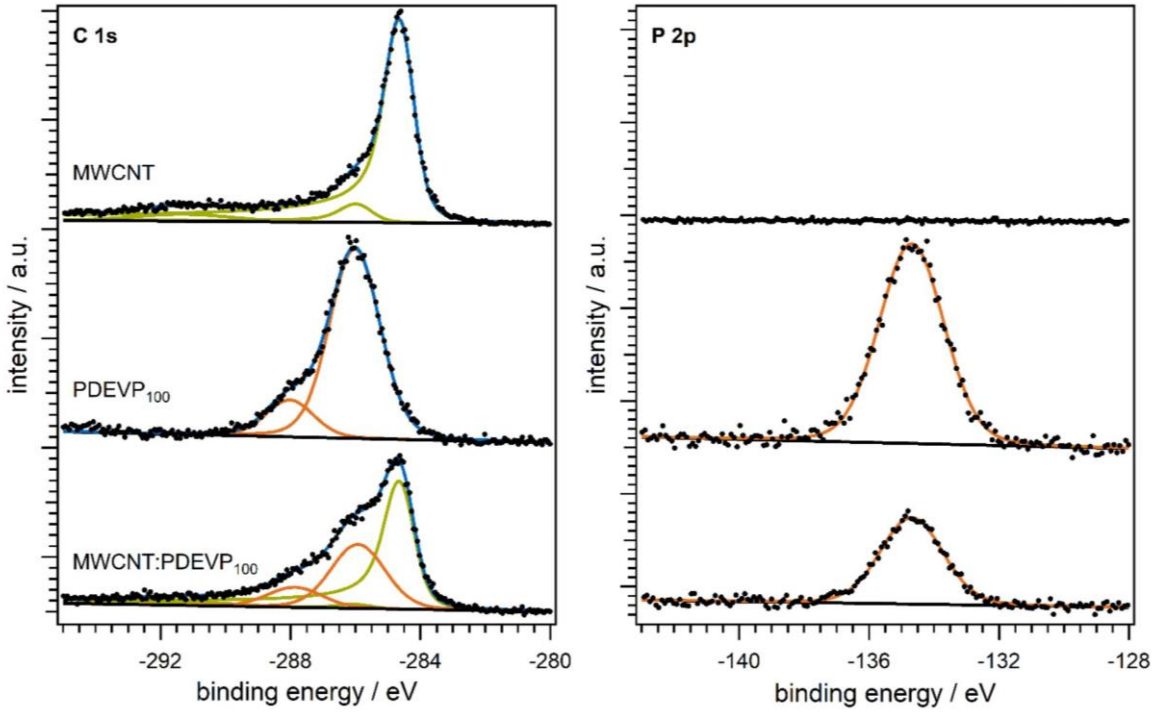

Figure S14: XPS detail spectra of the C 1s (left) and P 2p (right) core levels obtained from pristine MWCNT, pure PDEVP and MWCNT:$PDEVP_{100}$ = 1:5 (Table 3, entry 3). The intensity is scaled to the total C 1s peak area. Deconvolution of the C 1s core levels reveals that the MWCNT:$PDEVP_{100}$ spectrum is fully described by a superposition of both, the MWCNT and the PDEVP spectra without adding further components.

References

[1] K. C. Hultzsch, P. Voth, K. Beckerle, T. P. Spaniol, J. Okuda, *Organometallics.* **2000**, *19*, 228, DOI: 10.1021/om990583p.

[2] S. Salzinger, B. S. Soller, A. Plikhta, U. B. Seemann, E. Herdtweck, B. Rieger, *J. Am. Chem. Soc.* **2013**, *135*, 13030, DOI: 10.1021/ja404457f.

[3] C.-X. Cai, L. Toupet, C. W. Lehmann, J.-F. Carpentier, *J. Organomet. Chem.*. **2003**, *683*, 131, DOI: 10.1016/S0022-328X(03)00513-8.

[4] C. Schwarzenböck, A. Schaffer, P. Pahl, P. J. Nelson, R. Huss, B. Rieger, *Polym. Chem.* **2018**, *9*, 284, DOI: 10.1039/C7PY01796K.

[5] T. M. Pehl, M. Kränzlein, F. Adams, A. Schaffer and B. Rieger, *Catalysts.* **2020**, 10 (4), 448.

[6] a) M. Holzinger, J. Abraham, P. Whelan, R. Graupner, L. Ley, F. Hennrich, M. Kappes, A. Hirsch, *J. Am. Chem. Soc.* **2003**, *125*, 8566, DOI: 10.1021/ja029931w; b) J. Park, M. Yan, *Acc. Chem. Res.* **2013**, *46*, 181, DOI: 10.1021/ar300172h; c) A. Setaro, M. Adeli, M. Glaeske, D. Przyrembel, T. Bisswanger, G. Gordeev, F. Maschietto, A. Faghani, B. Paulus, M. Weinelt, R. Arenal, R. Haag, S. Reich, *Nat. Commun.* **2017**, *8*, 14281, DOI: 10.1038/ncomms14281; d) S. J. Pastine, D. Okawa, B. Kessler, M. Rolandi, M. Llorente, A. Zettl, J. M. J. Fréchet, *J. Am. Chem. Soc.* **2008**, *130*, 4238, DOI: 10.1021/ja8003446;

[7] a) C. Gao, H. He, L. Zhou, X. Zheng, Y. Zhang, *Chem. Mater.* **2009**, *21*, 360, DOI: 10.1021/cm802704c; b) M. S. Dresselhaus, G. Dresselhaus, R. Saito, A. Jorio, *Phys. Rep.* **2005**, *409*, 47, DOI: 10.1016/j.physrep.2004.10.006;

Supporting information of the addendum

Material and Methods

General consideration

Polymerizations with moisture and air-sensitive reactants were carried out in a *MBraun* LabMaster120 glovebox filled with argon 4.6 from *Westfalen* or using standard *Schlenk* techniques. All glassware was heat-dried prior to use. All chemicals were purchased from *Sigma-Aldrich*, ABCR, or TCI Europe and used without further purification unless otherwise stated. Dichloromethane, tetrahydrofuran, toluene, and pentane were dried using a *MBraun* SPS-800 solvent purification system and stored over 3 Å molecular sieve. Diethyl vinylphosphonate (DEVP) and were synthesized according to literature procedures followed by drying over CaH_2 for several days and distilled prior to use.[178] $LiCH_2TMS$, and $Cp_2YCH_2TMS(thf)$ were prepared according to literature procedures.[179, 180]

Electronspray Ionisation Mass Spectrometry (ESI-MS)

ESI-MS was measured using a Thermo Fisher Scientific Exactive Plus Orbitrap in positive mode in HPLC acetonitrile straight from the reaction mixture without quenching.

Fluorescence spectroscopy

Fluorescence spectroscopy was performed on a Jasco (Jasco FP-8300, Spectra Manager software 2.13). The concentration of polymers in methanol was determined to be 1.0 mg/mL. Corresponding substrates were prepared in 0.5 mM solutions. Fluorescence spectroscopy was performed on a Jasco (Jasco FP-8300, Spectra Manager software 2.13).

Lyophilization

The polymer samples subject to freeze-drying were dissolved in either ultrapure water or 1,4-dioxane and frozen under constant rotation in liquid nitrogen. For lyophilisation, a VaCo 5-II-D from Zirbus Technology GmbH was used, the pressure was adjusted to 2 mbar with a condenser temperature of -90 °C.

Nuclear magnetic resonance spectroscopy (NMR)

Nuclear magnetic resonance spectra were recorded on a *Bruker AVIII 400 HD* (400 MHz) or an *AVIII 500 cryo* (500 MHz). Deuterated solvents were purchased ($CDCl_3$, benzene-*d6*) from *Sigma-Aldrich*. Spectroscopic chemical shifts δ are reported in ppm and calibrated to the residual proton signals of the used solvents.

Size-exclusion chromatography multi-angle light scattering (SEC-MALS)

Molecular weights and polydispersity of the polymers (c = 2.5 mg/mL) were determined by SEC-MALS using a Wyatt Dawn Heleos II MALS light scattering unit and a Wyatt Optilab rEX

536 RI unit in THF: H_2O = 1:1 (with 9 g/L *tetra*-*n*-butyl-ammonium bromide and 272 mg/L 2,6-di-*tert*-butyl-4-methylphenol added) as eluent at 40 °C on two Agilent PolarGel-M columns; for absolute molecular weight (triple detection) determination of different polymers, the refractive index increments dn/dc = 0.0922 mL/g was used.

Iodo-2,6-dimethylpyridine (2)

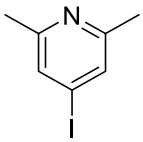

3.00 g (21.2 mmol, 1.0 eq.) 4-chloro-2,6-dimethylpyridine and 19.1 g (127 mmol, 6.0 eq.) sodium iodide were suspended in 50.0 mL acetonitrile. To this mixture, 2.27 mL (2.49 mg, 31.8 mmol, 1.5 eq.) acetyl chloride was added dropwise. The reaction mixture was stirred overnight at 140 °C. Following this, aqueous solutions of K_2CO_3 (25.0 mL, 10.0 wt%), Na_2SO_3 (25.0 mL, 5.00 wt%), and $Na_2S_2O_3$ (20.0 mL, concentrated solution) were added to the cold suspension. Ethyl acetate was added until phase separation could be occurred. After extracting the aqueous phase with ethyl acetate twice, the combined organic phases were dried over Na_2SO_4, and the solvent was removed in vacuo. Purification was achieved through sublimation with dry ice cooling (33.0 °C, p = 0.1 × 10^{-2} mbar), yielding in 2.26 g (9.69 mmol, 45%) 4-iodo-2,6-dimethylpyridine as a white solid.

^{1}H-NMR (500 MHz, $CDCl_3$, 300 K): δ (ppm) = 7.38 (s, 2H, H_{Ar}), 2.47 (s, 6H, CH_3).

^{13}C-NMR (101 MHz, $CDCl_3$, 300 K): δ (ppm) = 159.0 (s), 129.9 (s), 106.8 (s), 24.4 (s).

EA: calculated: C 36.08%, H 3.46%, N 6.01%, I 54.45%.

found: C 36.27%, H 3.33%, N 6.07%, I 54.04%.

The analytical data match those reported in the literature.[63]

2,6-Dimethyl-4-((Trimethylsilyl)ethynyl)pyridine (3)

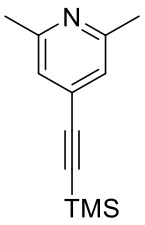

1.99 g (8.53 mmol, 1.00 eq.) 4-Iodo-2,6-dimethylpyridine and 120 mg (16.3 mmol, 0.02 eq.) bis(tri-phenylphosphine) palladium(II) dichloride were dissolved in 150 mL triethylamine. To this solution, 1.47 mL (1.17 mg, 11.9 mmol, 1.40 eq.) trimethylsilylacetylene and 16.3 mg (85.3 mmol, 0.01 eq.) copper (I) iodide were added, and the resulting rection mixture was stirred at 75 °C overnight. After filtration, the solvent was removed in vacuo. Purification via column chromatography (H/NEt_3 = 99:1, aluminium oxide as stationary phase) provided 1.16 g (5.70 mmol, 67%) 2,6-dimethyl-4-((trimethylsilyl)ethynyl)pyridine.

^{1}H-NMR (400 MHz, C_6D_6, 300 K): δ (ppm) = 6.84 (s, 2H, H_{Ar}), 2.29 (s, 6H, CH_3), 0.24 (s, 9H, $Si(CH_3)_3$).

ESI-MS: calculated: 204.1209 $[M–H]^+$, found: 204.1206 $[M–H]^+$.

EA: calculated: C 69.92%, H 8.53%, N 6.89%, I 13.81%.

found: C 70.68%, H 8.43%, N 6.99%, I 13.70%.

The analytical data match those reported in the literature.[181]

in-situ CH-bond activation of $Cp_2Y(CH_2TMS)(thf)$

The *in-situ* CH-bond activation of the methyl pyridine compound **3** was monitored *via* kinetic ^{1}H-NMR experiment in a J-Young NMR tube. Initially, 5.11 mg (0.0135 mmol, 1.0 eq.) $Cp_2YCH_2TMS(thf)$ were dissolved in 0.3 mL dry benzene-d_6. This solution was added to a solution containing 3.29 mg (0.0162 mmol, 1.2 eq.) 2,6-dimethyl-4-((trimethylsilyl)ethynyl)pyridine in 0.3 mL dry benzene-d_6 at room temperature. ^{1}H-NMR spectra are measured immediately after addition (5 minutes), subsequently at intervals of 15 minutes for one hour, and thereafter at hourly intervals for a total duration of 5 hours.

Polymerization of DEVP

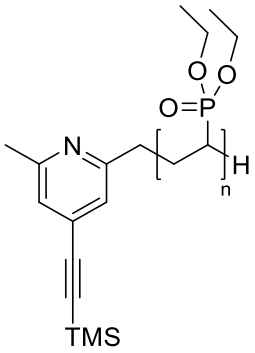

Upon full conversion of the CH-bond activation, the respective equivalents of *Michael* monomer were added in a single addition. An aliquot (0.1 mL) was taken and subsequently quenched with 0.4 mL wet methanol (calculation of conversion *via* ^{1}H-NMR spectroscopy). Once the full conversion was confirmed, the reaction mixture was then quenched by adding of 0.5 mL ethanol, followed by participation in 50 mL pentane. After centrifugation, the supernatant was decanted. The polymer was dissolved in 1,4-dioxane and lyophilized overnight, yielding a white solid product. Each aliquot was used for GPC-MALS analysis of the containing polymer species.

Table 11.1: Group-transfer polymerization results with *in-situ* activated $Cp_2Y(CH_2TMS)(thf)$

Entry	[DEVP]/ [Y][a]	X[b] [%]	$M_{n,theo}$[c] [kg/mol]	$M_{n,abs}$[d] [kg/mol]	$Đ$[d] [-]	I.E.[e] [%]
P1	50/1	99	8.7	19.6	1.09	44
P2	100/1	99	19.7	31.5	1.09	53
P3	200/1	99	33.7	66.1	1.05	50

[a] 13.5 µmol catalyst, 2 mL toluene, rt, 2 h; [b] conversion determined *via* integration of ^{31}P-NMR, [c] theoretical molecular weight determined as $M_{n,theo} = X \cdot M_{DEVP} \cdot [DEVP]/[Y] + M_{ini}$; [d] absolute molecular weight and polydispersity determined *via* SEC-MALS in THF:H_2O with added TBAF, 40 °C, dn/dc = 0.0922 mL/g; [e] initiator efficiency determined *via* I.E. = $M_{n,theo}/M_{n,abs} \cdot 100\%$.

^{1}H-NMR (400 MHz, $CDCl_3$, 300 K): δ (ppm) = 6.91 – 6.71 (m, $H_{ar,sym\text{-Collidin}}$), 4.13 (s, -OC*H*$_2CH_3$), 2.87 – 1.13 (m, $H_{backbone}$, -OCH$_2$C*H*$_3$), 0.22 (s, $H_{TMS\text{-}initiator}$).

^{31}P-NMR (203 MHz, $CDCl_3$, 300K): *δ* (ppm) = 33.2.

TMS deprotection procedure of PDEVP from group-transfer polymerization

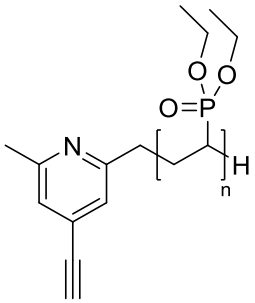

The alkyne functionalized PDEVP (1.0 eq.) was dissolved in methanol (5.00 mL solvent per 100 mg polymer). The calculated amount of K_2CO_3 (20 eq.) was suspended in the solution, and the resulting suspension was stirred overnight. Following the solvent removal, the mixture was dissolved in water and dialyzed for 24 h (MWCO 6-8 kDa). The deprotected polymer **P4** was obtained through lyophilization of the dialyzed solution.

Functionalization of polymer P4 with Coumarine-N_3 using azide-alkyne click reaction

The deprotected PDEVP **P4** (1.0 eq.) was dissolved in water (5.00 mL solvent per 100 mg polymer). Following this, a solution of 3-azido-7-coumarine (**6**) (10 eq., 2.17 µM in water) was added, along with a solution of Cp*Ru(COD)Cl (0.1 eq., 0.002 µM in water). The resulting reaction mixture was stirred overnight and subsequently dialyzed (MWCO 6-8 kDa). Lyophilization afforded the polymer **P5** in the form of a yellow solid.

11.4.2 Supporting Information Chapter 5

Supporting Information for the Manuscript Entitled *Allyl Group-Containing Polyvinylphosphonates as a Flexible Platform for the Selective Introduction of Functional Groups via Polymer-Analogous Transformations*†

Kerstin Halama,[‡a] Andreas Schaffer,[‡a] and Bernhard Rieger*[a]

[a]*WACKER-Chair of Macromolecular Chemistry, Catalysis Research Center, Technical University of Munich, Lichtenbergstraße 4, 85748 Garching near Munich, Germany. E-mail: rieger@tum.de.*

Table of Contents

1 Polymerization of DEVP and DAIVP to P(DEVP-*co*-DAIVP) P1

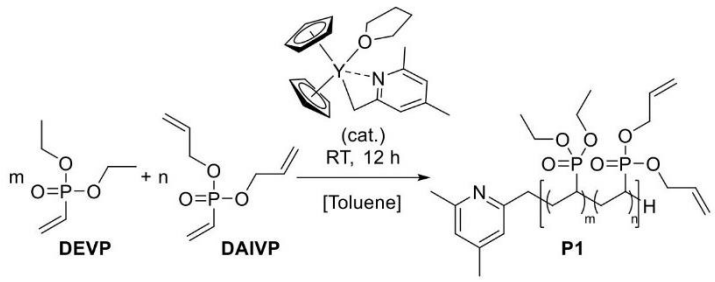

^{1}H-NMR (400 MHz, MeOD, 300 K): δ (ppm) = 7.22 – 6.85 (m, $CH_{Ar,}$ 2H), 6.04 (s, CH_{Allyl}, 22H), 5.42 (d, ^{3}J = 16.9 Hz, CH_{Allyl}, 22H), 5.28 (s, CH_{Allyl}, 22H), 4.63 (s, $POCH_{2,Allyl}$, 44H), 4.18 (s, $POCH_2$, 440H), 2.96 – 1.15 (m, polymer backbone, 363H), 1.38 (s, $POCH_2CH_3$, 660H).

^{31}P-NMR (203 MHz, MeOD, 300 K): δ (ppm) = 33.2.

IR (ATR): $\tilde{\upsilon}$ (cm^{-1}) = 3506 (br w), 2984 (m, ν_{C-H}), 2934 (m, ν_{C-H}), 2910 (m, ν_{C-H}), 1481 (w, δ_{C-H}), 1445 (m, δ_{C-H}), 1393 (m, δ_{C-H}), 1369 (w, δ_{C-H}), 1223 (st, $\nu_{P=O}$), 1164 (m, ν_{C-O}), 1098 (w), 1047 (w, ν_{P-O}), 1017 (st, ν_{P-O}), 952 (st), 780 (st).

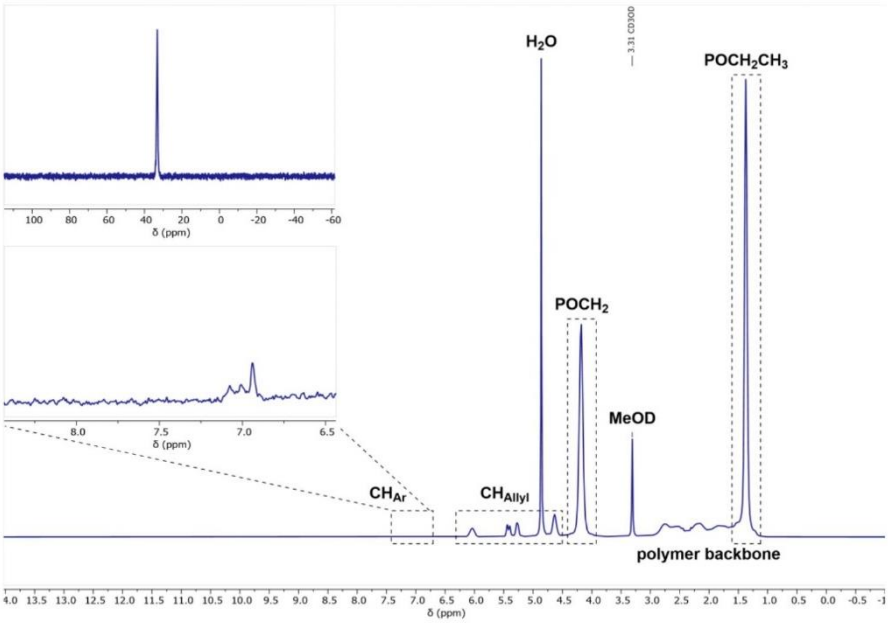

Fig. S1 ^{1}H- and zoom of ^{31}P-NMR spectrum of polymer **P1** in MeOD.

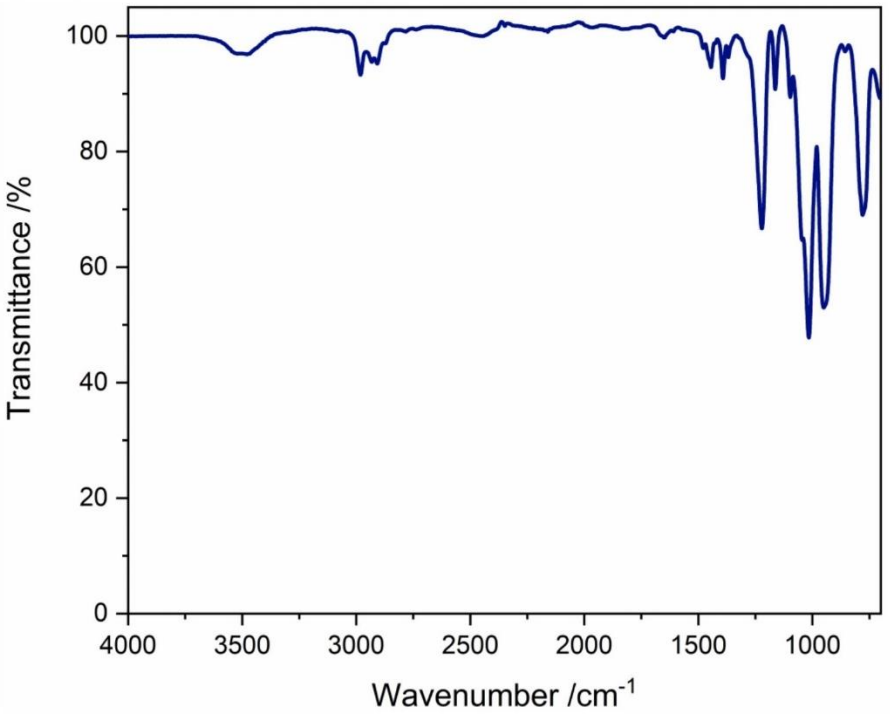

Fig. S2 IR spectrum of polymer **P1**.

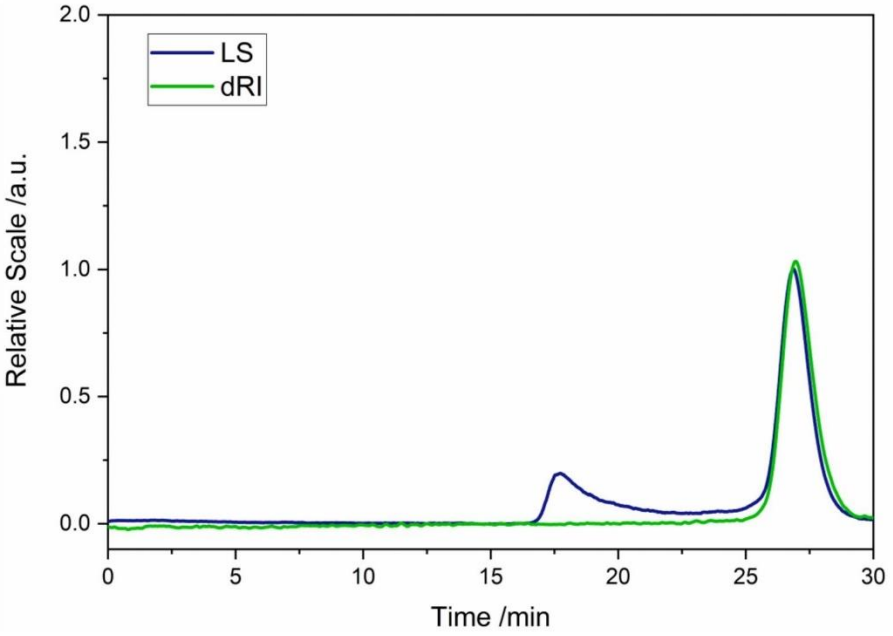

Fig. S3 GPC trace of polymer **P1** in THF/water measured via GPC-MALS.

2 Bromination and Follow-up Functionalizations

Bromination of P(DEVP-*co*-DAlVP) P1

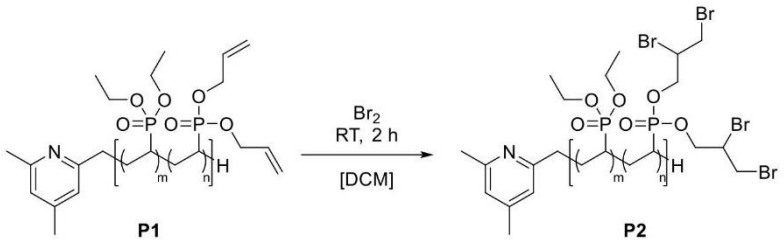

^{1}H-NMR (400 MHz, MeOD, 300 K): δ (ppm) = 7.76 – 7.65 (m, CH_{Ar}), 7.61 (s, CH_{Ar}), 4.63 – 4.48 (m, POCH_2CHBr), 4.20 (s, POCH_2), 4.04 – 3.86 (m, CHBr, CH_2Br), 3.67 – 3.46 (m, CHBr, CH_2Br), 2.91 – 1.16 (m, polymer backbone), 1.38 (s, POCH$_2CH_3$).

^{31}P-NMR (203 MHz, MeOD, 300 K): δ (ppm) = 33.1.

IR (ATR): $\tilde{\upsilon}$ (cm^{-1}) = 3349 (br w), 2989 (m, ν_{C-H}), 2937 (m, ν_{C-H}), 2910 (m, ν_{C-H}), 1481 (w, δ_{C-H}), 1447 (m, δ_{C-H}), 1394 (m, δ_{C-H}), 1370 (w, δ_{C-H}), 1209 (st, $\nu_{P=O}$), 1162 (m, ν_{C-O}), 1097 (w), 1043 (w, ν_{P-O}), 1022 (st, ν_{P-O}), 958 (st), 783 (st), 594 (w, ν_{C-Br}).

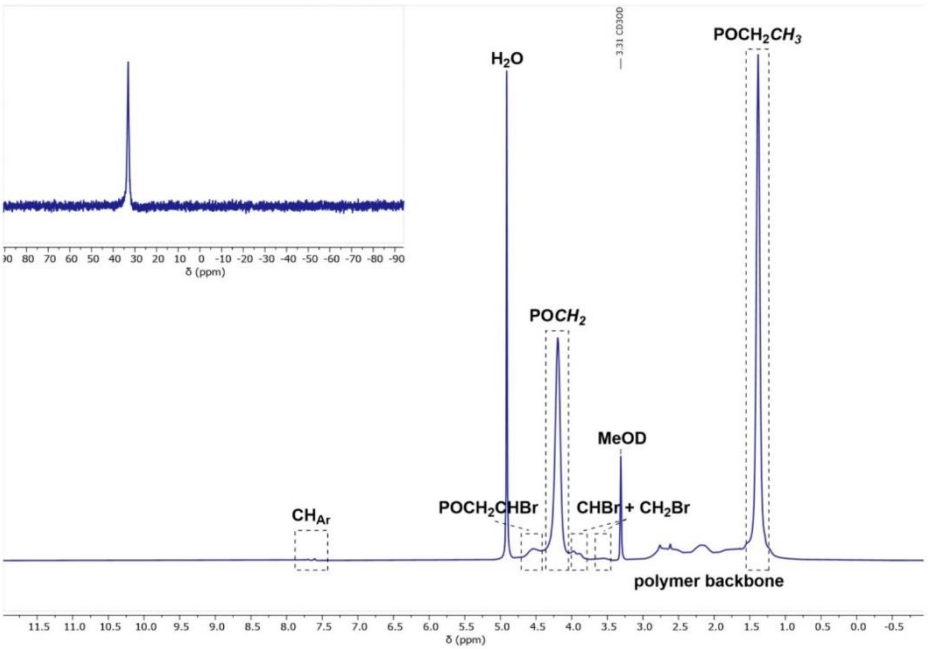

Fig. S4 ^{1}H- and zoom of ^{31}P-NMR spectrum of polymer **P2** in MeOD.

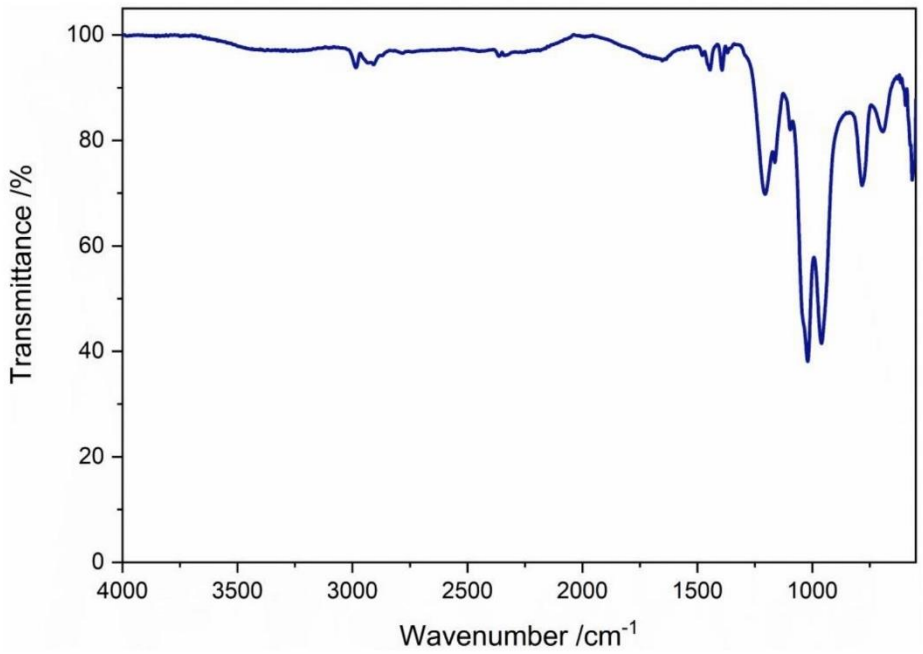

Fig. S5 IR spectrum of polymer **P2**.

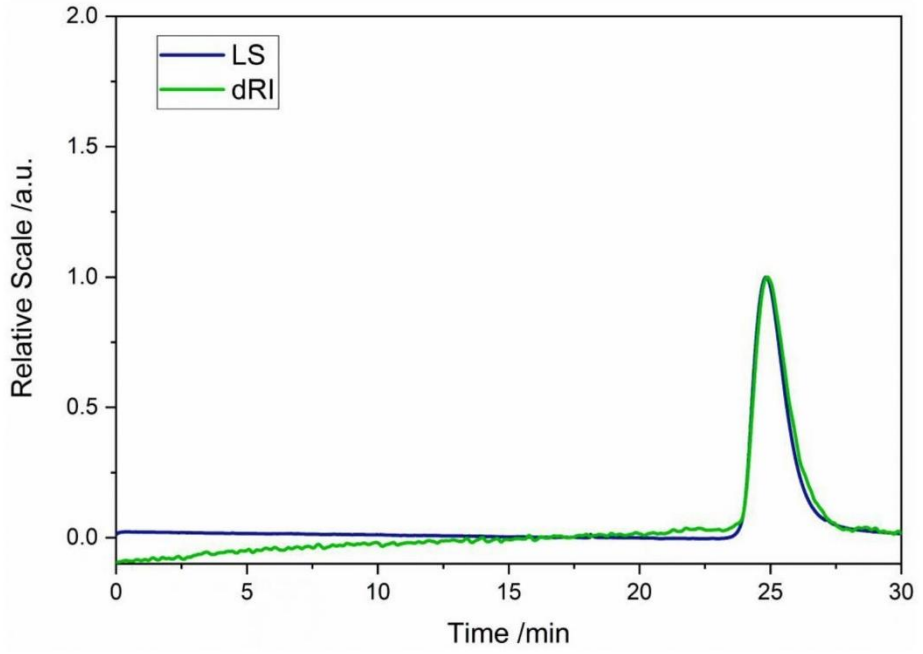

Fig. S6 GPC trace of polymer **P2** in THF/water measured via GPC-MALS.

Conversion of Brominated Polyvinylphosphonate P2 with Sodium Azide

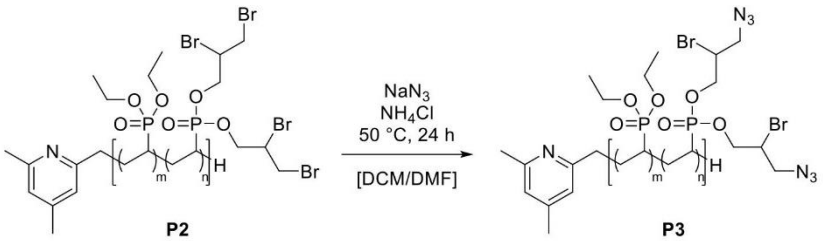

The brominated polyvinylphosphonate **P2** was dissolved in equal amounts of dichloromethane (4 mL per 100 mg of polymer) and *N*,*N*-dimethylformamide (4 mL per 100 mg of polymer) and treated with sodium azide (5.0 equiv. per C-Br bond). The reaction mixture was heated to 50 °C for 24 hours. Volatiles were then removed *in vacuo* and the residue was dissolved in deionized water. The polymer was dialysed against deionized water and freeze-dried from water.

^{1}H-NMR (400 MHz, MeOD, 300 K): δ (ppm) = 4.67 – 4.43 (m, non-converted POCH_2CHBr), 4.19 (s, POCH_2), 4.04 – 3.83 (m, non-converted CHBr), 3.03 – 1.13 (m, polymer backbone), 1.38 (s, POCH$_2CH_3$).

^{31}P-NMR (203 MHz, MeOD, 300 K): δ (ppm) = 33.1.

IR (ATR): $\tilde{\upsilon}$ (cm^{-1}) = 3375 (br w), 2981 (m, ν_{C-H}), 2929 (m, ν_{C-H}), 1481 (w, δ_{C-H}), 2111 (m, $\nu_{N=N=N}$), 1648 (m), 1445 (m, δ_{C-H}), 1392 (m, δ_{C-H}), 1368 (w, δ_{C-H}), 1211 (st, $\nu_{P=O}$), 1162 (m, ν_{C-O}), 1096 (w), 1041 (w, ν_{P-O}), 1019 (st, ν_{P-O}), 954 (st), 777 (st).

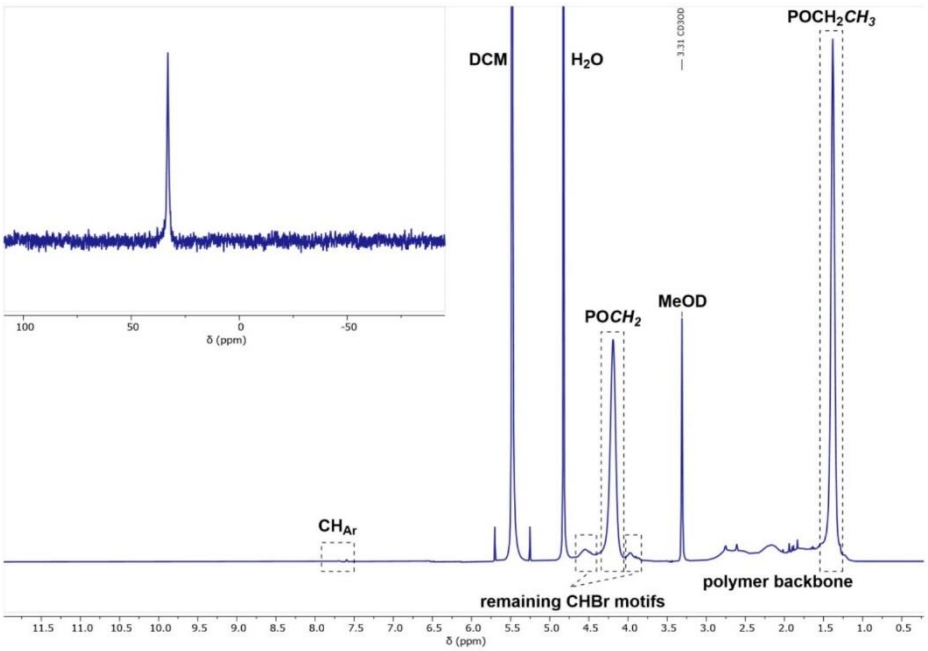

Fig. S7 ^{1}H- and zoom of ^{31}P-NMR spectrum of polymer **P3** in MeOD.

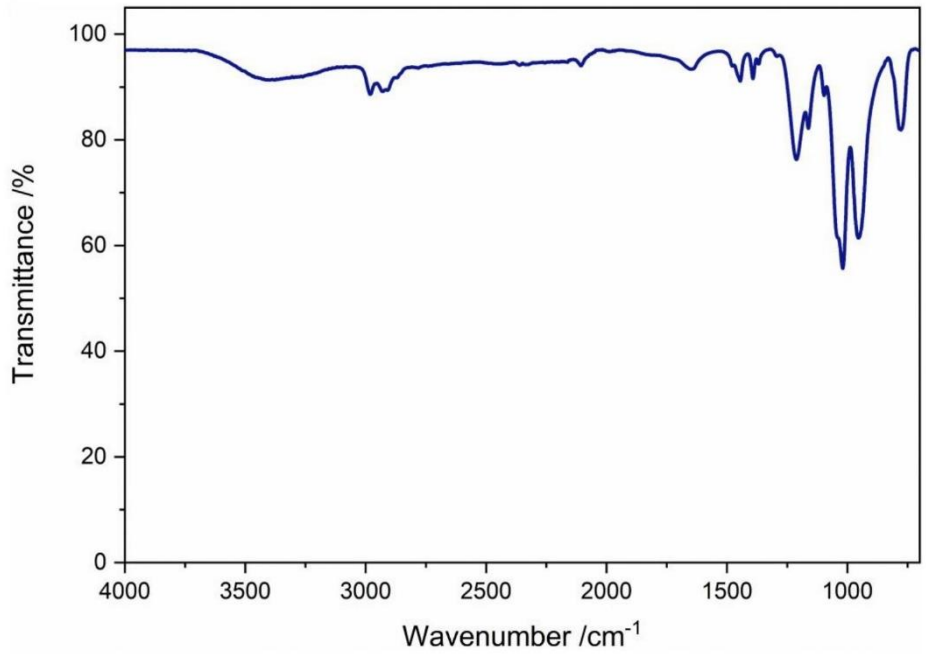

Fig. S8 IR spectrum of polymer **P3**.

3 Epoxydation Reactions and Follow-up Functionalizations

Epoxydation of P(DEVP-*co*-DAlVP) P1 with *OXONE* or *m*CPBA

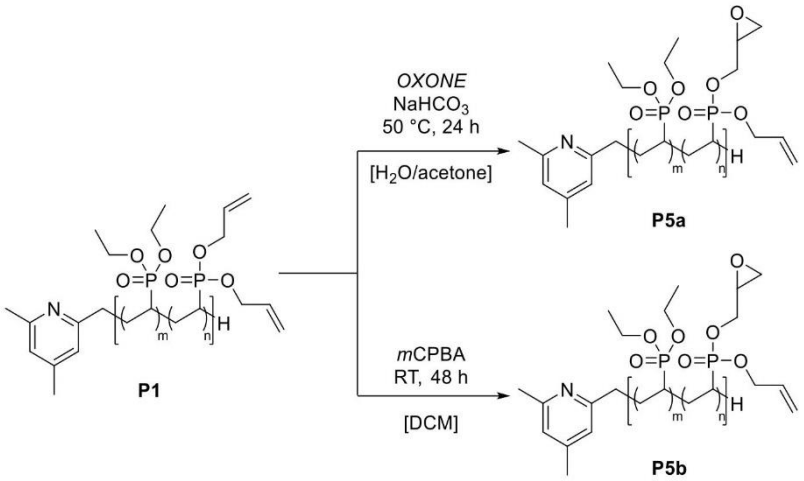

The crude reaction solutions were used immediately for the follow-up functionalization reaction to prevent cross-linking of the epoxide groups.

Analytical data of polymer **P5a**

^{1}H-NMR (400 MHz, MeOD, 300 K): δ (ppm) = 7.39 – 7.20 (m, CH_{Ar}), 6.04 (s, CH_{Allyl}), 5.42 (d, ^{3}J = 17.2 Hz, CH_{Allyl}), 5.27 (s, CH_{Allyl}), 4.65 (s, $POCH_{2,Allyl}$), 4.49 (s, $POCH_{2,Epxoide}$), 4.18 (s, $POCH_2$), 2.88 – 2.62 (m, $CH_{Epoxide}$), 2.98 – 1.08 (m, polymer backbone), 1.38 (s, $POCH_2CH_3$).

^{31}P-NMR (203 MHz, MeOD, 300 K): δ (ppm) = 33.1.

IR (ATR): $\tilde{\upsilon}$ (cm^{-1}) = 3466 (br w), 2983 (m, ν_{C-H}), 2931 (m, ν_{C-H}), 2909 (m, ν_{C-H}), 1652 (m), 1478 (w, δ_{C-H}), 1446 (m, δ_{C-H}), 1394 (m, δ_{C-H}), 1370 (w, δ_{C-H}), 1217 (st, $\nu_{P=O}$), 1164 (m, ν_{C-O}), 1099 (w), 1043 (w, ν_{P-O}), 1015 (st, ν_{P-O}), 953 (st), 783 (st).

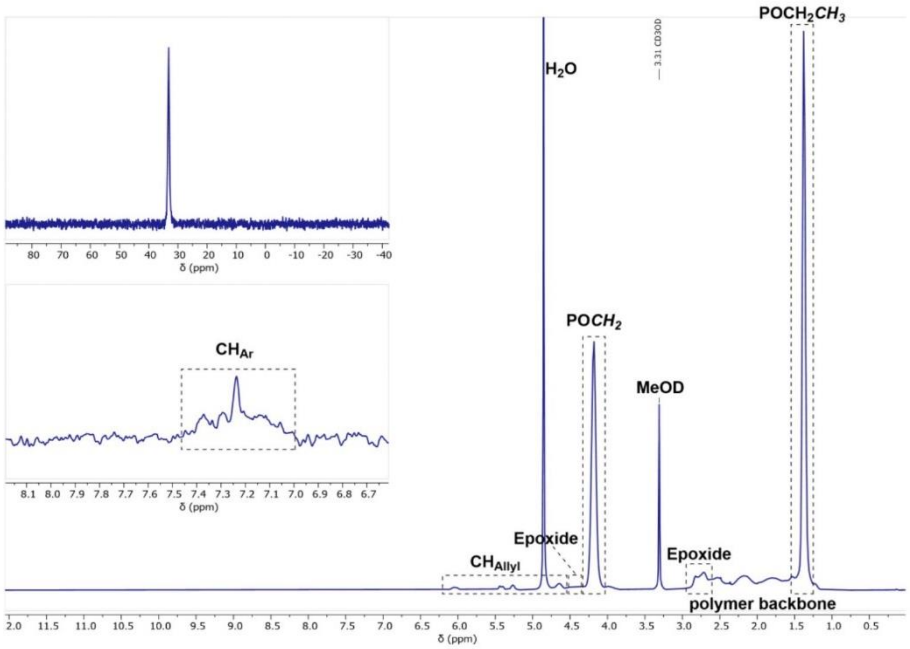

Fig. S9 ^{1}H- and zoom of ^{31}P-NMR spectrum of polymer **P5a** in MeOD.

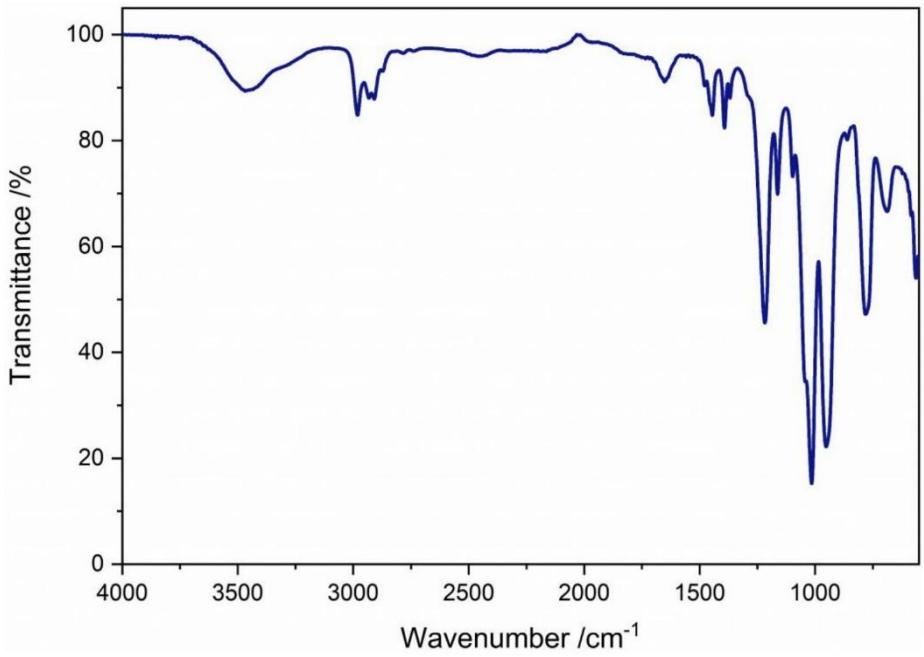

Fig. S10 IR spectrum of polymer **P5a**.

Analytical data of polymer **P5b**

^{1}H-NMR (400 MHz, MeOD, 300 K): δ (ppm) = 6.04 (s, CH_{Allyl}), 5.42 (d, ^{3}J = 17.2 Hz, CH_{Allyl}), 5.27 (s, CH_{Allyl}), 4.64 (s, $POCH_{2,Allyl}$), 4.18 (s, $POCH_2$), 2.88 – 2.67 (m, $CH_{Epoxide}$), 3.06 – 1.23 (m, polymer backbone), 1.38 (s, $POCH_2CH_3$).

^{31}P-NMR (203 MHz, MeOD, 300 K): δ (ppm) = 33.1

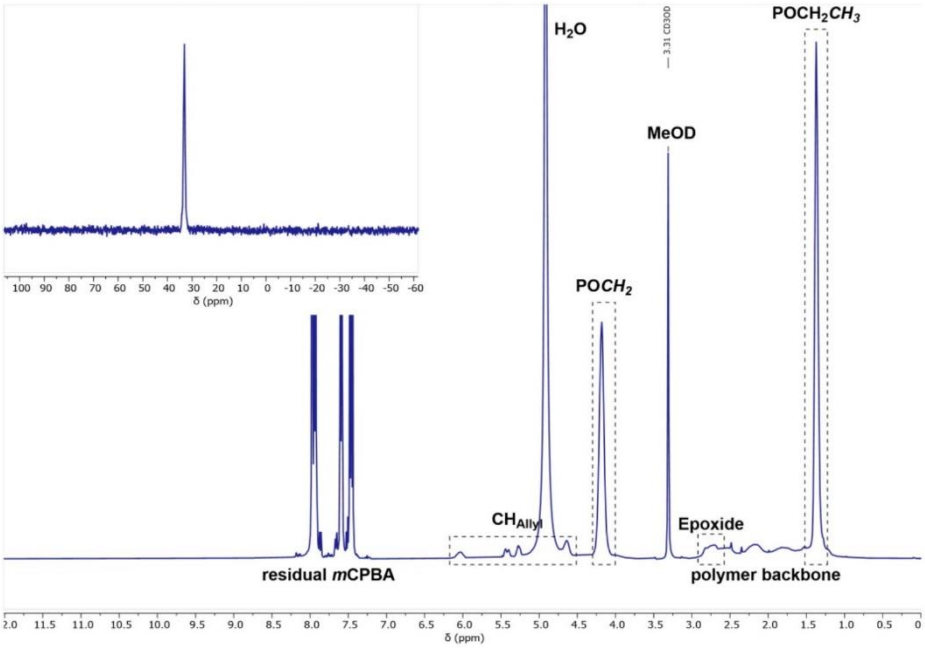

Fig. S11 ^{1}H- and zoom of ^{31}P-NMR spectrum of polymer **P5b** in MeOD.

Ring-Opening of Polyvinylphosphonate P5a with Phenol (2)

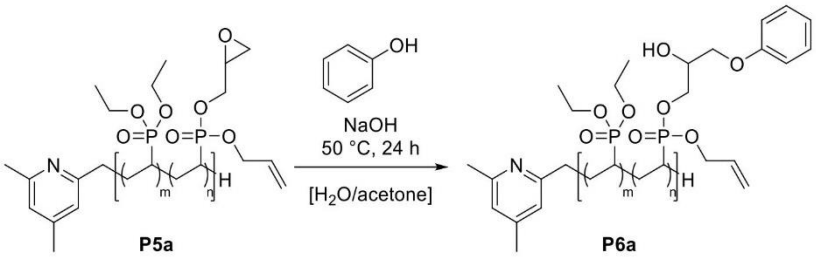

The crude solution of **P5a** in acetone/water (approximately 100 mg per 10 mL solvent) was treated with a solution of phenol (**2**) (8.8 equiv. per epoxide, 500 µmol in 750 µL H_2O) and sodium hydroxide (9.0 equiv. per epoxide, 511 µmol per 750 µL H_2O) in deionized water. Hereafter, the mixture was stirred for 24 hours at 50 °C. The conversion of the epoxide groups was checked via ^{1}H-NMR spectroscopy and the solution was cooled to room temperature. Acetone was removed under reduced pressure and the aqueous phase was purified via dialysis against water for 48 hours. The product was yielded via lyophilization from water.

^{1}H-NMR (400 MHz, MeOD, 300 K): δ (ppm) = 7.32 – 7.20 (m, $CH_{Ar,meta}$, 15H), 7.02 – 6.87 (m, $CH_{Ar,ortho}$, $CH_{Ar,para}$, 22H), 6.04 (s, $CH_{Allyl,}$), 5.42 (d, ^3J = 17.5 Hz, CH_{Allyl}), 5.23 (s, CH_{Allyl}), 4.63 (s, $POCH_{2,Allyl,}$ 9H), 4.18 (s, $POCH_2$, 475H), 2.91 – 1.14 (m, polymer backbone), 1.36 (s, $POCH_2CH_3$).

^{31}P-NMR (203 MHz, MeOD, 300 K): δ (ppm) = 33.3.

IR (ATR): $\tilde{\upsilon}$ (cm^{-1}) = 3466 (br w), 2983 (m, ν_{C-H}), 2931 (m, ν_{C-H}), 2909 (m, ν_{C-H}), 1652 (m), 1600 (m, $\nu_{C=C}$), 1497 (m, $\nu_{C=C}$), 1481 (w, δ_{C-H}), 1445 (m, δ_{C-H}), 1393 (m, δ_{C-H}), 1368 (w, δ_{C-H}), 1216 (st, $\nu_{P=O}$), 1162 (m, ν_{C-O}), 1097 (w), 1043 (w, ν_{P-O}), 1016 (st, ν_{P-O}), 952 (st), 780 (st).

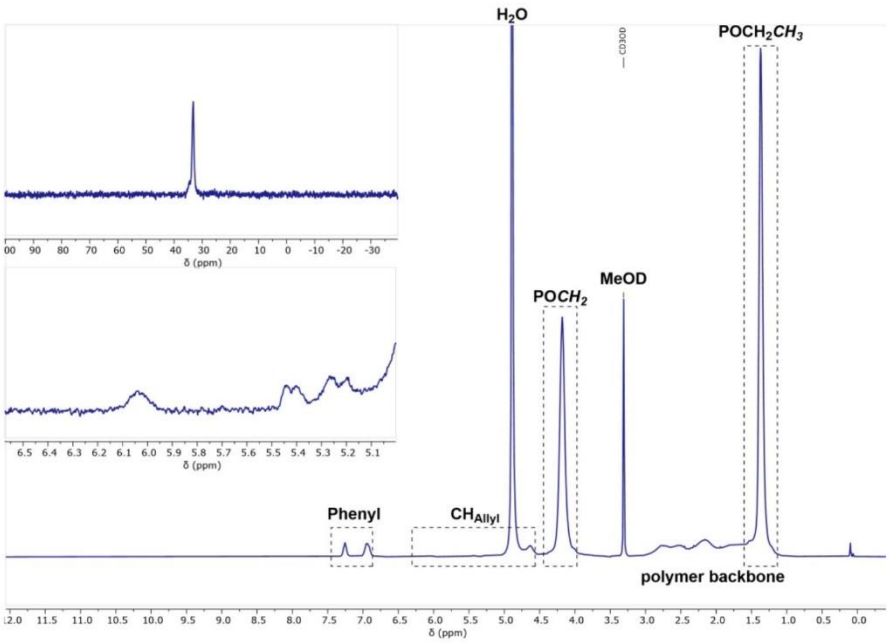

Fig. S12 ^{1}H- and zoom of ^{31}P-NMR spectrum of polymer conjugate **P6a** in MeOD.

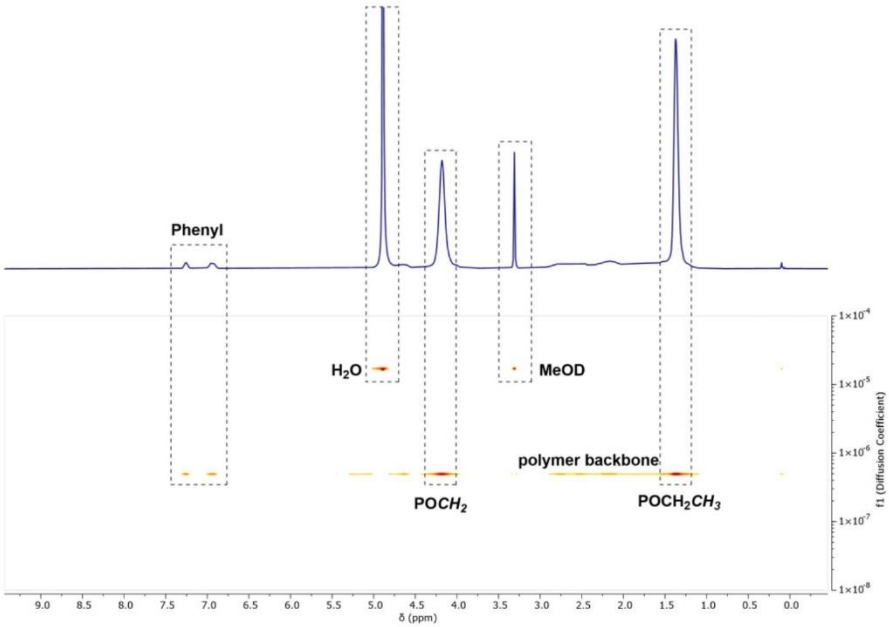

Fig. S13 DOSY spectrum of polymer **P6a** in MeOD.

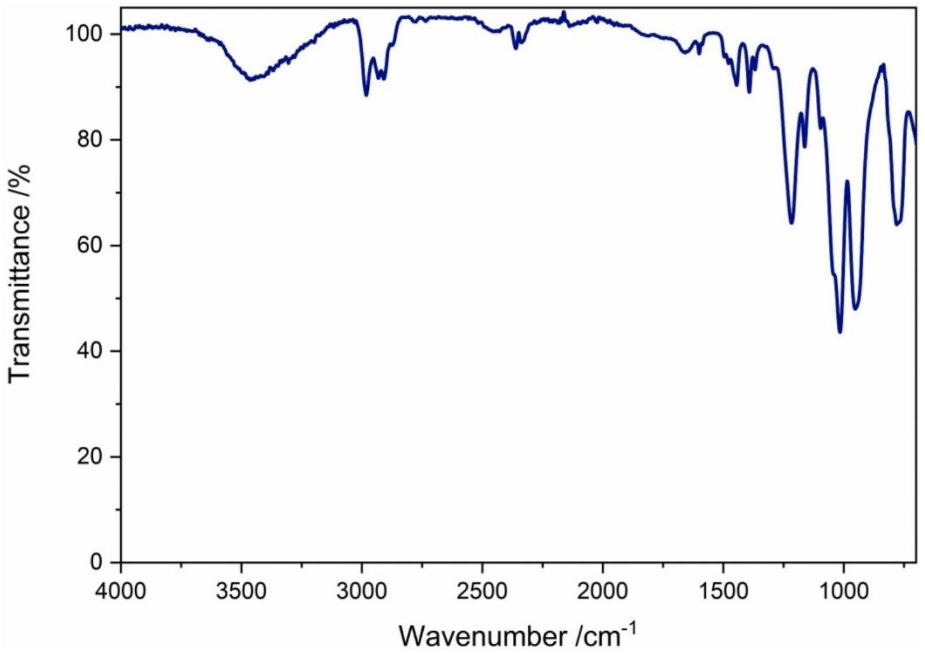

Fig. S14 IR spectrum of polymer conjugate **P6a**.

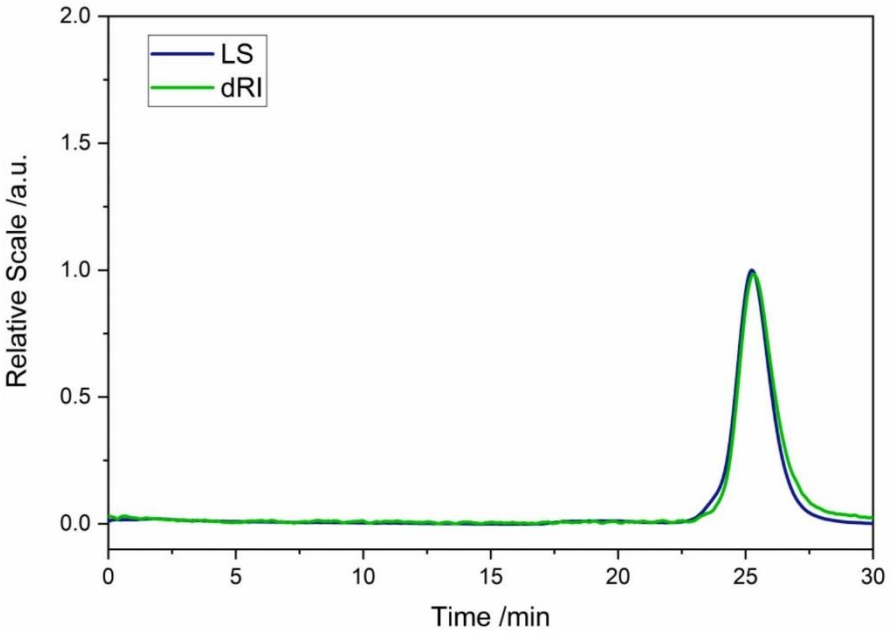

Fig. S15 GPC trace of polymer conjugate **P6a** in THF/water measured via GPC-MALS.

Ring-Opening of Polyvinylphosphonate P5a with Benzylamine (3)

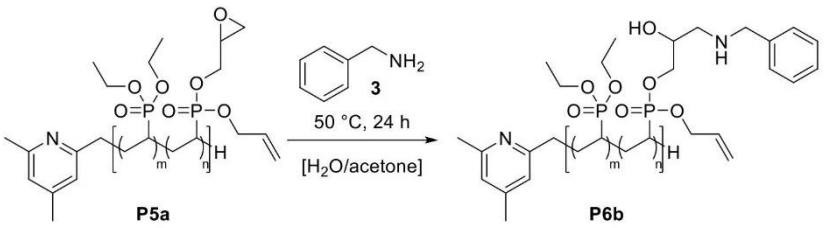

The crude solution of polymer **P5a** in acetone/water (approximately 100 mg per 10 mL solvent) was treated with benzylamine (**3**) (8.5 equiv. per epoxide). Hereafter, the mixture was stirred for 24 hours at 50 °C. The conversion of the epoxide groups was checked via ^{1}H-NMR spectroscopy and the solution was cooled to room temperature. Acetone was removed under reduced pressure and the aqueous phase was purified via dialysis against water for 48 hours. Freeze-drying from water yielded polymer conjugate **P6b**.

^{1}H-NMR (400 MHz, MeOD, 300 K): δ (ppm) = 7.77 – 7.07 (m, CH_{Ar}, 71H), 6.03 (s, CH_{Allyl}), 5.42 (d, ^{3}J = 17.1 Hz, CH_{Allyl}), 5.27 (s, CH_{Allyl}), 4.60 (s, $POCH_{2,Allyl}$, 13H), 4.18 (s, POCH_2, 471H), 3.65 (s, CH_2NH), 2.97 – 1.08 (m, polymer backbone), 1.38 (s, $POCH_2CH_3$).

^{31}P-NMR (203 MHz, MeOD, 300 K): δ (ppm) = 33.3.

IR (ATR): $\tilde{\upsilon}$ (cm^{-1}) = 3458 (br w), 2980 (m, ν_{C-H}), 2929 (m, ν_{C-H}), 2907 (m, ν_{C-H}), 1656 (m), 1496 (w, $\nu_{C=C}$), 1477 (w, δ_{C-H}), 1446 (m, δ_{C-H}), 1393 (m, δ_{C-H}), 1368 (w, δ_{C-H}), 1220 (st, $\nu_{P=O}$), 1163 (m, ν_{C-O}), 1096 (w), 1044 (w, ν_{P-O}), 1017 (st, ν_{P-O}), 950 (st), 787 (st).

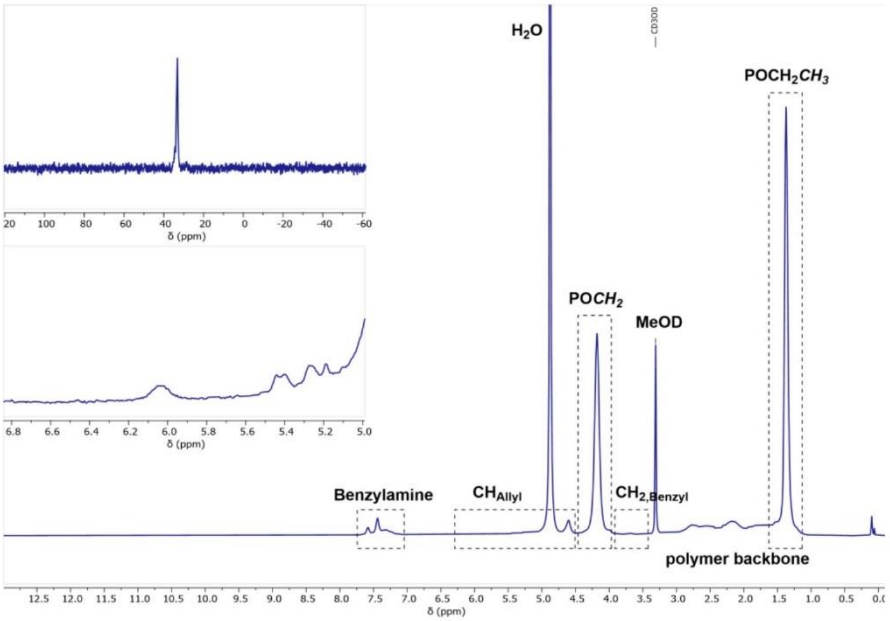

Fig. S16 ^{1}H- and zoom of ^{31}P-NMR spectrum of polymer conjugate **P6b** in MeOD.

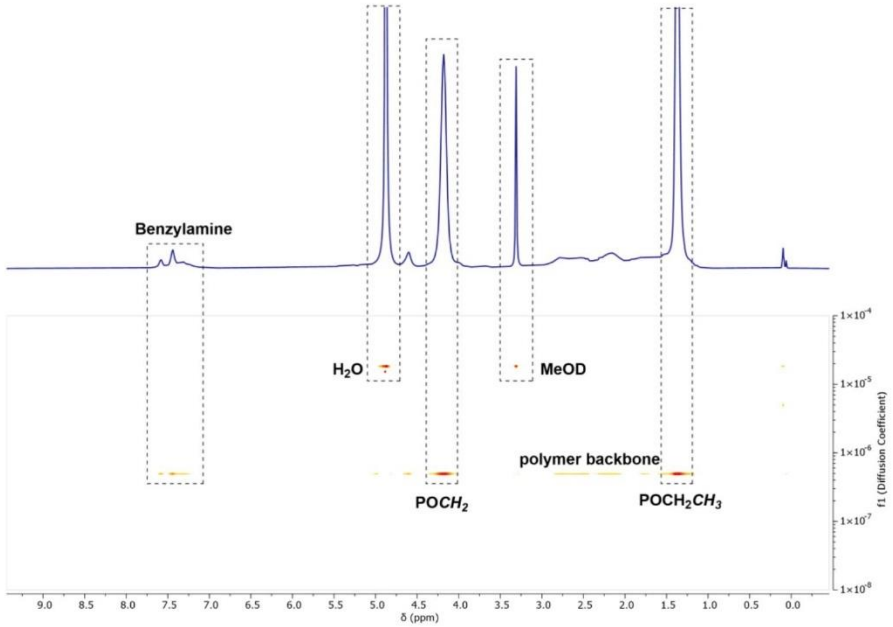

Fig. S17 DOSY spectrum of polymer **P6b** in MeOD.

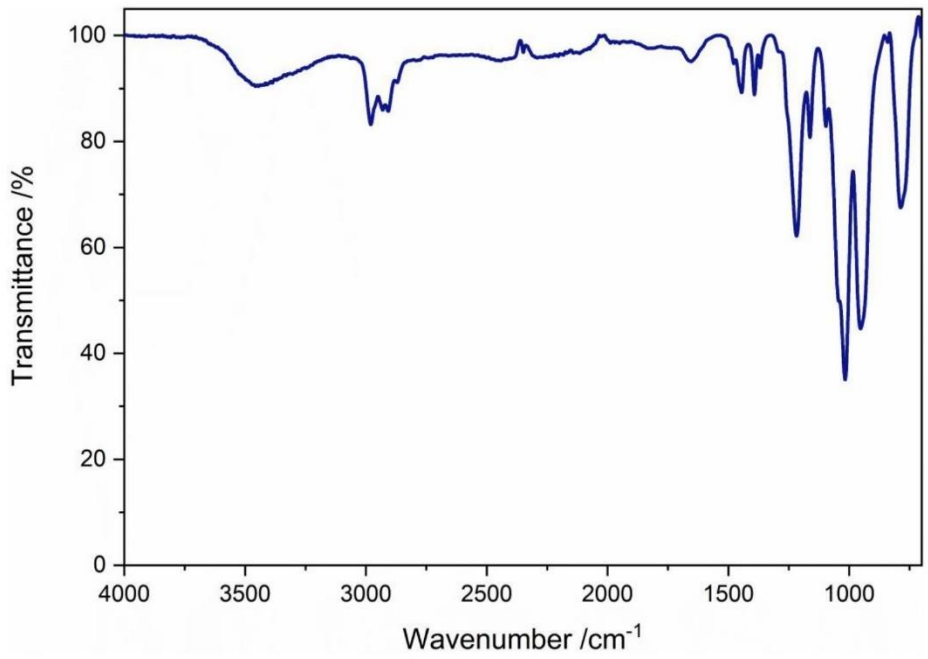

Fig. S18 IR spectrum of polymer conjugate **P6b**.

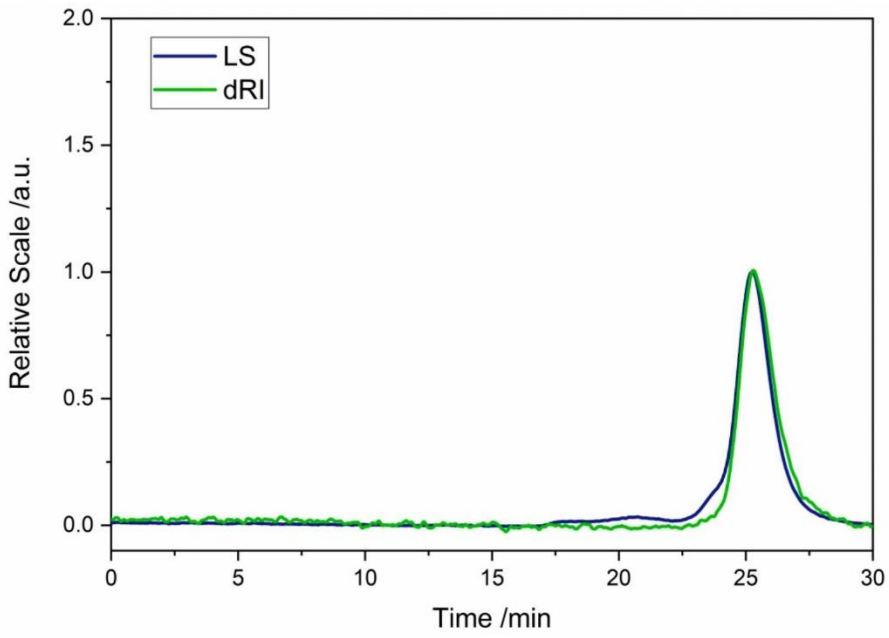

Fig. S19 GPC trace of polymer **P6b** in THF/water measured via GPC-MALS.

Ring-Opening of Polyvinylphosphonate P5a with 4-Amino-2,1,3-benzothiadiazole (4)

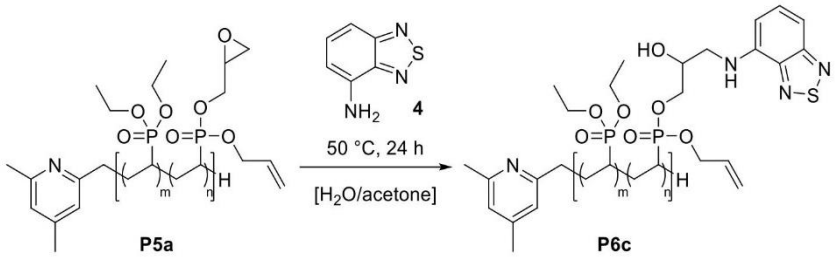

The crude solution containing polymer **P5a** in acetone/water (approximately 100 mg per 10 mL solvent) was treated with 4-amino-2,1,3-benzothiadiazole (**4**) (10 equiv. per epoxide). Hereafter, the mixture was stirred for 24 hours at 50 °C. The conversion of the epoxide groups was checked via ^{1}H-NMR spectroscopy and the solution was cooled to room temperature. Acetone was removed under reduced pressure and the remaining aqueous phase was purified via dialysis against water for 48 hours. Subsequent lyophilization from water yielded polymer conjugate **P6c**.

^{1}H-NMR (400 MHz, MeOD, 300 K): δ (ppm) = 7.41 (d, ^{3}J = 7.9 Hz, C*H*CHCHCNH, 6H), 7.20 (d, ^{3}J = 8.7 Hz, CHC*H*CHCNH, 5H), 6.63 (d, ^{3}J = 7.7 Hz, CHCHC*H*CNH, 6H), 4.18 (s, POCH_2, 484H), 2.88 – 1.16 (m, polymer backbone), 1.38 (s, POCH$_2CH_3$).

^{31}P-NMR (203 MHz, MeOD, 300 K): δ (ppm) = 33.2.

IR (ATR): $\tilde{\upsilon}$ (cm^{-1}) = 3454 (br w), 2980 (m, ν_{C-H}), 2930 (m, ν_{C-H}), 2908 (m, ν_{C-H}), 1629 (m), 1556 (m, $\nu_{C=N}$), 1497 (w, $\nu_{C=C}$) 1479 (w, δ_{C-H}), 1444 (m, δ_{C-H}), 1390 (m, δ_{C-H}), 1367 (w, δ_{C-H}), 1217 (st, $\nu_{P=O}$), 1161 (m, ν_{C-O}), 1097 (w), 1045 (w, ν_{P-O}), 1016 (st, ν_{P-O}), 953 (st), 781 (st).

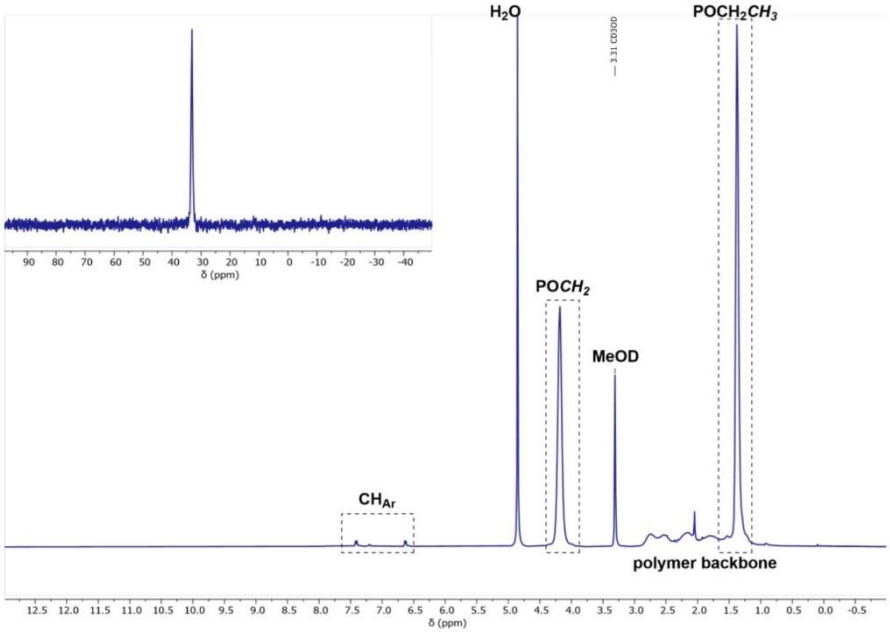

Fig. S20 ^{1}H- and zoom of ^{31}P-NMR spectrum of polymer conjugate **P6c** in MeOD.

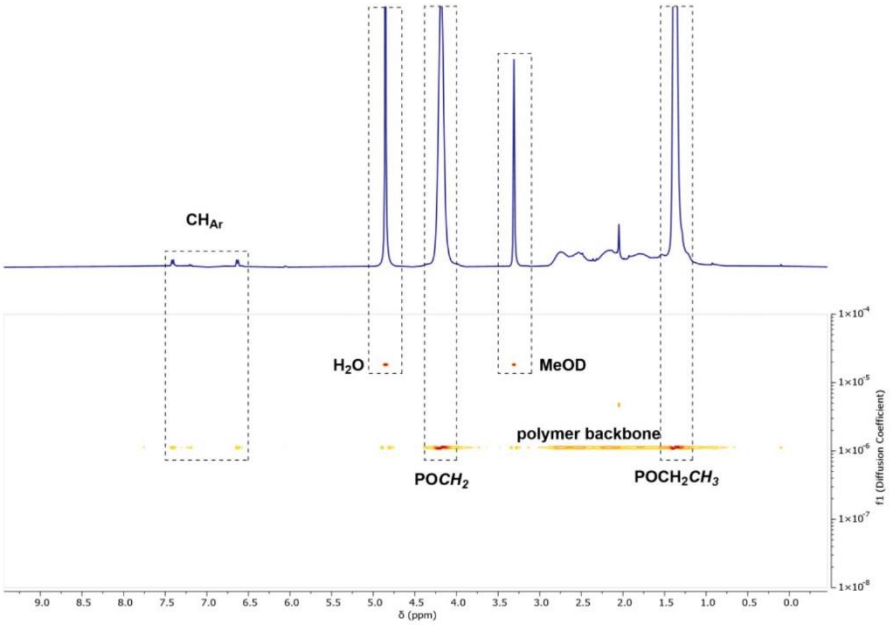

Fig. S21 DOSY spectrum of polymer **P6c** in MeOD.

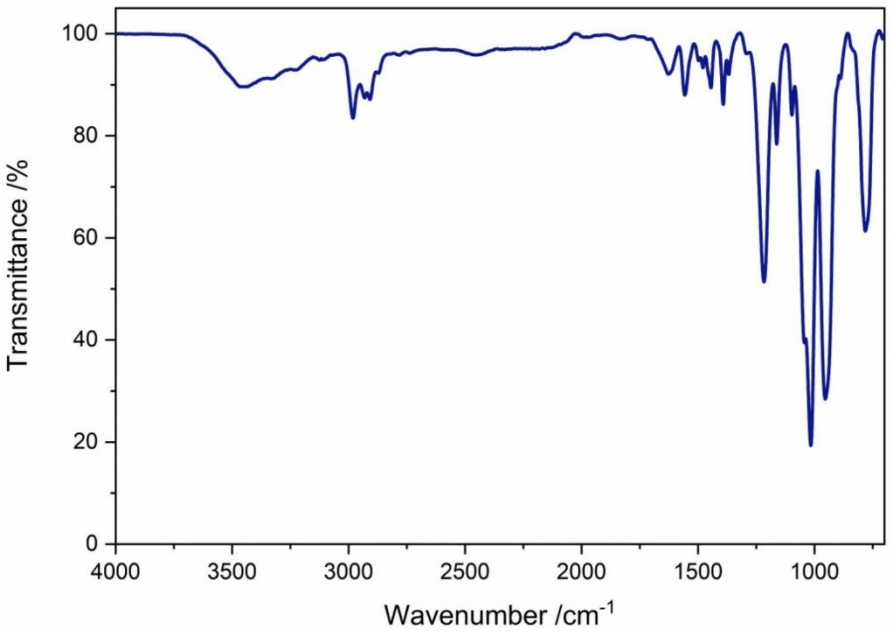

Fig. S22 IR spectrum of polymer conjugate **P6c**.

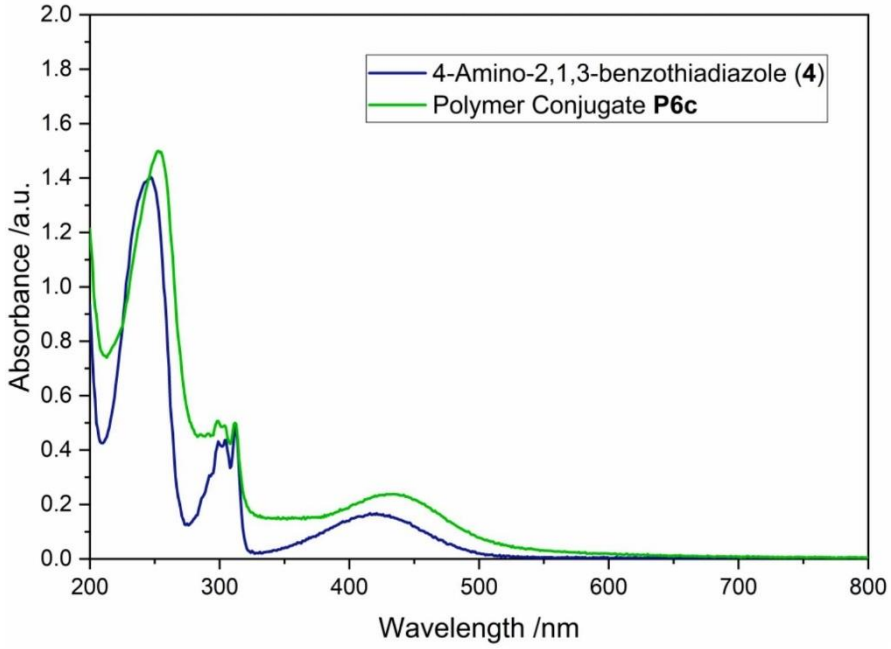

Fig. S23 UV/Vis spectrum of polymer conjugate **P6c** and 4-amino-2,1,3-benzpthiadiazole (**4**) in MeOH.

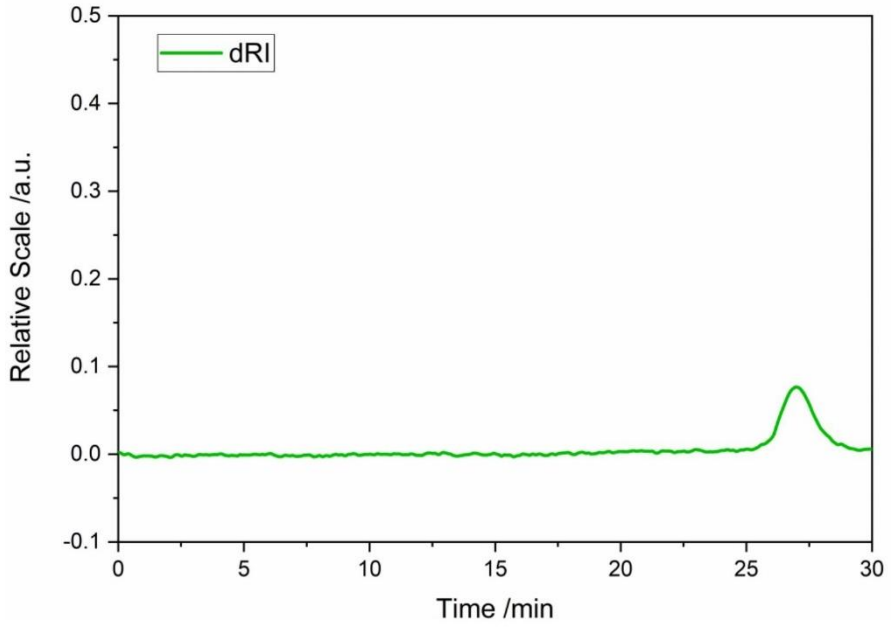

Fig. S24 GPC trace of polymer conjugate **P6c** in THF/water measured via GPC-MALS. Only the dRI trace is shown due to a strong interaction of the dye with MALS detector.

Ring-Opening of Polyvinylphosphonate P5b with Sodium Azide

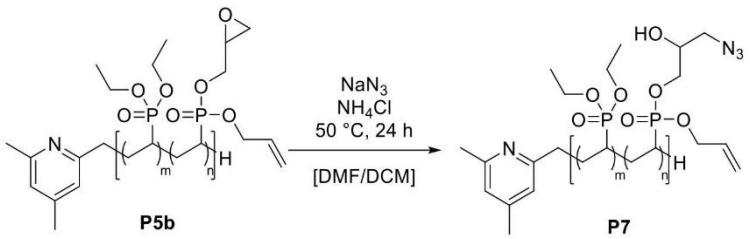

The crude solution containing polymer **P5b** was concentrated to a volume of approximately 3.00 mL (100 mg polymer per 3.0 mL DCM) and diluted with *N*,*N*-dimethylformamide (3.00 mL). The solution was treated with sodium azide (9.0 equiv. per epoxide) and ammonium chloride (9.0 equiv. per epoxide). Hereafter, the mixture was stirred for 24 hours at 50 °C and the conversion of the epoxide groups was checked via ^{1}H-NMR spectroscopy, which substantiated a quantitative consumption of the polymer-bound epoxides. The solvent was removed under reduced pressure and the crude product was dialysed against water for 48 hours. Subsequently, lyophilization from water yielded polymer **P7**.

^{1}H-NMR (400 MHz, MeOD, 300 K): δ (ppm) = 4.18 (s, PO*CH*$_2$, 440H), 2.88 – 1.16 (m, polymer backbone), 1.38 (s, POCH$_2$*CH*$_3$).

^{31}P-NMR (203 MHz, MeOD, 300 K): δ (ppm) = 33.2.

IR (ATR): $\tilde{\upsilon}$ (cm^{-1}) = 3427 (br w), 2981 (m, $\nu_{C\text{-}H}$), 2931 (m, $\nu_{C\text{-}H}$), 2907 (m, $\nu_{C\text{-}H}$), 2110 (m, $\nu_{N=N=N}$), 1713 (st), 1574 (m), 1477 (w, $\nu_{C=C}$) 1477 (w, $\delta_{C\text{-}H}$), 1429 (m, $\delta_{C\text{-}H}$), 1395 (m, $\delta_{C\text{-}H}$), 1369 (w, $\delta_{C\text{-}H}$), 1222 (st, $\nu_{P=O}$), 1193 (st), 1161 (m, $\nu_{C\text{-}O}$), 1101 (w), 1047 (w, $\nu_{P\text{-}O}$), 1017 (st, $\nu_{P\text{-}O}$), 960 (st), 791 (m), 750 (st).

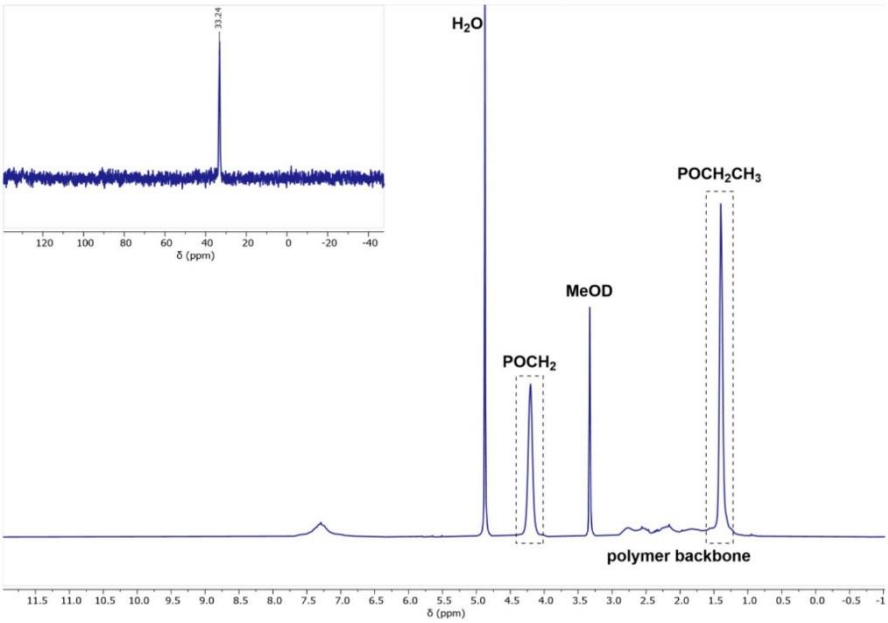

Fig. S25 ^{1}H- and zoom of ^{31}P-NMR spectrum of polymer **P7** in MeOD.

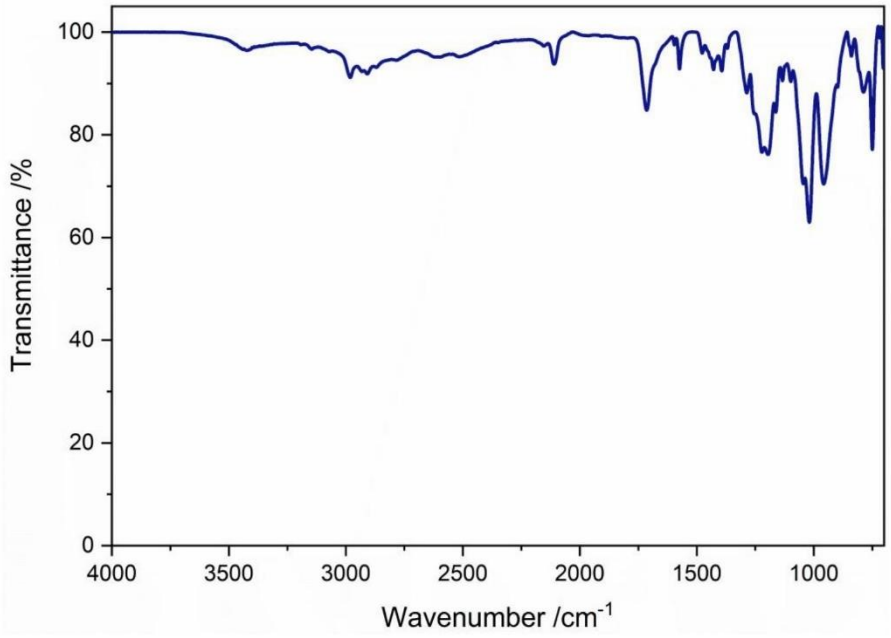

Fig. S26 IR spectrum of polymer **P7**.

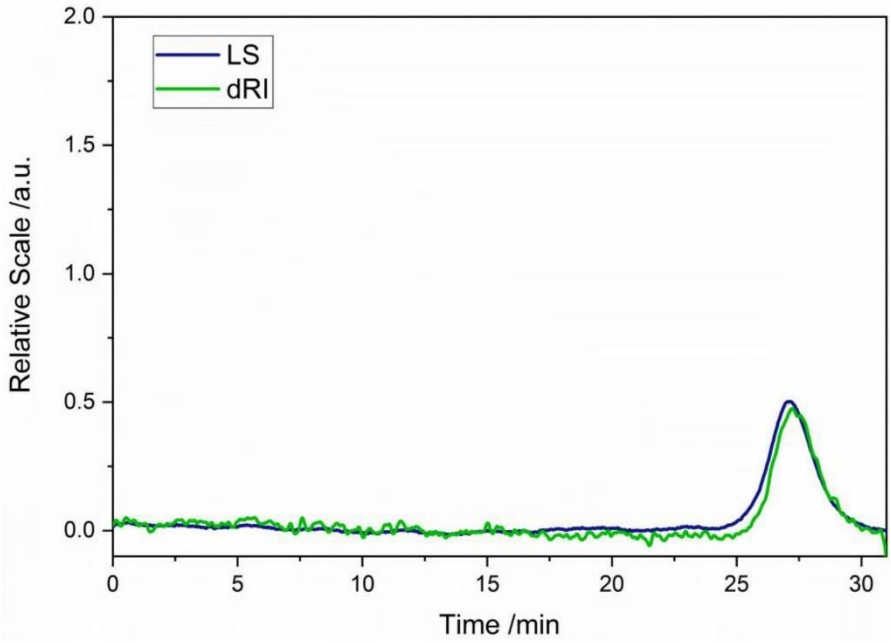

Fig. S27 GPC trace of polymer **P7** in THF/water measured via GPC-MALS.

Azide-Alkyne Click Coupling of Polyvinylphosphonate P7 with Phenylacetylene (1)

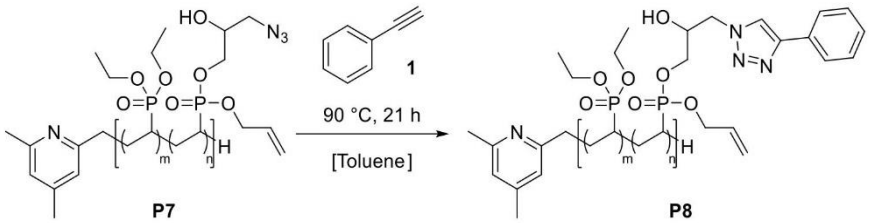

Polymer **P7** was dissolved in toluene (10 mg polymer per 1.0 mL solvent) and was treated with phenylacetylene (**1**) (8.0 equiv. per azide group; azide amount equal to epoxide amount in **P5b**). After heating to 90 °C, the reaction was stirred for 21 hours. ^{1}H- and DOSY-NMR spectroscopy was employed to check the outcome of the coupling reaction. Afterwards the polymer was washed with pentane to remove phenylacetylene and dialysed against water. Freeze-drying from water yielded conjugate **P8**.

^{1}H-NMR (400 MHz, MeOD, 300 K): δ (ppm) = 7.99 – 7.07 (m, Phenyl, 65H), 6.03 (s, CH_{Allyl}), 5.42 (d, ^{3}J = 17.3 Hz, CH_{Allyl}), 5.26 (s, CH_{Allyl}), 4.63 (s, $POCH_{2,Allyl}$, 10H), 4.18 (s, $PO\mathit{CH_2}$, 474H), 3.00 – 0.78 (m, polymer backbone), 1.37 (s, $POCH_2\mathit{CH_3}$).

^{31}P-NMR (203 MHz, MeOD, 300 K): δ (ppm) = 33.2.

IR (ATR): $\tilde{\upsilon}$ (cm^{-1}) = 3471 (br w), 2981 (m, ν_{C-H}), 2928 (m, ν_{C-H}), 2909 (m, ν_{C-H}), 1773 (m), 1713 (st), 1652 (br m), 1573 (w, $\nu_{C=C}$), 1480 (w, δ_{C-H}), 1444 (m, δ_{C-H}), 1392 (m, δ_{C-H}), 1368 (w, δ_{C-H}), 1216 (st, $\nu_{P=O}$), 1193 (st), 1162 (m, ν_{C-O}), 1097 (w), 1044 (w, ν_{P-O}), 1015 (st, ν_{P-O}), 951 (st), 778 (st).

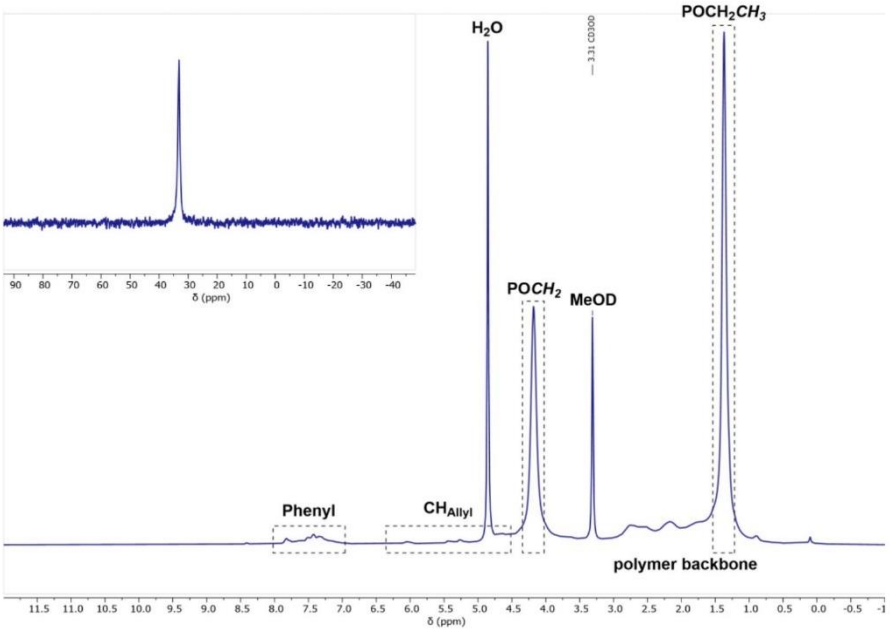

Fig. S28 ^{1}H- and zoom of ^{31}P-NMR spectrum of polymer **P8** in MeOD.

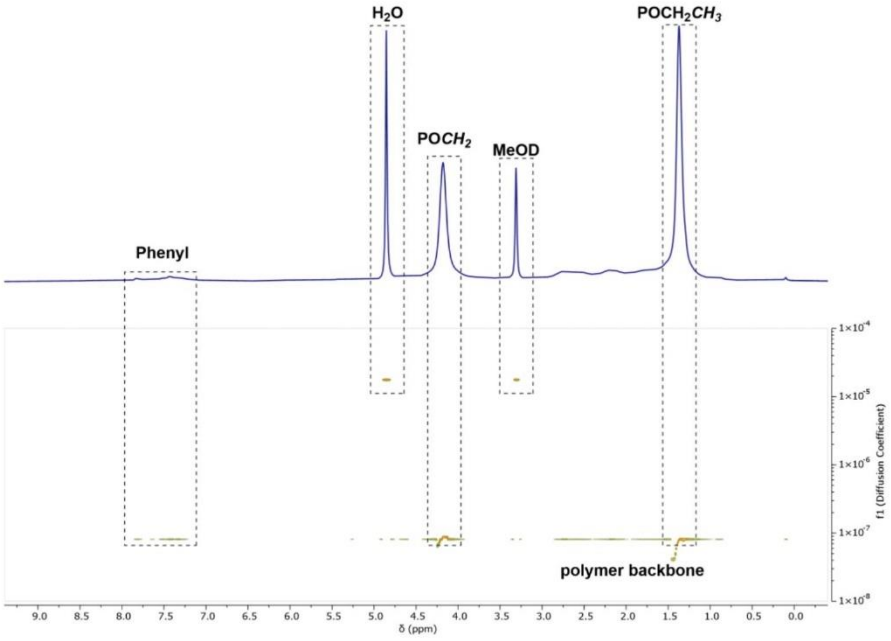

Fig. S29 DOSY spectrum of polymer **P8** in MeOD.

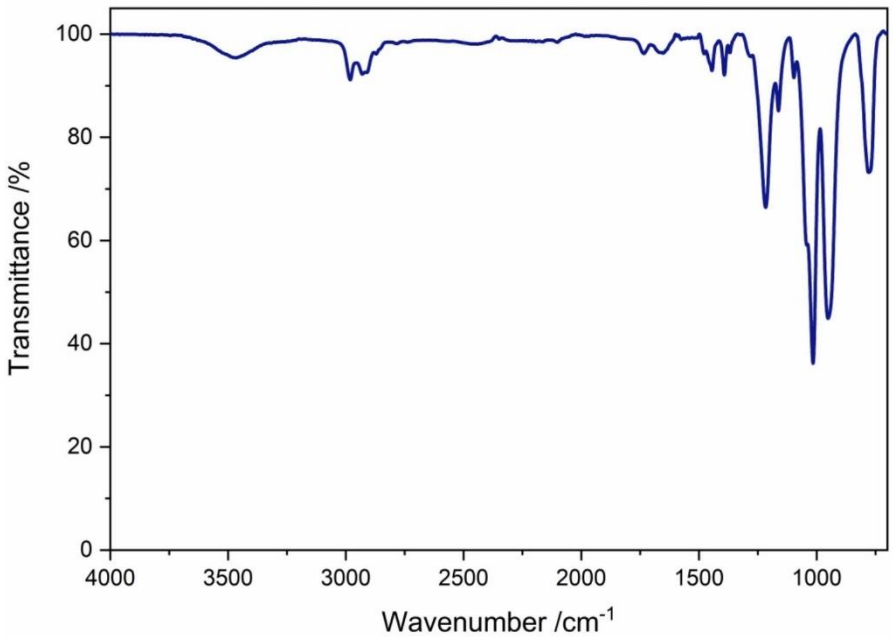

Fig. S30 IR spectrum of polymer **P8**.

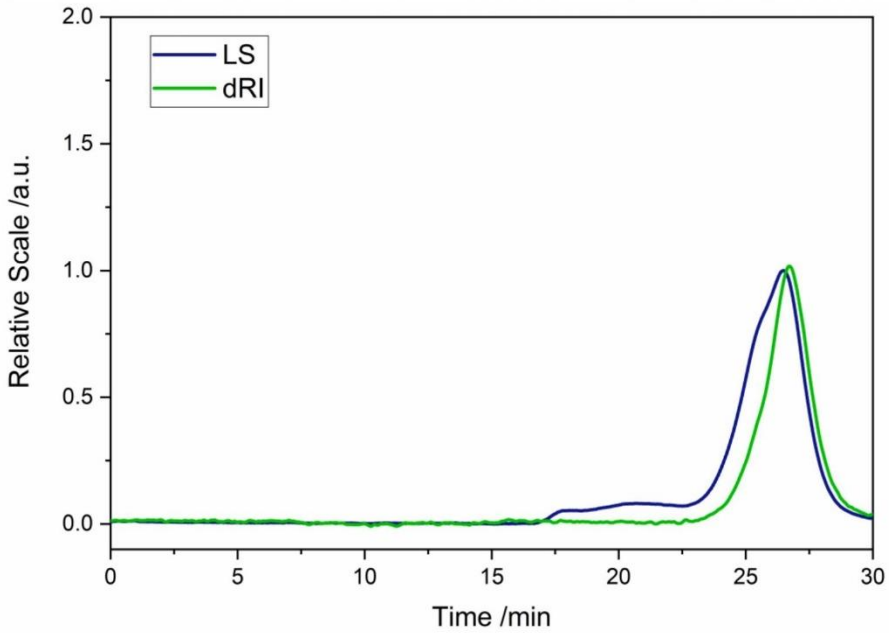

Fig. S31 GPC trace of polymer **P8** in THF/water measured via GPC-MALS.

4 Synthesis of Dual-Functionalized Polyvinylphosphonates

Follow-up Functionalization of P6b with Thiocholesterol (5) via Thiol-Ene Click Chemistry

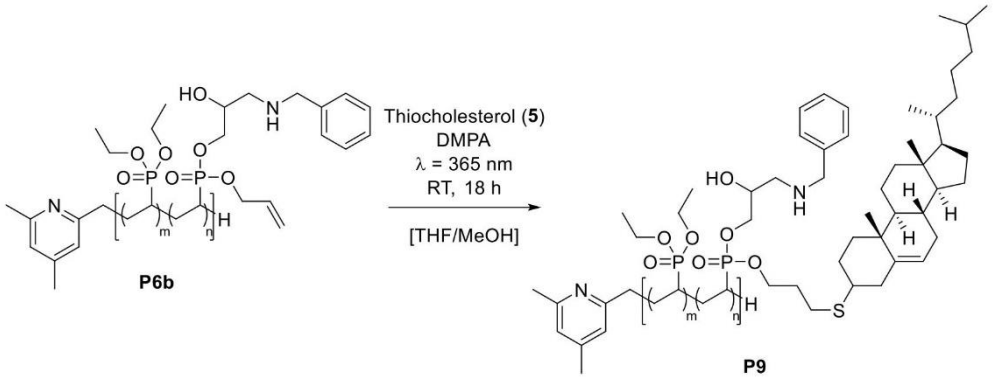

Polymer **P6b** (100 mg per 10 mL solvent) was dissolved in a mixture of THF/water (5/1). This solution was treated with thiocholesterol (**5**) (4.0 equiv. per remaining allyl group) and catalytic amounts of the photoinitiator 2,2-dimethoxy-2-phenylacetophenone. The reaction mixture was degassed (drawing vacuum and refilling with argon; 15 iterations) and irradiated at $\lambda = 365$ nm for 18 hours at room temperature. The consumption of the allyl groups was monitored by ^{1}H-NMR spectroscopy. Volatiles were then removed *in vacuo* and the crude polymer was washed several times with pentane to remove excess thiocholesterol, when the quantitative conversion of the allyl groups was observed via NMR. Hereafter, the conjugate was purified by dialysis against water and freeze-dried to yield substrate **P9**.

^{1}H-NMR (400 MHz, MeOD, 300 K): δ (ppm) = 7.70 – 7.11 (m, benzylamine, 71H), 5.39 (s, CH_{Chol}), 4.18 (s, POCH_2, 484H), 2.91 – 1.14 (m, polymer backbone), 1.38 (s, POCH$_2CH_3$), 1.03 (s, $CH_{3,Chol}$), 0.95 (d, $^{3}J = 6.2$ Hz, $CH_{3,Chol}$), 0.88 (d, $^{3}J = 6.6$ Hz, 2 x $CH_{3,Chol}$), 0.72 (s, $CH_{3,Chol,}$ 13H).

^{31}P-NMR (203 MHz, MeOD, 300 K): δ (ppm) = 33.2.

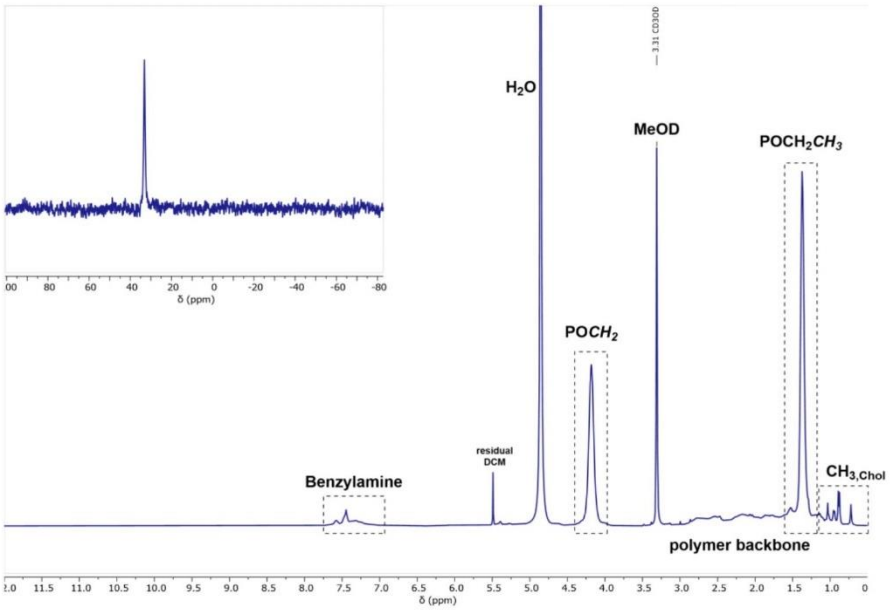

Fig. S32 ^{1}H- and zoom of ^{31}P-NMR spectrum of polymer **P9** in MeOD.

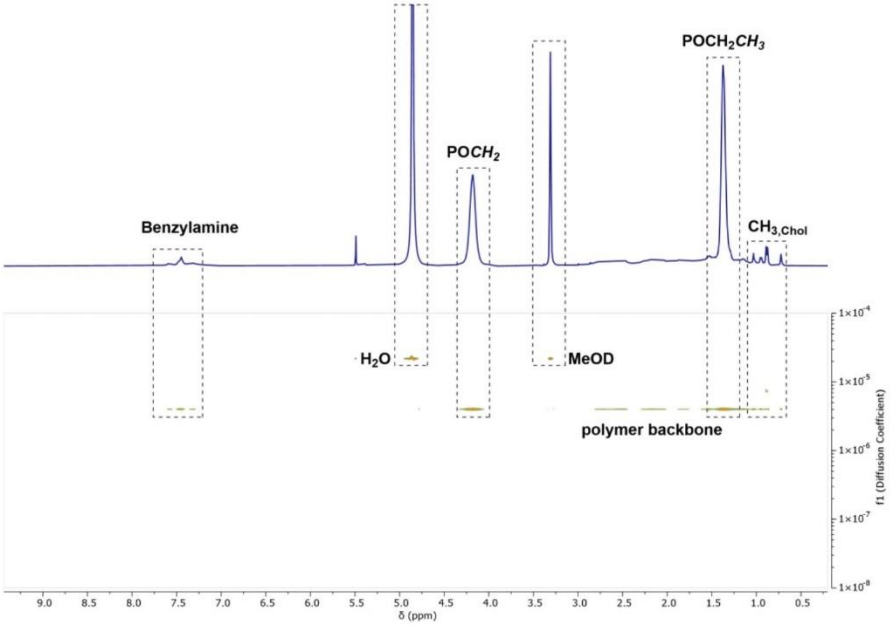

Fig. S33 DOSY spectrum of **P9** in MeOD.

Follow-up Functionalization of P8 with Thiocholesterol (5) via Thiol-Ene Click Chemistry

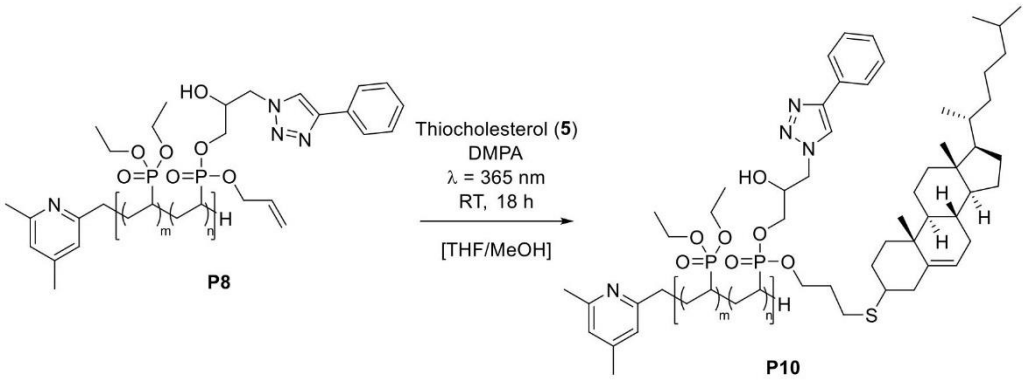

Polymer **P8** (100 mg per 10 mL solvent) was dissolved in a mixture of THF/water (5/1). This solution was treated with thiocholesterol (**5**) (4.0 equiv. per remaining allyl group) and catalytic amounts of the photoinitiator 2,2-dimethoxy-2-phenylacetophenone. The reaction mixture was degassed (drawing vacuum and refilling with argon; 15 iterations) and irradiated at λ = 365 nm for 18 hours at room temperature. The consumption of the allyl groups was monitored by ^{1}H-NMR spectroscopy. Volatiles were then removed *in vacuo* and the crude polymer was washed several times with pentane to remove excess thiocholesterol, when the quantitative conversion of the allyl groups was observed by NMR. Hereafter, the conjugate was purified by dialysis against water and lyophilized to yield substrate **P10**.

^{1}H-NMR (400 MHz, MeOD, 300 K): δ (ppm) = 8.16 – 6.89 (m, Phenyl, 65H), 4.18 (s, POC*H*$_2$, 484H), 2.96 – 1.11 (m, polymer backbone), 1.38 (s, POCH$_2$*CH*$_3$), 0.95 (d, ^{3}J = 6.4 Hz, CH$_{3,Chol}$), 0.88 (d, ^{3}J = 6.5 Hz, 2 x CH$_{3,Chol}$), 0.72 (s, C*H*$_{3,Chol}$, 11H).

^{31}P-NMR (203 MHz, MeOD, 300 K): δ (ppm) = 33.2.

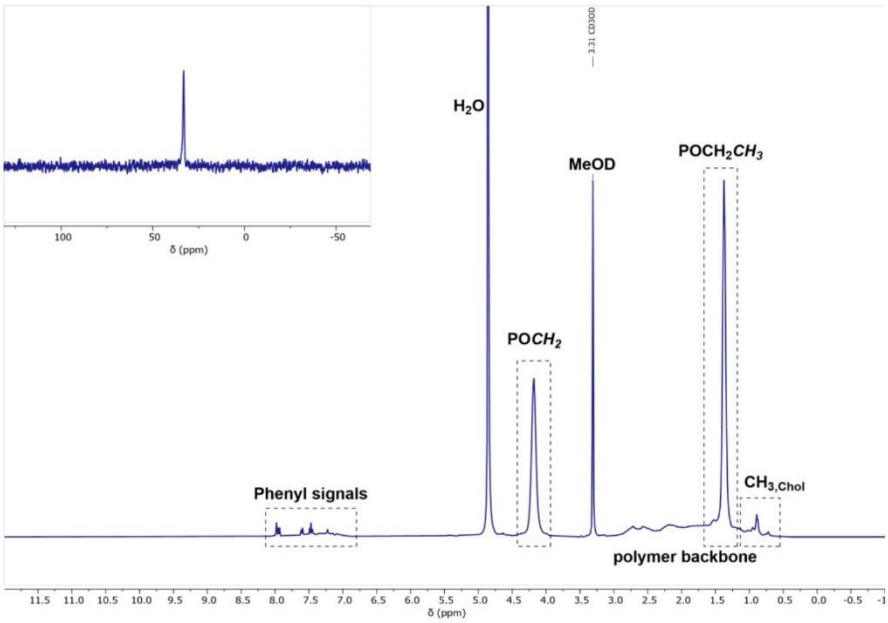

Fig. S34 ^{1}H- and zoom of ^{31}P-NMR spectrum of polymer **P10** in MeOD.

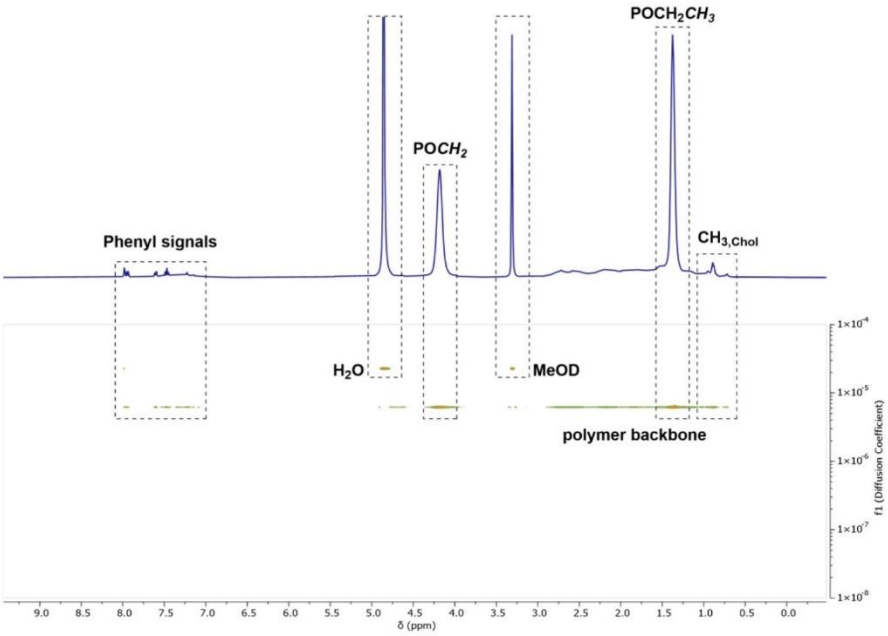

Fig. S35 DOSY spectrum of **P10** in MeOD.

5 Introduction of Hydrazone Linkages in P(DEVP-*co*-DAlVP) P1

Thiol-Ene Coupling of Methyl Thioglycolate (6) with P(DEVP-*co*-DAlVP) P1

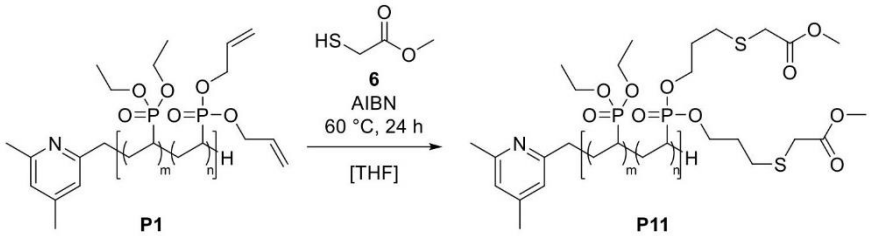

Polyvinylphosphonate **P1** (500 mg, 25.0 µmol) was dissolved in THF (30 mL) in a pressurizable schlenk flask. Methyl thioglycolate (**6**) (236 µL, 2.64 mmol, 5.00 equiv. per allyl group) and catalytic amounts of azobisisobutyronitrile were added and the solution was degassed via repeated evacuation and filling with argon (20 iterations). The mixture was heated to 60 °C and stirred for 24 hours at this temperature. After this time period ^{1}H-HMR spectroscopy confirmed the quantitative conversion of the allyl groups. The solvent was removed *in vacuo*, the residue was dissolved in deionized water, and the aqueous solution was purified by dialysis against deionized water. After replacing the dialysate after two and four hours, the mixture was dialysed against water for additional 20 hours and the polymer-containing solution was freeze-dried to yield **P11** as a colourless solid.

^{1}H-NMR (400 MHz, MeOD, 300 K): δ (ppm) = 4.18 (br s, PO*CH$_2$*), 3.71 (s, methyl ester), 2.82 (s, SCH$_2$(C=O), CH$_2$S), 2.96 – 1.07 (m, polymer backbone), 2.04 (s,), 1.38 (br s, POCH$_2$*CH$_3$*).

^{13}C-NMR (126 MHz, MeOD, 300 K): δ (ppm) = 172.6 (s, C=O), 65.9 (s, POCH$_2$), 63.5 (s, POCH$_2$), 52.8 (s, OCH$_3$), 33.8 (s, CH$_2$), 34.4 – 28.5 (m, polymer backbone), 31.1 (s, CH$_2$), 29.6 (s, CH$_2$), 17.2 (s, POCH$_2$*CH$_3$*).

^{31}P-NMR (203 MHz, MeOD, 300 K): δ (ppm) = 33.2.

IR (ATR): $\tilde{\upsilon}$ (cm^{-1}) = 3472 (br w), 2980 (m, ν_{C-H}), 2930 (m, ν_{C-H}), 2909 (m, ν_{C-H}), 1736 (m, $\nu_{C=O}$), 1477 (w, δ_{C-H}), 1443 (m, δ_{C-H}), 1392 (m, δ_{C-H}), 1368 (w, δ_{C-H}), 1219 (st, $\nu_{P=O}$), 1162 (m, ν_{C-O}), 1097 (w), 1043 (w, ν_{P-O}), 1015 (st, ν_{P-O}), 952 (st), 781 (st).

EA:

calculated*:	C 43.24	H 7.75	N 0.06	S 2.53
found:	C 43.34	H 7.82	N 0.12	S 2.47

*with 1.5 wt-% residual water after freeze-drying

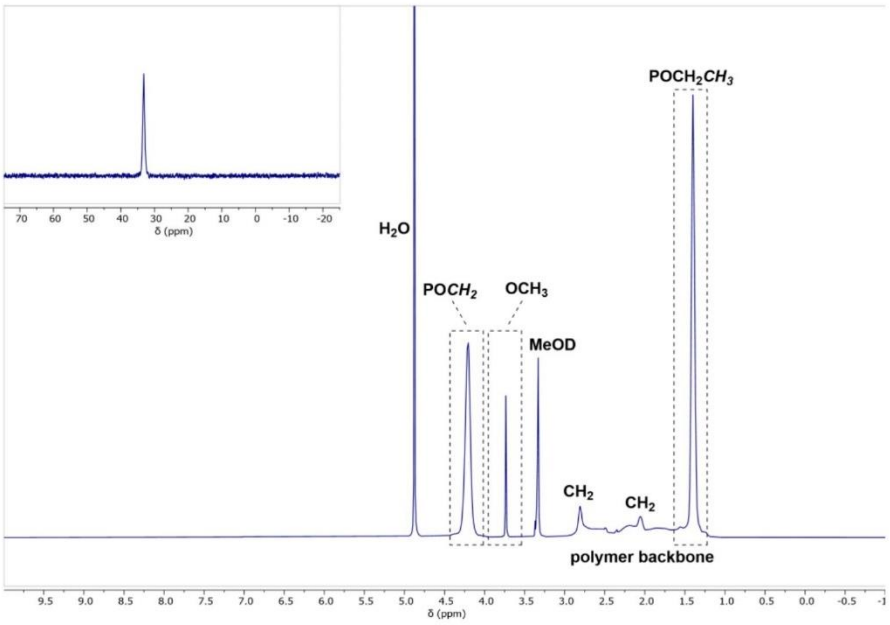

Fig. S36 ^{1}H- and zoom of ^{31}P-NMR spectrum of polymer **P11** in MeOD.

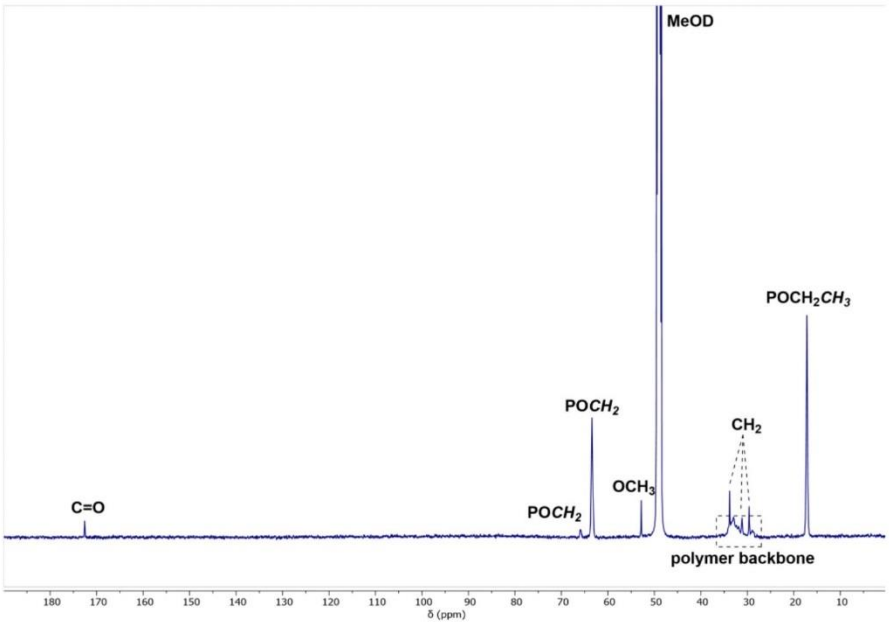

Fig. S37 ^{13}C-NMR spectrum of polymer **P11** in MeOD.

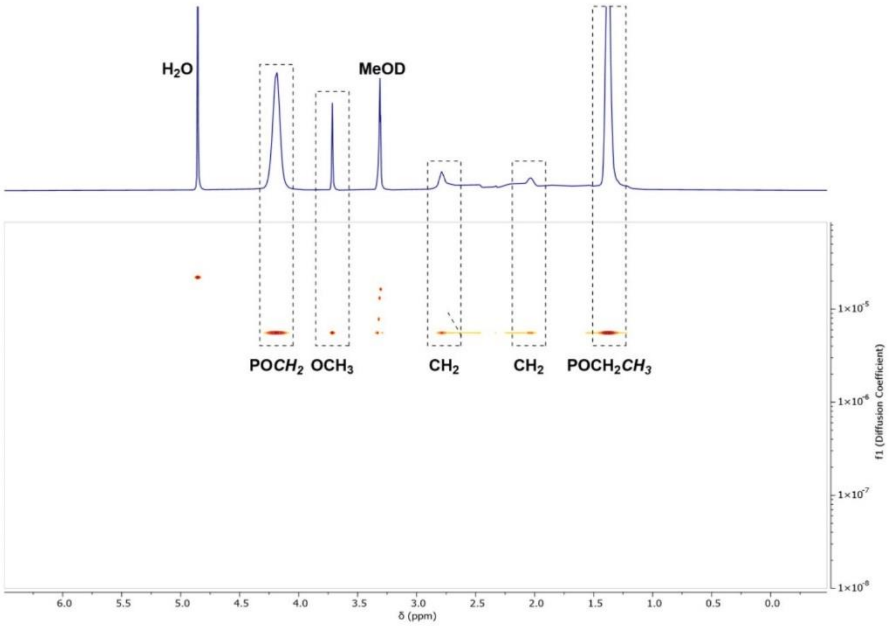

Fig. S38 DOSY-NMR of polymer **P11** in MeOD.

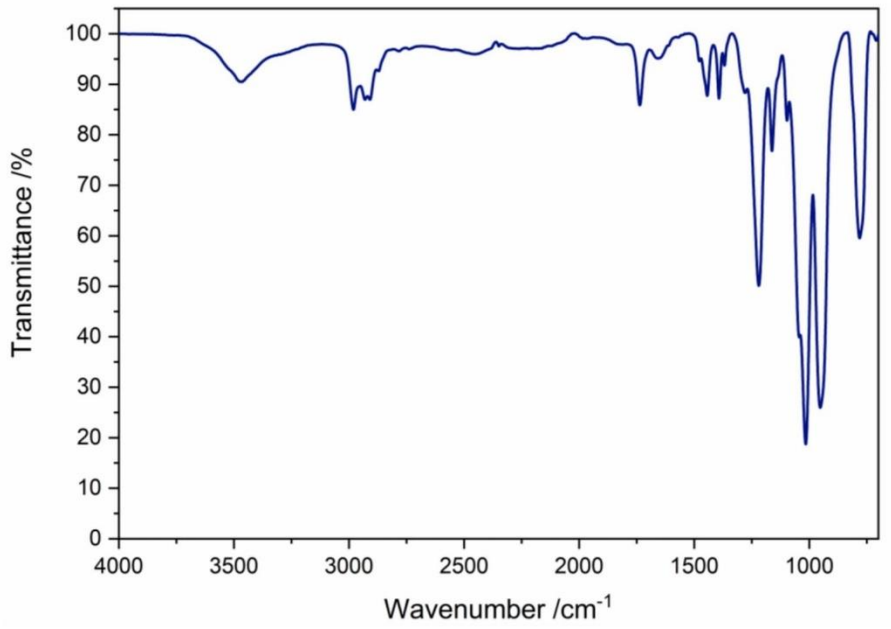

Fig. S39 IR spectrum of polymer **P11**.

Formation of Hydrazide P12

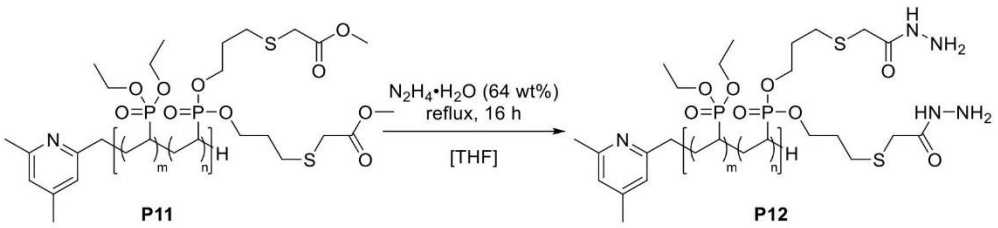

Under an argon atmosphere 300 mg of the thiol-ene adduct **P11** (13.5 µmol) were dissolved in absolute THF (30 mL) and treated with hydrazine-hydrate (700 µL, 14.3 mmol, 50.0 equiv. per ester). The mixture was refluxed for 24 hours and the quantitative conversion of the ester was confirmed by ^{1}H-NMR spectroscopy. Hereafter, the volatiles were removed *in vacuo* using an external cooling trap. Excess hydrazine was rendered harmless by addition of diluted hydrogen peroxide. The polymeric residue was dissolved in deionized water and purified by dialysis for 24 hours. The polymer-containing solution was lyophilized to yield hydrazide **P12** as a colourless solid.

^{1}H-NMR (400 MHz, MeOD, 300 K): δ (ppm) = 4.18 (br s, POCH_2), 3.20 (s, SCH_2(C=O)), 2.76 (s, CH_2S), 2.96 – 1.16 (m, polymer backbone), 1.99 (s, CH_2), 1.38 (br s, POCH$_2CH_3$).

^{13}C-NMR (126 MHz, MeOD, 300 K): δ (ppm) = 171.6 (s, C=O), 66.1 (s, POCH_2), 63.5 (s, POCH_2), 34.1 (s, CH_2), 31.6 (s, CH_2), 35.0 – 28.2 (m, polymer backbone), 29.6 (s, CH_2), 17.2 (s, POCH$_2CH_3$).

^{31}P-NMR (203 MHz, MeOD, 300 K): δ (ppm) = 33.2.

IR (ATR): $\tilde{\upsilon}$ (cm^{-1}) = 3411 (br m), 2981 (m, ν_{C-H}), 2930 (m, ν_{C-H}), 2910 (m, ν_{C-H}), 1660 (m, $\nu_{C=O}$), 1478 (w, δ_{C-H}), 1444 (m, δ_{C-H}), 1392 (m, δ_{C-H}), 1368 (w, δ_{C-H}), 1212 (st, $\nu_{P=O}$), 1162 (m, ν_{C-O}), 1096 (w), 1041 (w, ν_{P-O}), 1014 (st, ν_{P-O}), 954 (st), 783 (st).

EA:

calculated*:	C 42.25	H 7.86	N 2.27	S 2.53
found	C 41.74	H 7.79	N 2.04	S 2.42

*with 3.0 wt-% residual water after freeze-drying

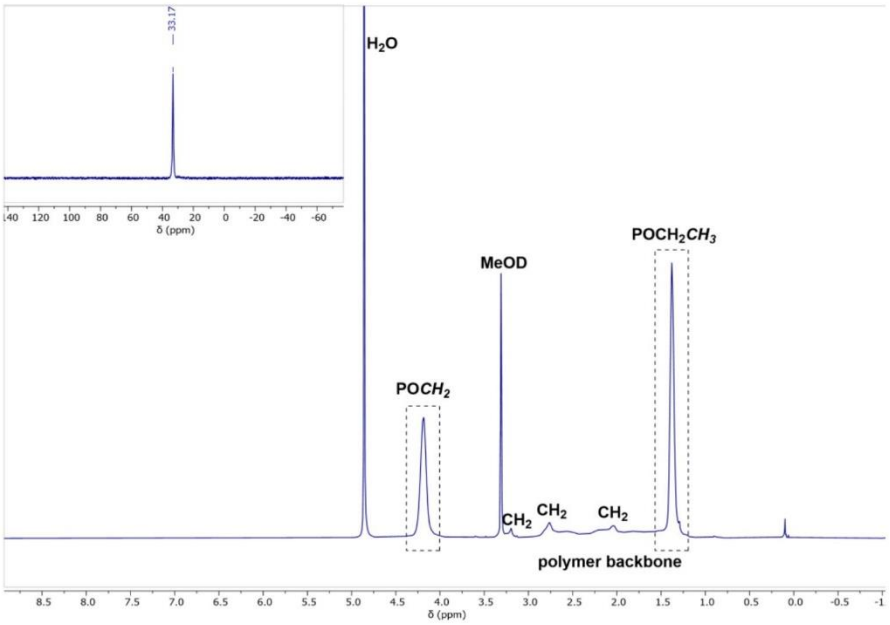

Fig. S40 ^{1}H- and zoom of ^{31}P-NMR spectrum of polymer **P12** in MeOD.

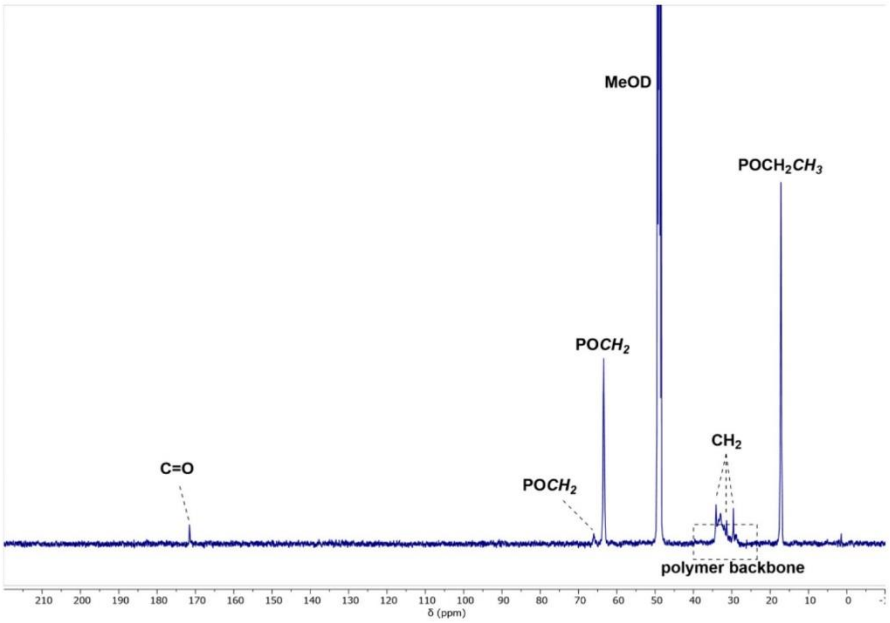

Fig. S41 ^{13}C-NMR spectrum of polymer **P12** in MeOD.

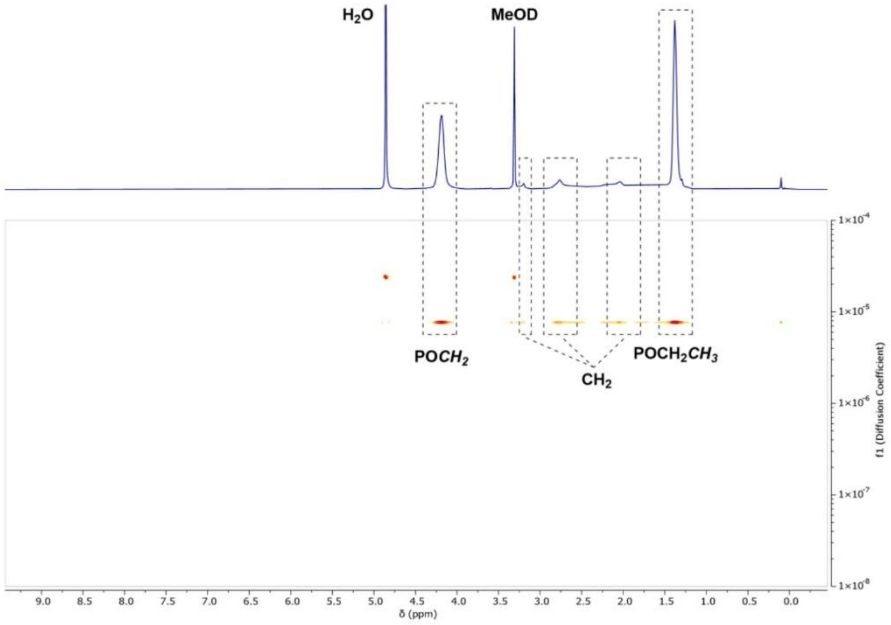

Fig. S42 DOSY-NMR of polymer **P12** in MeOD.

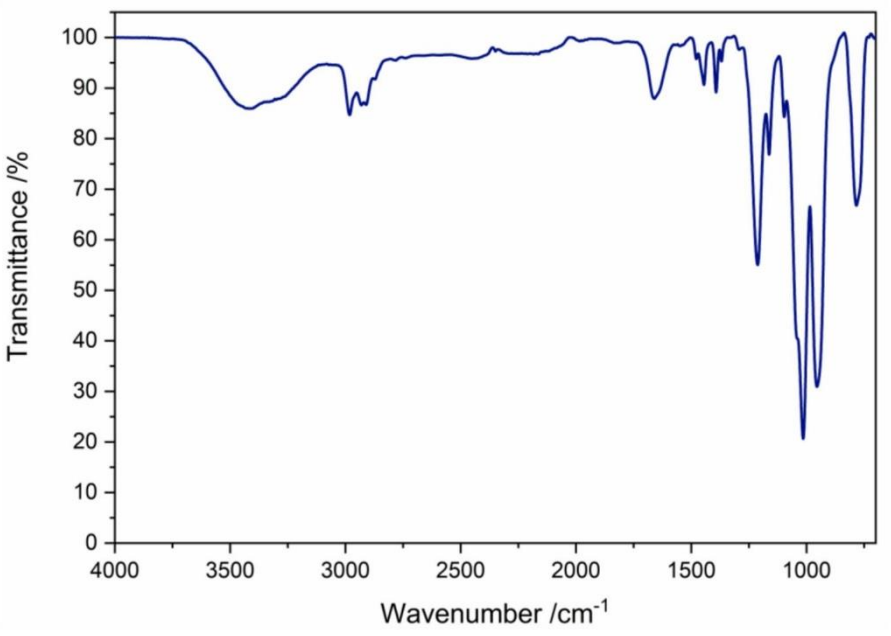

Fig. S43 IR spectrum of polymer **P12**.

Formation of Hydrazone P13

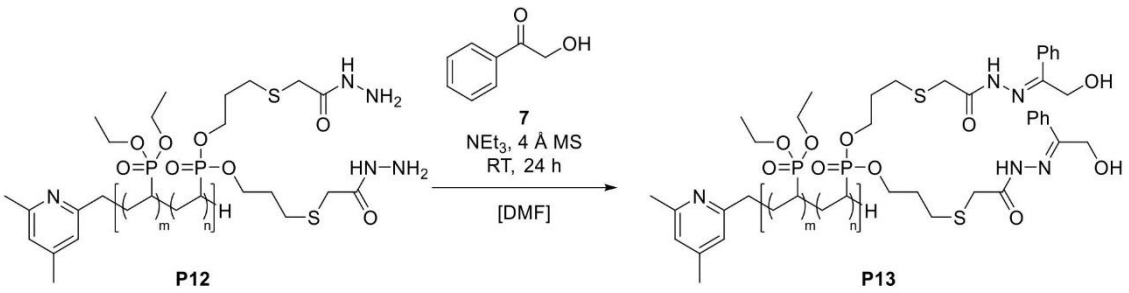

Under an argon atmosphere hydrazide **P12** (150 mg, 6.74 µmol) was dissolved in anhydrous DMF (6.0 mL) and treated with triethylamine (50 µL, 142 µmol, 2.50 equiv. per hydrazide motif) and 2-hydroxyacetophenone (**7**) (48.2 mg, 142 µmol, 2.50 equiv. per hydrazide motif). In the presence of molecular sieves (4 Å) the solution was stirred at room temperature. The progress of the reaction was monitored by ^{1}H-NMR spectroscopy and the reaction was stopped after 24 hours. Remains of the molecular sieves were filtrated off, volatiles were removed in high vacuum, and the yellowish residue was dissolved in deionized water. The hydrazone adduct was purified by dialysis against deionized water for 24 hours. Lyophilization of the aqueous polymer solution yielded compound **P13** as a yellow solid.

^{1}H-NMR (400 MHz, MeOD, 300 K): δ (ppm) = 8.55 (s, $NH_{Hydrazone}$), 8.28 – 6.84 (m, Ph), 4.18 (s, $POCH_2$), 3.99 (s, CH_2OH), 3.19 (s, CH_2), 2.76 (s, CH_2), 2.04 (s, CH_2), 2.94 – 1.06 (m, polymer backbone), 1.37 (s, $POCH_2CH_3$).

^{13}C-NMR (126 MHz, MeOD, 300 K) δ (ppm) = 169.9 (s, C=O), 157.9 (s, C=N), 134.4 (s, C_{Ar}), 133.3 (s, C_{Ar}), 129.9 (s, C_{Ar}), 128.7 (s, C_{Ar}), 65.8 (weak s, PO*CH_2*), 63.5 (s, PO*CH_2*), 33.1 (s, CH_2), 30.8 (s, CH_2), 35.6 – 27.8 (m, polymer backbone), 23.7 (s, CH_2), 17.2 (s, $POCH_2$*CH_3*).

^{31}P-NMR (203 MHz, MeOD, 300 K): δ (ppm) = 33.2.

IR (ATR): $\tilde{\upsilon}$ (cm^{-1}) = 3407 (br m), 2980 (m, ν_{C-H}), 2927 (m, ν_{C-H}), 1680 (m, $\nu_{C=N}$), 1595 (m, $\nu_{C=O}$), 1478 (w, δ_{C-H}), 1444 (m, δ_{C-H}), 1391 (m, δ_{C-H}), 1368 (w, δ_{C-H}), 1215 (st, $\nu_{P=O}$), 1162 (m, ν_{C-O}), 1096 (w), 1043 (w, ν_{P-O}), 1018 (st, ν_{P-O}), 957 (st), 783 (st).

UV/Vis (MeOH): λ_{max} [nm] ($\varepsilon \times 10^3$ [L mol^{-1} cm^{-1}]) = 300 (5.2).

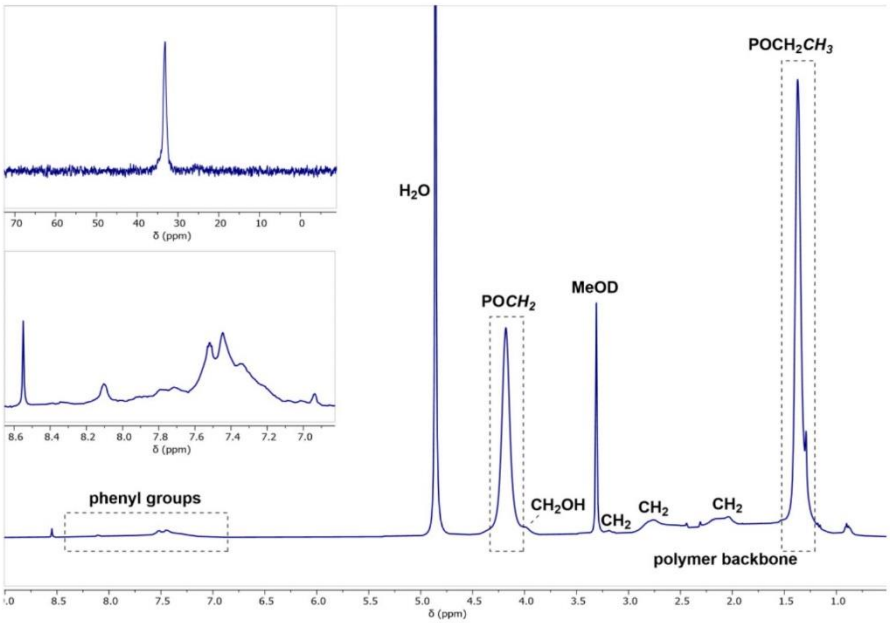

Fig. S44 ^{1}H-NMR, zoom of the aromatic region and ^{31}P-NMR spectrum of polymer **P13** in MeOD.

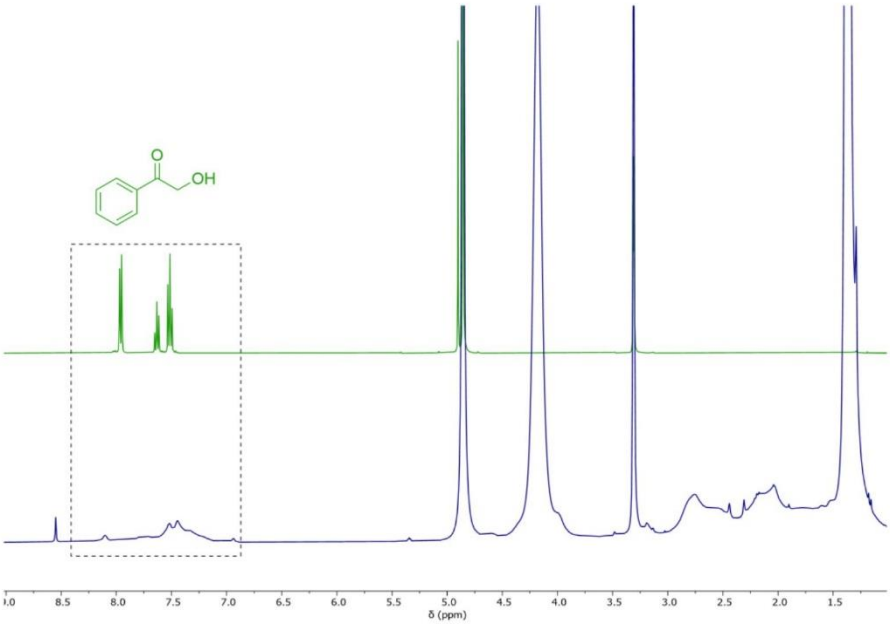

Fig. S45 NMR comparison of 2-hydroxyacetophenon (**7**) and polymer **P13** in MeOD.

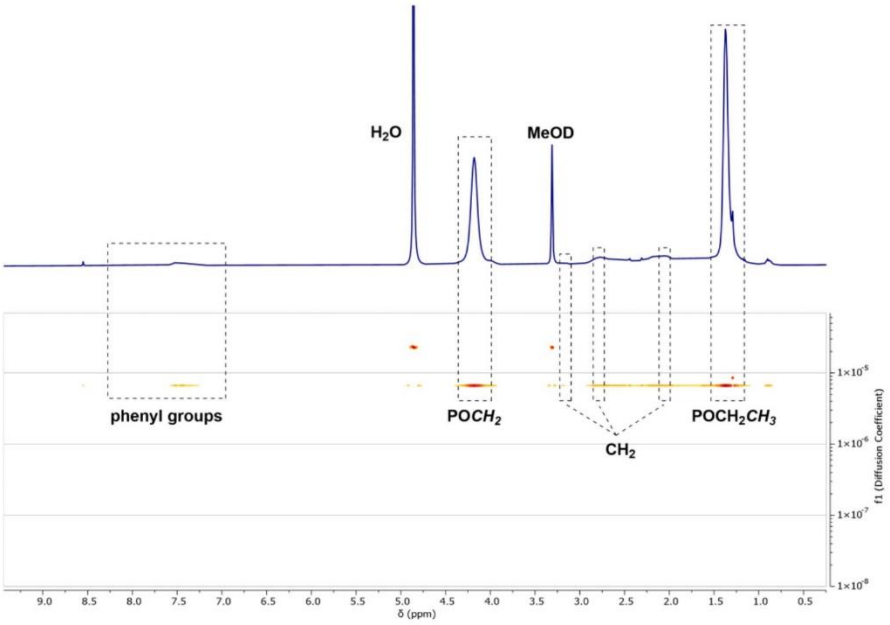

Fig. S46 DOSY-NMR of polymer **P13** in MeOD.

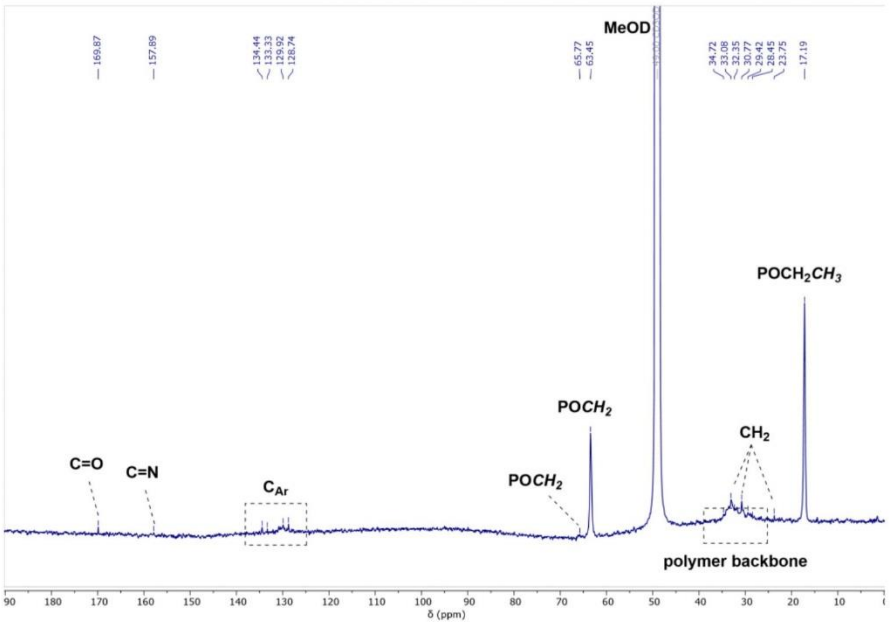

Fig. S47 ^{13}C-NMR of polymer **P13** in MeOD.

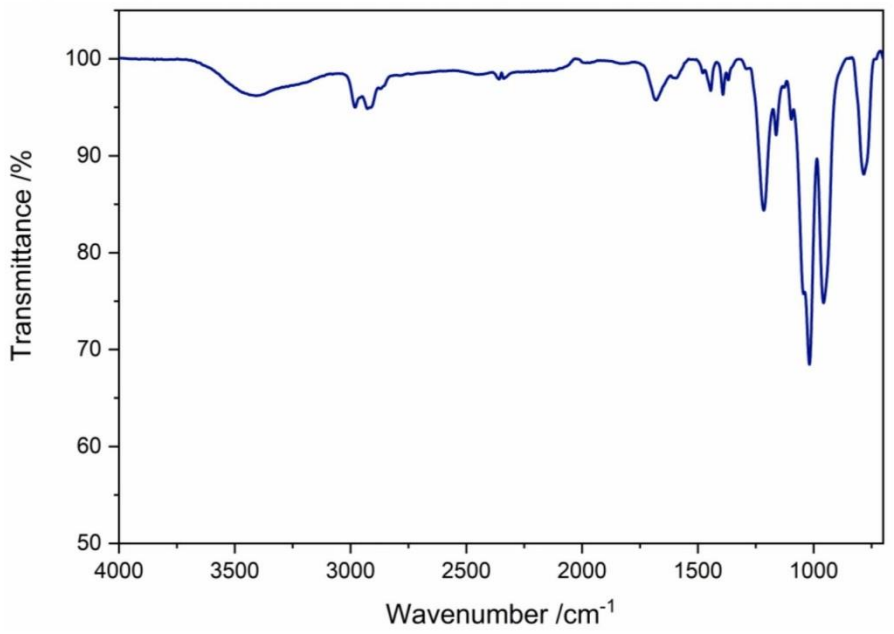

Fig. S48 IR spectrum of polymer **P13**.

11.4.3 Supporting Information Chapter 6

Cytocompatible Triblock Copolymers with Controlled Microstructure enabling Orthogonally Functionalized Bio-Polymer-Conjugates

Kerstin Halama[a], Molly Tzu-Yu Lin[b], Andreas Schaffer[a], Marvin Foith[a], Friederike Adams[b,c], Bernhard Rieger[a]*

[a] WACKER-Chair of Macromolecular Chemistry, Catalysis Research Center, Department of Chemistry, Technical University of Munich, Lichtenbergstr. 4, 85748 Garching (Germany)

[b] Institute for Ophthalmic Research, University of Tübingen,Elfriede-Aulhorn-Strasse 7,72076 Tübingen, Germany

[c] Chair of Macromolecular Materials and Fiber Chemistry, Institute of Polymer Chemistry, University of Stuttgart, Pfaffenwaldring 55, 70569 Stuttgart, Germany

TABLE OF CONTENTS

1. GENERAL EXPERIMENTAL

All reactions and polymerizations with moisture and air-sensitive reactants were carried out in an M*Braun* LabMaster120 glovebox filled with argon 4.6 from *Westfalen* or using standard *Schlenk* techniques. All glassware was heat-dried before use. All chemicals were purchased from *Sigma-Aldrich*, ABCR, or TCI Europe and used without further purification unless otherwise stated. Dichloromethane, tetrahydrofuran, toluene, and pentane were dried using an M*Braun* SPS-800 solvent purification system and stored over a 3 Å molecular sieve. Diethyl vinyl phosphonate and diallyl vinyl phosphonate were dried over CaH_2 for several days and distilled before use. $Y(CH_2TMS)_3(thf)$[1], the precursor catalyst $Cp_2Y(CH_2TMS)(thf)$[2], diallyl vinyl phosphonate[3], dichloro vinyl phosphonate[4], (3-(trimethylsilyl)propargyl alcohol[5], thiocholesterol[6] and azido-functionalized folate[7] were prepared according to literature procedures.

Cell Viability Assay was used for evaluating the biocompatibility of polymers with spontaneously immortalized human *Müller* cell line (MIO-M1). The polymers were prepared at a stock concentration of 1.5 mg/mL in distilled water and vortex until dissolved before use. MIO-M1 (P41) was seeded in a transparent 96-well plate at the density of 10,000 cells in pre-warmed high glucose (4.5 g/L) DMEM medium (Gibco; Thermo*Fisher* Scientific, Taufkirchen, Germany) supplemented with 10% fetal bovine serum and 1% penicillin/streptomycin (Thermo*Fisher* Scientific, Karlsruhe, Germany). After 24 hours, the medium was aspirated, and each well was treated with 100 µL of different concentrations of polymers (5, 15, 25, 50, 100, 150, 200, 250, and 500 µg/mL) prepared in the medium. Following 24 hours of treatment at 37°C and 5% CO_2, an MTS assay was carried out to evaluate the metabolic activity of the treated cells by adding 20 µL of the CellTiter 96 ® Aqueous One Solution Reagent (Promega Corporation, Madison, WI, USA) directly to each well and incubated at 37°C for 90 minutes. Subsequently, the absorbance was

measured at 490 nm with a reference wavelength set at 690 nm for background correction using a a Tecan Reader (NanoQuant infinite M200). All data is shown as mean ± SD from five replicates after normalizing to the untreated control wells representing 100% cell viability.

Dynamic light scattering (DLS) was performed at a Zetasizer Nano ZS (*Malvern*). The diameter was averaged over three independent values consisting each of 10 measurements. The samples were dissolved in water at a concentration of 2.5 mg/mL.

Elemental analysis (EA) was performed by the Laboratory of Microanalytics at the Institute of Inorganic Chemistry at the Technical University of Munich, Department of Chemistry, Catalysis Research Center.

Electrospray Ionization Mass Spectrometry (ESI-MS) was measured using a Thermo *Fisher* Scientific Exactive Plus Orbitrap in a positive mode in HPLC methanol straight from the reaction mixture without quenching.

Fluorescence spectroscopy was performed on a Jasco (Jasco FP-8300, Spectra Manager software 2.13). The concentration of polymers in methanol was determined to be 1.0 mg/mL. Corresponding substrates were prepared in 0.5 mM solutions. Fluorescence spectroscopy was performed on a Jasco (Jasco FP-8300, Spectra Manager software 2.13).

Lyophilization was performed on a VaCO 5-II-D at a pressure of 1 mbar and -90 °C condenser temperature from either 1,4-dioxane or water.

Nuclear magnetic resonance (NMR) spectra were recorded on a Bruker AV-400HD, AV-500HD, or AV-II-500 spectrometer at 400 or 500 MHz (^{1}H), 125 MHz (^{13}C), 203 MHz (^{31}P) and 99 MHz (^{29}Si). NMR spectroscopical shifts δ were reported in ppm relative to the deuterated

solvent's residual proton or carbon signal. Deuterated solvents ($CDCl_3$, benzene-d_6, MeOD, DMSO-d_6) were purchased from Sigma-Aldrich or Deutero and dried over 3 Å molecular sieves before use. DOSY-NMR measurements were performed for the characterization of polymer conjugates.

Size-exclusion chromatography multi-angle light scattering (SEC-MALS) was used to determine molecular weights and polydispersity of the polymers (c = 2.5 mg/mL) with a Wyatt Dawn Heleos II MALS light scattering unit and a Wyatt Optilab rEX 536 RI unit in THF: H_2O = 1:1 (with 9 g/L *tetra-n*-butyl-ammonium bromide and 272 mg/L 2,6-di-*tert*-butyl-4-methylphenol added) as eluent at 40 °C on two Agilent PolarGel-M columns; for absolute molecular weight (triple detection) determination of the polyvinyl phosphonates the refractive index increment dn/dc = 0.0922 mL/g[8] was used.

UV/vis spectroscopy (UV/vis) was measured on a Varian Cary 50 Scan UV visible spectrophotometer. Spectra were measured from 200 nm to 800 nm at 25 °C. The samples were dissolved in methanol and analyzed in a QS 10×10 mm quartz glass cuvette from *Hellma* GmbH & Co. KG. A baseline correction with the pure solvent was performed before sample measurements.

2. SYNTHESIS PROCEDURES

DI (3-(TRIMETHYLSILYL)PROP-2-YN-1-YL) VINYL PHOSPHONATE (DPRTMSVP)

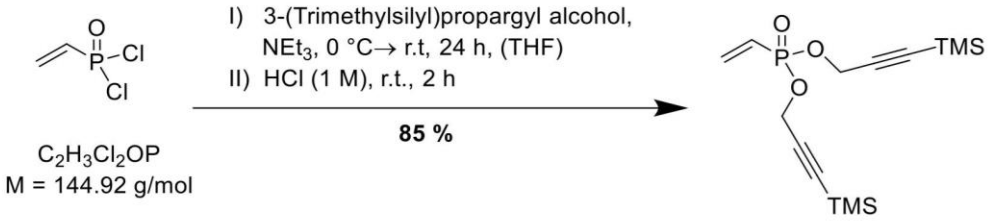

$C_2H_3Cl_2OP$
M = 144.92 g/mol

$C_{14}H_{25}O_3PSi_2$
M = 328.49 g/mol

5.15 mL (7.25 g, 50.0 mmol, 1.0 eq.) vinyl phosphonic dichloride and 16.3 mL (14.1 g, 110 mmol, 2.2 eq.) were dissolved in 250 mL of THF in a *Schlenk* flask. Under vigorous stirring, 27.8 mL (20.2 g, 200 mmol, 4.0 eq.) triethyl amine was added at 0 °C. After stirring the solution overnight at room temperature, the reaction course was monitored via ^{31}P NMR spectroscopy. With complete conversion, the reaction is then quenched with 50 mL of water. The solution was filtered and washed with water (2 × 100 mL). The aqueous phase was extracted with ethyl acetate (2 × 200 mL). The combined organic phases were dried over sodium sulfate before the solvent was removed in vacuo. Purification via sublimation with dry iced cooling (75.0 °C, p= 5.0×10^{-6} mbar) yielded 14.0 g (42.5 mmol, 85%) di (3-(trimethylsilyl) prop-2-yn-1-yl)vinyl phosphonate as light yellow oil.

^{1}H-NMR (500 MHz, $CDCl_3$, 300K): δ (ppm) = 6.37 – 5.90 (m, 3H, CH_{Vinyl}), 4.36 (q, 4H, CH_2), 0.12 (s, 18H, $Si(CH_3)_3$).

^{13}C-NMR (126 MHz, $CDCl_3$, 300K): δ (ppm) = 136.4 (s, C_{Vinyl}), 125.1 (d, J_{PC}= 185.6 Hz, PC_{Vinyl}), 99.2 (s, C), 92.9 (s, Si-C), 54.4 (s, CH_2), -0.4 (s, CH_3).

^{31}P-NMR (203 MHz, $CDCl_3$, 300K): δ (ppm) = 19.5.

^{29}Si-NMR (99 MHz, $CDCl_3$, 300K): δ (ppm) = -17.1.

ESI-MS: calculated: 329.11 $[M–H]^+$, found: 329.11 $[M–H]^+$.

EA: calculated: C 51.19%, H 7.67%, P 9.43%.

found: C 51.20%, H 7.74%, P 9.42%.

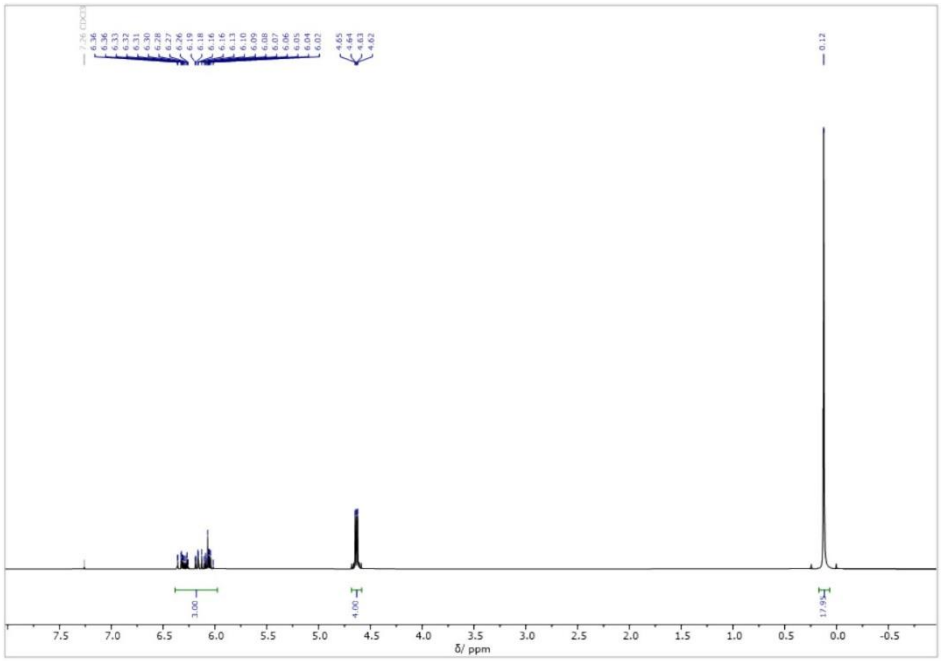

Figure S1: ^{1}H-NMR (500 MHz, $CDCl_3$, 300 K) of di (3-(trimethylsilyl)prop-2-yn-1-yl) vinyl phosphonate (DPrTMSVP).

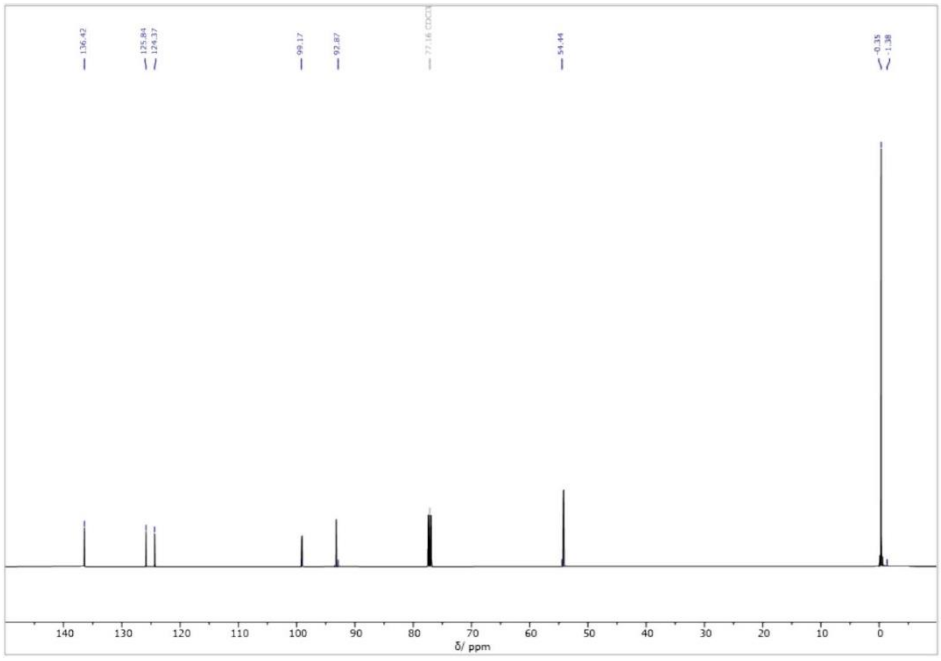

Figure S2: ^{13}C-NMR (126 MHz, $CDCl_3$, 300 K) of di (3-(trimethylsilyl)prop-2-yn-1-yl) vinyl phosphonate (DPrTMSVP).

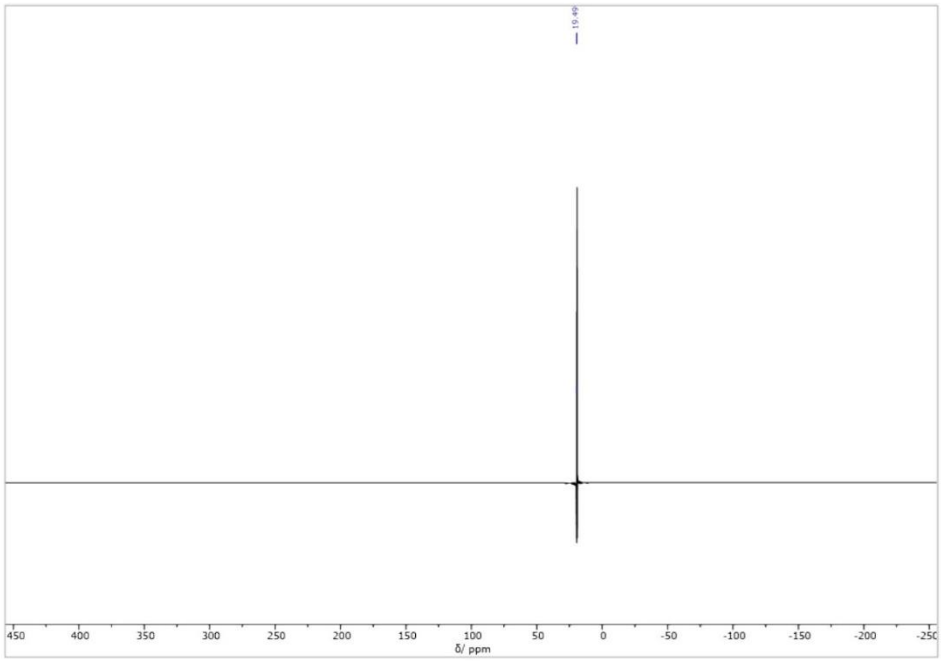

Figure S3: ^{31}P-NMR (203 MHz, $CDCl_3$, 300 K) of di (3-(trimethylsilyl)prop-2-yn-1-yl) vinyl phosphonate (DPrTMSVP).

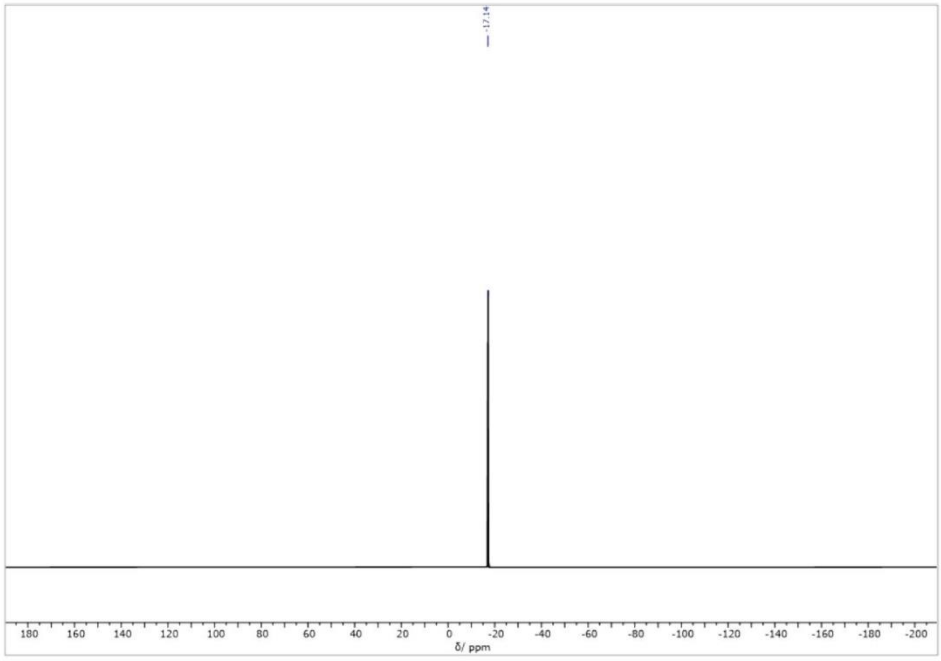

Figure S4: ^{29}Si-NMR (99 MHz, $CDCl_3$, 300 K) of di (3-(trimethylsilyl)prop-2-yn-1-yl) vinyl phosphonate (DPrTMSVP).

3. POLYMERIZATION PROCEDURE

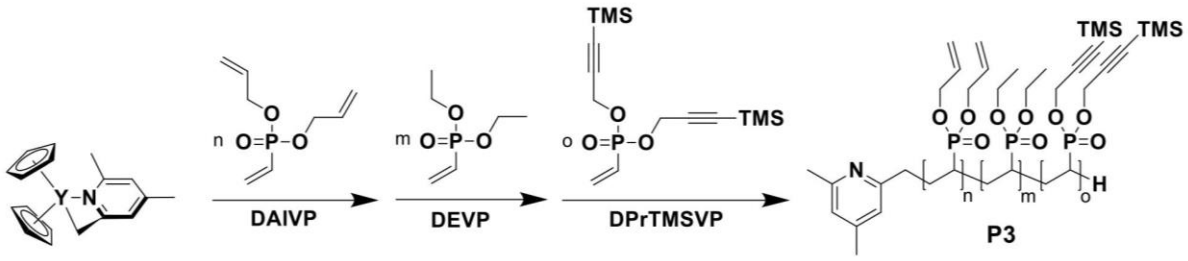

For the C–H bond activation, 75.7 mg (200 µmol, 1.0 eq.) $Cp_2Y(CH_2TMS)(thf)$ was dissolved in 5.0 mL absolute toluene, and 24.3 mg (200 µmol, 1.0 eq.) *sym*-collidin was added to the solution. The *in-situ* activation of the catalyst is performed at room temperature for two hours. For the polymerization, firstly, 188 mg (1.00 mmol, 5.0 eq.) diallyl vinyl phosphonate was added, and an aliquot of PDAlVP **P1** (0.50 mL) was withdrawn after one minute. Secondly, 10.5 mL absolute toluene was refilled after three minutes, and 2.30 g (14.0 mmol, 80 eq.) diethyl vinyl phosphonate was added. 1.00 mL of the reaction solution is used for an aliquot of P(DAlVP-*co*-DEVP) **P2**. For the final polymerization step, 294 mg (825 µmol, 5.0 eq) di (3-(trimethylsilyl)prop-2-yn-1-yl) vinyl phosphonate was used. The polymerization was performed at room temperature overnight before an aliquot of P(DAlVP-DEVP-DPrTMSVP) **P3** is withdrawn, and the reaction was quenched by adding wet methanol. The polymer participated from pentane, subject to centrifugation, and the supernatant was decanted. The residual polymer is dissolved in 1,4-dioxane before being freeze-dried. The purified polymer is analyzed using $^{1}H/^{31}P$/DOSY-NMR and SEC-MALS.

Polyvinyl phosphonate P3

^{1}H-NMR (400 MHz, $CDCl_3$, 300K): δ (ppm) = 6.88 – 6.60 (m, 2H, $H_{ar,sym\text{-Collidin}}$), 5.87 (s, 14H, $-OCH_2CHCH_2$), 5.33 – 5.04 (m, 28H, $-OCH_2CHCH_2$), 4.79 (s, 8H, $-CH_2C{\equiv}CSi(CH_3)_3$)), 4.49 (s, 28H, $-OCH_2CHCH_2$), 4.08 (s, 404H, $-OCH_2CH_3$), 2.87 – 0.96 (m, 936H, backbone, OCH_2CH_3), 0.13 (s, 36H, $-CH_2C{\equiv}CSi(CH_3)_3$).

^{31}P-NMR (203 MHz, $CDCl_3$, 300K): δ (ppm) = 33.2.

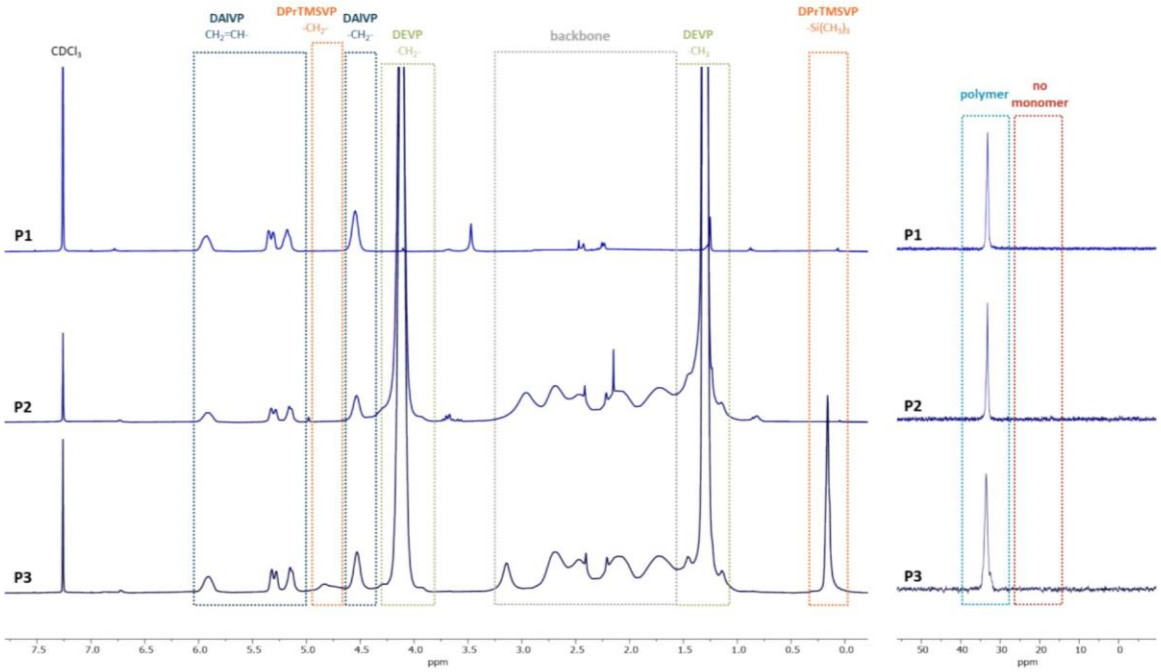

Figure S5: ^{1}H (400 MHz, $CDCl_3$, 300K) (right) and ^{31}P (203 MHz, $CDCl_3$, 300K) (left) of the polyvinyl phosphonates PDAlVP **P1**, P(DAlVP-*co*-DEVP) **P2** and P(DAlVP-DEVP-DPrTMSVP) **P3**.

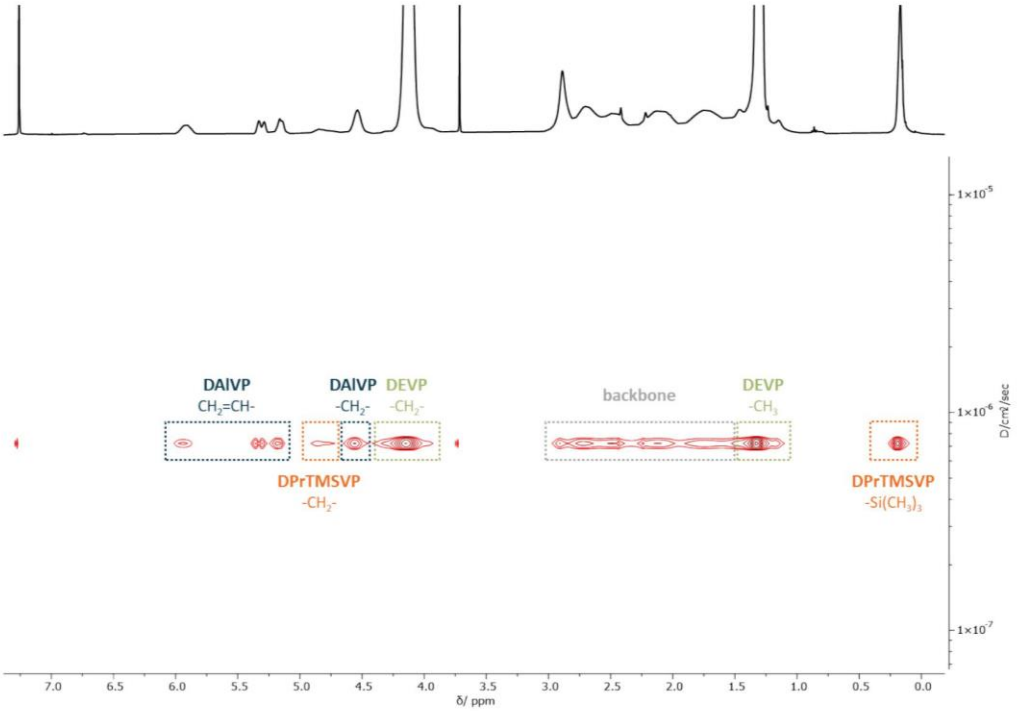

Figure S6: DOSY-NMR of and P(DAlVP-DEVP-DPrTMSVP) **P3.**

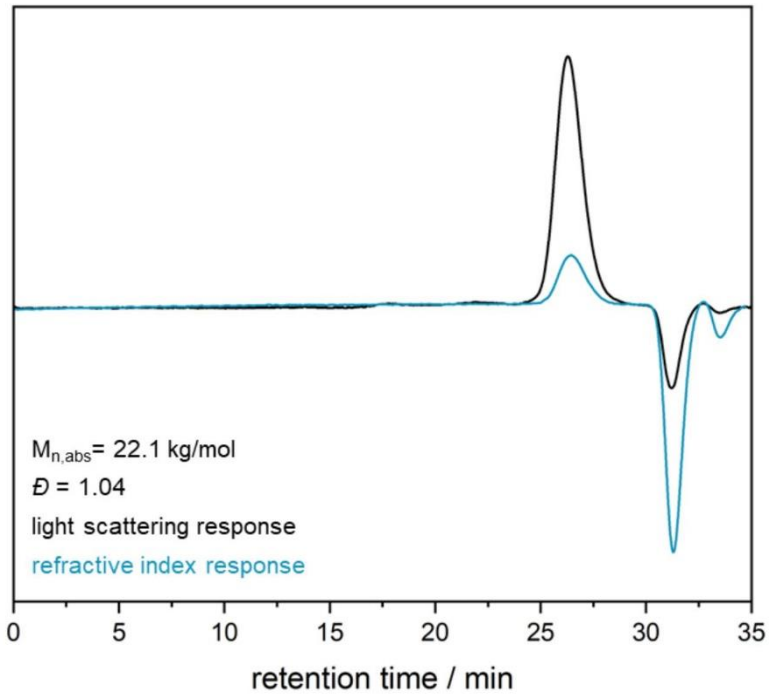

Figure S7: SEC-MALS of P(DAlVP-DEVP) **P2**.

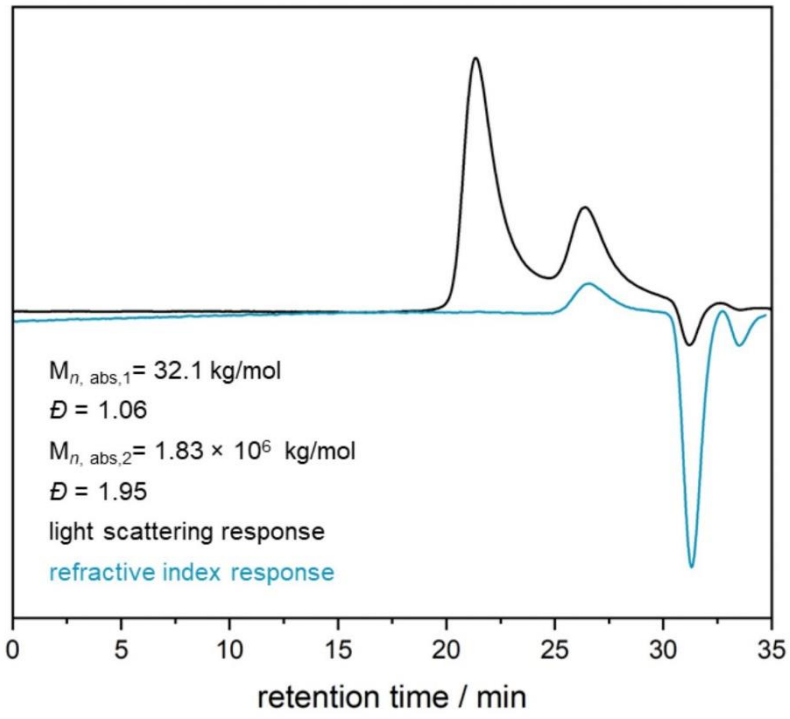

Figure S8: SEC-MALS of P(DAlVP-DEVP-DPrTMSVP) **P3**.

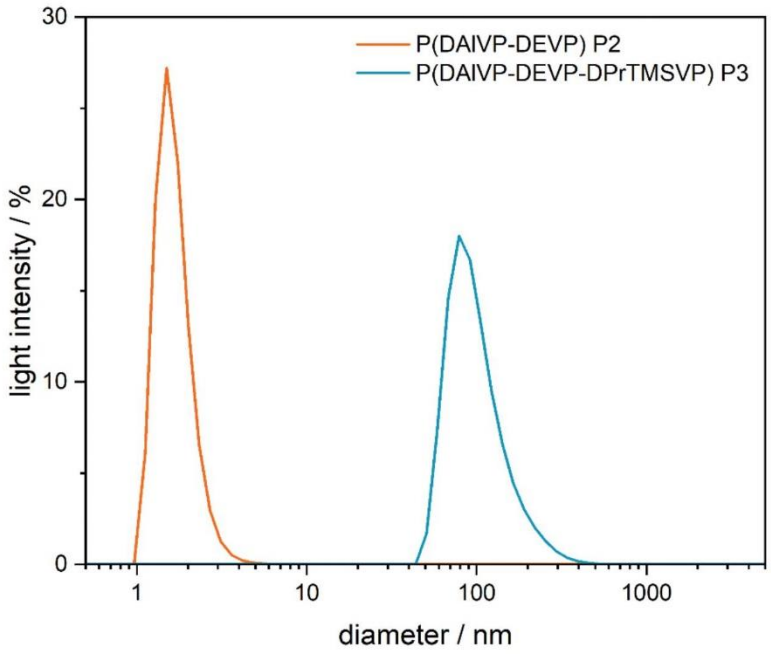

Figure S9: DLS spectra of **P2** (d = 26.5 ± 1.90 nm, PDI = 0.835) and **P3** (d = 128 ± 1.20 nm, PDI = 0.361).

4. POST-POLYMERISATION FUNKTIONALISATION

DEPRODECTION OF PROPARGYL GROUPS (DPRTMSVP)

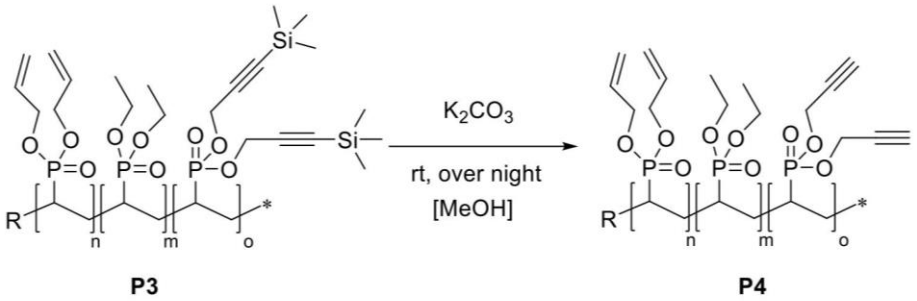

P3 **P4**

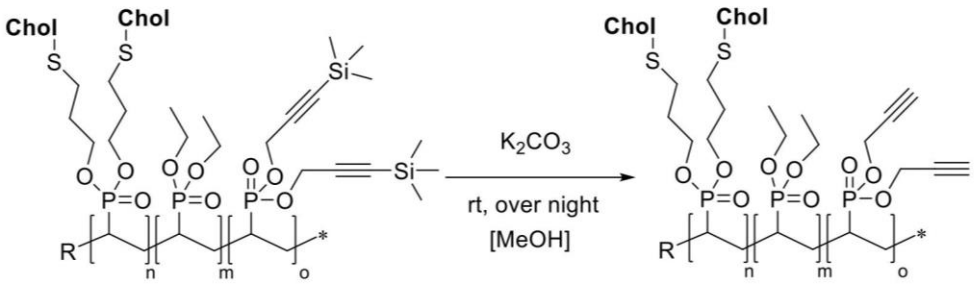

P8 **P9**

For deprotection of the propargyl groups, the polyvinyl phosphonates were dissolved in methanol (5.00 mL solvent per 100 mg polymer), and potassium carbonate (5.0 eq. per propargyl group) was added. The reaction solution was stirred overnight at room temperature before the volatiles were removed under reduced pressure. The residue was purified by dialysis against water and freeze-dried to yield the deprotected polymer.

Deprotection of P3 = P4

^{1}H-NMR (400 MHz, $CDCl_3$, 300K): δ (ppm) = 6.91 – 6.68 (m, $H_{ar,sym\text{-Collidin}}$), 5.92 (s, -$OCH_2CHCH_2$), 5.43 – 5.04 (m, -$OCH_2CHCH_2$), 4.55 (s, -$OCH_2CHCH_2$), 4.13 (s, -$OCH_2CH_3$), 2.87 – 0.96 (m, backbone, OCH_2CH_3,-$OCH_2C{\equiv}CH$).

^{31}P-NMR (203 MHz, $CDCl_3$, 300K): δ (ppm) = 33.2.

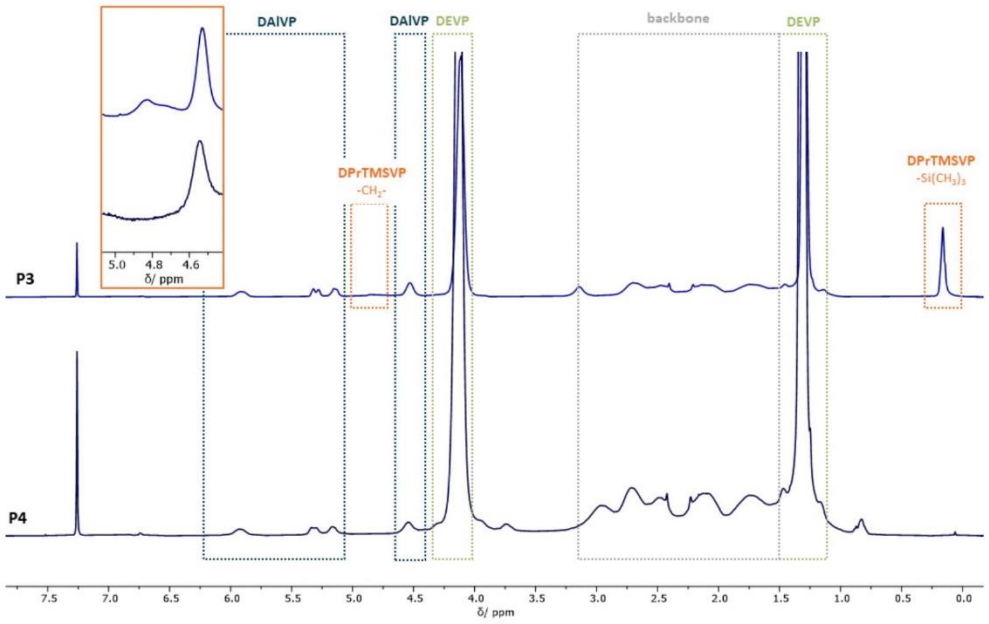

Figure S 10: ^{1}H-NMR (400 MHz, $CDCl_3$, 300K) of the polyvinyl phosphonates P(DAlVP-DEVP-DPrTMSVP) **P3** and P(DAlVP-DEVP-DPrVP) **P4.**

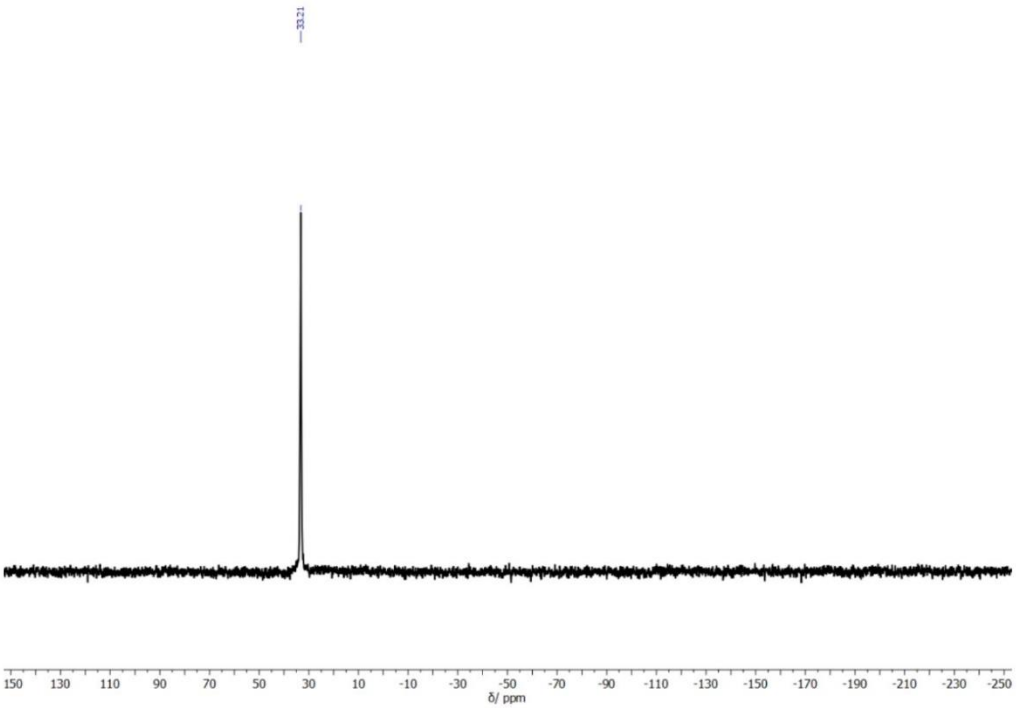

Figure S 11: ^{31}P-NMR (203 MHz, $CDCl_3$, 300K) of P(DAlVP-DEVP-DPrVP) **P4.**

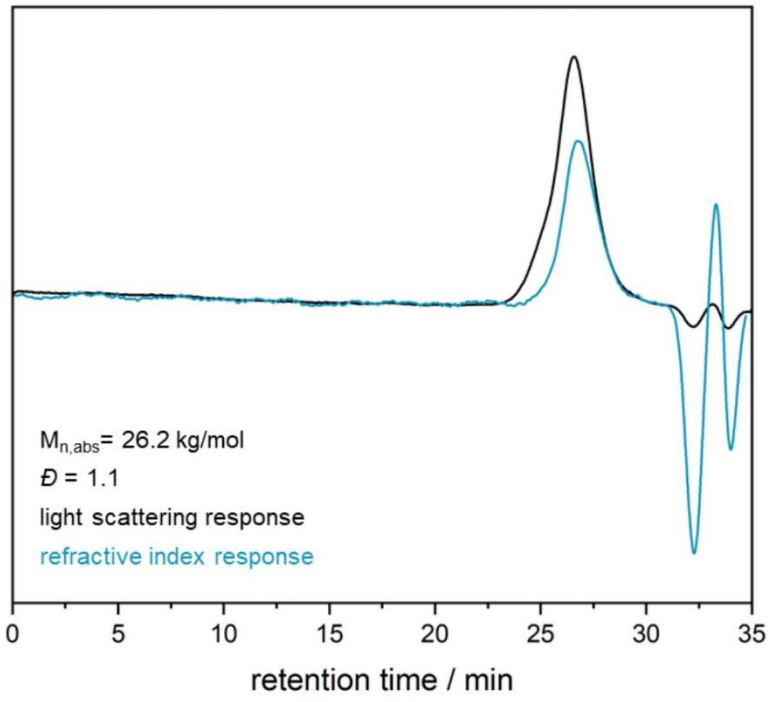

Figure S13: SEC-MALS of P(DAIVP-DEVP-DPrVP) **P4**.

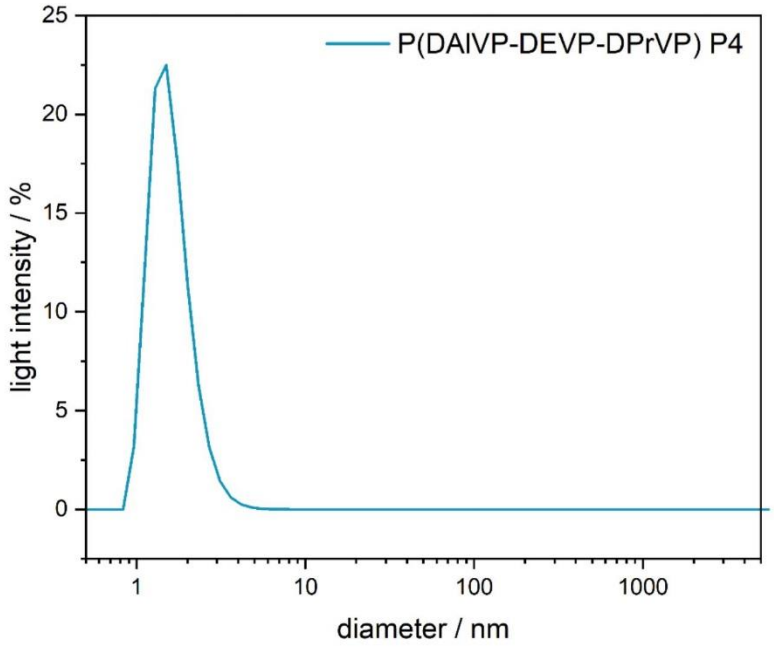

Figure S14: DLS spectra of **P4** (d = 8.10 ± 0.20 nm, PDI = 0.334).

Deprotection of P8 = P9

^{1}H-NMR (400 MHz, $CDCl_3$, 300K): δ (ppm) = 6.89 – 6.70 (m, $H_{ar,sym\text{-}Collidin}$), 5.94 (s, -$OCH_2CHCH_2$), 5.54 – 5.13 (m, -$OCH_2CHCH_2$), 4.54 (s, -$OCH_2CHCH_2$), 4.13 (s, -$OCH_2CH_3$), 3.72 (s, -$CH_2C{\equiv}CH$), 2.79 – 0.98 (m, backbone, OCH_2CH_3, $H_{cholesterol}$), 0.99 – 0.81 (m, -$CH3_{3,\ cholesterol}$).

^{31}P-NMR (400 MHz, $CDCl_3$, 300K): δ (ppm) = 33.2.

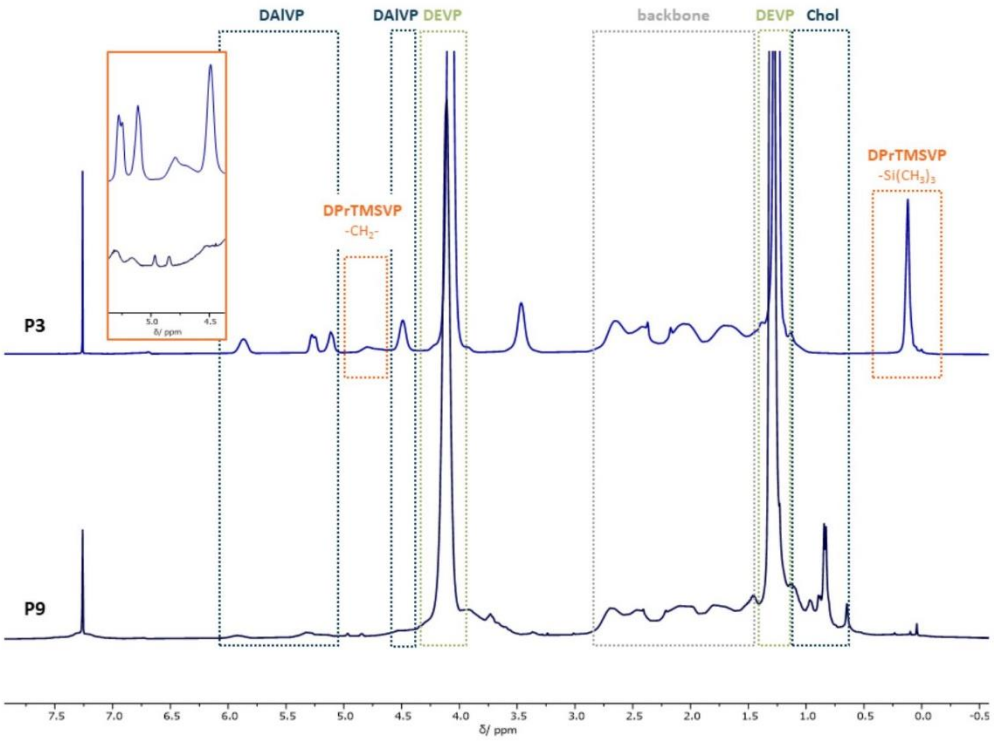

Figure S15: ^{1}H-NMR (400 MHz, $CDCl_3$, 300K) of the polyvinyl phosphonates **P3** and **P9.**

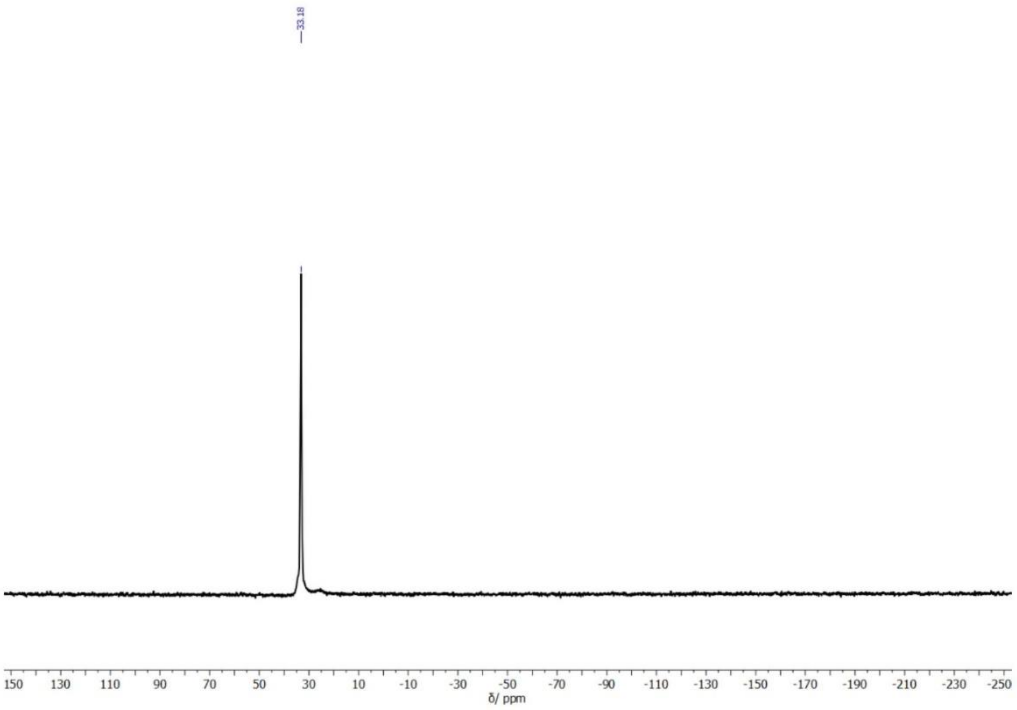

Figure S 16: ^{31}P-NMR (203 MHz, $CDCl_3$, 300K) of P(DAlVP-DEVP-DPrVP) **P9.**

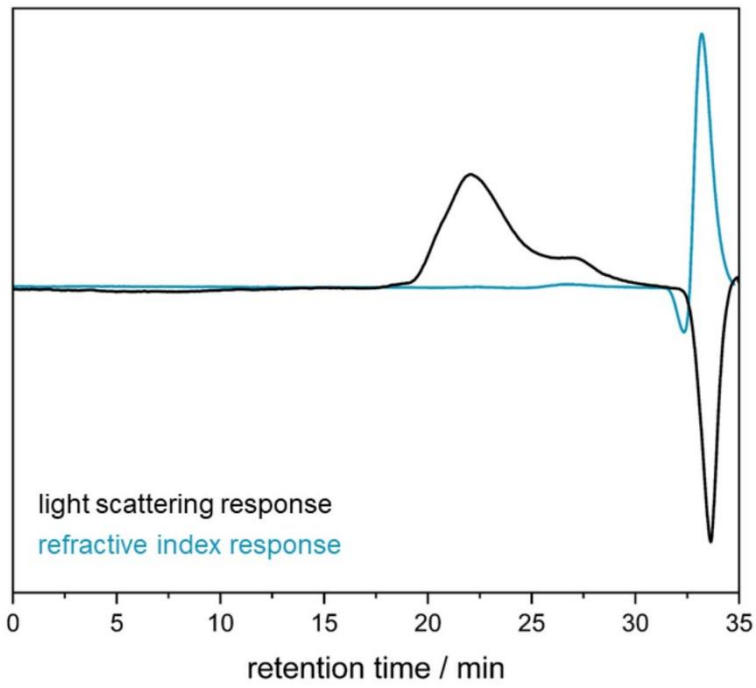

Figure S17: SEC-MALS of polyvinyl phosphonate **P9**.

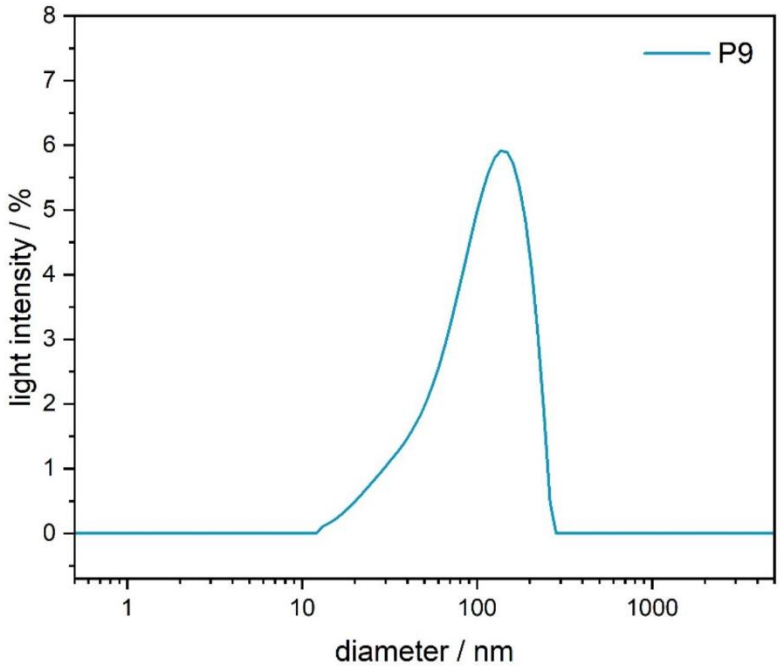

Figure S18: DLS spectra of **P9** (d = 164 ± 21.1 nm, PDI = 0.467).

MODIFICATION OF DPRVP VIA ALKYNE-AZIDE CYCLOADDITION (AAC)

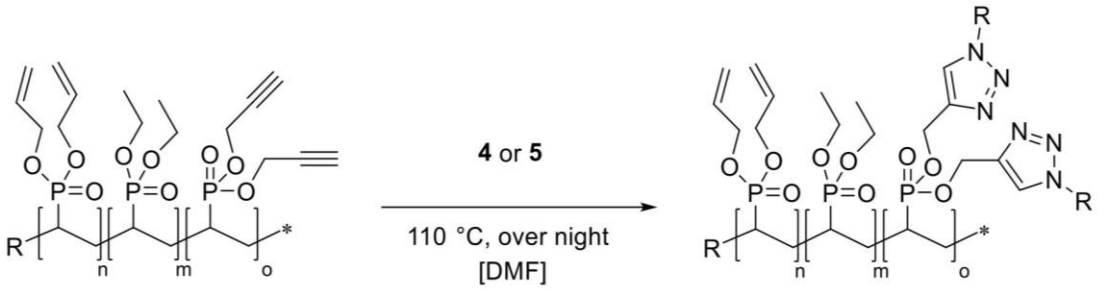

P4

P5 (R= Bn)
P6 (R= hydroxycoumarin)

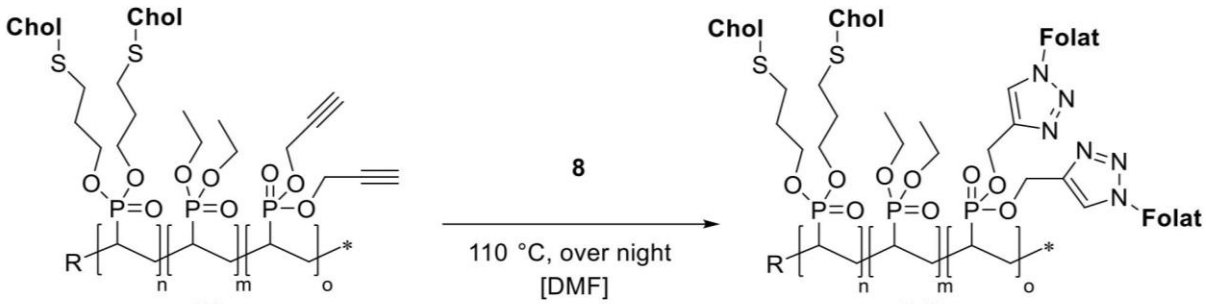

P9 **P10**

The polymer and the respective azide (3.0 eq. per propargyl group) were dissolved in *N*,*N*-dimethylformamid (5.00 mL solvent per 100 mg polymer) before the reaction solution was stirred for 48 hours at 110 °C. The solvent was removed under reduced pressure, and the crude product was purified in different ways.

Modification of P4 with benzylazide 4 = P5

The crude polymer **P5** was dissolved in water and ethanol (water/ethanol = 5/1) and purified by dialysis. In the beginning, against water/ethanol = 5/1, then against water. The functionalized substrate is yielded through freeze-drying.

^{1}H-NMR (400 MHz, MeOD, 500K): δ (ppm) = 8.57 (s, $H_{triazol}$), 7.69 – 7.24 (m, $H_{ar,\ Benzyl}$), 6.01 (s, -OCH$_2$C*H*CH$_2$), 5.47 – 5.20 (m, -OCH$_2$CHC*H*$_2$), 4.60 (s, -OC*H*$_2$CHCH$_2$), 4.18 (s, -OC*H*$_2$CH$_3$), 2.90 – 1.16 (m, backbone, OC*H*$_2$CH$_3$,-OCH$_2$C≡C*H*).

^{31}P-NMR (400 MHz, MeOD, 300K): δ (ppm) = 33.2.

MODIFICATION OF DPRVP VIA ALKYNE-AZIDE CYCLOADDITION (AAC)

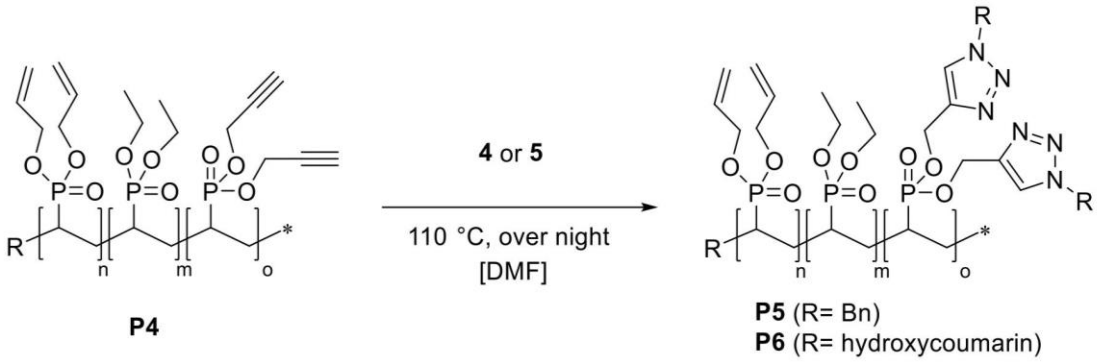

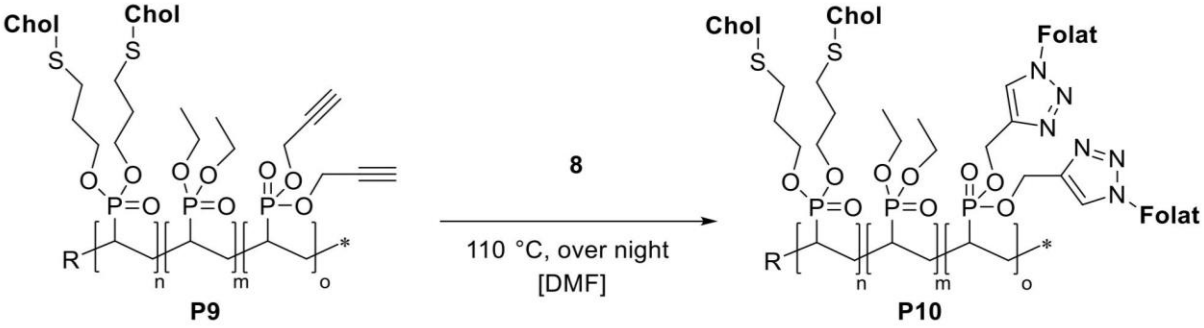

The polymer and the respective azide (3.0 eq. per propargyl group) were dissolved in *N*,*N*-dimethylformamid (5.00 mL solvent per 100 mg polymer) before the reaction solution was stirred for 48 hours at 110 °C. The solvent was removed under reduced pressure, and the crude product was purified in different ways.

Modification of P4 with benzylazide 4 = P5

The crude polymer **P5** was dissolved in water and ethanol (water/ethanol = 5/1) and purified by dialysis. In the beginning, against water/ethanol = 5/1, then against water. The functionalized substrate is yielded through freeze-drying.

^{1}H-NMR (400 MHz, MeOD, 500K): δ (ppm) = 8.57 (s, $H_{triazol}$), 7.69 – 7.24 (m, $H_{ar,\ Benzyl}$), 6.01 (s, -OCH$_2$C*H*CH$_2$), 5.47 – 5.20 (m, -OCH$_2$CHC*H*$_2$), 4.60 (s, -OC*H*$_2$CHCH$_2$), 4.18 (s, -OC*H*$_2$CH$_3$), 2.90 – 1.16 (m, backbone, OC*H*$_2$CH$_3$,-OCH$_2$C≡C*H*).

^{31}P-NMR (400 MHz, MeOD, 300K): δ (ppm) = 33.2.

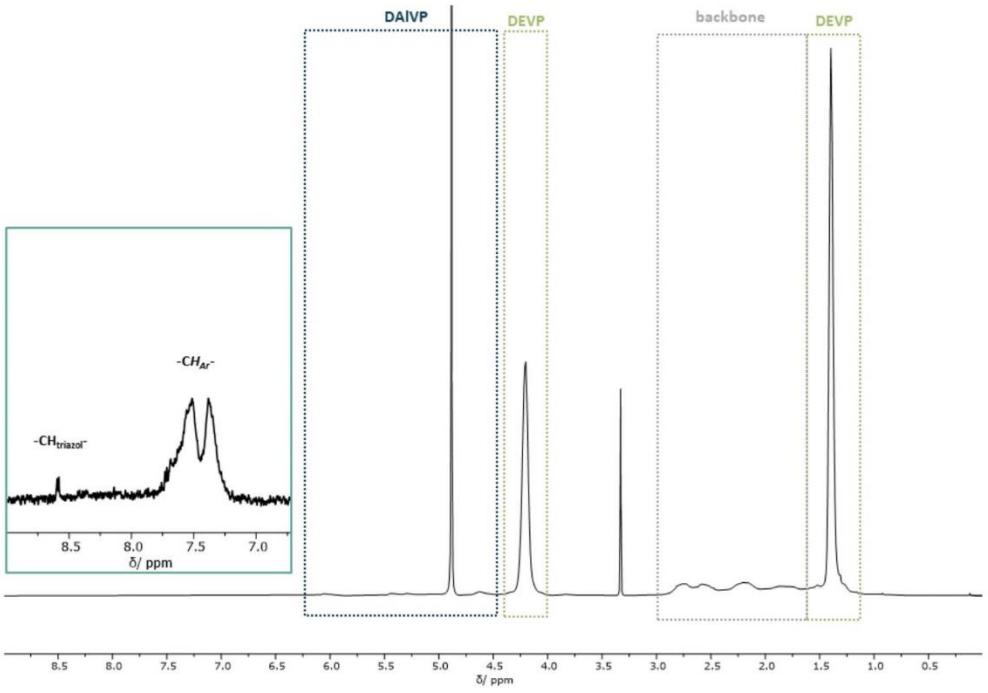

Figure S19: ^{1}H-NMR (400 MHz, MeOD, 300K) of the polyvinyl phosphonates **P5.**

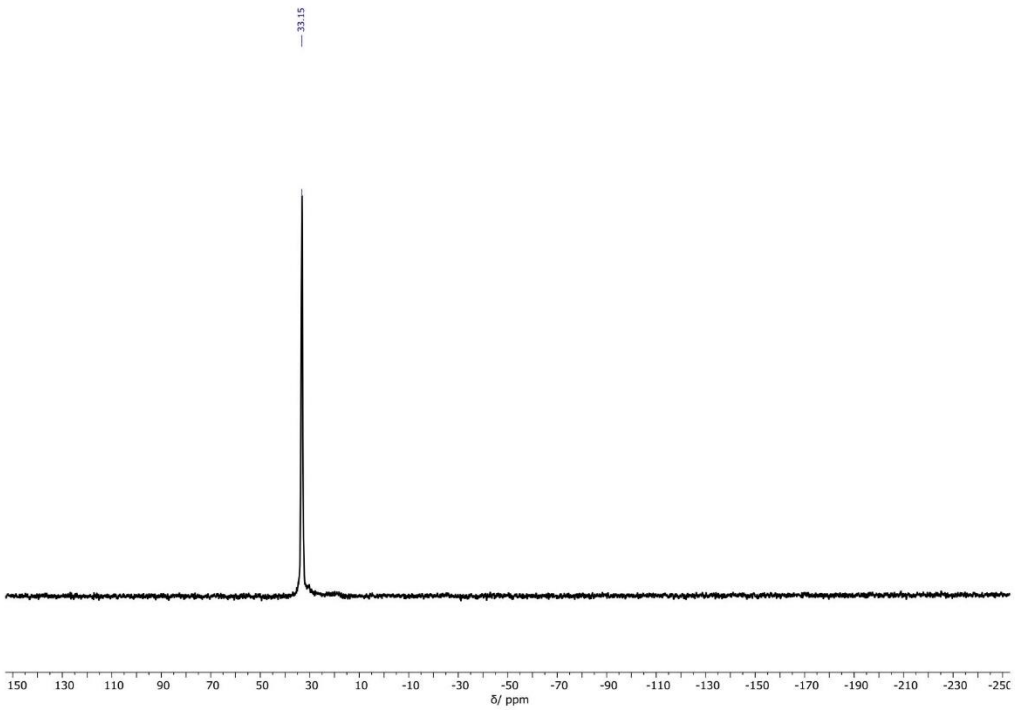

Figure S20: ^{31}P-NMR (203 MHz, $CDCl_3$, 300K) of polyvinyl phosphonate **P5**.

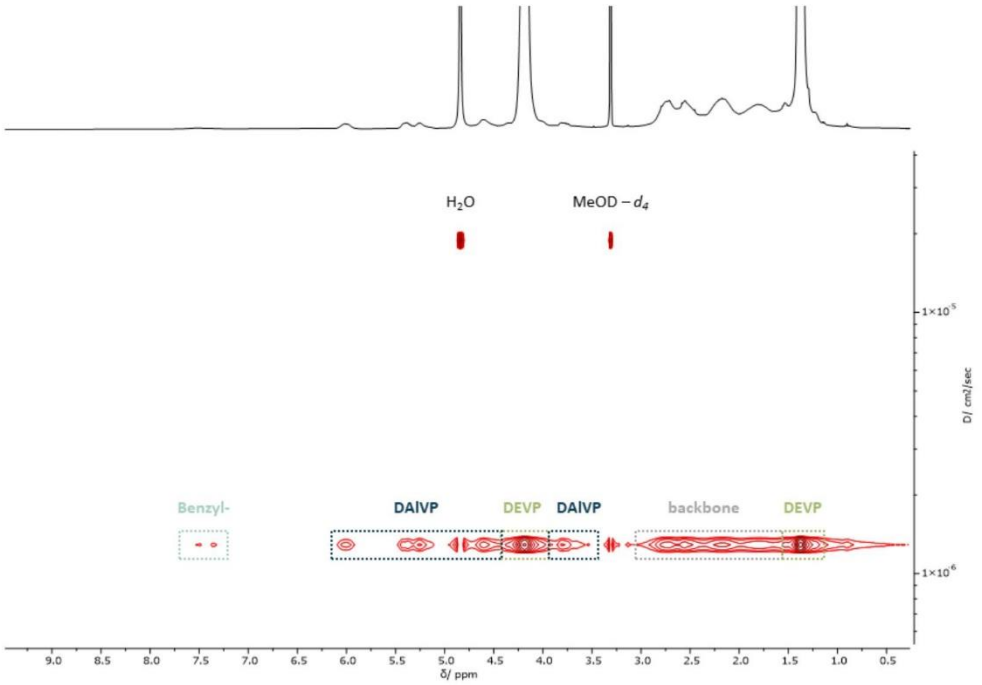

Figure S21: DOSY-NMR of polyvinyl phosphonate **P5.**

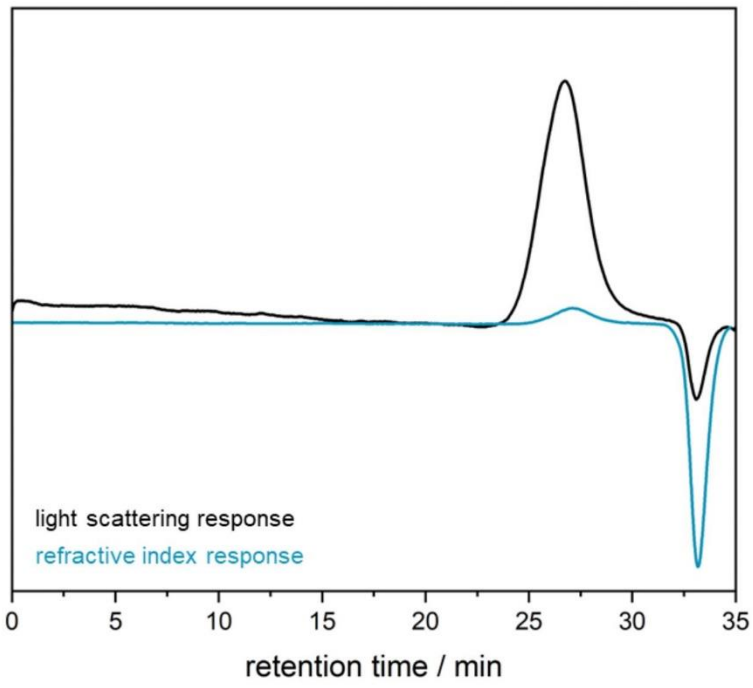

Figure S22: SEC-MALS of polyvinyl phosphonate **P5**.

Modification of P4 with 3-azide-7-hydroxycoumarin 5 = P6

The polymer **P6** was purified via dialysis against water before freeze-drying.

^{1}H-NMR (400 MHz, MeOD, 500K): δ (ppm) = 8.47 (s, $H_{triazol}$), 7.79 – 7.34 (m, $H_{ar,\ Coumarin}$), 7.03 – 6.62 (m, $H_{ar,\ Coumarin}$), 6.00 (s, -OCH$_2$C*H*CH$_2$), 5.51 – 5.15 (m, -OCH$_2$CHC*H*$_2$), 4.58 (s, C*H*$_2$CHCH$_2$), 4.18 (s, -OC*H*$_2$CH$_3$), 2.91 – 1.15 (m, backbone, OC*H*$_2$CH$_3$,-OCH$_2$C≡C*H*).

^{31}P-NMR (400 MHz, MeOD, 300K): δ (ppm) = 33.1.

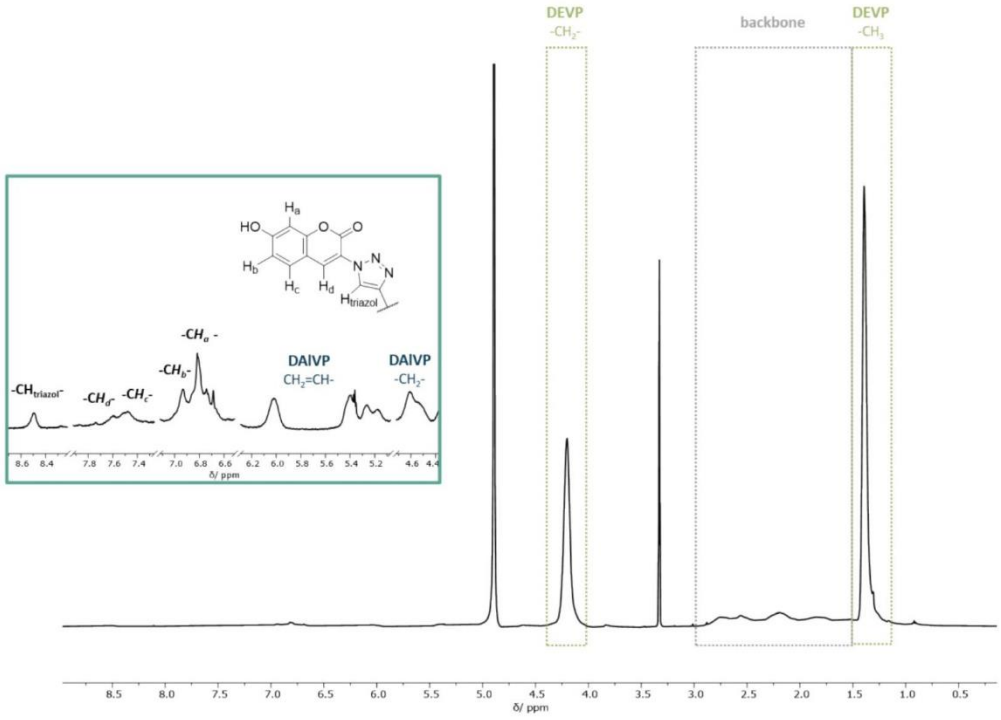

Figure S23: ^{1}H-NMR (400 MHz, $CDCl_3$, 300K) of the polyvinyl phosphonates **P6.**

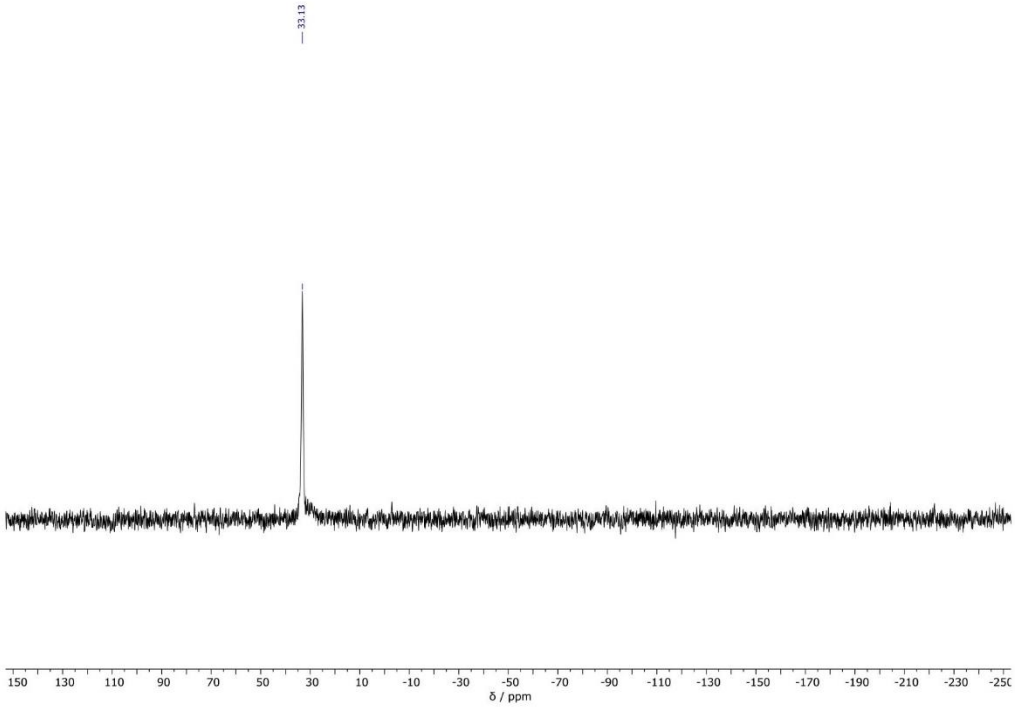

Figure S24: ^{31}P-NMR (203 MHz, MeOD, 300K) of polyvinyl phosphonate **P6.**

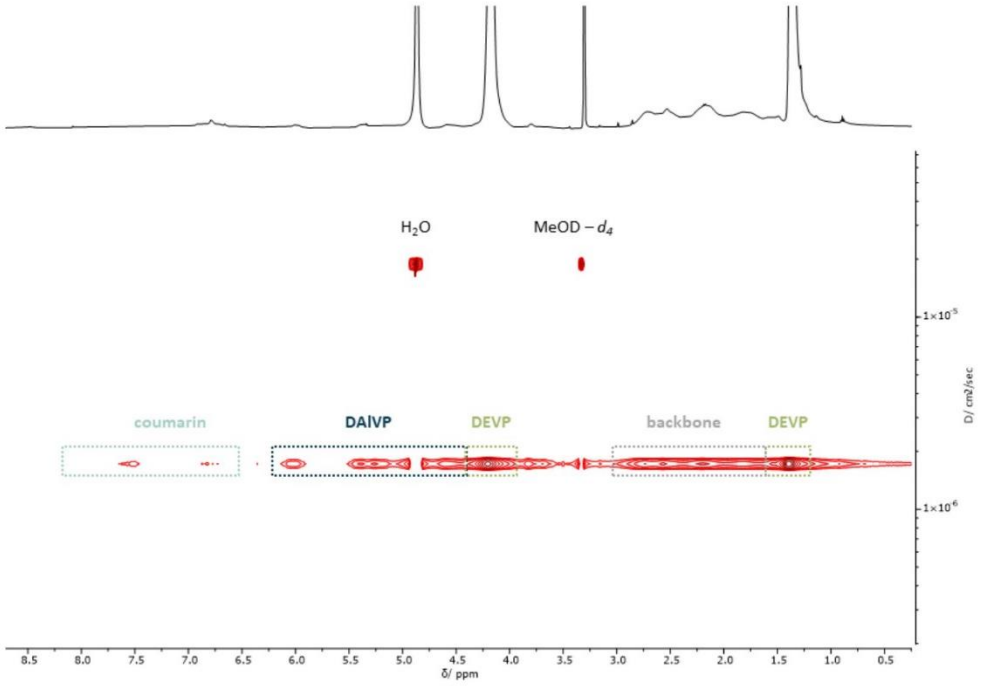

Figure S25: DOSY-NMR of polyvinyl phosphonate **P6.**

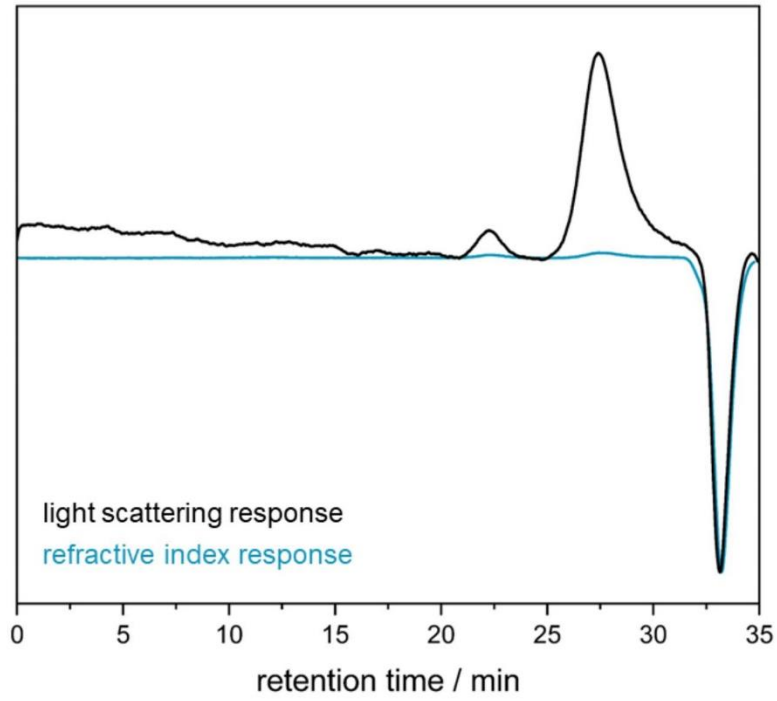

Figure S26: SEC-MALS of polyvinyl phosphonate **P6**.

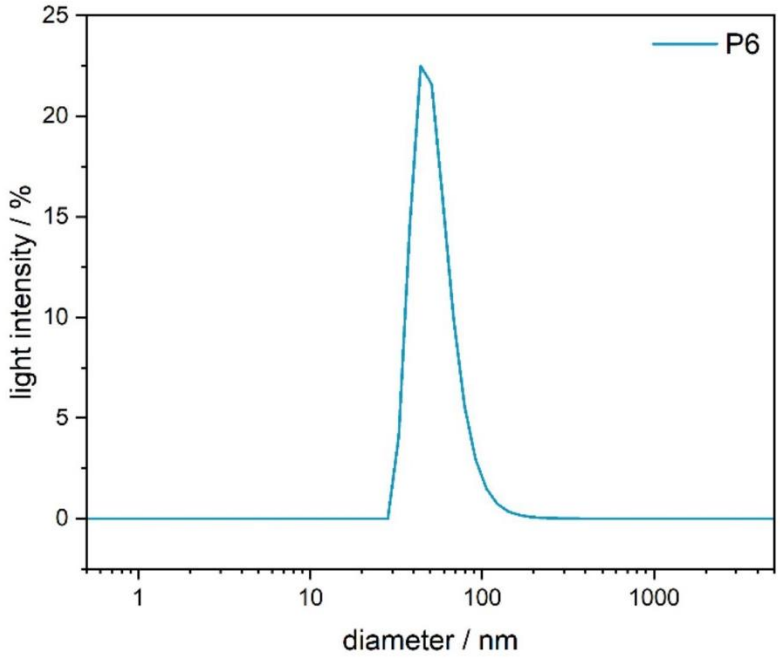

Figure S27: DLS spectra of **P6** (d = 97.8 ± 0.50 nm, PDI = 0.17).

Modification of P9 with folic acid azide 8 = P10

The crude polymer **P10** was dissolved in a NaOH solution (1 M) and purified by dialysis. In the beginning, against NaOH solution (1 M), then against water. The functionalized substrate is yielded through freeze-drying.

^{1}H-NMR (400 MHz, DMSO-*d6*, 500K): δ (ppm) = 8.47 – 6.48 (m, H_{Folate}), 7.61 (s, $H_{triazol}$), 4.01 (s, -OCH_2CH$_3$), 2.78 – 0.99 (m, backbone, OCH_2CH$_3$, $H_{cholesterol}$), 0.99 – 0.71 (m, -CH3$_{3,\ cholesterol}$).

^{31}P-NMR (400 MHz, DMSO-*d6*, 300K): δ (ppm) = 32.9.

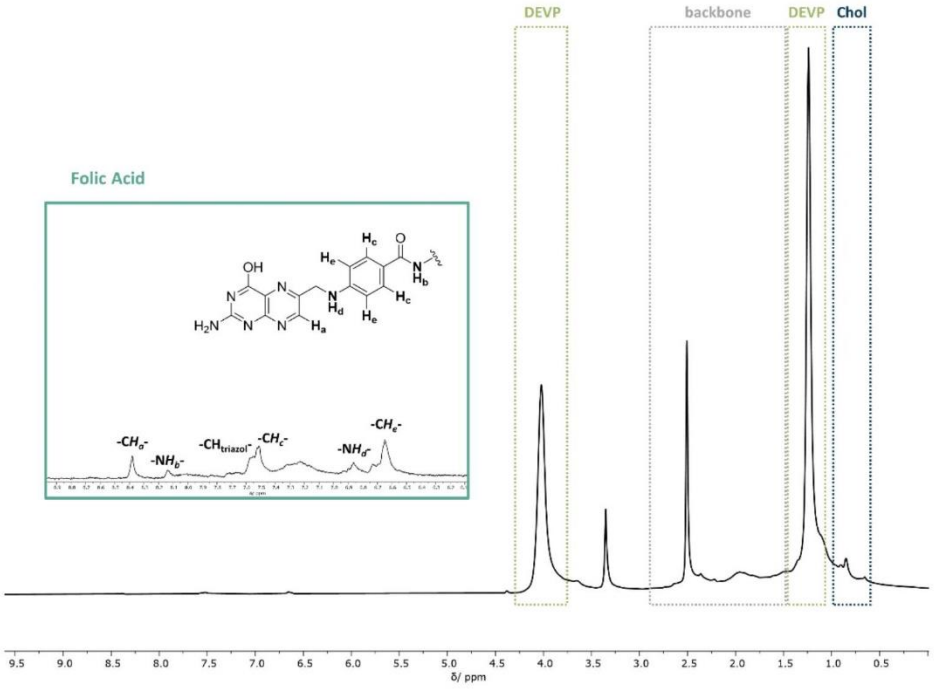

Figure S28: ^{1}H-NMR (400 MHz, DMSO-*d6*, 300K) of the polyvinyl phosphonates **P10.**

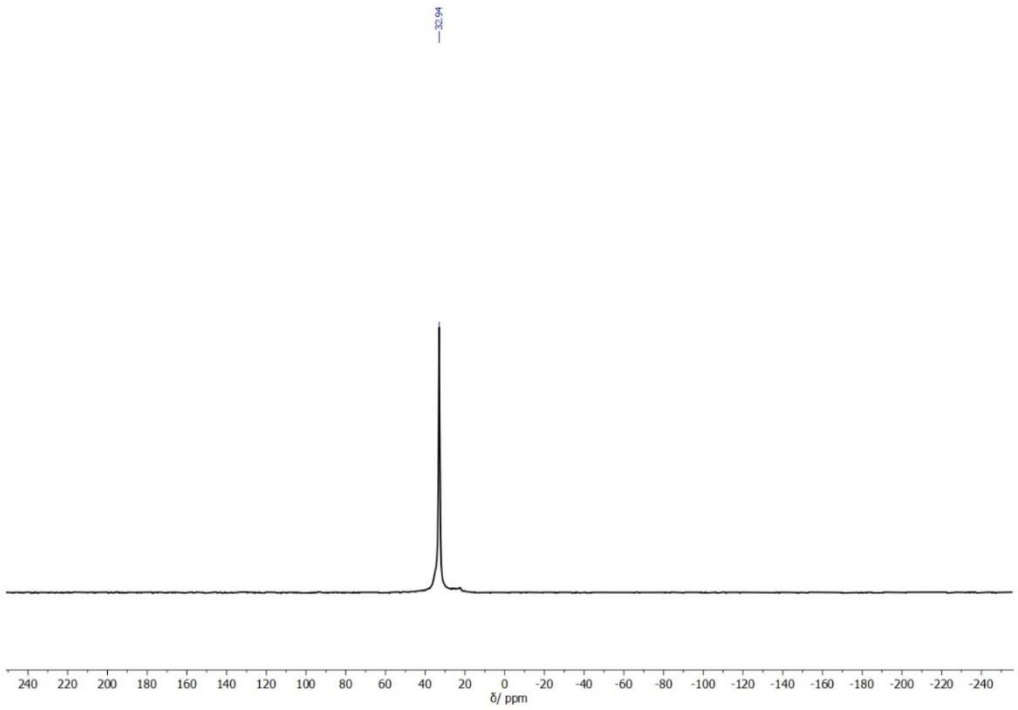

Figure S29: ^{31}P-NMR (203 MHz, DMSO-*d6*, 300K) of polyvinyl phosphonate **P10.**

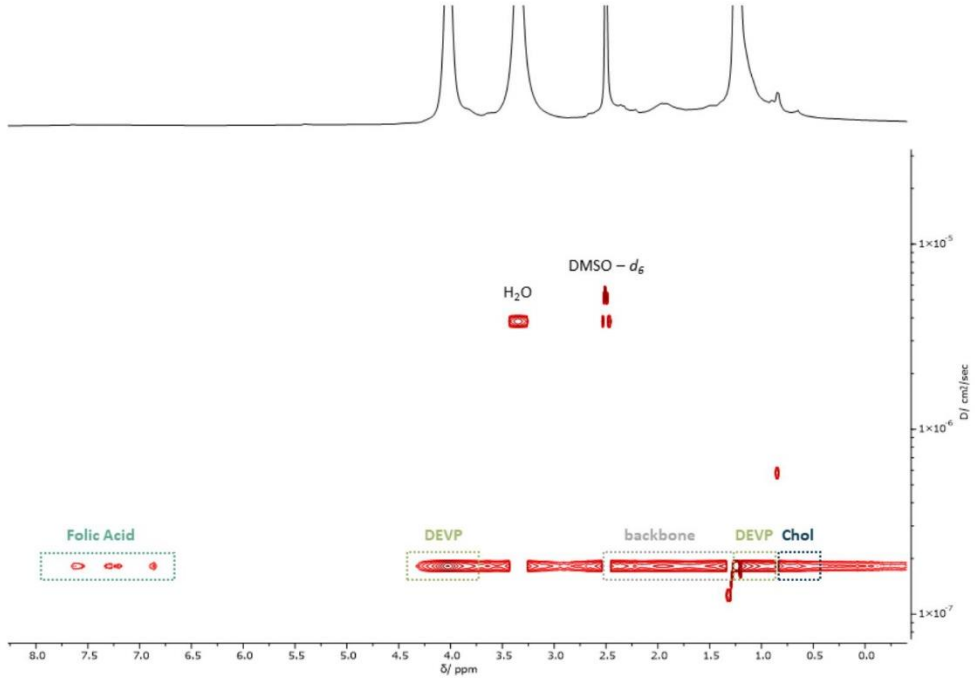

Figure S30: DOSY-NMR of polyvinyl phosphonate **P10.**

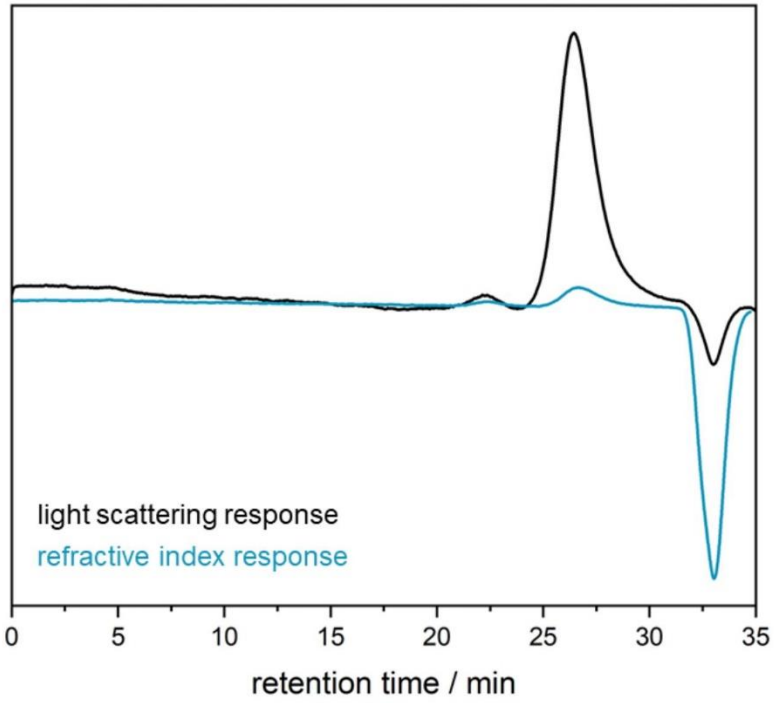

Figure S31: SEC-MALS of polyvinyl phosphonate **P10**.

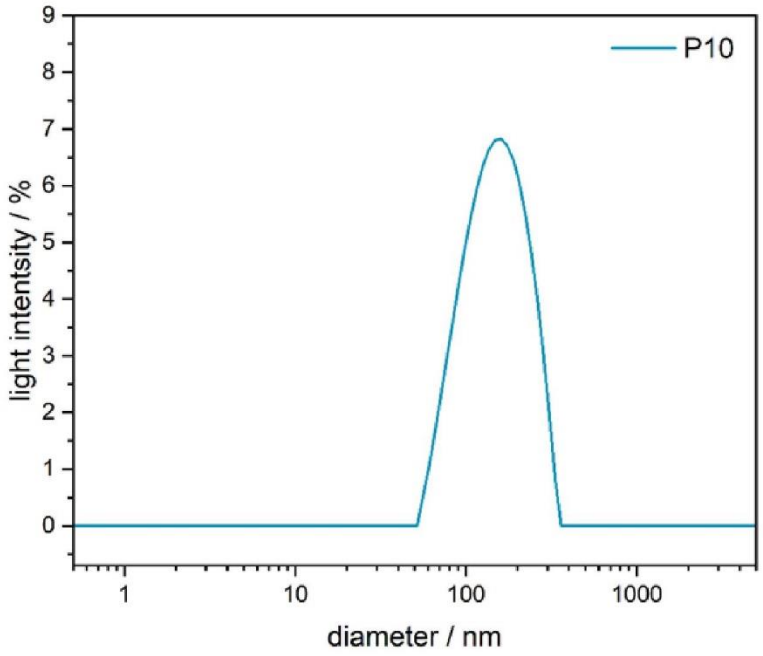

Figure S32: DLS spectra of **P10** (d = 183 ± 8.70 nm, PDI = 0.433).

FUNCTIONALIZATION OF DALVP VIA THIOL-EN CLICK REACTION

MODIFICATION OF P5 WITH CYSTEIN P7

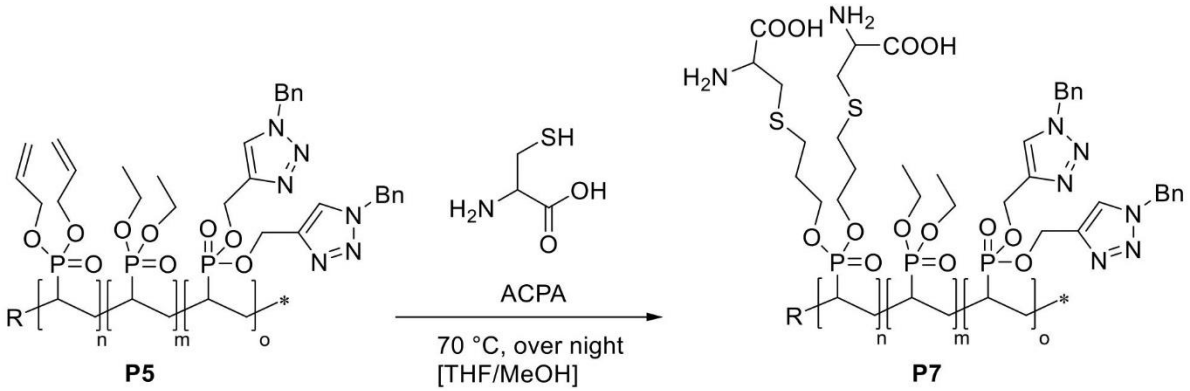

Polyvinyl phosphonate **P5**, L-cysteine (2.0 eq. per allyl group in the polymer), and 4,4'-azobis(4-cyanopentanoic acid) (ACPA) (0.1 eq. per allyl group in the polymer) were dissolved in 25.0 mL water. The mixture was degassed via repeated evacuation and filling with argon (20 iterations) before heating at 70 °C for 15 hours. After purification by dialysis against water, the aqueous solution was freeze-dried to yield the functionalized substrates **P7**.

^{1}H-NMR (400 MHz, MeOD, 300K): δ (ppm) = 8.57 (s, $H_{triazol}$) 7.69 – 7.24 (m, $H_{ar,\ Benzyl}$), 4.18 (s, -OC*H*$_2$CH$_3$), 2.90 – 1.16 (m, backbone, OC*H*$_2$CH$_3$,-OCH$_2$C≡C*H*).

^{31}P-NMR (400 MHz, MeOD, 300K): δ (ppm) = 33.2.

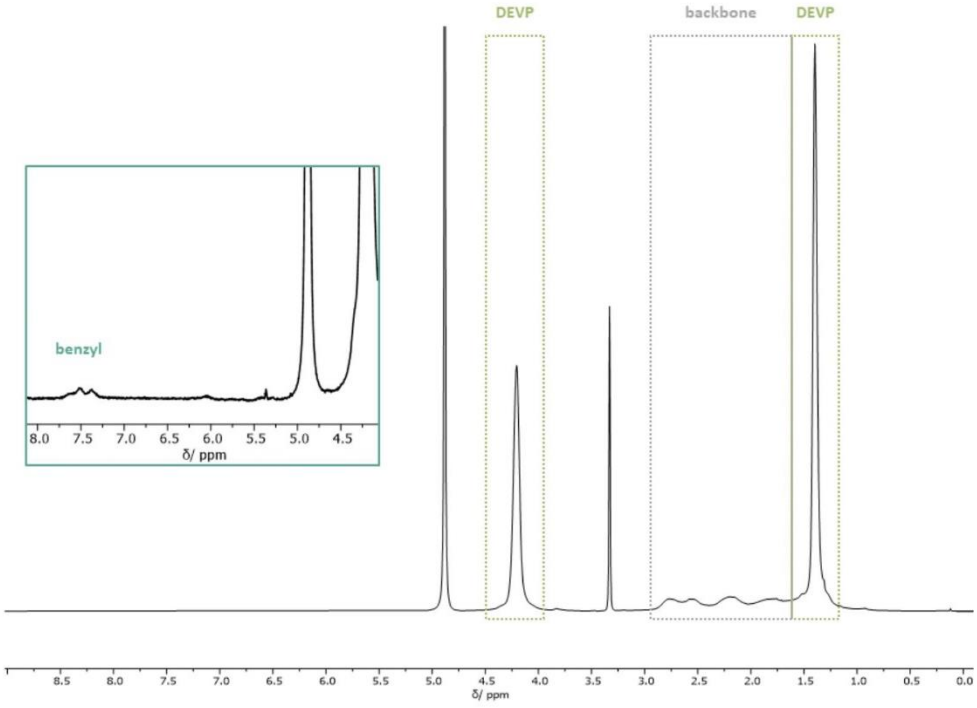

Figure S33: ^{1}H-NMR (400 MHz, MeOD, 300K) of the polyvinyl phosphonates **P7.**

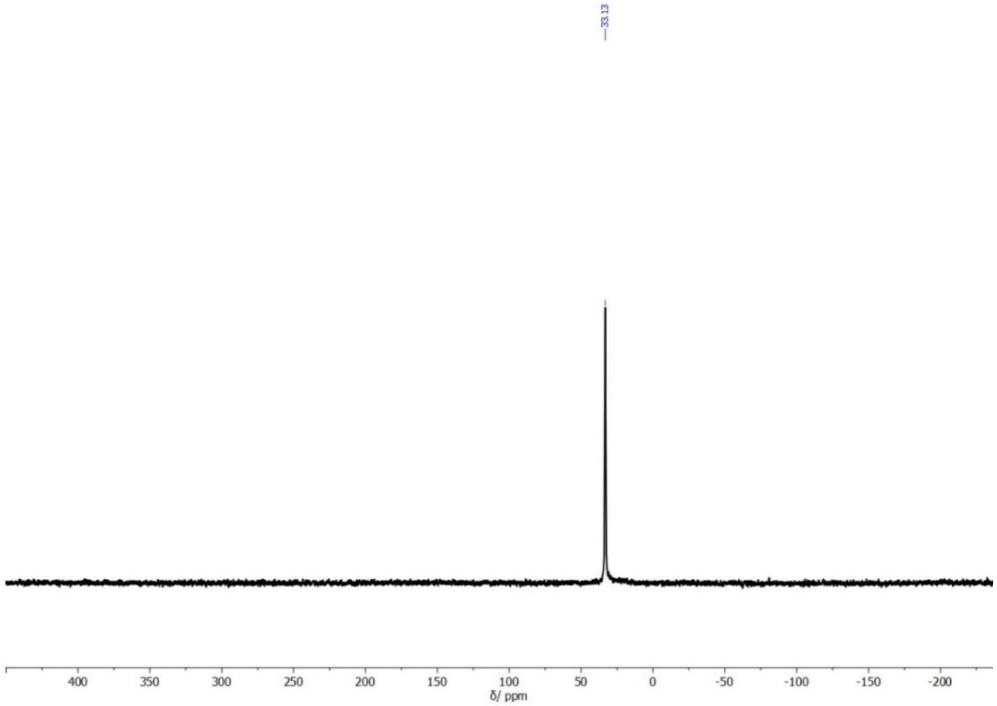

Figure S34: ^{31}P-NMR (203 MHz, MeOD, 300K) of polyvinyl phosphonate **P7.**

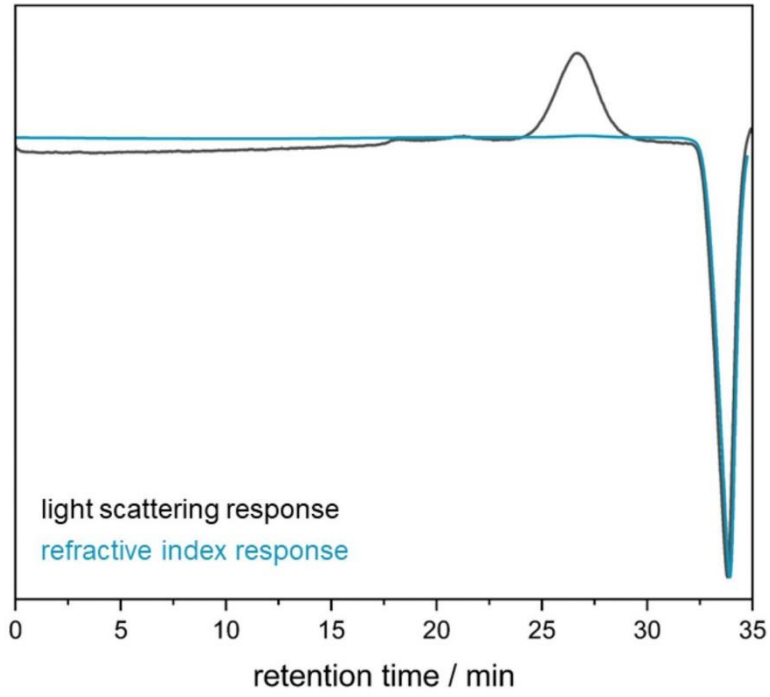

Figure S35: SEC-MALS of polyvinyl phosphonate **P7**.

MODIFICATION OF P3 WITH THIOCHOLESTEROL P8

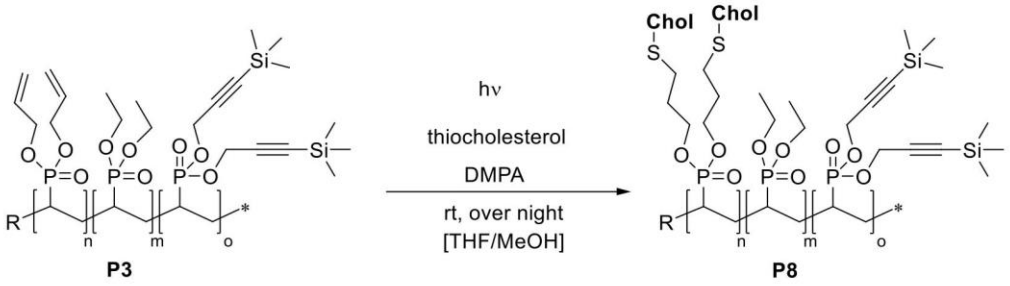

The polymer **P3** was dissolved in a mixture of tetrahydrofuran and methanol (THF/MeOH = 5/1) (15 mL solvent per 100 mg polymer). The thiocholesterol (0.9 eq. per allyl group in the polymer) and 2,2-dimethoxy-2-phenylacetophenone (DMPA) (0.1 eq. per allyl group in the polymer) were added. The mixture was degassed via repeated evacuation and filling with argon (20 iterations) before irradiating (λ = 365 nm) for 18 hours at room temperature. After removing the solvent under reduced pressure, the residue was dissolved in water and tetrahydrofuran (H_2O/THF = 95/5) and purified by dialysis against water. The aqueous solution was freeze-dried to yield the functionalized substrates.

^{1}H-NMR (400 MHz, $CDCl_3$, 500K): δ (ppm) = 6.89 – 6.70 (m, $H_{ar,sym\text{-Collidin}}$), 5.92 (s, -$OCH_2CHCH_2$), 5.50 – 5.06 (m, -$OCH_2CHCH_2$), 4.71 (s, -$CH_2C{\equiv}CSi(CH_3)_3$)), 4.54 (s, -$OCH_2CHCH_2$), 4.12 (s, -$OCH_2CH_3$), 2.79 – 0.98 (m, backbone, OCH_2CH_3, $H_{cholesterol}$), 0.99 – 0.81 (m, $-CH3_{3,\ cholesterol}$), 0.13 (s, -$CH_2C{\equiv}CSi(CH_3)_3$).

^{31}P-NMR (400 MHz, $CDCl_3$, 300K): δ (ppm) = 33.2.

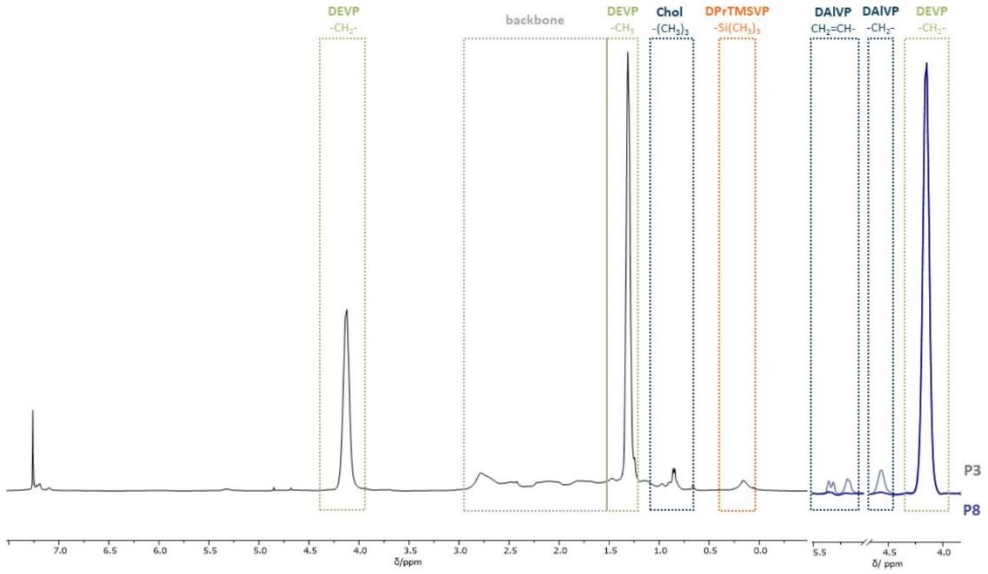

Figure S36: ^{1}H-NMR (400 MHz, $CDCl_3$, 300K) of the polyvinyl phosphonates **P8.**

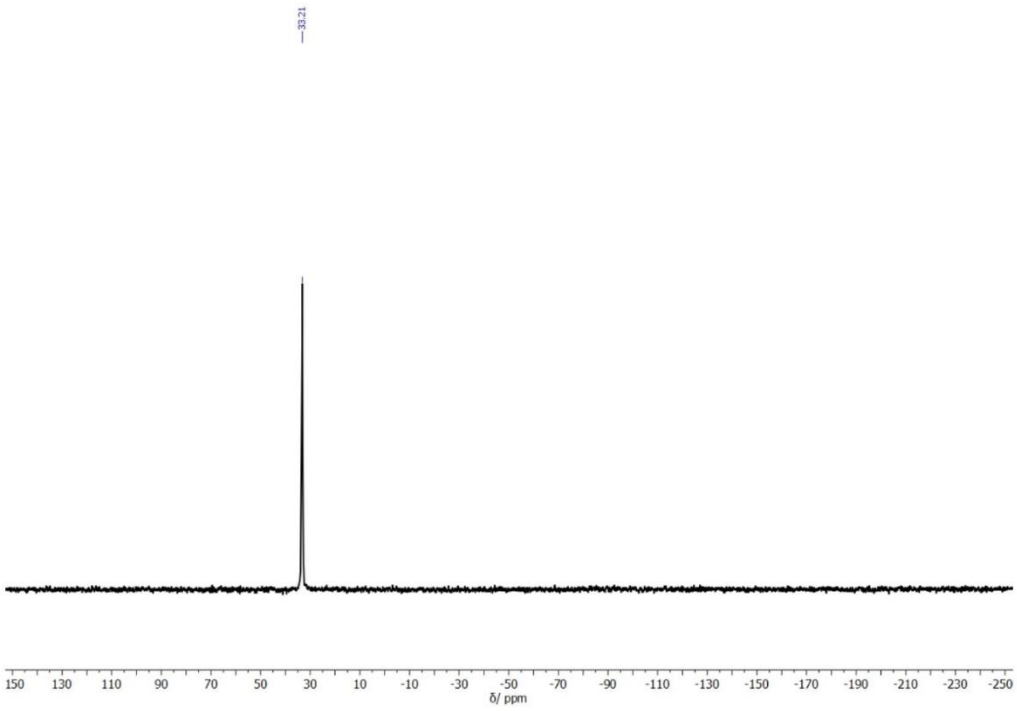

Figure S37: ^{31}P-NMR (203 MHz, $CDCl_3$, 300K) of polyvinyl phosphonate **P8.**

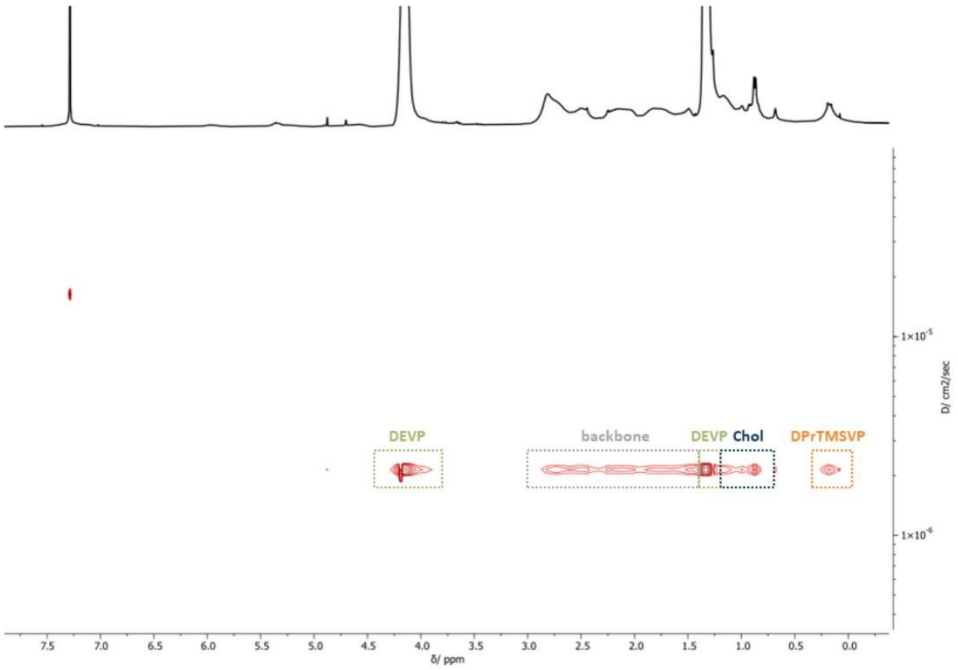

Figure S38: DOSY-NMR of polyvinyl phosphonate **P8.**

5. REFERENZES

(1) Hultzsch, K. C.; Voth, P.; Beckerle, K.; Spaniol, T. P.; Okuda, J. Single-Component Polymerization Catalysts for Ethylene and Styrene: Synthesis, Characterization, and Reactivity of Alkyl and Hydrido Yttrium Complexes Containing a Linked Amido−Cyclopentadienyl Ligand. *Organometallics* **2000**, *19* (3), 228-243.

(2) Salzinger, S.; Soller, B. S.; Plikhta, A.; Seemann, U. B.; Herdtweck, E.; Rieger, B. Mechanistic Studies on Initiation and Propagation of Rare Earth Metal-Mediated Group Transfer Polymerization of Vinylphosphonates. *Journal of the American Chemical Society* **2013**, *135* (35), 13030-13040.

(3) Schwarzenböck, C.; Nelson, P. J.; Huss, R.; Rieger, B. Synthesis of next generation dual-responsive cross-linked nanoparticles and their application to anti-cancer drug delivery. *Nanoscale* **2018**, *10* (34), 16062-16068.

(4) Pehl, T. M.; Adams, F.; Kränzlein, M.; Rieger, B. Expanding the Scope of Organic Radical Polymers to Polyvinylphosphonates Synthesized via Rare-Earth Metal-Mediated Group-Transfer Polymerization. *Macromolecules* **2021**, *54* (9), 4089-4100. DOI: 10.1021/acs.macromol.1c00217.

(5) Yang, Q.; Draghici, C.; Njardarson, J. T.; Li, F.; Smith, B. R.; Das, P. Evolution of an oxidative dearomatization enabled total synthesis of vinigrol. *Organic & Biomolecular Chemistry* **2014**, *12* (2), 330-344.

(6) Schwarzenböck, C.; Schaffer, A.; Pahl, P.; Nelson, P. J.; Huss, R.; Rieger, B. Precise synthesis of thermoresponsive polyvinylphosphonate-biomolecule conjugates via thiol–ene click chemistry. *Polymer Chemistry* **2018**, *9* (3), 284-290, 10.1039/C7PY01796K.

(7) Liu, L.; Zheng, M.; Renette, T.; Kissel, T. Modular Synthesis of Folate Conjugated Ternary Copolymers: Polyethylenimine-graft-Polycaprolactone-block-Poly(ethylene glycol)-Folate for Targeted Gene Delivery. *Bioconjugate Chemistry* **2012**, *23* (6), 1211-1220.

(8) Pehl, T. M.; Kränzlein, M.; Adams, F.; Schaffer, A.; Rieger, B. C–H Bond Activation of Silyl-Substituted Pyridines with Bis(Phenolate)Yttrium Catalysts as a Facile Tool towards Hydroxyl-Terminated Michael-Type Polymers. *Catalysts* **2020**, *10* (4), 448.

11.4.4 Supporting Information Chapter 7

Material and Methods

General consideration

Polymerizations with moisture and air-sensitive reactants were carried out in a *MBraun* LabMaster120 glovebox filled with argon 4.6 from *Westfalen* or using standard *Schlenk* techniques. All glassware was heat-dried prior to use. All chemicals were purchased from *Sigma-Aldrich*, ABCR, or TCI Europe and used without further purification unless otherwise stated. Dichloromethane, tetrahydrofuran, toluene, and pentane were dried using a *MBraun* SPS-800 solvent purification system and stored over 3 Å molecular sieve. Diethyl vinylphosphonate (DEVP) were synthesized according to literature procedures followed by drying over CaH_2 for several days and distilled prior to use.[178] $LiCH_2TMS$, and $Cp_2YCH_2TMS(thf)$ prepared according to literature procedures.[179, 180]

Dynamic light scattering (DLS)

DLS experiments were conducted on Litesizer 500 in the measurement mode of particle size series. The measurements were measured with an automatic angle and an equilibration time of 10 s. Each measurement consisted of 3 acquisitions. The LCST was measured by a temperature program that increased and decreased in the range from 25 to 50 °C in two-degree steps, equilibrating for 5 min once the measurement temperature was achieved. The samples were dissolved in water in a concentration of 2.5 mg/mL.

Lyophilization

The polymer samples subject to freeze-drying were dissolved in either ultrapure water or 1,4-dioxane and frozen under constant rotation in liquid nitrogen. For lyophilisation, a VaCo 5-II-D from Zirbus Technology GmbH was used, the pressure was adjusted to 2 mbar with a condenser temperature of –90 °C.

Nuclear magnetic resonance spectroscopy (NMR)

Nuclear magnetic resonance spectra were recorded on a *Bruker AVIII 400 HD* (400 MHz) or an *AVIII 500 cryo* (500 MHz). Deuterated solvents were purchased ($CDCl_3$, benzene-*d6*) from *Sigma-Aldrich*. Spectroscopic chemical shifts δ are reported in ppm and calibrated to the residual proton signals of the used solvents.

Size-exclusion chromatography multi-angle light scattering (SEC-MALS)

Molecular weights and polydispersity of the polymers (c = 2.5 mg/mL) were determined by SEC-MALS using a Wyatt Dawn Heleos II MALS light scattering unit and a Wyatt Optilab rEX

536 RI unit in THF: H_2O = 1:1 (with 9 g/L *tetra-n*-butyl-ammonium bromide and 272 mg/L 2,6-di-*tert*-butyl-4-methylphenol added) as eluent at 40 °C on two Agilent PolarGel-M columns; for absolute molecular weight (triple detection) determination of different polymers, the refractive index increments dn/dc = 0.0922 mL/g was used.

Transmission electron microscopy (TEM)

TEM analysis of coacervate core micelle samples was performed on a JEOL JEM 1400 plus instrument at an acceleration voltage of 120 kV. TEM grids were hydrophilized by glow discharge for 30 s before sample preparation. Then 0.5 µL of the sample (c= 0.5 mg/mL in MilliPore water) was placed onto the hydrophilized carbon-coated copper mesh grid and incubated for 30 s. Excess liquid was paper-blotted afterward. The dried grid was then stained with an aqueous 2 wt% uranyl acetate solution for 30 s, and the excess liquid was blotted again with filter paper before imaging.

Turbidity measurements

Turbidity measurements were performed on a Varian Cary 50 Scan UV visible spectrophotometer in a QS 10×10 mm quartz glass cuvette from *Hellma* GmbH & Co. KG. The cloud point of the aqueous polymer solution (c = 2.5 mg/mL) was determined by spectrophotometric detection of the change in transmittance at λ = 500 nm. The samples were heated/cooled at a rate of 1.0 K/min in one-degree steps followed by a 5 min long period of constant temperature to ensure equilibration. The cloud point was defined as the temperature corresponding to a 10% decrease in optical transmittance.

Photoluminescence measurements

The photoluminescence measurements were performed on AVA-Spec 2048 from *Avantes*. For the excitation of the samples, PS cuvettes were placed in a 90° cuvette holder consisting of a *Prizmatix* current controller as a light source irradiated with light of a wavelength of 365 nm.

Polymerization

For the C–H bond activation, a solution of *sym*-collidin (1.00 equiv.) in dry toluene (1.00 mL) was added to a solution of $Cp_2Y(CH_2TMS)(thf)$ (2.00 equiv.) in absolute toluene (1.00 mL). After the quantitative conversion, the reaction mixture was diluted with 8.00 mL of dry toluene, and the respective amount of DEVP was added in one portion. After 5 min, one aliquot was taken (0.1 mL quenched with 0.4 mL of MeOD-d_4), the conversion of PDEVP was determined by ^{1}H-NMR, and then DPrTMSVP was added to the solution in one portion. After stirring overnight, another aliquot was taken (0.1 mL quenched with 0.4 mL of MeOD-d_4), and the conversion of DEVP was determined via ^{31}P-NMR. The polymer participated from pentane, subject to centrifugation, and the supernatant was decanted. The residual polymer is dissolved in 1,4-dioxane before being freeze-dried. The purified polymer is analyzed using ^{1}H/^{31}P/DOSY-NMR and SEC-MALS.

^{1}H-NMR (400 MHz, $CDCl_3$, 300 K): δ (ppm) = 6.91 – 6.71 (m, $H_{ar,sym\text{-Collidin}}$), 4.84 (s, -C$H_2$C≡CSi($CH_3$)$_3$)), 4.13 (s, -OC$H_2CH_3$), 2.87 – 1.13 (m, $H_{backbone}$, -OCH$_2$CH_3), 0.18 (s, -CH2C≡CSi(CH_3)$_3$).

^{31}P-NMR (203 MHz, $CDCl_3$, 300K): *δ* (ppm) = 33.2.

Characterization of polymer micelles

Cell viability assay

The biocompatibility of polymers was evaluated with spontaneously immortalized human *Müller* cell line (MIO-M1). The polymers were prepared at a stock concentration of 1.5 mg/mL in distilled water and vortex until dissolved before use. MIO-M1 (P41) was seeded in a transparent 96-well plate at the density of 10,000 cells in pre-warmed high glucose (4.5 g/L) DMEM medium (Gibco; *Thermo Fisher* Scientific, Taufkirchen, Germany) supplemented with 10% fetal bovine serum and 1% penicillin/streptomycin (*Thermo Fisher* Scientific, Karlsruhe, Germany). After 24 hours, the medium was aspirated, and each well was treated with 100 µL of different concentrations of polymers (5, 15, 25, 50, 100, 150, 200, 250, and 500 µg/mL) prepared in the medium. Following 24 hours of treatment at 37°C and 5% CO_2, an MTS assay was carried out to evaluate the metabolic activity of the treated cells by adding 20 µL of the CellTiter 96 ® Aqueous One Solution Reagent (Promega Corporation, Madison, WI, USA) directly to each well and incubated at 37°C for 90 minutes. Subsequently, the absorbance was measured at 490 nm with a reference wavelength set at 690 nm for background correction using a Tecan Reader (NanoQuant infinite M200). All data is shown as mean ± SD from five replicates after normalizing to the untreated control wells representing 100% cell viability.

CMC determination

The CMC values of amphiphilic polymers were determined with the help of Nile red (NR). In this regard, a stock solution of NR (c = 1.26 mg/mL) was prepared by dissolving the dye in DMSO. Concentrated stock solutions of each polymer were prepared in Milli-Q water (c = 0.0015, 0.15 and 3.0 mg/mL) and combined with the dye solution (a volume of 2 µL of dye was added to each polymer concentration). Afterward, 15 different concentrations ranging from 0.00001 to 2 mg/mL were prepared using further dilution with Milli-Q water. The solutions were incubated at room temperature for 5 hours. Once the solutions had been transferred to black bottom 96-well microplates (*Thermo* Scientific, Nunclon™, Germany), samples were allowed to equilibrate for 30 minutes at 25 °C. Excitation/emission wavelengths for all fluorescence measurements were 485/636 nm, respectively, and measured on a plate reader at 25 °C (TECAN Spark, TECAN, Maennedorf, Switzerland). Based on the plot of fluorescence intensity versus polymer concentration, two distinguished lines were created using the low initial fluorescence before NR is taken up by the micelles and the first polymer concentrations of the linear increase in fluorescence indicating micelle formation. The CMC value for each polymer was derived from the intersection of these two lines.

Loading and release experiments

To obtain fluorescein-loaded vehicles, firstly, fluorescein was dissolved in DMSO (c = 0.3 mg/mL). Under continuous stirring, the fluorescein solution was added dropwise to an ice-cooled polymer solution (polymer/fluorescein = 12/1). The mixture was then stirred for 1 h on ice and 90 min at ambient temperature. Subsequently, five dialysis membranes were filled with 600 µL each of this solution and were dialyzed against deionized water night. For the release studies, the five dialysis tubes were placed in 90 mL water at different temperatures (T = room temperature, 37 °C, 40 °C, and 42 °C). Samples (1.5 mL) were taken at regular intervals (hourly during the first 7 hours, then after 24, 30, 48 and 72 hours) and the removed volume was backfilled with 1.5 mL of the related medium. Each sample taken was later conducted to photoluminescence spectroscopy. The amount of fluorescein was then determined from the relative irradiance at each measuring point using calibration curves. The calibration curves were generated *via* photoluminescence measurements using fluorescein solutions in water and the citrate-buffer solutions with varying concentrations. With help of the reference sample (vide infra, initial amount of fluorescein) the fraction of released fluorescein was calculated.

11.4.5 Supporting Information Chapter 8

Material and Methods

General consideration

Polymerizations with moisture and air-sensitive reactants were carried out in a *MBraun* LabMaster120 glovebox filled with argon 4.6 from Westfalen or using standard *Schlenk* techniques. All glassware was heat-dried prior to use. All chemicals were purchased from *Sigma-Aldrich*, ABCR, or TCI Europe and used without further purification unless otherwise stated. Dichloromethane, tetrahydrofuran, toluene, and pentane were dried using a *MBraun* SPS-800 solvent purification system and stored over 3 Å molecular sieve. Diethyl vinylphosphonate (DEVP) was synthesized according to literature procedures followed by drying over CaH_2 for several days and distilled prior to use.[178] $LiCH_2TMS$, $Cp_2YCH_2TMS(thf)$, dichloro vinyl phosphonate and (3-(trimethylsilyl)propargyl alcohol were prepared according to literature procedures.[27, 179, 180, 182]

Column chromatography

Silica gel (grain size: 60-200µm) from *Acros Organics* was used for purification *via* column chromatography, corresponding solvent ratios are given in the appropriate procedures.

Elemental Analysis

The elemental analysis was performed by the microanalytical laboratory at the Department of Inorganic Chemistry at the Technical University of Munich on a Vario EL from *Elementar.*

Dialysis

Purification *via* dialysis were performed with a Spectra/Por 1 dialysis tube (regenerated cellulose) with a molecular weight cut-off (MWCO) of 6000 8000 (*Spectrumlabs*). Before use membranes are flushed with deionized water. Typical solvent for dialysis was water. However, if specific solvents are used for dialysis, it will be given in the corresponding procedures.

Nuclear magnetic resonance spectroscopy (NMR)

Nuclear magnetic resonance spectra were recorded on a *Bruker AVIII 400 HD* (400 MHz) or an *AVIII 500 cryo* (500 MHz). Deuterated solvents were purchased from *Sigma-Aldrich*. Spectroscopic chemical shifts δ are reported in ppm and calibrated to the residual proton signals of the used solvents.

Size-exclusion chromatography multi-angle light scattering (SEC-MALS)

Molecular weights and polydispersity of the polymers (c = 2.5 mg/mL) were determined by SEC-MALS using a Wyatt Dawn Heleos II MALS light scattering unit and a Wyatt Optilab rEX 536 RI unit in THF: H_2O = 1:1 (with 9 g/L *tetra-n*-butyl-ammonium bromide and 272 mg/L 2,6-di-*tert*-butyl-4-methylphenol added) as eluent at 40 °C on two Agilent PolarGel-M columns; for

absolute molecular weight (triple detection) determination of different polymers, the refractive index increments dn/dc = 0.0922 mL/g was used.

Thin-layer chromatography (TLC)

Thin-layer chromatography was performed on silica coated aluminum sheets (F254) from *Sigma-Aldrich*. Compounds were detected by either UV-light (λ = 254nm, λ = 366 nm) or $KMNO_4$-solution followed by heating to 200 °C-250 °C. The detection method used is specified in the corresponding procedure.

UV/vis spectroscopy (UV/vis)

UV/vis spectra were measured on a *Varian* Cary 50 Scan UV visible spectrophotometer from 200 nm to 800 nm at 25 °C. The samples were dissolved in methanol and analyzed in a QS 10×10 mm quartz glass cuvette from *Hellma* GmbH & Co. KG. A baseline correction with the pure solvent was performed before sample measurements.

Synthesis of nucleobase- derivates

9-(2-bromoethyl)-9H-purin-6-amine

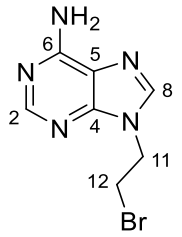

3.50 g (25.9 mmol, 1.00 eq.) adenine and 10.74 g (77.7 mmol, 3.00 eq.) potassium carbonate were dissolved in 180 ml DMF. Afterward, 10.0 ml (21.9 g, 117 mmol, 4.50 eq.) 1,2-dibromoethane was added to the solution, which was stirred for 48 h at room temperature. Subsequently, the solution was extracted three times with 250 ml chloroform. The combined organic phases were washed with brine, followed by drying sodium sulfate, followed by removing the volatiles. The crude product was purified via recrystallization in methanol, yielding 2.46 g (10.2 mmol, 39%) 9-(2-bromoethyl)-9*H*-purin-6-amine.

^{1}H-NMR (400 MHz, DMSO-d_6, 300 K): δ (ppm) = 8.17 (s, 1H, H-8), 8.15 (s, 1H, H-2), 7.25 (s, 2H, -NH2), 4.56 (t, $^{3}J_{H,H}$ = 6.1 Hz, 2H, H-11), 3.94 (t, $^{3}J_{H,H}$ = 6.1 Hz, 2H,H-12).

^{13}C-NMR (101 MHz, DMSO-d_6, 300 K): δ (ppm) = 156.00 (C-6), 152.51 (C-2), 149.48 (C-4), 140.91 (C-8), 118.69 (C-5), 44.65 (C-11), 31.57 (C-11).

EA: calculated: C 34.73%, H 3.33%, N 28.93%, Br 28.93%.

found: C 34.91%, H 3.21%, N 28.60%, Br 31.80%.

9-(2-azidoethyl)-9H-purin-6-amine

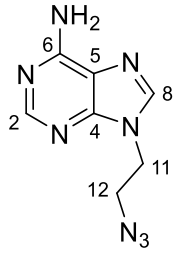

1.20 g (4.94 mmol, 1.00 eq.) 9-(2-bromoethyl)-9H-purin-6-amine was dissolved in 85.0 ml DMSO. After addition of 964 mg sodium azide, the solution was stirred at 80°C for 24 h. The reaction was quenched by adding water, and the resulting mixture was extracted with EtOAc. The combined organic phases were washed with brine, and dried using sodium sulfate, and the solvent was removed under vacuum. The crude product is washed with hexane to yield 488 mg (2.39 mmol, 49%) 9-(2-azidoethyl)-9*H*-purin-6-amine.

^{1}H-NMR (400 MHz, DMSO-d_6, 300 K): δ (ppm) = 8.16 (s, 2H, H-2, H-8), 7.25 (s, 2H,-NH_2), 4.34 (t, $^{3}J_{H,H}$ = 5.7 Hz, 2H, H-11), 3.81 (t, $^{3}J_{H,H}$ = 5.8 Hz, 2H, H-12).

^{13}C-NMR (101 MHz, DMSO-d_6, 300 K): δ (ppm) = 155.99 (C-6), 152.54 (C-2), 149.62 (C-4), 140.89 (C-8), 118.71 (C-5), 49.71 (C-12), 42.45 (C-11).

EA: calculated: C 41.17%, H 3.95%, N 54.88%.

found: C 41.10%, H 3.85%, N 53.30%.

3-benzoyl-5-methylpyrimidine-2,4(1H,3H)-dione

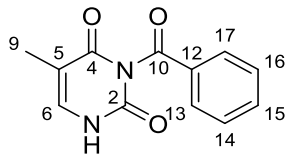

5.04 g (40.0 mmol, 1.00 eq.) thymine was dissolved in 24.0 ml pyridine and 16.0 ml acetonitrile (MeCN). Afterward, 10.7 ml (12.9 g, 92.0 mmol, 2.30 eq.) benzoyl chlorid was added dropwise at room temperature, and the resulting solution was stirred overnight at room temperature. Subsequently, the solution was portioned between 200 ml DCM and 200 ml water. The aqueous phase was extracted three times with 200 ml DCM, the combined organic phases were dried over sodium sulfate, and the volatiles were removed. The resulting solid was dissolved in 80.0 ml dioxane, followed by the addition of 3.00 g (21.7 mmol, 0.50 eq.) potassium carbonate and 40.0 ml water. The solution was stirred for 2 h at room temperature. Then, the pH of the solution was adjusted to pH = 5 with concentrated acetic acid, followed by concentrating the solution. 160 ml of saturated sodium hydrogen carbonate solution was added to the concentrated solution and stirred for 1 h at room temperature. The resulting suspension was filtered, and the isolated solid was washed with ice-cold water. The solid was recrystallized in acetone, yielding 5.50 g (23.9 mmol, 60%) 3-benzoyl-5-methylpyrimidine-2,4(1*H*,3*H*)-dione.

^{1}H-NMR (400 MHz, DMSO-d_6, 300 K): δ (ppm) = 7.93 (d, $^{3}J_{H,H}$ = 7.7 Hz, 2H, H-13,H-17), 7.77 (t, $^{3}J_{H,H}$ = 7.4 Hz, 1H, H-15), 7.59 (t, $^{3}J_{H,H}$ = 7.6 Hz, 2H, H-14, H-16), 7.53 (s, 1H, H-6), 1.81 (s, 3H, H-9).

^{13}C-NMR (101 MHz, DMSO-d_6, 300 K): δ (ppm) = 1170.25 (C-10), 163.59 (C-4), 150.13 (C-2), 139.20 (C-6), 135.30 (C-15), 131.45 (C-12), 130.20 (C-13, C-17), 129.46 (C-14, C-16), 107.74 (C-5), 11.71 (C-9).

EA: calculated: C 62.61%, H 4.38%, N 12.17%.

found: C 62.47%, H 4.27%, N 12.09%.

3-benzoyl-1-(2-bromoethyl)-5-methylpyrimidine-2,4(1H,3H)-dione

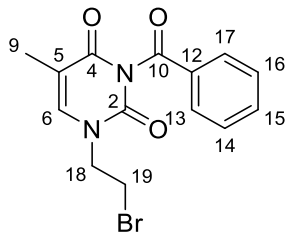

2.00 g (8.69 mmol, 1.00 eq.) 3-benzoyl-5-methylpyrimidine-2,4(1H,3H)-dione and 3.60 g (26.1 mmol, 3.00 eq.) potassium carbonate were dissolved in 90.0 ml DMF. Following this, 3.37 ml (7.34 g, 39.1 mmol, 4.50 eq.) 1,2-dibromoethane was added and the solution was stirred for 48 h at room temperature. The solution was portioned between 150 ml chloroform, and the organic phase was washed with brine, dried over sodium sulfate, and the solvent was removed under vacuum. The crude product is purified via column chromatography (SiO_2, hexane: EtOAc; 2:8), isolating 1.49 g (4.42 mmol, 51%) 3-benzoyl-1-(2-bromoethyl)-5-methylpyrimidine-2,4(1*H*,3*H*)-dione.

TLC: R_f = 0.65 (hexane:EtOAc; 2:8) SiO_2, [UV].

^{1}H-NMR (400 MHz, DMSO-d_6, 300 K): δ (ppm) = 7.94 (d, $^3J_{H,H}$ = 7.1 Hz, 2H, H-13,H-17), 7.84 (s, 1H, H-6), 7.78 (t, $^3J_{H,H}$ = 7.5 Hz, 1H, H-15), 7.60 (t, $^3J_{H,H}$ = 7.7 Hz, 2H, H-14, H-16), 4.12 (t, $^3J_{H,H}$ = 6.4 Hz, 2H, H-18), 3.76 (t, $^3J_{H,H}$ = 6.3 Hz, 2H, H-19), 1.85 (s, 3H, H-9).

^{13}C-NMR (101 MHz, DMSO-d_6, 300 K): δ (ppm) = 169.52 (C-10), 162.80 (C-4), 149.38 (C-2), 142.38 (C-6), 135.51 (C-15), 131.10 (C-12), 130.25 (C-13, C-17), 129.52 (C-14, C-16), 108.43 (C-5), 48.89 (C-18), 30.38 (C-19), 11.86 (C-9).

EA: calculated: C 49.87%, H 3.89%, N 8.31%, Br 23.70%.

found: C 50.42%, H 3.85%, N 8.21%, Br 22.90%.

1-(2-azidoethyl)-5-methylpyrimidine-2,4(1H,3H)-dione

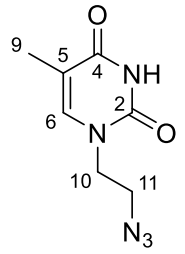

2.37 g (7.03 mmol, 1.00 eq.) 3-benzoyl-1-(2-bromoethyl)-5-methylpyrimidine-2,4(1*H*,3*H*)-dione was dissolved in 130 ml DMSO, followed by the addition of 1.37 g (21.1 mmol, 3.00 eq.) sodium azide. The resulting solution was stirred for 24 h at 80°C. Subsequently, the solution was quenched with water and three times extracted with EtOAc. The combined organic phases were washed with brine and dried over sodium sulfate. The volatiles were removed, and the resulting crude product was purified via column chromatography (SiO_2, hexane: EtOAc; 2:8). 669 mg (3.28 mmol, 59%) 1-(2-azidoethyl)-5-methylpyrimidine-2,4(1*H*,3*H*)-dione could be isolated.

TLC: R_f = 0.35 (hexane:EtOAc; 2:8) SiO_2, [UV].

^{1}H-NMR (400 MHz, DMSO-d_6, 300 K): δ (ppm) = 11.3 (s, 1H, -NH-), 7.53 (s, 1H, H-6), 3.82 (t, $^3J_{H,H}$ = 5.7 Hz, 2H, H-10), 3.58 (t, $^3J_{H,H}$ = 5.7 Hz, 2H, H-11), 1.75 (s, 3H, H-9).

^{13}C-NMR (101 MHz, DMSO-d_6, 300 K): δ (ppm) = 164.25 (C-4), 150.90 (C-2), 141.40 (C-6), 108.59 (C-5), 49.02 (C-11), 46.54 (C-10), 11.94 (C-9).

EA: calculated: C 43.08%, H 4.65%, N 8.31%, Br 35.88%.

found: C 42.89%, H 4.57%, N 8.21%, Br 31.99%.

Polymerization

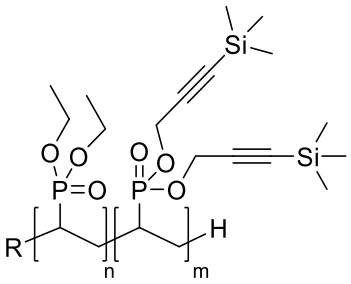

A solution of *sym*-collidine (1.00 equiv.) in absolute toluene (5.00 mL) was added to a solution of $Cp_2Y(CH_2TMS)(thf)$ (1.00 equiv.) in absolute toluene (5.00 mL). After stirring for two hours, the mixture was diluted with additional toluene (80.0 mL). A mixture of DEVP (90 eq.) and DPrTMSVP (10 eq.) in absolute toluene (5.00 mL) was then added to the solution in one portion. After four hours, the completion of the polymerization was detected by ^{31}P-NMR spectroscopy. The reaction was quenched by the addition of MeOH, and the polymer was precipitated in pentane. The supernatant solvent was decanted, and the residual polymer was dissolved in water and freeze-dried to yield the pure polymer as a colorless solid.

^{1}H-NMR (400 MHz, $CDCl_3$, 300 K): δ (ppm) = 4.84 (s, -C*H*$_2$C≡CSi(CH$_3$)$_3$)), 4.12 (s, -OC*H*$_2$CH$_3$), 2.95 – 0.95 (m, $H_{backbone}$, -OCH$_2$C*H*$_3$), 0.17 (s, -Si(C*H*$_3$)$_3$).

^{31}P-NMR (203 MHz, $CDCl_3$, 300K): *δ* (ppm) = 33.2.

TMS deprotection procedure of PDEVP from group-transfer polymerization

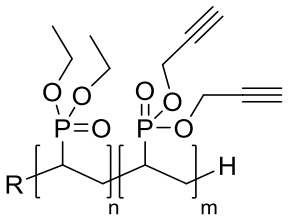

The alkyne functionalized PDEVP (1.0 eq.) was dissolved in methanol (5.00 mL solvent per 100 mg polymer). The calculated amount of K_2CO_3 (20 eq. per propargyl group) was suspended in the solution, and the resulting suspension was stirred overnight. Following the solvent removal, the mixture was dissolved in water and dialyzed for 24 h (MWCO 6-8 kDa). The deprotected polymer **P4** was obtained through lyophilization of the dialyzed solution.

^{1}H-NMR (400 MHz, $CDCl_3$, 300 K): δ (ppm) = 4.12 (s, -OC*H_2*CH_3), 2.97 – 0.89 (m, $H_{backbone}$, -OCH_2C*H_3*).

^{31}P-NMR (203 MHz, $CDCl_3$, 300K): *δ* (ppm) = 33.2.

Post-polymerization functionalization with nucleobases

Adenine functionalization of P(DEVP-co-DPrVP) via CuAAC

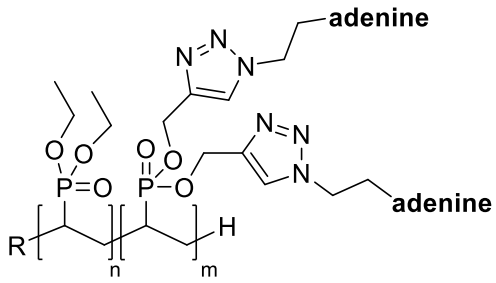

The polymer (1.0 eq.) was dissolved in water (5.0 mL solvent for 100 mg polymer), followed by the addition of sodium ascorbate (5.0 eq). After degassing, $CuSO_4 \cdot 5H_2O$ (5.0 eq.), and a solution of 9-(2-azidoethyl)-9*H*-purin-6-amine (5.0 eq. in DMF) were added to the solution and stirred at room temperature for 48 h. Afterward, the EDTA was added, and the solution was stirred at room temperature for another 24 hours. The solution is dialyzed against water for 48 h providing water exchanges until the sample is colorless, followed by its lyophilization.

UV/vis (MeOH): λ_{max} = 259 nm.

^{1}H-NMR (400 MHz, $CDCl_3$, 300 K): δ (ppm) = 8.28 (bs, $CH_{triazole}$, $CH_{adenine}$), 4.12 (s,-POC*H*$_2$CH$_3$), 2.81-0.91 (m, $H_{backbone}$, -OCH$_2$C*H*$_3$).

^{31}P-NMR (203 MHz, $CDCl_3$, 300K): *δ* (ppm) = 33.1.

Adenine functionalization of P(DEVP-co-DPrVP) via Huisgen-AAC

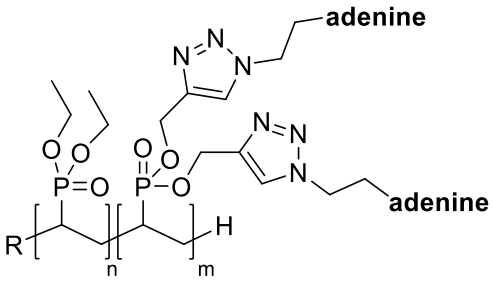

The polymer (1.0 eq.) is dissolved in a solvent (5.0 mL solvent for 100 mg polymer) and a solution of 9-(2-azidoethyl)-9*H*-purin-6-amine in DMF was added. After stirring for 48 h, the crude reaction solution was dialyzed for 48 h. Subsequently, the polymer was purified *via* lyophilization.

Table 11.2: Post-polymerization functionalization of P(DEVP-*co*-DPrVP) with adenine *via Huisgen*-AAC

Entry	Nucleobase (eq.)	solvent	T [°C]
P13	adenine **7**	H_2O:DMSO (2:5)	90
P16	adenine **7**	DMF	130
P17	adenine **7**	DMAc	150

UV/vis (MeOH): λ_{max} = 259 nm.

^{1}H-NMR (400 MHz, $CDCl_3$, 300 K): δ (ppm) = 8.28 (bs, $CH_{triazole}$, $CH_{adenine}$), 4.12 (s,-POC*H*$_2$CH$_3$), 2.81-0.91 (m, $H_{backbone}$, -OCH$_2$C*H*$_3$).

^{31}P-NMR (203 MHz, $CDCl_3$, 300K): *δ* (ppm) = 33.1.

Thymine functionalization of P(DEVP-co-DPrVP) via CuAAC

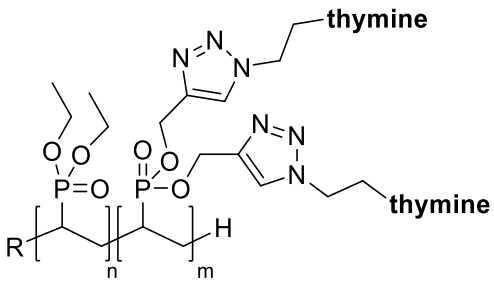

The polymer (1.0 eq.) was dissolved in water (5.0 mL solvent for 100 mg polymer), followed by the addition of sodium ascorbate (5.0 eq.). After degassing, $CuSO_4 \cdot 5H_2O$ (5.0 eq.), and a solution of 1-(2-azidoethyl)-5-methylpyrimidine-2,4(1*H*,3*H*)-dione (5.0 eq. in DMF) were added to the solution and stirred at room temperature for 48 h. Afterward, the EDTA was added, and the solution was stirred at room temperature for another 24 hours. The solution is dialyzed against water for 48 h providing water exchanges until the sample is colorless, followed by its lyophilization.

UV/vis (MeOH): λ_{max} = 268 nm.

^{1}H-NMR (400 MHz, $CDCl_3$, 300 K): δ (ppm) = 11.3 (bs, $NH_{thymine}$), 8.21 (bs, $CH_{triazole}$), 7.25 (bs, $CH_{thymine}$), 6.87 (bs, $CH_{Ar,\ initiator)}$, 4.62 (bs, CH_2, $H_{ethylene\ linker}$), 4.03 (s, -POC*H*$_2$CH$_3$), 3.83 (bs, CH_2, $H_{ethylene\ linker)}$, 2.88-0.85 (m, $H_{backbone}$, -OCH$_2$C*H*$_3$).

^{31}P-NMR (203 MHz, $CDCl_3$, 300K): *δ* (ppm) = 32.9.

Thymine functionalization of P(DEVP-co-DPrVP) via Huisgen-AAC

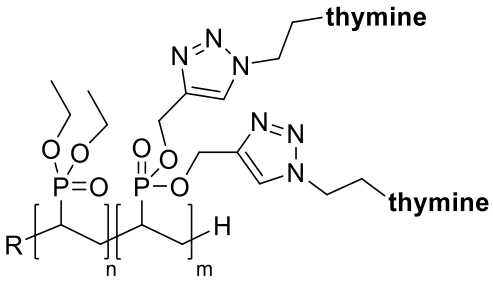

The polymer (1.0 eq.) is dissolved in a solvent (5.0 mL solvent for 100 mg polymer) and a solution of 1-(2-azidoethyl)-3-benzoyl-5-methylpyrimidine-2,4(1*H*,3*H*)-dione (5.0 eq., in DMF) was added. After stirring for 48 h, the crude reaction solution was dialyzed for 48 h. Subsequently, the polymer was purified via lyophilization.

UV/vis (MeOH): λ_{max} = 268 nm.

^{1}H-NMR (400 MHz, $CDCl_3$, 300 K): δ (ppm) = 11.3 (bs, $NH_{thymine}$), 8.21 (bs, $CH_{triazole}$), 7.25 (bs, $CH_{thymine}$), 6.87 (bs, $CH_{Ar,\ initiator)}$, 4.62 (bs, CH_2, $H_{ethylene\ linker}$), 4.03 (s, -POC*H*$_2$CH$_3$), 3.83 (bs, CH_2, $H_{ethylene\ linker)}$, 2.88-0.85 (m, $H_{backbone}$, -OCH$_2$C*H*$_3$).

^{31}P-NMR (203 MHz, $CDCl_3$, 300K): *δ* (ppm) = 32.9.

11.5 Statutory Declaration

Ich, Kerstin Halama, erkläre an Eides statt, dass ich die bei der promotionsführenden Einrichtung

TUM School of Natural Science /TUM Graduate School

der TUM zur Promotionsprüfung vorgelegte Arbeit mit dem Titel:

Expanding the Biomedical Application Scope: Tailoring of Poly(vinyl phosphonates) via Side- and End-Group Functionalization unter der Anleitung und Betreuung durch: Prof. Dr. Dr. h.c. Berhard Rieger

ohne sonstige Hilfe erstellt und bei der Abfassung nur die gemäß § 7 Abs. 6 und 7 angegebenen Hilfsmittel benutzt habe.

☒ Ich habe keine Organisation eingeschaltet, die gegen Entgelt Betreuer*innen für die Anfertigung von Dissertationen sucht, oder die mir obliegenden Pflichten hinsichtlich der Prüfungsleistungen für mich ganz oder teilweise erledigt.

☒ Ich habe die Dissertation in dieser oder ähnlicher Form in keinem anderen Prüfungsverfahren als Prüfungsleistung vorgelegt.

☒ Teile der Dissertation wurden in RSC Advances (RSC), Macromolecular Materials and Engineering (WILEY) and Macromolecules (ACS) veröffentlicht.

☒ Ich habe den angestrebten Doktorgrad noch nicht erworben und bin nicht in einem früheren Promotionsverfahren für den angestrebten Doktorgrad endgültig gescheitert.

☐ Ich habe bereits am _____ bei der promotionsführenden Einrichtung _____ der Hochschule _____ unter Vorlage einer Dissertation mit dem Thema _____

die Zulassung zur Promotion beantragt mit dem Ergebnis:

_____

☒ Ich habe keine Kenntnis über ein strafrechtliches Ermittlungsverfahren in Bezug auf wissenschaftsbezogene Straftaten gegen mich oder eine rechtskräftige strafrechtliche Verurteilung mit Wissenschaftsbezug.

Die öffentlich zugängliche Promotionsordnung sowie die Richtlinien zur Sicherung guter wissenschaftlicher Praxis und für den Umgang mit wissenschaftlichem Fehlverhalten der TUM sind mir bekannt, insbesondere habe ich die Bedeutung von § 27 PromO (Nichtigkeit der Promotion) und § 28 PromO (Entzug des Doktorgrades) zur Kenntnis genommen. Ich bin mir der Konsequenzen einer falschen Eidesstattlichen Erklärung bewusst.

Mit der Aufnahme meiner personenbezogenen Daten in die Alumni-Datei bei der TUM bin ich

☒ einverstanden, ☐ nicht einverstanden.

Ort, Datum, Unterschrift